NASA Conference Publication 10103

Fourth Aircraft Interior Noise Workshop

Compiled by
David G. Stephens
Langley Research Center
Hampton, Virginia

Compilation of material presented at a workshop sponsored by the National Aeronautics and Space Administration, the Society of Automotive Engineers, and the German Aerospace Research Establishment and held in Friedrichshafen, Germany May 19–20, 1992

JULY 1992

National Aeronautics and Space Administration

Langley Research Center
Hampton, Virginia 23665-5225

PREFACE

The fourth in a series of NASA/SAE Interior Noise Workshops was held on May 19 and 20, 1992 at the Graf Zeppelin Haus in Friedrichshafen, Germany. The theme of the workshop was new technology and applications for aircraft interior noise with emphasis on source noise prediction; cabin noise prediction; cabin noise control, including active and passive methods; and cabin interior noise test procedures. This report is a compilation of the presentations made at the meeting which addressed the above issues.

Appreciation is extended to all of those who participated in the workshop and particularly to those that made presentations. In addition, Dr. Ingo Borchers of Dornier Luftfahrt GmbH served as an excellent workshop host as well as tour guide of the acoustic facilities at Dornier. Finally, special thanks are extended to Ms. Loriot of Dornier and Ms. Sutherland of NASA for managing the myriad of arrangements and correspondence associated with this very successful workshop.

David G. Stephens, NASA Langley Research Center
Hanno Heller, DLR Institute for Design Aerodynamics

TABLE OF CONTENTS

4TH NASA/SAE/DLR AIRCRAFT INTERIOR NOISE WORKSHOP

AGENDA

Tuesday, May 19, 1992

8:00 a.m. REGISTRATION

9:00 a.m. WELCOME
Ingo U. Borchers, Dornier Luftfahrt GmbH

9:20 a.m. INTRODUCTORY COMMENTS
David G. Stephens, Chief, Acoustics Division, NASA Langley Research Center and Hanno Heller, Deutsche Forschungsanstalt für Luft- und Raumfahrt

9:40 a.m. I - AIRCRAFT CASE STUDIES

Acoustic Loads on Jet Aircraft
N. N. Reddy, Lockheed Aeronautical Systems Company

MD-80 Aft Cabin Noise Control - A Case History
M. A. Simpson, Douglas Aircraft Co.

The Dornier 328 Acoustic Test Cell (ATC) for Interior Noise Tests and Selected Test Results
H. J. Hackstein, Dornier Luftfahrt GmbH

11:00 a.m. BREAK AND DISCUSSION PERIOD

11:20 a.m. II - PREDICTION AND DIAGNOSTIC TECHNIQUES

Vibro-Acoustic FE Analyses of the Saab 2000 Aircraft
Inge S. Green, Saab Aircraft AB, Linköping, Sweden

Sound Intensity Scanning Technique for Aircraft Interior Noise Measurements
Dr. G. Krishnappa, National Research Council, Canada

Recent Advances in SEA
Ken H. Heron, Defense Research Agency, RAE Farnborough

Use of SEA to Predict Structureborne Noise in Aircraft
Jerome E. Manning, Cambridge Collaborative

12:40 p.m. DISCUSSION

1:00 p.m. LUNCH

2:30 p.m. III - ACTIVE CONTROL OF NOISE TRANSMISSION

Advanced Study for Active Noise Control in Aircraft (ASANCA)
I. U. Borchers, Dornier Luftfahrt Gmbh

Active Control of Noise Transmission through Stiff Lightweight Fuselage Constructions
Dean Thomas, ISVR, Southampton University

Sound Transmission Reduction with 'Intelligent' Panel Systems
Chris R. Fuller, Virginia Polytechnic Institute & State University

Active Control Using Piezo Actuators for Aircraft Interior Noise - Analytical and Experimental Results
Richard J. Silcox, NASA Langley Research Center

3:50 p.m. BREAK AND DISCUSSION

Wednesday, May 20, 1992

9:00 a.m. IV - SUBJECTIVE ACOUSTICS

Measurement of Sleep Response
Dr. John B. Ollerhead, Civil Aviation Authority, London

Pilots Noise Exposure During a B 747-400 Long Haul Flight - Ambient Noise and Acoustic-Head Recording and Analysis of Data
Knut Hoffman, Deutsche Lufthansa AG

Pilots Noise Exposure During a B 747-400 Long Haul Flight - Judgement of Noise Analysis in Respect to Hearing Impairment of Pilots and Discussion of Possible Measures
Hans Jürgen Hoorman, Deutsche Insurance

10:00 a.m. BREAK AND DISCUSSION

10:30 a.m. V - ACTIVE CONTROL AND INTERIOR NOISE

Active Vibration and Noise Control for Turboprop Applications - Research Program Activities
Antonio Paonessa, Alenia Aeronautica

Active Sychrophasing of Propeller Unbalance
Dick Kaptein, Fokker Aircraft B. V.

A Lightweight Loudspeaker for Aircraft Communications and Active Noise Control
Glenn E. Warnaka, Applied Acoustic Research

11:30 a.m. DISCUSSIONS AND ADJOURNMENT

12:00 p.m. LUNCH

1:00 p.m. TOUR OF DORNIER FACILITIES

Lockheed

ACOUSTIC LOADS PREDICTION ON JET AIRCRAFT

N. N. REDDY

NASA/SAE/DLR INTERIOR NOISE WORKSHOP
FRIEDRICHSHAFEN, GERMANY
MAY 1992

Lockheed

AIRCRAFT NOISE SOURCES

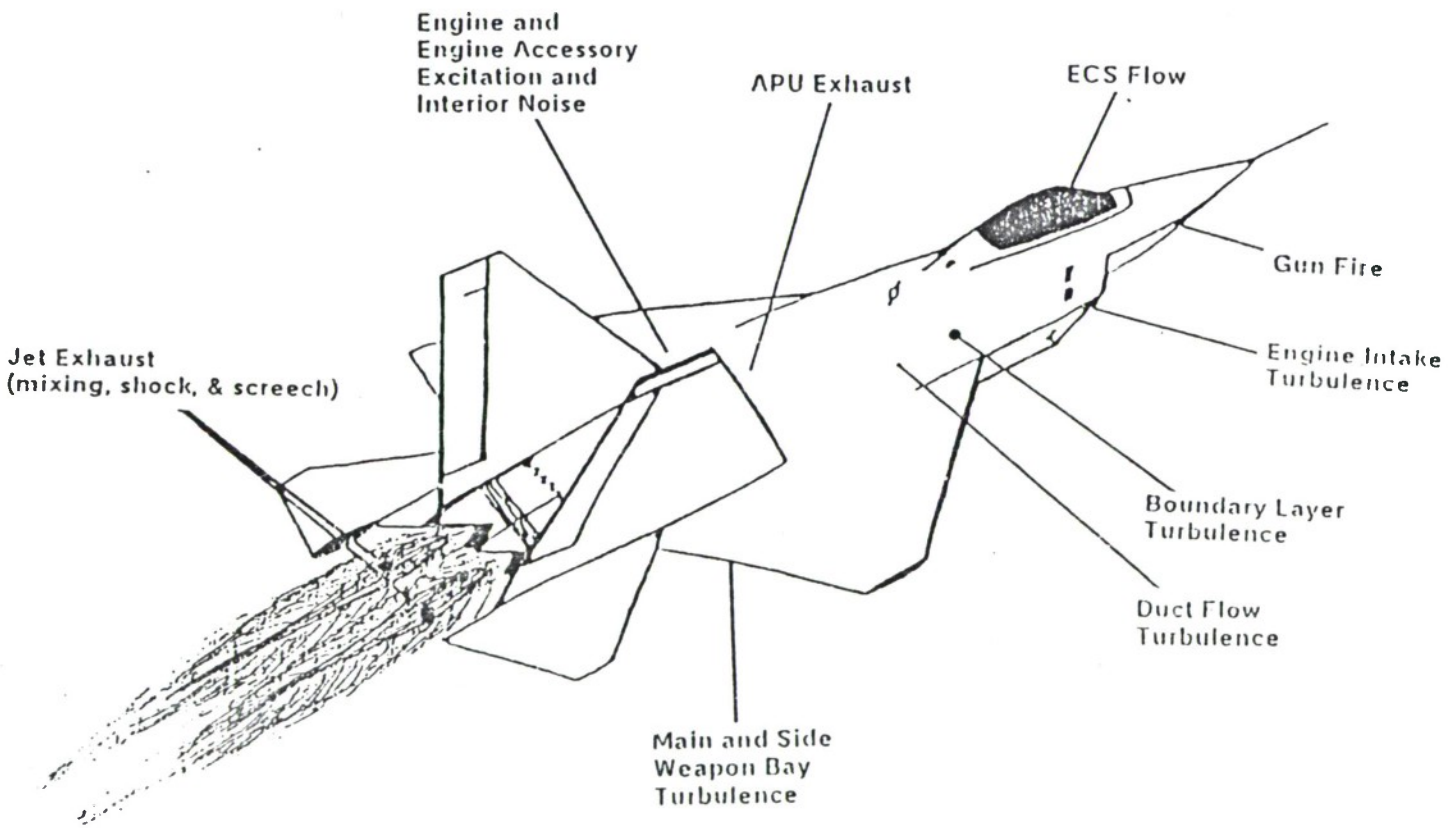

Lockheed

NEARFIELD AIRCRAFT NOISE PREDICTION PROGRAM

DOMINANT SOURCES

- Jet Turbulent Mixing Noise
- Jet Broadband Shock Noise
- Fluctuating Pressure Under Turbulent Boundary Layer

1/3-OCTAVE BAND SOUND PRESSURE LEVELS

FREQUENCY RANGE: 25 Hz - 10,000 Hz

Lockheed

JET TURBULENT MIXING NOISE

PREDICTION METHOD - SEMI-EMPIRICAL PROCEDURE

Swift and Mungur

LFC Noise Criteria - NASA CR-159104

APPLICABLE TO:

Single Flow Circular Jets

Dual Flow Coaxial Circular Jets

Plug Nozzles

Lockheed

FLIGHT EFFECTS ON JET MIXING NOISE

FORWARD MOTION EFFECTS

RELATIVE VELOCITY EFFECT ON ACOUSTIC POWER GENERATION

$$M_{eff} = M_j \, (1 - V_a/V_j)^{0.75}$$

DYNAMIC AMPLIFICATION EFFECT

$(1 + M_a \cos\theta)^{-1}$ Factor

ALTITUDE EFFECTS

AMBIENT DENSITY (ρ_a/ρ_{sl})

AMBIENT SOUND SPEED (c_a/c_{sl})

} ACOUSTIC IMPEDANCE

Lockheed

BROADBAND NEARFIELD SHOCK NOISE

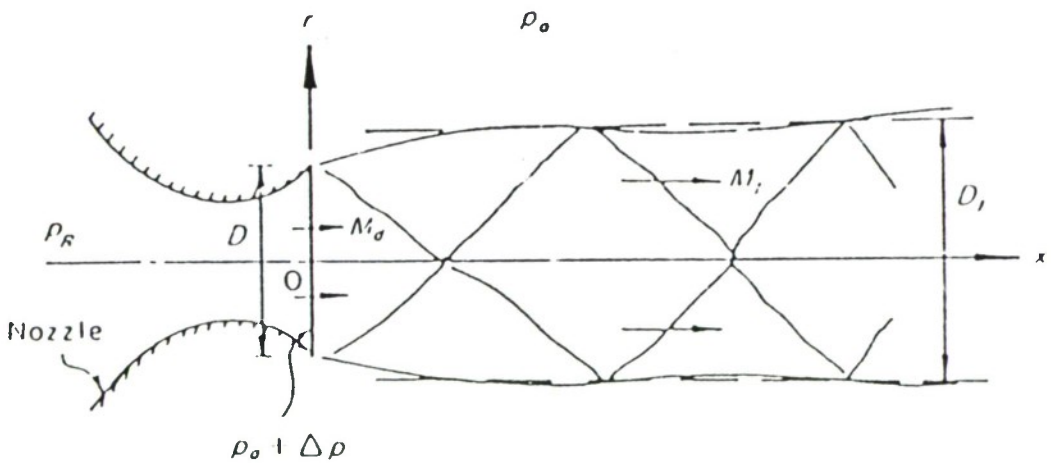

Lockheed

EFFECT OF JET MACH NUMBER ON SHOCK NOISE INTENSITY

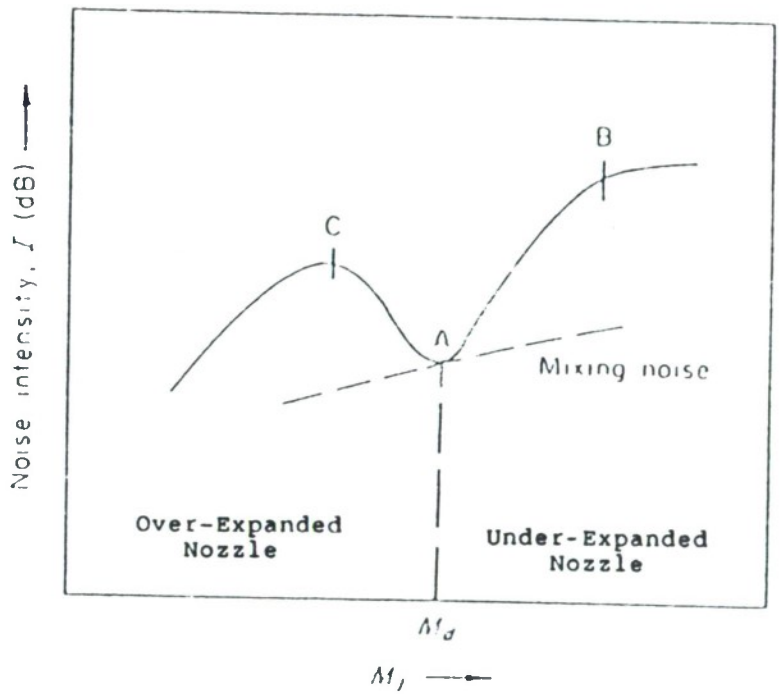

Lockheed

JET SHOCK BROADBAND NOISE PREDICTION METHODS

METHOD BASED ON RECENT THEORETICAL DEVELOPMENT
TAM - JSV (1987)

- SINGLE FLOW CONVERGENT OR CONVERGENT-DIVERGENT NOZZLES
- OVEREXPANDED ($M_j < M_d$) OR UNDEREXPANDED ($M_j > M_d$) MODES
- HEATED JETS
- AGREES WELL WITH EXPERIMENTAL DATA
  (Comparison with Yu's data)

Lockheed

COMPARISON OF JET MIXING NOISE AND SHOCK NOISE PREDICTIONS

Nozzle Exit Diameter = 2.4 ft
Jet Total Temperature = 1500 deg R
Standard Atmosphere
Jet Velocity = 2156 ft/s
Jet Mach Number = 1.32

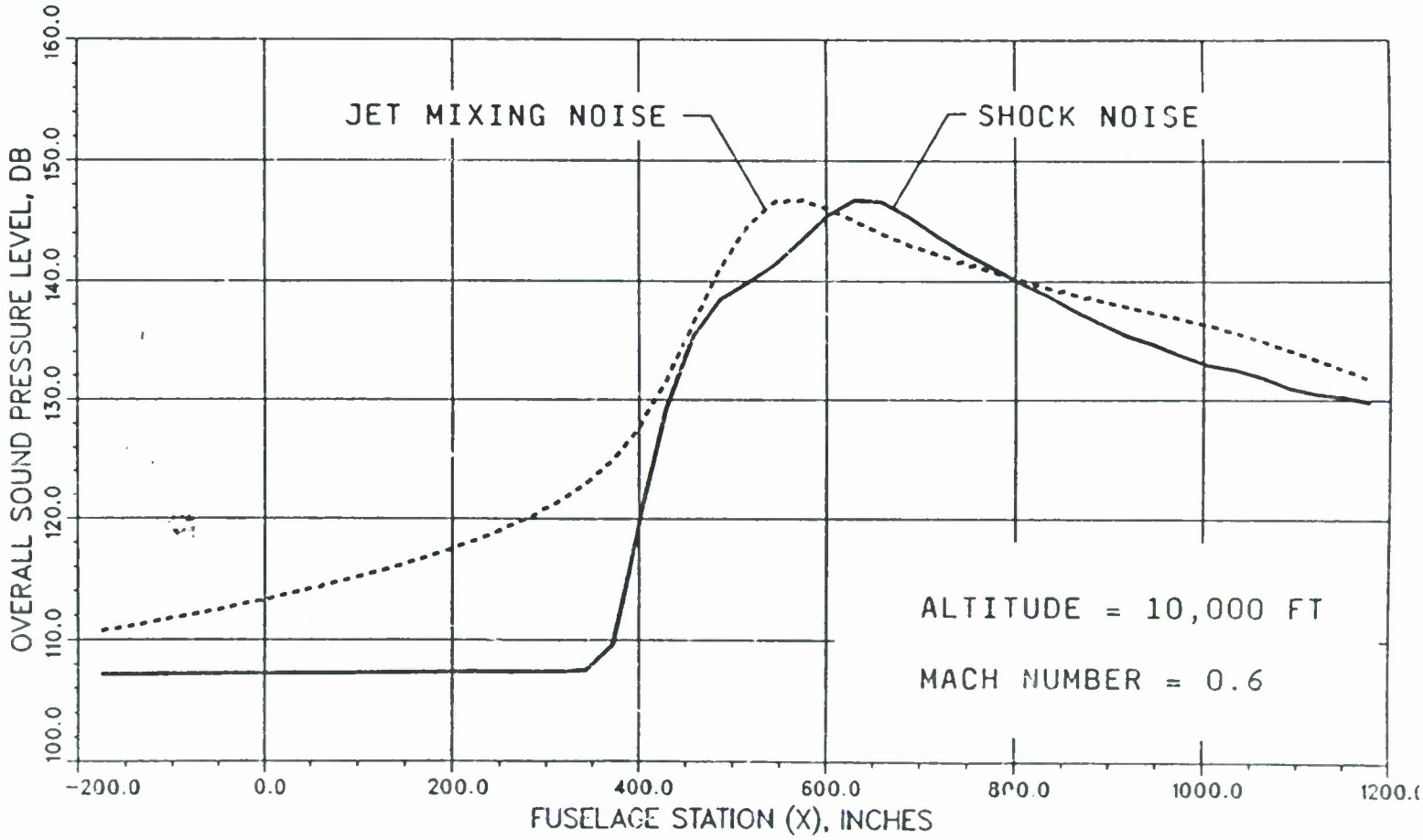

7-MAY-92

Lockheed

FLUCTUATING PRESSURE UNDER TURBULENT BOUNDARY LAYER

PREDICTION METHOD

- SEMI-EMPIRICAL PROCEDURE
- SUBSONIC FLIGHT
- BASED ON EXPERIMENTAL WALL PRESSURE SPECTRA
  - Empirical Curve Fit Equation
- DYNAMIC PRESSURE SCALING

Lockheed

SMOOTH WALL B.L. PRESSURE SPECTRA
FIGURE 8-16 OF BLAKE

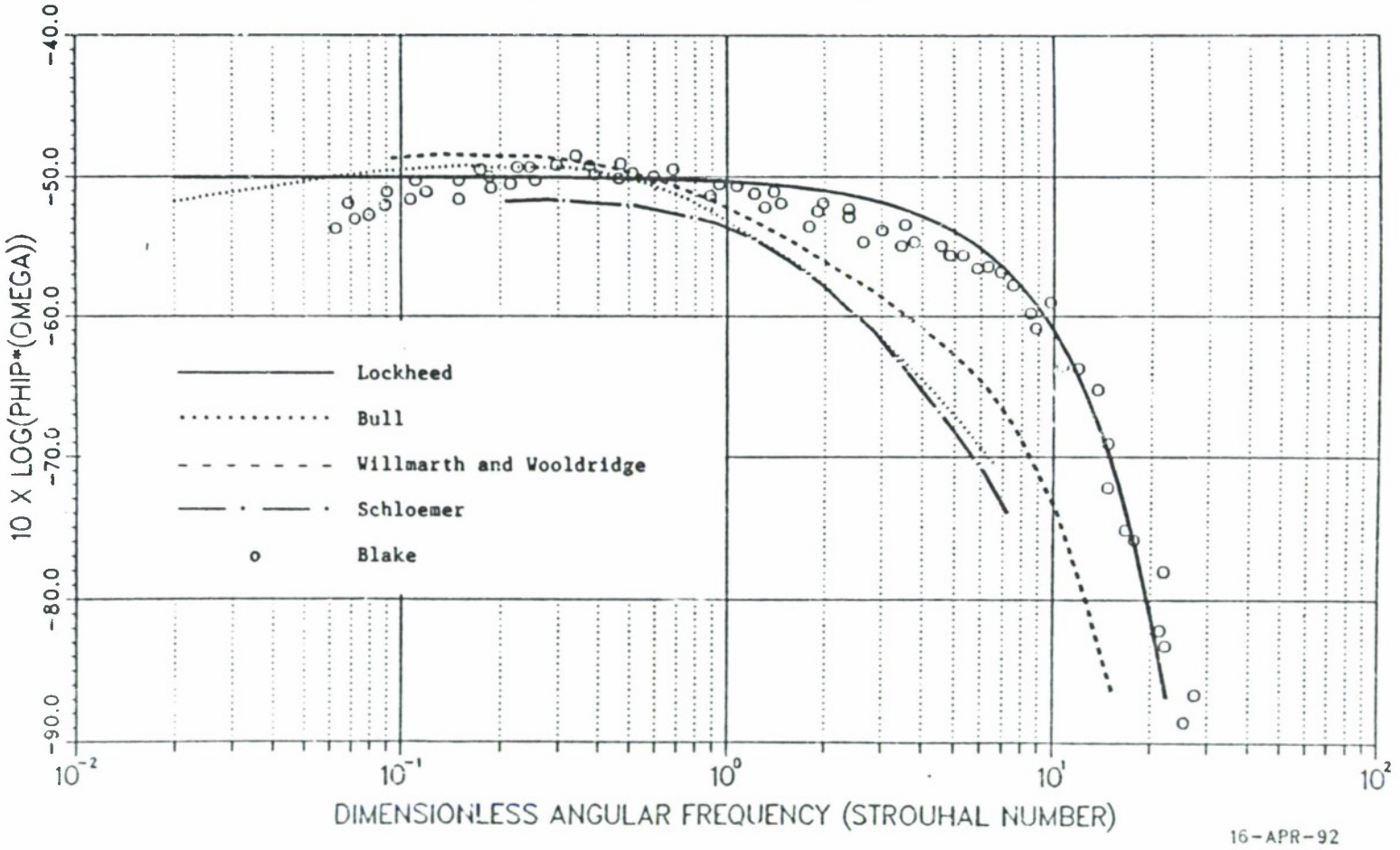

Lockheed

TYPICAL NEARFIELD NOISE SPECTRA ON FUSELAGE

Nozzle Exit Diameter = 2.4 ft
Jet Total Temperature = 1500 deg R
Flight Mach Number = 0.6
Standard Atmosphere

Jet Velocity = 2156 ft/s
Jet Mach Number = 1.32
Altitude = 10,000 ft

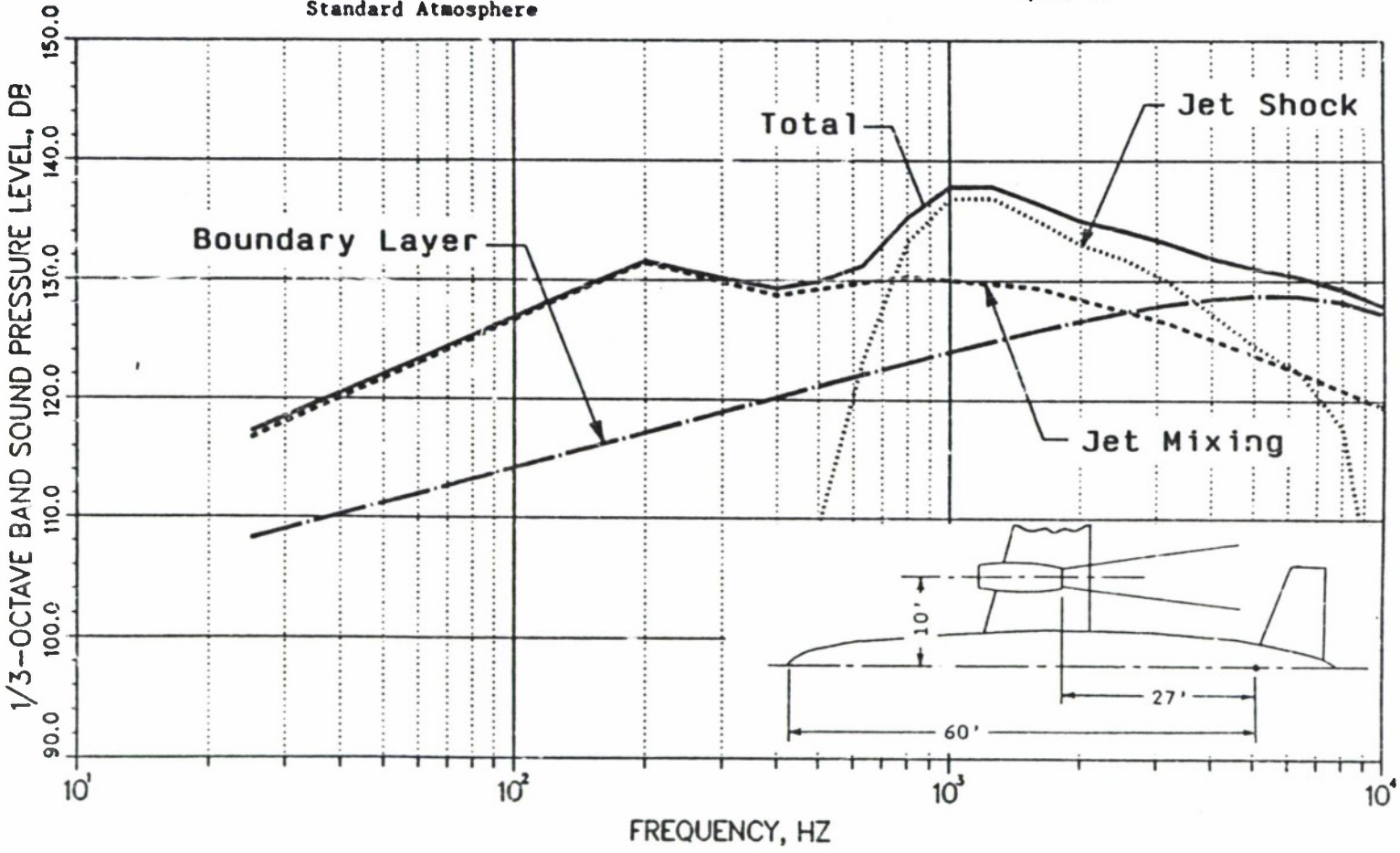

N92
32950
UNCLAS

MD-80 AFT CABIN NOISE CONTROL – A CASE HISTORY

M.A. Lang, D.R. Lorch, D.N. May, and M.A. Simpson

Douglas Aircraft Company
McDonnell Douglas Corporation
Long Beach, California, USA

Presented at
NASA/SAE/DLR 4th Aircraft Interior Noise Workshop
Friedrichshafen, Germany

May 19, 1992

SUMMARY

This presentation discusses the results of an interior noise technology program conducted in 1991 to improve the noise environment in the aft cabin of MD-80 twin jet aircraft. The noise environment in the aft cabin includes tone noise levels occurring at the shaft rotational frequencies of the engine. Engine vibration levels at these frequencies are transmitted through the engine pylon to the cabin. The objective of this program was to reduce the levels of three specific tones, one which occurs during ground idle operations (the lower frequency tone, termed the lo-tone) and two which occur during cruise (the lo-tone and a higher frequency tone termed the hi-tone).

Two potential noise control treatments were identified, studied in ground and flight tests at Douglas Aircraft Company, and then evaluated on a production, in-service aircraft. The treatments are both vibration absorber devices which are designed to reduce vibration at and around the frequencies at which they are tuned. Frame vibration absorbers consist of an absorber mass with an elastomer spring, and are installed on the four aft-most frames and floor beams in the cabin. Engine vibration absorbers consist of an absorber mass on a long stem, and are installed on the forward engine mount yoke of each engine pylon.

Prototype frame absorbers tuned to the lo-tone frequency were tested on a DC-9 fuselage test section, excited by a shaker attached to the pylon. Results of these tests showed a 10 dB reduction in aft seat lo-tone noise levels in an unfurnished cabin, and a 5 dB reduction when the cabin was furnished. Engine vibration absorbers were tested during ground and flight tests of an MD-80 test aircraft. Several absorber configurations were tested, involving different combinations of absorbers tuned to reduce the lower or the higher frequency tones (termed the "lo-tone" and the "hi-tone" absorbers). These tests showed a 6 to 10 dB reduction of the lo-tone when all lo-tone absorbers were installed, and a 4 to 6 dB reduction of the hi-tone when all hi-tone absorbers were installed.

A series of ground and flight evaluation tests using an in-service aircraft was then conducted, for several configurations of frame and engine vibration absorbers. For each configuration the test data were analyzed to yield the average sound pressure level in 1 Hz bandwidths over the operating range of the aircraft, and these levels were averaged over three seats in the aft cabin. Further, a composite tone noise reduction was computed which incorporated the reductions measured for the three tones. The results of this evaluation showed that frame absorbers alone and lo-tone engine absorbers alone each provided significant reductions, but the combination of frame and lo-tone absorbers provided the highest composite tone reduction, 6 dB relative to an untreated configuration. This combined treatment is currently being implemented by one major airline on their MD-80 aircraft.

MD-80 AFT CABIN NOISE CONTROL – A CASE HISTORY

M.A. Lang, D.R. Lorch, D.N. May, M.A. Simpson
Douglas Aircraft Company
McDonnell Douglas Corporation

Presented at
NASA/SAE/DLR 4th Aircraft Interior Noise Workshop
Friedrichshafen, Germany
May 19, 1992

MD-80 AFT CABIN NOISE CONTROL

Key Team Participants

<u>Acoustics</u>
A. Burke
G. Cunto (Alenia)
E. Harvey
D. May
M. Simpson

<u>Structures</u>
D. Lorch

<u>Test/Analysis</u>
M. Lang
O. Angell

MD-80 AFT CABIN NOISE CONTROL

- Program conducted in response to airline desire for quieter aft cabin
- Cabin noise caused by engine vibration transmitted through pylon to cabin surfaces

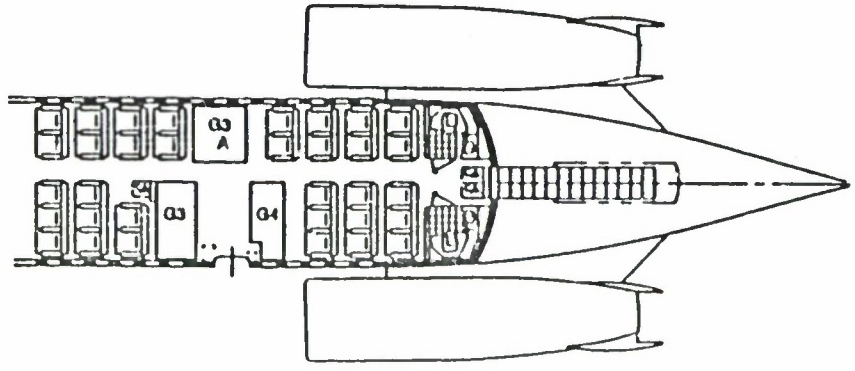

AFT CABIN TONES

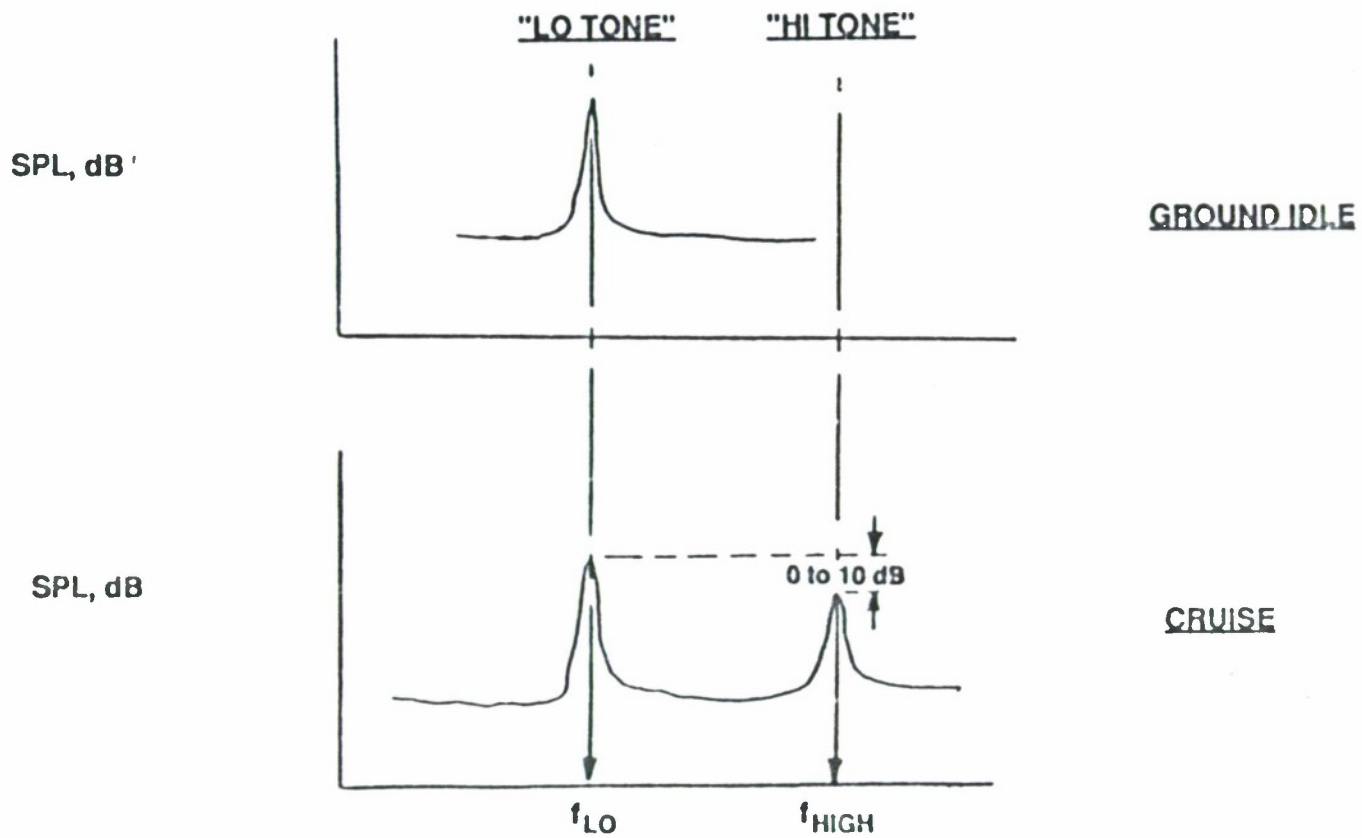

NOISE REDUCTION SOLUTIONS

FRAME VIBRATION ABSORBERS

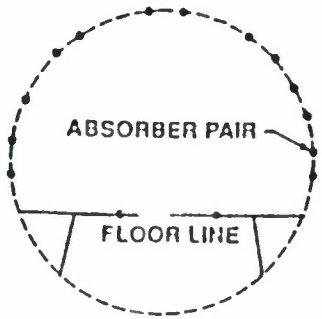

AFT FOUR CABIN FRAMES
- 24-28 ABSORBERS PER FRAME
- 104 ABSORBERS PER AIRCRAFT

- REDUCES FRAME RESONANCE BY INDUCING VIBRATION OF ABSORBER MASS
- NEW TO DOUGLAS TWIN JETS

ENGINE VIBRATION ABSORBERS

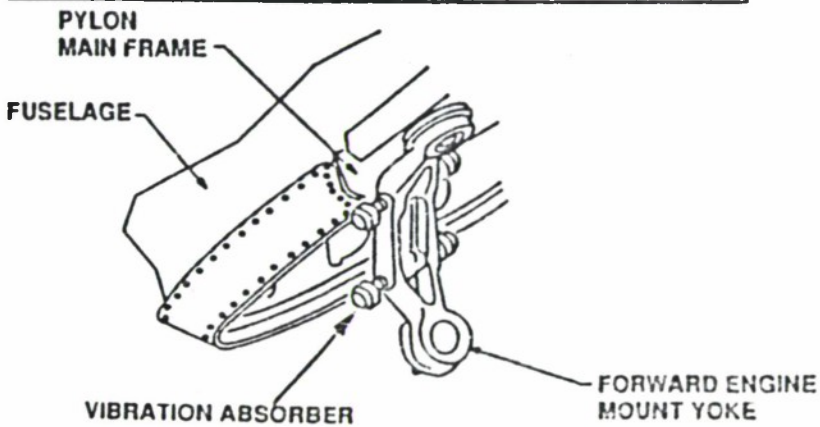

- REDUCES ENGINE VIBRATION INPUT TO CABIN
- USES 4 LO-TONE ABSORBERS INSTEAD OF CURRENT MIX OF 2 LO-TONE + 1 HI-TONE ABSORBERS
- LOW COST, USES EXISTING PARTS

Typical Installation of Frame Dynamic Absorber

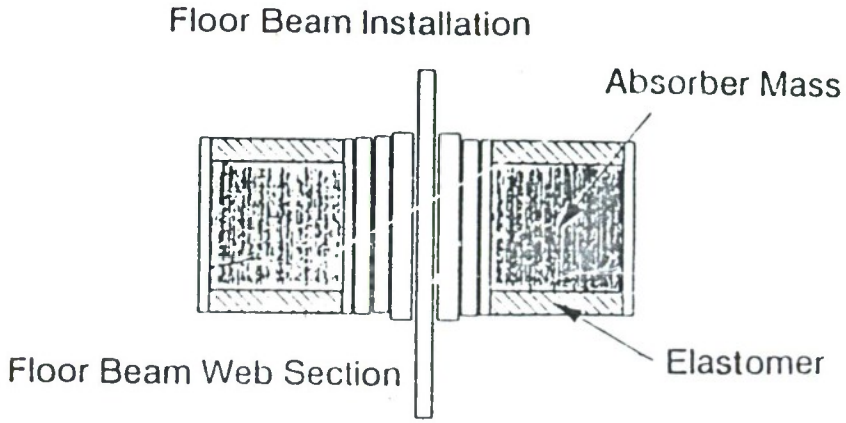

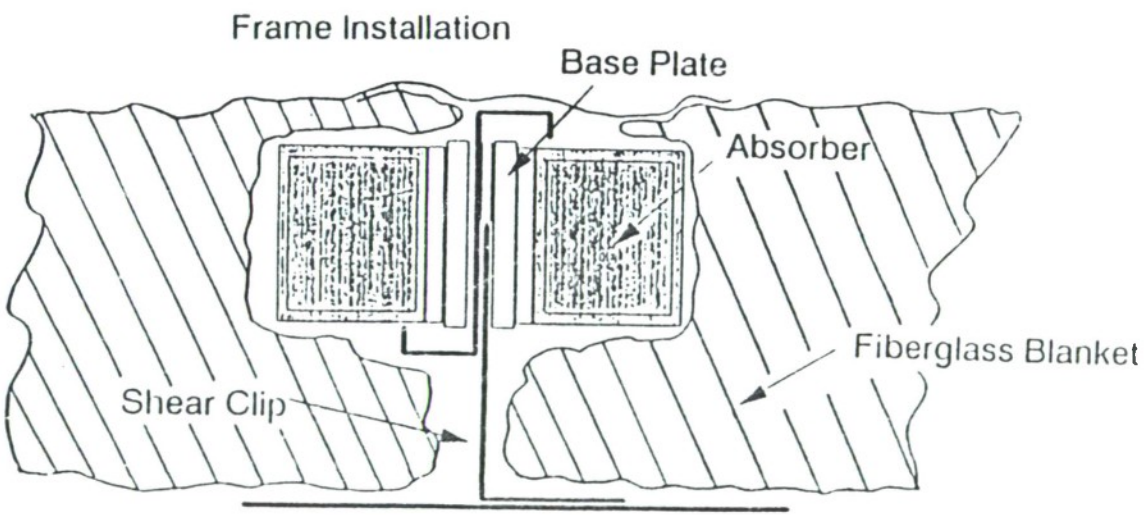

ENGINE VIBRATION ABSORBER

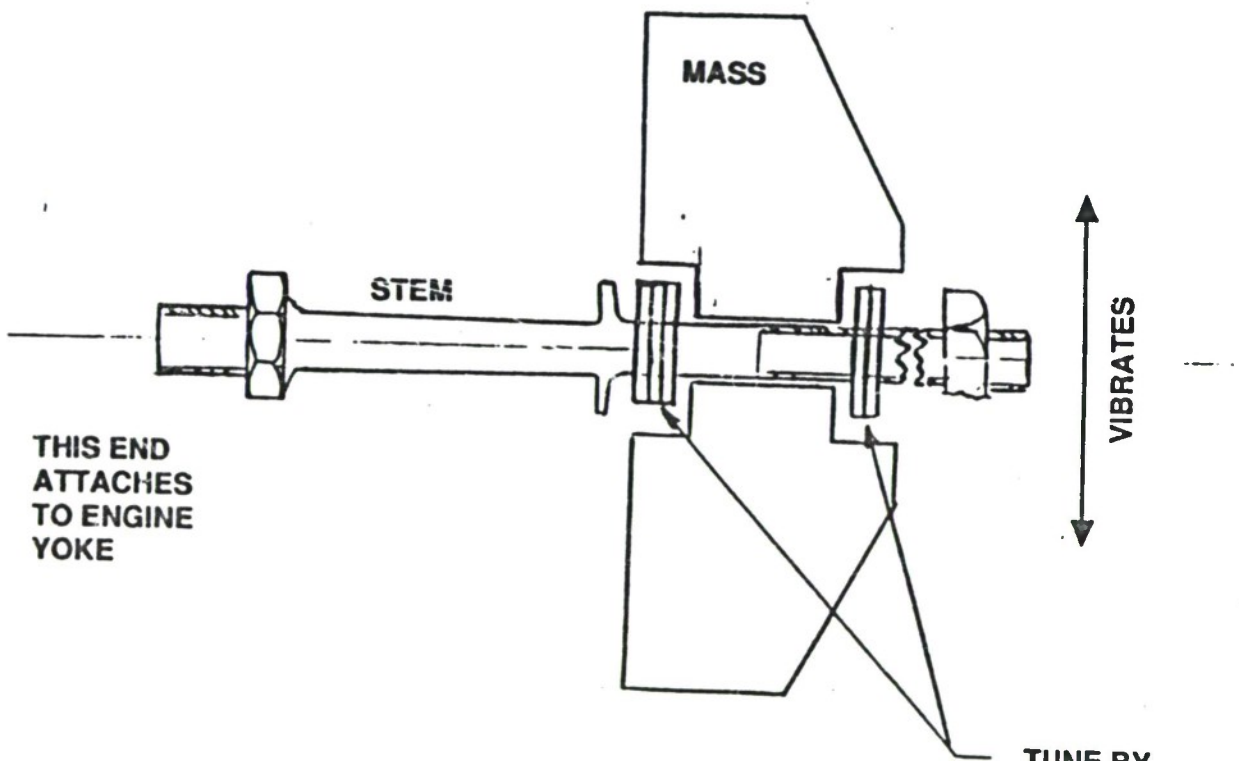

EXPLODED VIEW

DEVELOPMENT TESTS – FRAME VIBRATION ABSORBERS

- Lab tests conducted on a DC-9 fuselage test section
- Prototype absorbers installed on aft 4 frames
- Fuselage excited by 20 lb shaker mounted at engine pylon, at lo-tone frequency
- Test results:
  - Unfurnished cabin – 10 dB reduction
  - Furnished cabin – 5 dB reduction

SAMPLE LAB TEST RESULTS – PROTOTYPE FRAME ABSORBERS
(UNFURNISHED FUSELAGE)

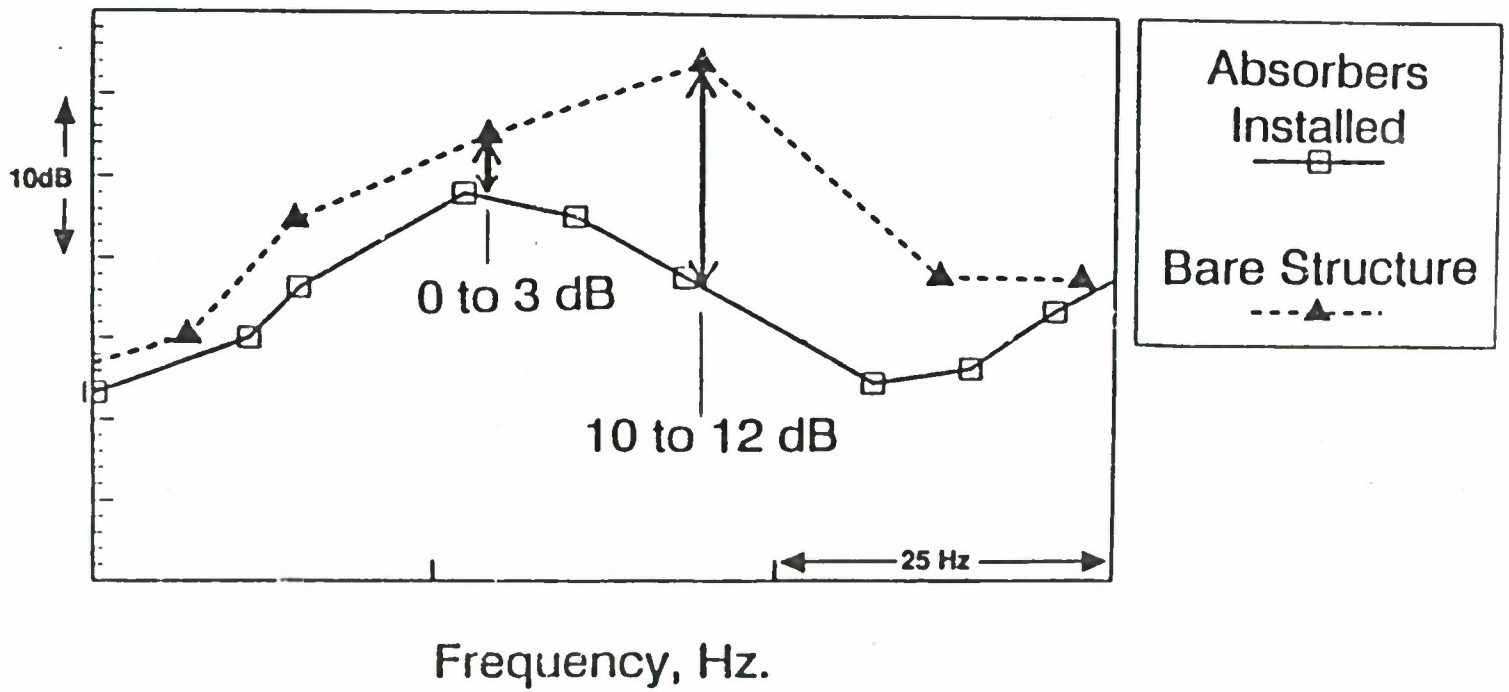

* DUE TO 20 LB LAB SHAKER INPUT, MEASURED IN AFT SEAT ROW, WINDOW SEAT

DEVELOPMENT TESTS – ENGINE VIBRATION ABSORBERS

- Ground and flight tests conducted on an MD-80 test aircraft
- Noise spectra obtained for engine sweeps (up and down) and steps (up, at 1% rpm increments) at 3 seats in aft seat row
- Configurations evaluated:
  - 4, 3, or 2 lo-tone absorbers
  - 4, 3, or 2 hi-tone absorbers
  - 2 lo-tone and 1 hi-tone absorbers (production configuration)
  - no absorbers
- Test results (average reduction over 3 seats, 8 Hz):
  - 4 lo-tone absorbers – 6 - 10 dB reduction
  - 4 hi-tone absorbers – 4 - 6 dB reduction
  - Fewer absorbers yield proportionately lower reductions

SAMPLE FLIGHT TEST RESULTS – ENGINE ABSORBER CONFIGURATIONS

(4 LO-TONE ABSORBERS, CRUISE CONDITIONS)

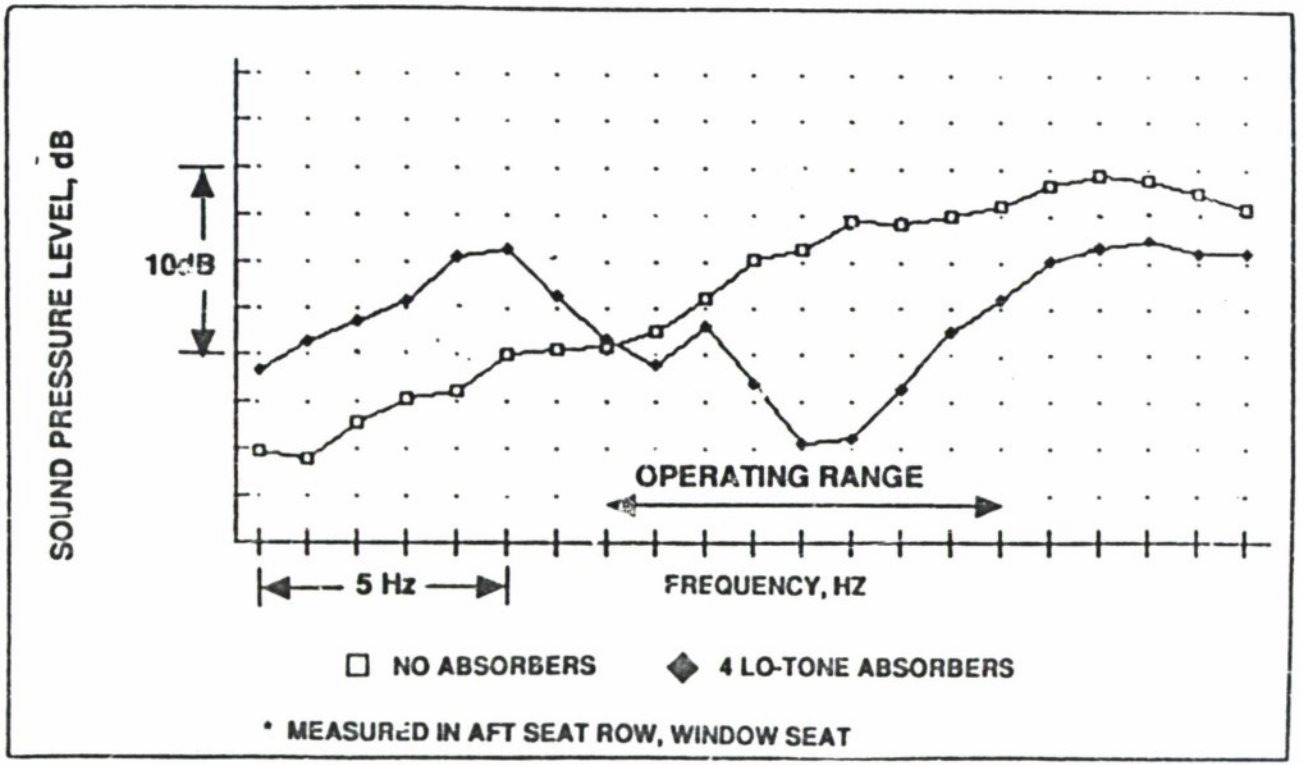

IN-SERVICE EVALUATION TESTS

NOISE CONTROL TREATMENTS

- Production engine absorbers (4 lo-tone + 2 hi-tone)
- 8 lo-tone engine absorbers
- 8 hi-tone engine absorbers
- 104 frame absorbers
- Combinations of frame and engine absorbers

MEASUREMENTS

- Ground tests at low power to measure "ground idle" noise, and at high power to simulate "cruise" noise – all treatments
- Flight tests to measure "cruise" noise – selected treatments
- Engine rpm varied in sweeps (up and down), and steps (up)
- 3 microphones (seats 37A, C, E)

SAMPLE TEST RESULTS – SPECTRA AT INDIVIDUAL SEATS

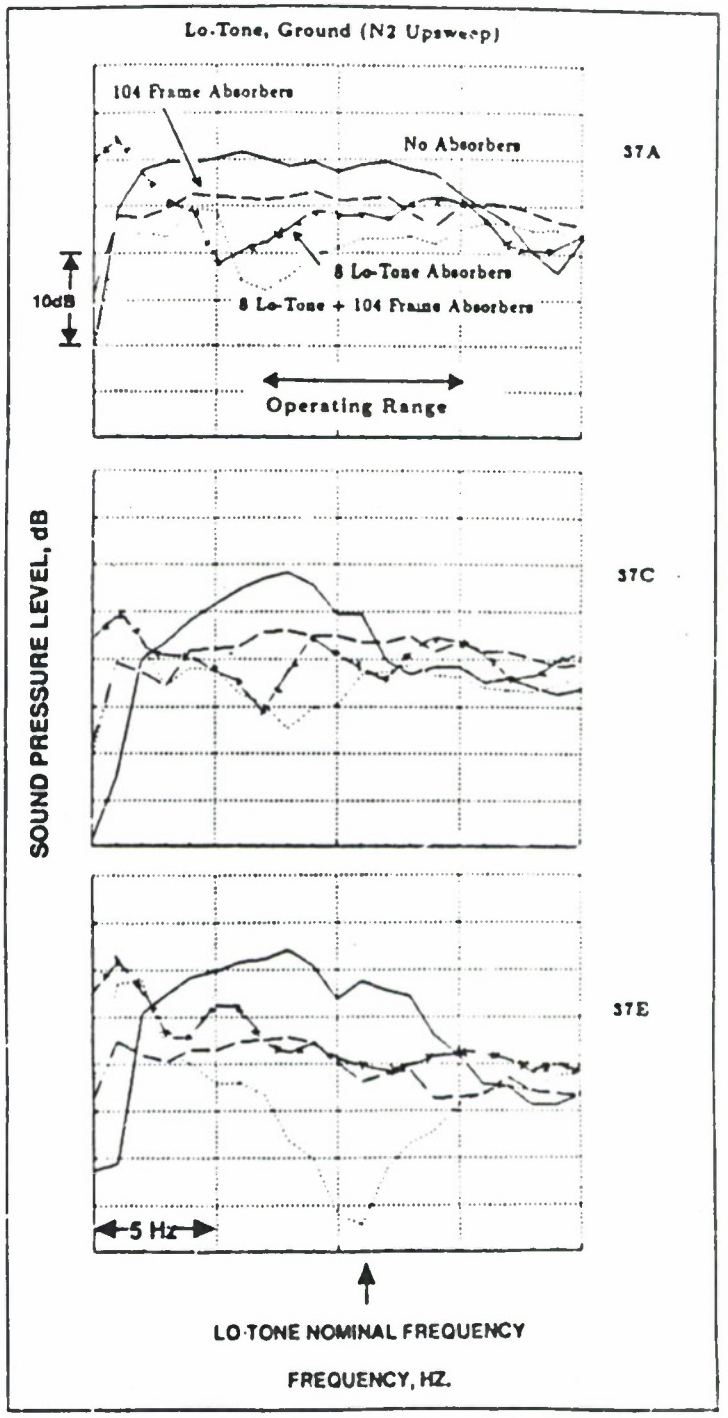

IN-SERVICE EVALUATION TESTS

ANALYSIS

- Average Sound Pressure Level (SPL) calculated in 1 Hz bandwidths across operating range

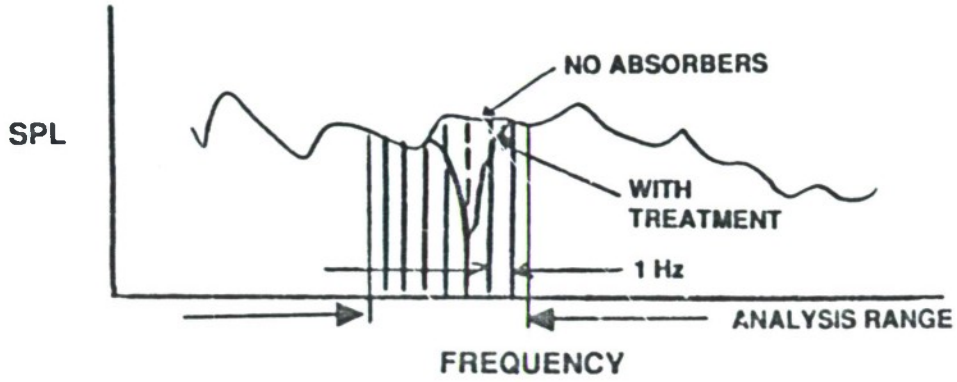

INTERPRETATION

- Average noise reduction (SPL difference) for each treatment across 3 seats for each problem tone
- Three problem tone noise reductions for each treatment combined to give a single-number benefit – "Composite ground and flight noise reduction"

NOISE REDUCTION VS. ADDED TREATMENT WEIGHT – Cases Calculated

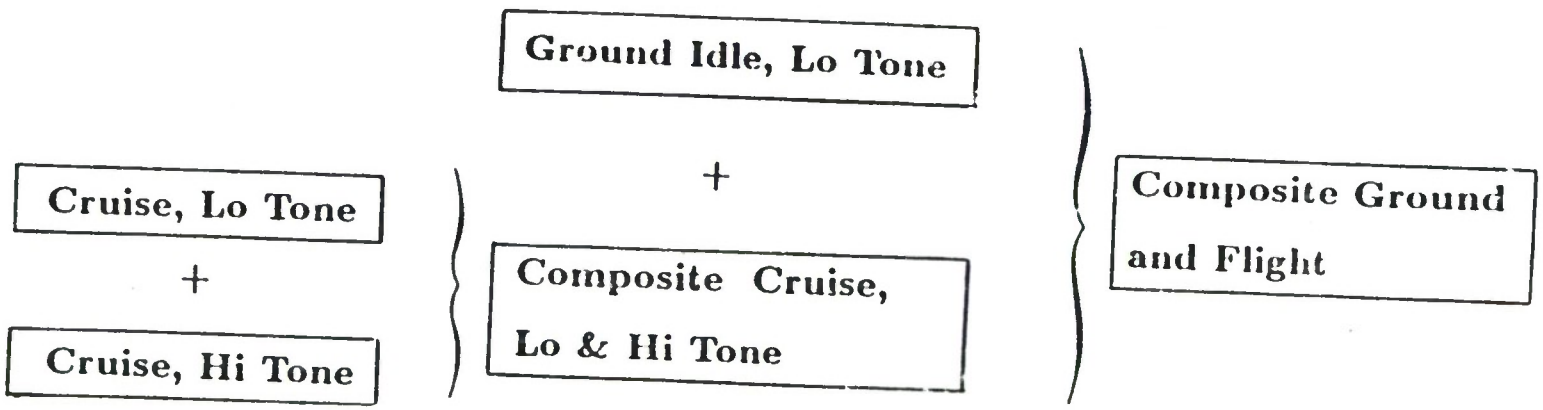

NOISE TREATMENT MANAGEMENT APPROACH

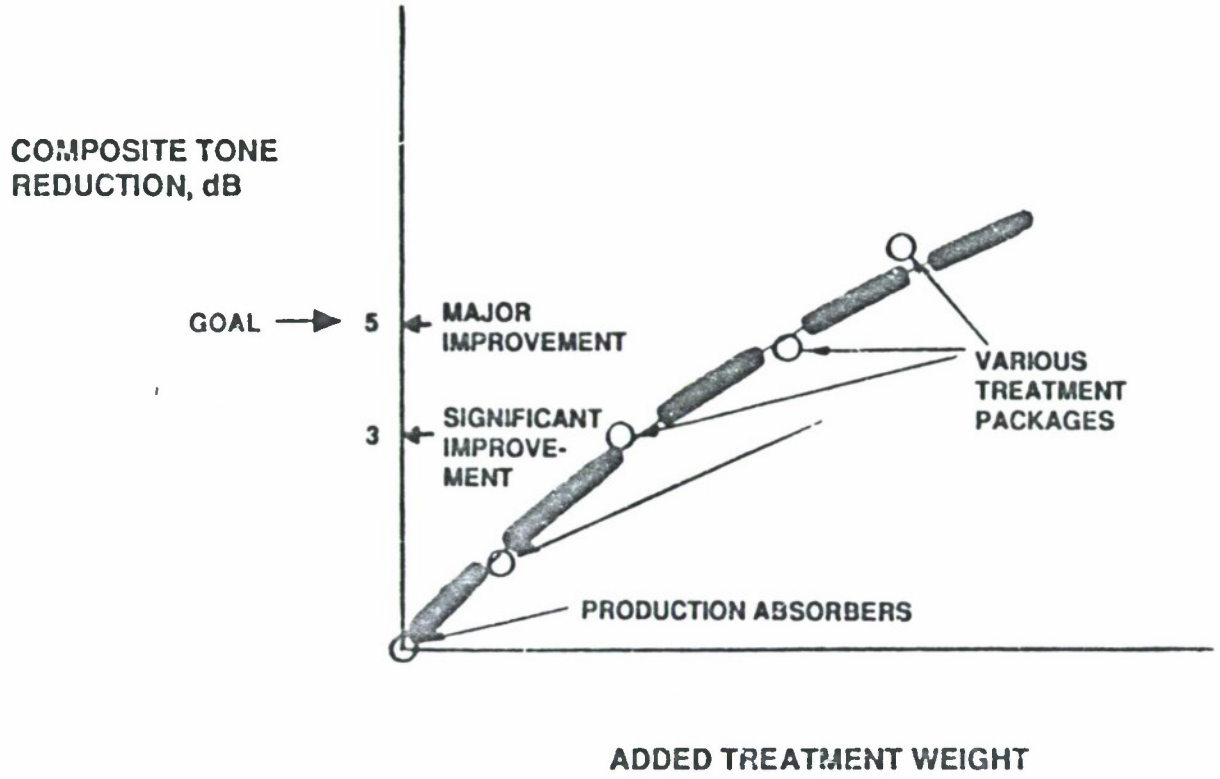

TONE NOISE REDUCTIONS FOR EACH TREATMENT

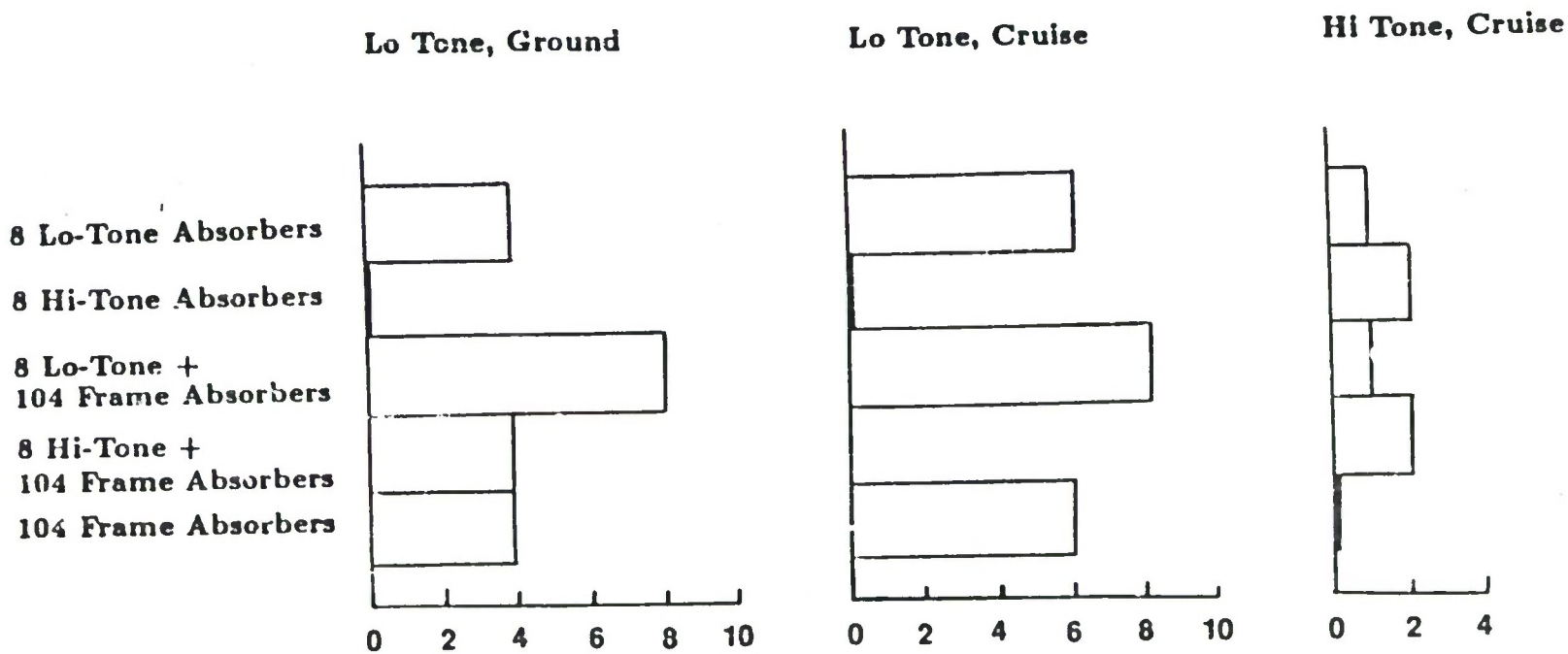

Tone Noise Reduction, dB
(Relative to Production Absorber Configuration)

FRAME & ENGINE VIBRATION ABSORBER NOISE BENEFIT

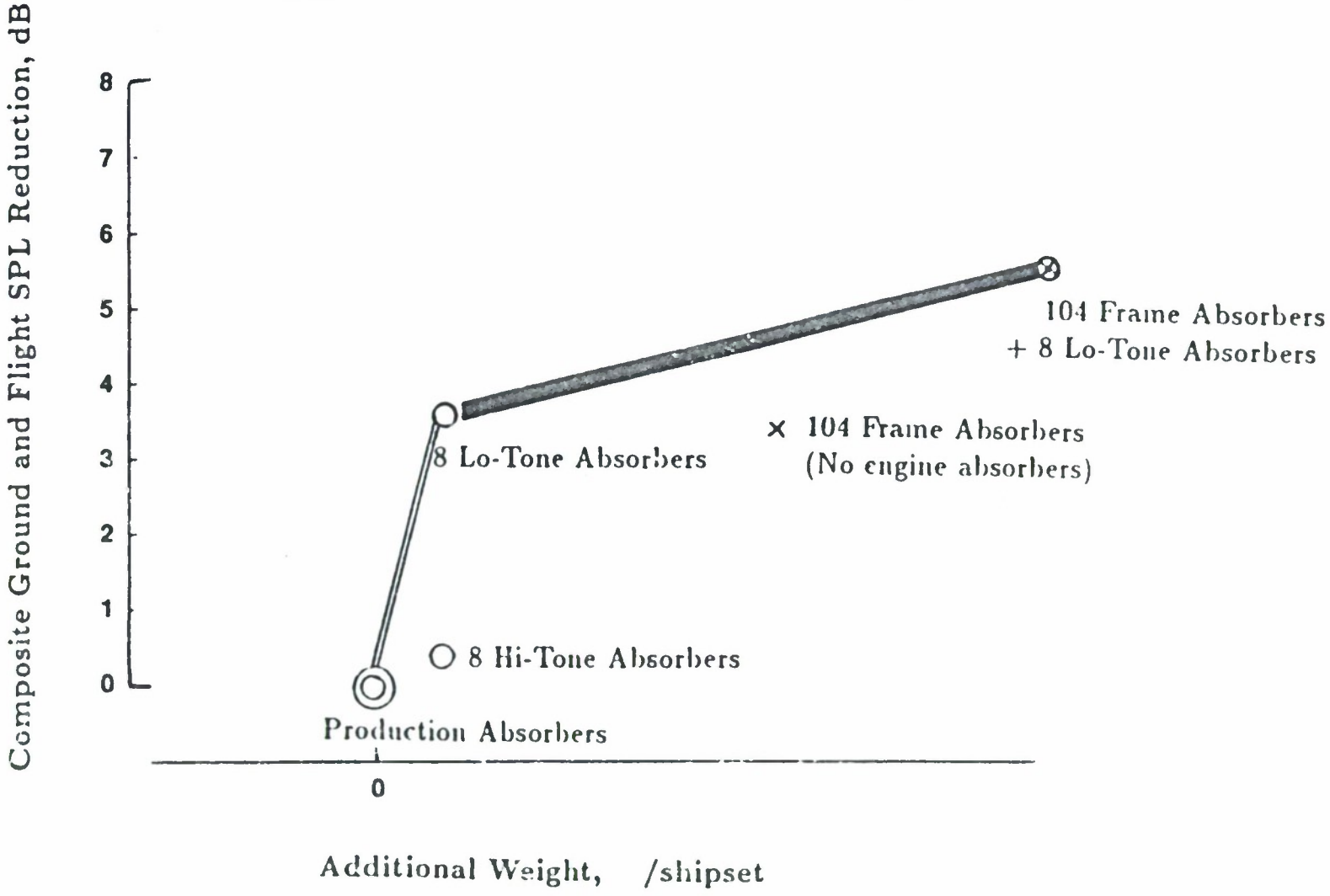

CONCLUSIONS

- Frame absorbers and lo-tone engine absorbers each give significant noise reductions – combined treatments give the highest reduction
- Recommended treatment configuration: 104 frame absorbers plus 4 lo-tone engine absorbers
- Airline pleased with success of aft cabin noise reduction program
- Implementation of the recommended treatment has begun
- Also recommended on-going monitoring program

DGLR / AIAA-92-02-164

The Dornier 328 Acoustic Test Cell (ATC) for Interior Noise Tests and Selected Test Results

H.J. Hackstein, I.U. Borchers, K. Renger, K. Vogt
Dornier Luftfahrt GmbH, Friedrichshafen, Germany

DGLR/AIAA 14th Aeroacoustics Conference
May 11-14, 1992 / Aachen, Germany

THE DORNIER 328 ACOUSTIC TEST CELL (ATC) FOR INTERIOR NOISE TESTS AND SELECTED TEST RESULTS

H. Josef Hackstein

Ingo U. Borchers

Klaus Renger

Konrad Vogt

Dornier Luftfahrt GmbH, Friedrichshafen, Germany

ABSTRACT

To perform advanced acoustic studies for achieving low interior noise levels for the Dornier 328, an acoustic test cell (ATC) of the Dornier 328 has been build. The ATC consists of a fuselage section with full cabin length, a realistic fuselage suspension and three exterior noise simulation rings equiped with 60 loudspeakers. To generate and control the noise excitation and to store and evaluate the large number of the ATC measurement data, a complex digital 60 channel computer/amplifier noise generation system as well as multichannel digital data aquisition and evaluation systems have been used.
The noise control tests started with vibration measurements for supporting acoustic data interpretation. Then acoustic tests followed which first have been carried out without noise reduction measures. Since synchrophasing is an important noise reduction mean, in the second test phase extensive tests on this topic have been performed. In addition, experiments have been carried out on dynamic vibration absorbers, the most important passive noise reduction measure for the low frequency propeller noise. The tests included different kinds of such absorbers and measurements for different RPM's and synchrophaser angles.
The present paper gives a detailed description of the design and the arrangement of the ATC. Furthermore, the exterior noise simulation as well as data aquisition and evaluation are explained. The most interesting results of the measurements showing very promising noise reductions due to synchrophasing and dynamic vibration absorbers are presented.

1. INTRODUCTION

Low cabin noise levels are required by the airlines for new propeller driven regional aircraft as it is an important factor for successful operation. Thus, for the Dornier 328 a goal of 78dB(A) on at least 75% of the passenger seats for a maximum cruise at 1050 RPM in 25000 ft has been specified. Also for the climb condition at 1100 RPM the levels should not be much louder. To reach this goal an extensive interior noise control program has been established and is currently in progress. One powerful tool for this interior noise control program is the Acoustic Test Cell (ATC) of the Dornier 328 shown in Figure 1.

The intention for building the ATC was to have a test rig which comes as near as possible to the real aircraft including the full cabin cavity and a realistic exterior noise simulation. A great advantage of the ATC is a reduced number of expensive flight hours and the opportunity of testing more variations of noise control measures without effecting flight certification.

2. DESIGN OF THE DORNIER 328 ATC

The ATC fuselage with a total length of 12.2 m consits of three parts, the center part with a length of 6.95 m , a front extension cylinder with a length of 1.85 m and an aft extension cylinder with a length of 3.4 m, see Figure 2.

The center part of the ATC is excited by the external noise generation system and is used for suspending the ATC. It has almost the same structure as the Dornier 328 fuselage. Only minor changes, as for example the kind of rivets, had to be made for simplification. Thus it could be expected that the eigenfrequencies and eigenmodes of the ATC in the region of the highest excitation levels are about the same as for the Dornier 328.

As could be seen from earlier finite element calculations [1] not only the vibrational behaviour of the fuselage is important for the interior noise but also the coupling of the structursl modes with the modes of the enclosed air volume, the cavity modes. Therefore, the total cabin lenght should be represented. Because of cost saving reasons this was established by adding the aft extension cylinder,a cylinder with a simplified aluminum frame and stringer structure, to the center part by riveting. A simulation of the cockpit air volume, which may couple across an open cockpit door to the cabin volume, was realized by the front extension cylinder consisting of the same simplified structure as the aft extension cylinder. At the end of the extension parts the ATC is closed by wooden plates.

Inside the ATC the floor is manufactured by wooden plates which are covered by a carpet with similar material as planned for the real aircraft. To separate the cockpit from the cabin, a wooden wall is installed including a door. A view into the ATC is

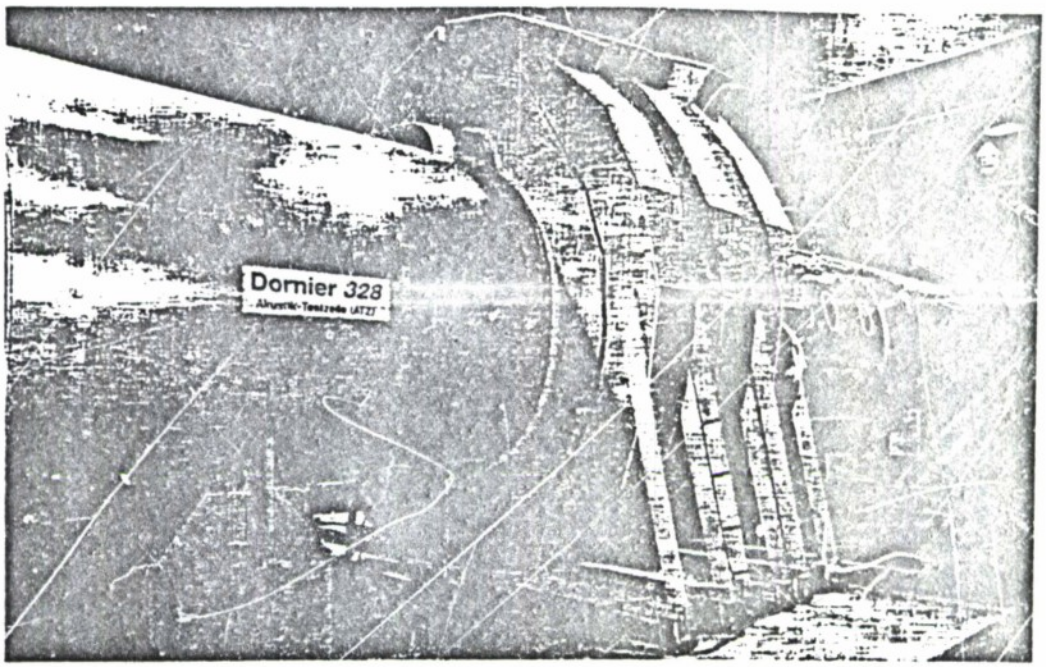

Figure 1: The Dornier 328 Acoustic Test Cell (ATC)

given in Figure 3. Until now, no interior equipment for the tests have been used. For the near future it is planned to install thermal insulation, interior trim and seats.

The ATC fuselage is mounted in the large acoustically treated test chamber of Dornier Luftfahrt GmbH. The suspension is realized by a steel constuction which holds the ATC on four original wing ettachement points.

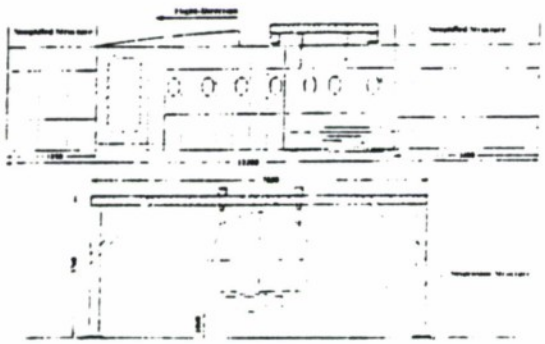

Figure 2: Structure and suspension of the ATC

3. SIGNAL GENERATION SYSTEM

A very complex part of the ATC is the signal generation system designed to generate propeller noise on the fuselage as close as possible to reality. With this system, based on a 60 channel computer/ amplifier noise generation group, it is possible to simulate calculated and measured propeller noise fields with the correct amplitude and phase at 60 points on the fuselage skin. Different synchrophasing angles can be adjusted within a few seconds, enabling parameter studies on this important subject. For special measurements it is also possible, to generate broadband random noise for example to simulate boundary layer and jet noise .

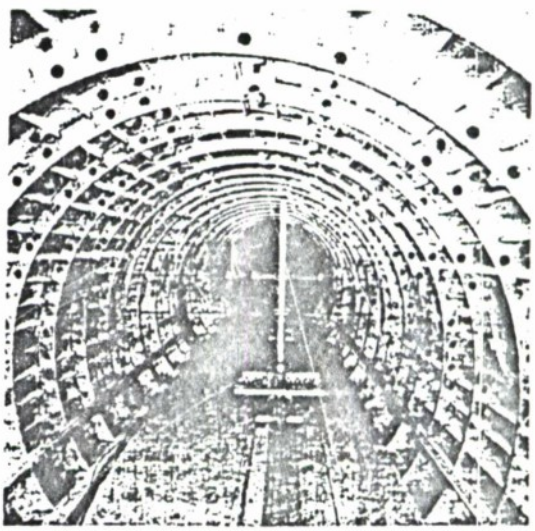

Figure 3: Interior of the ATC including microphone antenna

3.1 Signal Generation System Hardware

The set-up of the total system is given in Figure 4. The 60 loudspeakers are located in three planes, the propeller plane, a quarter of the wavelength of the fundamental tone in front and a quarter of a wavelengh behind the propeller plane, cover the part of the fuselage most strongly excited. For each of these planes two wooden loudspeaker sections formed as half rings, one on the left and one of the right side, have been build containing 10 loudspeakers each, see Figure 5.

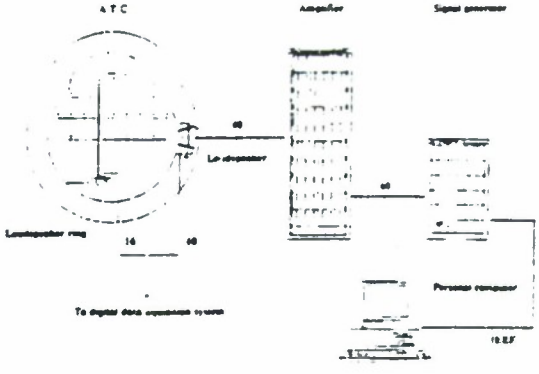

Figure 4: Flow chart of the ATC noise excitation and measurement system

The exterior excitation noise is monitored by microphones mounted on the outer fuselage skin under each loudspeaker. To enable easy access to these microphones every half ring is fitted on wheels for easy loudspeaker section disassembly. The wheels are guided by aluminium profils to ensure that allways the same position on the fuselage is reobtained. Every loudspeaker has its own closed chamber, which can be accessed by a door at the backside of the loudspeaker rings. Thus it is also possible to change the loudspeakers from the backside without moving the wooden half ring.

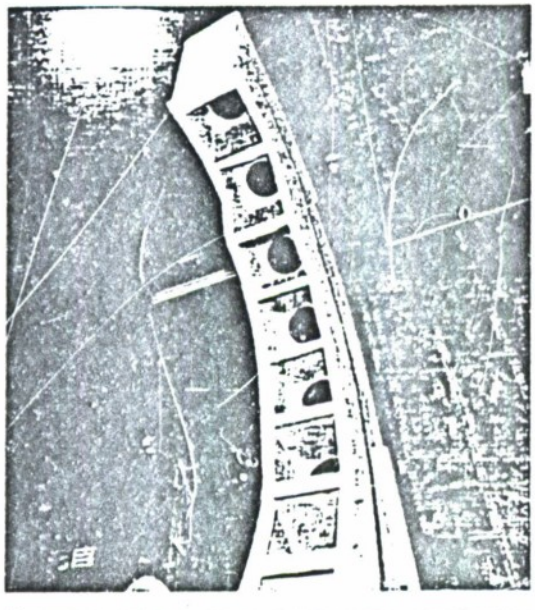

Figure 5: View into a loudspeaker half ring

Between the fuselage and the loudspeaker boxes a layer of weak insulation wool is used to ensure that the ATC has no contact to the wooden construction and that the loudspeakers will not influence each other. The loudspeakers are driven by 60 independant 130 Watt special amplifiers resulting in a power rack with about 8000 Watt continous output power.
The output power of the amplifiers is fixed to maximum for highest accuracy. The amplitude of the signals is controlled by the signal generator cards. Also for accuracy reasons the frequency range of the amplifiers is limited to 2000 Hz. For possible future, different applications it is very easy to change this limit. Also it is planned to make the output power adjustable, if needed.

The noise signal is generated by 60 signal generator cards shown in Figure 6. Every card has its own memory and processor, so that it is able to operate independant from the computer. To ensure the correct phase relationship between the cards, the first card provides also the master clock impulse for the remaining 59 ones. For special tests, it is also possible to trigger the total system by an external clock impulse.

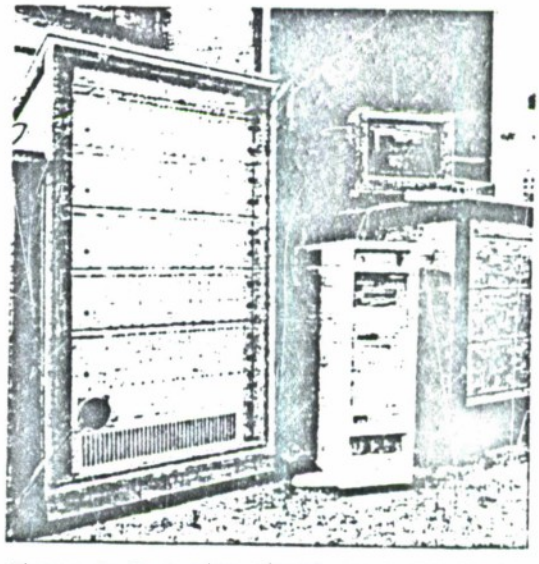

Figure 6: Rack with signal generator cards connected to a personal computer

The signal generator cards are fully controlled by a personal computer. The periodic time functions to be downloaded for different selected flight cases contain phase and normalized amplitude information for each loudspeaker/ amplifier channel. The period of the time function certainly equals the period of the fundamental propeller tone.

For operation it is only necessary to download once two periods of the digitized periodic time function from the computer into the memory of the different loudspeaker signal generator cards. The phase shift between the different loudspeaker signals is obtained by telling each card, at which point of the digitized time function it shall start the period of the output signal. With this technique it is very easy to change the phase relationship between the signals

An additional very important function of each signal generator card is the possibility of changing the amplitude of the signal during signal output. This is done by a second D/A converter on the card, providing the reference voltage for the main D/A converter. The second converter can be accessed during operation. Thus it is possible to use the full dynamic range of the main D/A converter. For standard propeller noise fields the corresponding settings of the second D/A converters are stored in files.

3.2 System Software Options

The generated loudspeaker signals and a corresponding correction signal can be superimposed for compensating the phase- and amplitude errors caused by the loudspeaker/amplifier combination. This correction signal was previously measured for every channel.

With a time delay setting, the phase of each channel can be set based on its reference channel. This makes it very easy to change the synchronnasing angle, because all left-hand channels refere to the first channel of the left side and all right-hand channels refere to the first channel of the right side. The first channel of the right side referes to the first channel of the left side, so that only the time delay of the first right-hand channel has to be changed to adjust a new synchrophasing angle.
Furthermore it is possible to change the output frequency of the signal generator cards in minimum steps of 1 µs. The simulated propeller fundamental frequency is given by the selected number of points for one period at a fixed output frequency of the points.

To preserve the loudspeakers, the output starts automaticaly from zero amplitude by slow amplitude rising to the adjusted level. For the same reason the system level is decreasing slowly when the output is switched off. After changing any parameter of the system, the setting is restored to the signal generator cards.

Finaly it is possible to store any current system set-up in a file on disc and reload it. Also it should be noted that all measurements showed an impressive stability of the sound generating system.

4. MEASUREMENT SYSTEM

For each measurement, first all 60 microphones under the loudspeakers of the sound generating system are measured. Then the interior sound field is recorded in 12 planes using a moveable microphone antenna with 15 microphones leading to a total number of 180 interior noise measurement points. In addition one fixed reference microphone is measured during the recording at each plane, giving a total of 252 signal records for every complete measurement.

For such a large number of measurement positions a user programable digital data aquisition system is needed and was used. In the current configuration the used system handles 32 channels parallel and a total maximum number of 126 channels using software controlled channel switches.
It is capable to connect every microphone to its geometric location, so that various noise distribution plots can be generated.

The user software developed by Dornier for the measurements in the ATC, sets the calibration factors for each channel depending on the channel switch settings, the microphone coordinates depending on the position of the antenna in the ATC, and the name of the current recording depending on the synchrophasing angle and the position of the antenna. With this, it is possible to measure all locations for one paramater set of synchropnasing angles, e.g., 6 angles, within 80 minutes. For every plane all 6 synchrophasing angles are measured before moving the antenna to the next plane. In general, all data are measured as time records and stored on optical discs or DAT tapes. This enables various analyses later if needed.

For the standard data analysis also a software package has been developed, which automaticaly calculates the averaged FFT's for each location and measurement, the average of all spectra, and selected spectra, e.g., the average spectra at the passengers ear positions, the sound distribution over cabin length, etc. All results are given in dB as well as dB(A), as absolute noise levels as well as noise reductions.

It is possible to perform several measurements in one day and to do the data analysis software-controlled automatically during the night. Thus a lot of parameter variations can be tested rather effectively.

5. NOISE AND VIBRATION MEASUREMENTS ON THE BARE ATC

All noise and vibration measurements described in this paper have been performed without interior treatment as for example thermal insulation, interior trim and seats.

5.1 Exterior Noise Field

Following the Dornier 328 specification, the ATC has been excited by two different pure tone propeller noise spectra. One of these was the propeller noise for the condition maximum cruise with 1050 RPM at 345 kts. The other was the condition maximum cruise with 1100 RPM and 345kts as the worst case of a quick cruise climb. Because of not available flight test data of the propeller noise (the ATC tests

started before first flight) the exterior sound field has been calculated. The free field propeller noise was provided by Hartzell for its Dornier 328 six-bladed propeller and has been corrected for installation effects estimated by Dornier. The propeller noise spectra for both excitations in dB(A) averaged over all 60 loudspeakers are given in Figure 7. It can be seen that for both spectra the fundamental has the highest levels and the the harmonics are continously decreasing. This behaviour is typical for a six bladed propeller, while four bladed propellers often show higher A-weighted levels for the second and third blade passage frequency (BPF). The spectrum for 1050 RPM has for all tones lower levels than that for 1100 RPM. For the fundamental, the difference is about 2 dB(A) but for the higher harmonics this difference is increasing up to about 7 dB(A) at the fourth tone. This behaviour can be explained by the higher helical tip Mach number at 1100 RPM. The difference in total noise is about 3 dB(A).

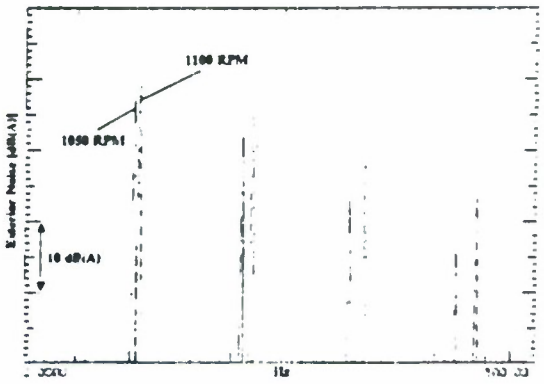

Figure 7: Spectra of total averaged simulated exterior propeller noise (1050 RPM and 1100 RPM)

5.2 Vibration Measurements

Information on the bare ATC structural dynamics in form of eigenfrequencies and modeshapes as well as operational deflection shapes has been obtained from vibration measurements on the ATC. First an experimental modal analysis with multiple point shaker excitation at 10 reference points grouped in three points for each individual measurement run was carried out. For exicitation the burst random technique was used. For the calculation of the mode shapes only those reference points have been applied which showed the best values for the indicator functions. Six frames have been analyzed using a total of 170 accelerometers.

Up to 235 Hz 16 modes could be identified. Figure 8 shows the mode shapes for Mode 7 at 95.7 Hz and Mode 8 at 116.8 Hz. These two modes are the nearest to the fundamentals of the simulated propeller noise with 105 Hz and 110 Hz, respectively. It can be seen that Mode 7 at 95.7 Hz has five antinodes above the floor. Below the floor the structural displacement is not so strong but the floor itself shows in the region of the aisle stronger displacements. For Mode 8 at 116.8 Hz the nodal lines can not be as clearly identified as those of Mode 7. Nevertheless six antinodes can be discovered above the floor. Another one can be detected below the floor. The floor deflections are for Mode 8 smaller than for Mode 7.

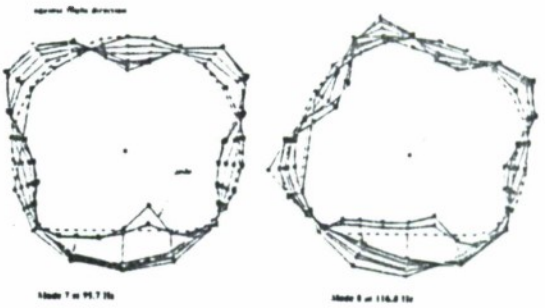

Figure 8: Selected eigenmodes of the ATC

To get knowledge about the motion of the ATC structure during propeller noise excitation, operational deflection shapes have been determined. The used technique is described in [2]. The operational deflection shapes shown in the present paper have been measured for two frames and contain the fundamental as well as four harmonics but they are dominated by the fundamental. Figure 9 presents the operational deflection shapes at the simulated propeller noise field for 1050 RPM for two different synchrophasing angles, 0° and 40°. For the synchrophasing angle of 0° a nearly symmetrical deflection shape with five antinodes above the floor can be seen. This shape is very similar to that of the Mode 7 at 95.7 Hz. Thus this eigenmode might have been strongly excited by the simulated propeller noise field at 1050 RPM. Changing the synchrophasing angle to 40 ° leads to a rotation of the vibration pattern and a reduction of deflection amplitudes.

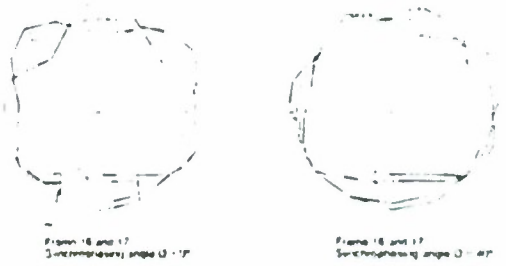

Figure 9: Operational deflection shapes for simulated propeller noise (1050 RPM)

5.3 Interior Noise

The interior noise measurements have been carried out as described in Section 4. Figure 10 shows an example of the A-weighted interior noise levels for the first three blade passage frequencies and the total noise as a function of the synchrophasing angle. The levels are average values of all 180 measurement positions in the cabin of the ATC. It can clearly be seen that synchrophasing leads to a significant total noise reduction of about 4 dB(A). This total noise reduction is dominated by the the interior noise field at the first BPF. Similar as the total noise, the noise at the first BPF shows a maximum at 10° and a minimum at 40°. The noise at the second BPF shows two maxima at 10° and 40° and two minima at 0° and 30°. Also for this BPF a difference between maximum and minimum of 4 dB(A) occured. Because the levels for the second BPF are much lower than those of the first the minimum of the total noise at 0° is not affected. For the third BPF nearly no influence due to synchrophasing can be observed. An explanation for the overall noise reduction may be found in the above mentioned reduction of the vibrational deflection due to synchrophasing. In addition, the coupling between structure and cavity may reduce due to the rotation of the deflection shape.

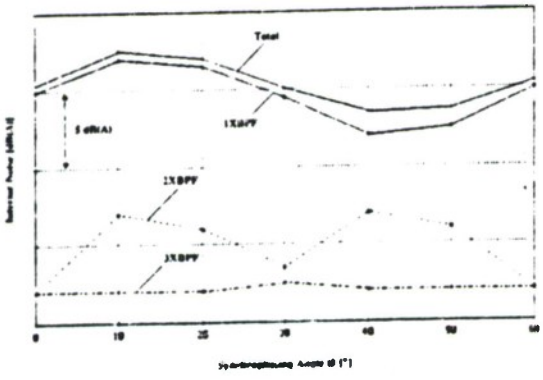

Figure 10: Total averaged interior noise levels for simulated propeller (1050 RPM)

The noise distribution in the cabin with and without synchrophasing is given in Figure 11. This figure represents the noise levels at 12 axial positions averaged at each axial position over three microphones in a typical passenger ear height. It can be seen that the noise reduction due to synchrophasing is effective over the whole cabin length.

For a simulated propeller noise excitation with 1100 PPM the results are given in Figure 12. Also for this excitation the synchrophasing angle has a great influence and leads to a noise reduction of 4 dB(A). The maximum and minimum can be found at 20° and 50°, respectively. Similar as for 1050 RPM this behaviour is mainly caused by the

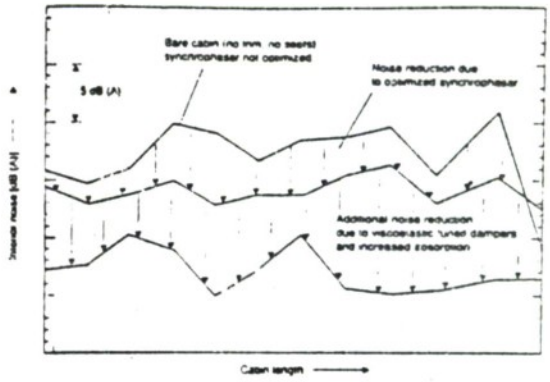

Figure 11: Interior noise distributions averaged at the passenger ear positions for simulated propeller noise (1050 RPM)

first BPF, which had a maximum at 20° and a minimum at 50°. However the interior levels for the second and third BPF are much closer to the levels of the first BPF than for 1050 RPM. The levels for the third BPF are even higher than those for the second BPF. This is caused first by the higher levels at higher harmonics for the 1100 RPM excitation and secondly by a worse noise reduction at these higher harmonics than for the first BPF. The interior levels for the second BPF show similar as for 1050 RPM two maxima and two minima but at the minimum for the first BPF also a minimum for the second BPF occurs. The third BPF is nearly not influenced by synchrophasing.

During the preparation of this this paper a first in-flight spot-test on the Dornier 328 could be performed. At this test the exterior noise on the fuselage was measured at the two points with minimum propeller tip clearance. In addition, the interior noise in the propeller plane at the positions of the outer seats were recorded. A first evaluation showed good agreement of the noise reductions of the Dornier 328 and the ATC.

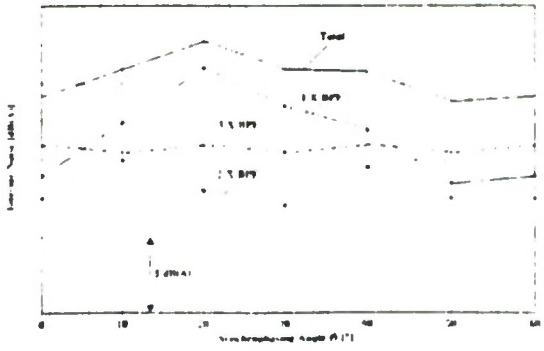

Figure 12: Total averaged interior noise levels for simulated propeller noise (1100 RPM)

6. NOISE AND VIBRATION MEASUREMENTS ON THE ATC EQUIPED WITH DYNAMIC VIBRATION ABSORBERS

As noted in Chapter 5.1, for the Dornier 328 two RPMs are defined: 1050 RPM for cruise and 1100 RPM for climb. Therefore special dynamic vibration absorbers (DVAs) had to be developed which are effective on both RPMs. This behaviour can be achieved with two types of these new absorbers: broadband viscoelastic tuned dampers and double tuned narrow band vibration absorbers.

For the first one, the spring part consists of a special rubber piece with damping just sufficient to obtain a bandwith covering both frequencies. This kind of dampers had been developed together with Anatrol GmbH. The second type is based on a flight-proven single frequency design provided by Fokker. The related new establisned damper type has two dicrete peeks at the required frequencies.

The ATC investigations had been carried out with both types of these dynamic vibration absorbers.

6.1 Vibration Measurements

These vibration measurements were performed with viscoelastic tuned dampers attached to the frames. For the initial damper arrangement a symmetric positioning of 8 damper pairs around the frames was chosen. More dampers than antinodes were used to avoid that the structure finds nodes at the damper locations. Eight frames were treated with the same damper positioning. Figure 13 shows for this example the comparison of operational deflection modes at 1050 RPM with and without dampers. It can clearly be seen that the dampers cause a strong reduction of the deflections. Only on the right side of the fuselage some minor vibretions are remaining.

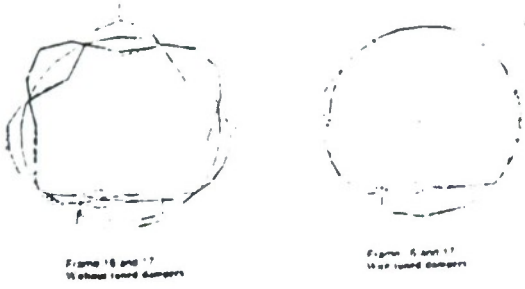

Figure 13: Operational deflection shapes for simulated propeller noise (1050 RPM)

6.2 Interior Noise

The effect of the viscoelastic tuned dampers in the above mentioned initial arrangement on the interior noise in the ATC for 1050 RPM is given in Figure 11. Significant noise reductions up to 8 db(A) are obtained over the whole cabin length in the ear positions of the passengers in addition to the synchrophasing effect. Additional 2 dB(A) could be gained by attaching 120 mm foam to the aft wooden end plate of the ATC as indicated in Figure 11.

Following these initial investigations, the damper positions and number of dampers per frame were attempted to be optimized. Three further damper arrangements have been tested. The first one consists of 5 pairs of tuned dampers per frame with a symmetric distribution at 9 frames. The result can be seen in Figure 14 where the interior noise levels in dB(A) averaged over all messurement positions is shown as a function of the synchrophasing angle. For most synchrophasing angles also this first new configuration leads to lower interior noise levels than without tuned dampers but the levels are up to 4 dB(A) higher than the levels for the initial configuration, depending on the synchrophasing angle.

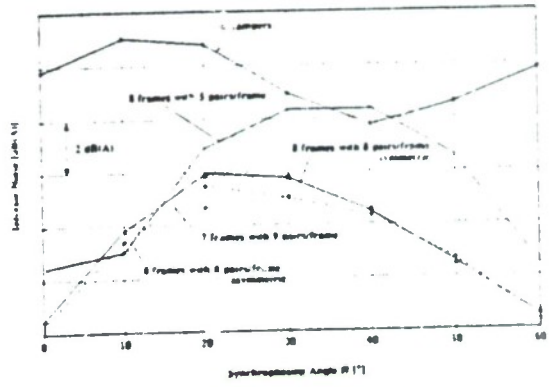

Figure 14: Total averaged interior noise levels for simulated propeller noise (1050 RPM)

The second new damper arrangement included 8 pairs of tuned dampers per frame mounted to eight frames with an asymmetric distribution including four dampers on the left side, one in the center, and three on the right side. This arrangement was wae born out of the operational deflection shape given in Figure 13, where the biggest remaining vibrations after attaching the initial tuned damper configuration could be observed on the left side. This new asymmetric configuration shows a further improvement against the initial configuration.

For the tested third new damper arrangement nine pairs of dampers per frame were mounted at seven frames. This configuration gave no further improvement and was slightly worse than the second new arrangement.

In Figure 14 it also can be seen that the optimum sychrophasing angle for all considered four arrangements has been shifted to 0°.

The averaged spectral total noise reduction of the whole cabin due to the tuned dampers in the favourable second new arrangement for 1050 RPM is given in Figure 15. The measured reduction values are about 8 dB(A) for the first, 9 dB(A) for the second and 3 dB(A) for the third BPF. The high reduction at the second BPF is strongly due to the changing of synchrophasing angle from the optimal 40° for the untreated ATC to the optimal 0° for the ATC equiped with tuned dampers. As can be seen in Figure 10 the second BPF of the untreated ATC has a maximum at 40° and a minimum at 0° with a level difference of about 5 dB(A). Therefore, the efficiency of the tuned dampers at the second BPF is 4 dB(A). The 3 dB(A) reduction for the third tone may be explained by a pure mass effect.

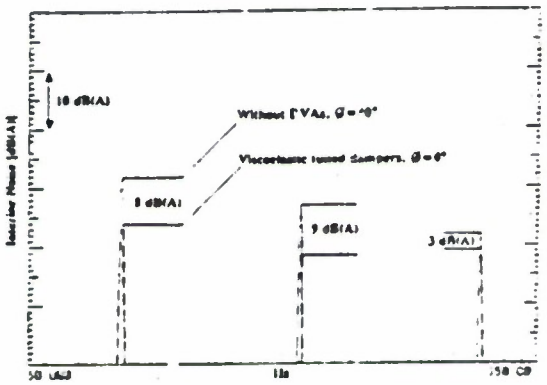

Figure 15: Total averaged interior noise spectra for simulated propeller noise (1050 RPM)

The length distributions of the A-weighted interior noise for the four investigated tuned damper arrangements for a simulated propeller noise with 1050 RPM are given in Figure 16. This figure shows again and more significant that the asymmetric damper distribution with 6 dampers per frame at 8 frames (second new arrangement) leads to the lowest interior noise levels.

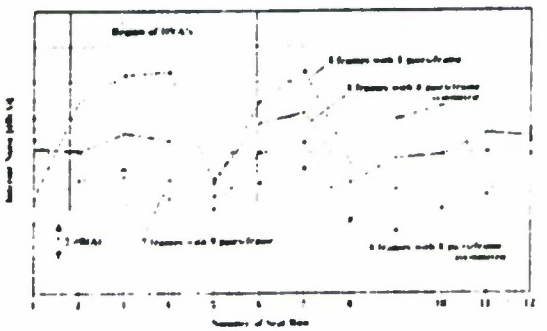

Figure 16: Interior noise distributions averaged at the passenger ear positions for simulated propeller noise (1050 RPM)

At the positions of the favourable second new arrangement also double tuned narrow band vibration absorbers have been attached followed by corresponding measurements. The obtained result is shown in Figure 17 in form of averaged interior noise axial distributions for the plane of the passenger heads compared to the favourable result for the viscoelastic tuned dampers. The use

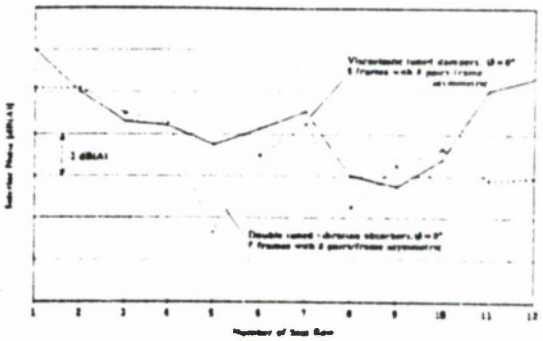

Figure 17: Interior noise distributions averaged at the passenger ear positions for simulated propeller noise (1050 RPM)

of the double tuned vibration absorbers leads in the position of seat rows 1, 5, 8, 11 and 12 to improvements up to 4 dB(A). For the other seat rows the levels remain nearly constant. This very good result is related with an average total cabin noise reduction of about 11 dB(A) for the fundamental tone, see Figure 18. For the second tone a noise reduction of 6 dB(A) can be observed of which 1 dB is due to the absorbers according to explanation given above. The 3 db(A) reduction for the third tone may be also here explained as a pure mass effect.

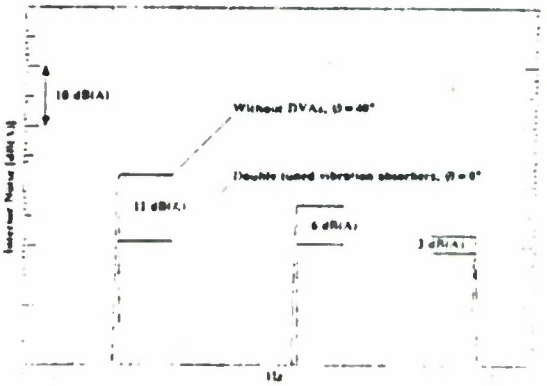

Figure 18: Total averaged interior noise spectra for simulated propeller noise (1050 RPM)

For 1100 RPM also damper tests have been performed. In general it can be stated that for this RPM the noise reduction due to the dynamic vibration absorbers is lower than for 1050 RPM. A related example is given in Figure 19, which shows the comparison between A-weighted interior noise levels as

a function of synchrophasing angle without and with viscoelastic tuned dampers in the favourable arrangement described above. Here the difference between the interior noise without dampers at optimum synchro-

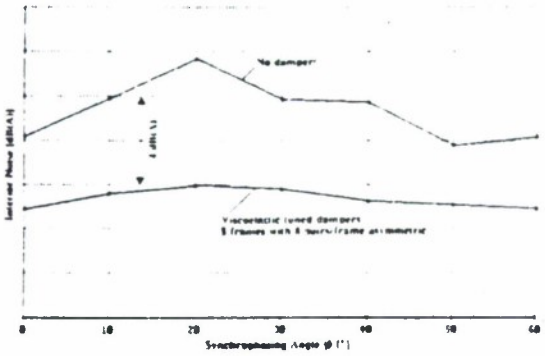

Figure 19: Interior noise distributions averaged at the passenger ear positions for simulated propeller noise (1050 RPM)

phaser angle and the interior noise with dampers at optimum synchrophasing angle is only about 3 dB(A). Figure 20 shows the spectral comparison for the same cases as in Figure 19. The interior noise is reduced by about 4 dB(A) on the first BPF, about 3 db(A) on the second BPF and about 3.5 dB(A) on the third BPF. Nevertheless, this result corresponds also to an interesting noise reduction in the cabin.

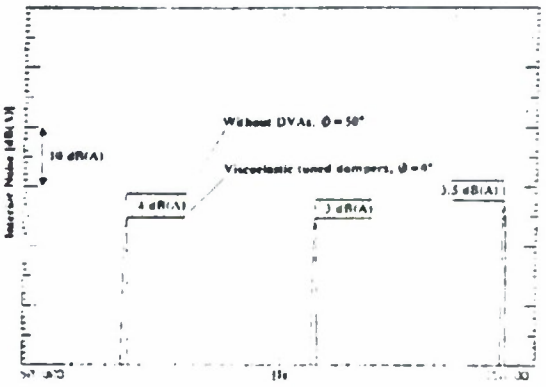

Figure 20: Total averaged interior noise spectra for simulated propeller noise (1100 RPM)

7. SUMMARY

In order to study and identfiy effective interior noise control measures for the Dornier 328 with limited impact on project flight schedule an acoustic test cell (ATC) of the Dornier 328 has been build. The ATC consists of a fuselage section with full cabin length, a realistic fuselage suspension and three exterior noise simulation rings equiped with 60 loudspeakers. The signals for the speakers have been provided by a complex 60 channel computer/amplifier noise generation system. With this system it was possible to simulate propeller noise excitation at 60 points on the fuselage skin including realistic phase distribution.

Prior to the acoustic measurements vibration measurements had been carried out for data interpretation. These measurements without noise control treatment showed eigenmodes at 95.7 Hz and 116 Hz near the two excitation fundamental tones of 105 Hz and 110 Hz,respectively, of the considered two different propeller noise spectra. For simulated propeller noise excitation at 1050 RPM and 1100 RPM the deflection shapes looked very similar to the eigenmode at 95.7 Hz. Simulated synchrophasing yielded a rotation of the deflection shape and a reduction of the deflection amplitudes.

The noise measurements showed a great effect of synchrophasing on the interior noise levels. About 4 dB(A) difference of total averaged interior noise of the whole cabin between worst and best synchrophasing angle have been measured for 1050 RPM and 1100 RPM with best synchrophasing angles at 40° and 50°, respectively. In both cases this effect is dominated by the noise at the first BPF. The noise improvement may be explained by the reduced vibration amplitudes in connection with a reduced coupling of structure and cavity, due to rotation of the operational vibration shapes.

Attaching viscoelastic dampers to eight frames of the ATC led a significant reduction of the vibration amplitudes. The following noise measurements showed promising noise reductions in the whole cabin. Improvements at the plane of the passenger heads up to about 8 db (A) have been measured. Also for these measurements an influence of synchrophasing angle could be observed shifting the optimal angle to 0° for both RPMs. An attempt to optimize the number and positioning of the viscoelastic dampers yielded further improvements to the interior noise, especially with respect to a uniform noise distribution in the cabin.

Also double tuned vibration absorbers have been tested in the ATC at the identified most favourable positions. The measurements showed up to 4dB(A) better results at certain axial locations in the cabin than the tests on the viscoelastic tuned dampers.

For 1100 RPM reduced efficiencies of both the viscoelastic tuned dampers and the double tuned vibration absorbers were measured. Nevertheless, still a total noise reduction in the hole cabin of 3 dB(A) could be identifia for the viscoelastic tuned dampers.

REFERENCES

[1] I.U. Borchers, H. J. Hackstein, P. Bartels, M. Grünewald, C. Wenigwieser:
Summary of Dornier 328 Interior Noise Control Study, The 1990 International Conference on Noise Control Engineering, Gothenburg, Sweden,1990

[2] W. Kreder:
Time Domain Movement Analysis (TDMA) Operational Deflection Shapes Computed from Time Histories, Sixt International Modal Analysis Conference, 1988

4th NASA/SAE/DLR Aircraft Interior Noise Workshop
Friedrichshafen, Germany
May 19 - 20, 1992

Inge S. Green
Saab Aircraft AB
Linköping, Sweden

Vibro-acoustic FE analyses of the Saab 2000 Aircraft

- Coupled acoustic/structural aircraft FE-model
- Creation of modal database
- BPF pressure field excitation
- Frequency response analyses
- Model validation analysis
- Planned analyses
- Model development

Vibro-acoustic FE analyses of the Saab 2000 Aircraft

- Coupled acoustic/structural aircraft FE-model
  - Acoustic model
  - Structural model
  - Coupled Acoustic-Structural model
- Creation of modal database
  - Substructuring/Modal synthesis
  - Acoustic eigenmodes
  - Structural eigenmodes
  - Coupled eigenmodes
- BPF pressure field excitation
  - Cruise flight nearfield BPF noise prediction
  - Inclusion of fuselage scattering

- Frequency response analyses
  - Scheme of computation
  - Modal contribution to BPF response
  - Structural response (Operating deflection shape)
  - Cabin cavity response (Pressure field in dB)

- Model validation analysis
  - Experimental modal analysis, Fuselage Test Rig
  - Fuselage Rig shaker test simulation

- Planned analyses
  - Tuned Damper installation and optimization
  - Structure-borne path identification
  - Active Vibration Control analyses

- Model development
  - Fuselage sections with interior
  - Active Noise Control analyses

4th NASA/SAE/DLR Aircraft Interior Noise Workshop
Friedrichshafen, Germany
May 19 - 20, 1992

Inge S. Green
Saab Aircraft AB
Linköping, Sweden

VIBRO-ACOUSTIC FE ANALYSES OF THE SAAB 2000 AIRCRAFT

SUMMARY

FE-models of the Saab 2000 fuselage structure and the interior cavity have been created in order to compute the noise level in the passenger cabin due to propeller noise (page 1).

The FE-system ASKA was used for these analyses. The total number of degrees of freedom (dof) for the models is over 400000. To make the analysis possible substructuring was used in addition to several levels of "midnets" and modal component synthesis. This way the number of dof at each level was reduced to give acceptable computer times (page 2 - 6).

Examples are shown of Acoustic modes (page 7 - 8) and dominant structure modes (page 9 - 10) from the modal database.

BPF pressure field at cruise flight was predicted and applied to the aircraft (page 11 - 12).

Scheme of computations (Normal mode analysis and Frequency response analysis) are outlined in page 13.

From the frequency response analysis, modal contribution (page 14), structural response (page 15) and cabin cavity response (page 16) are shown.

From Fuselage Test Rig modal analysis a first validation of the FE-model is made (page 17).

Validation with the Frequency Response Function method is under way (page 18 - 19).

Planned analyses with the Saab 2000 AFEM model is shown in page 20 and proposed model development in page 21.

SAAB

SAAB 2000 COUPLED STRUCTURE-CAVITY FE MODEL

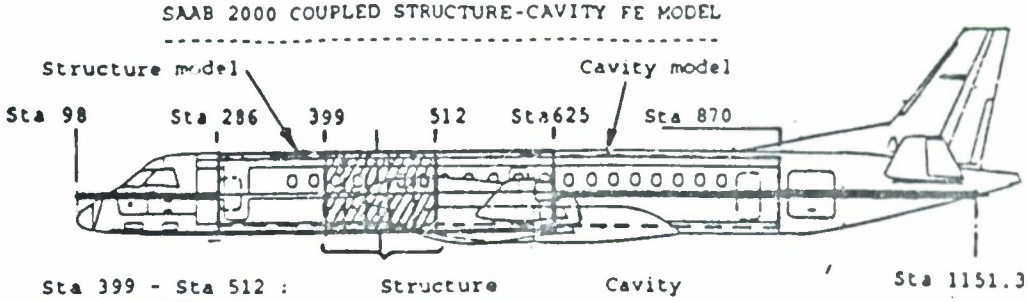

Sta 399 - Sta 512 :	Structure Main Net 290	Cavity
Number of Nodal points :	22681	62118
Number of Elements :	10153	3599
Number of Substructures:	10	10

Database from
Eigenvalue analysis :720 eigenvalues (11.2-342.5 Hz)

Structure Subnets

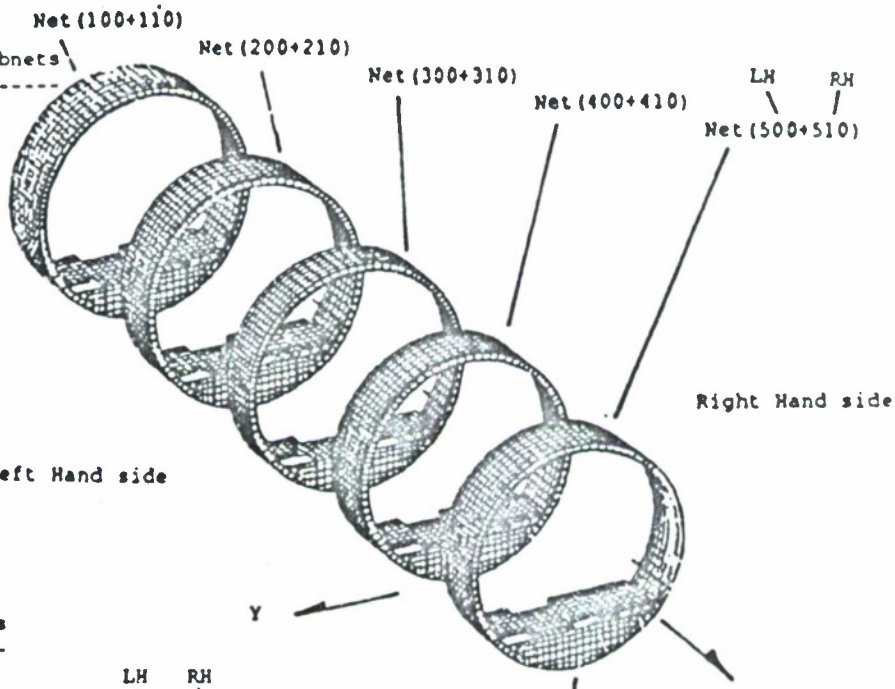

Acoustic Nets

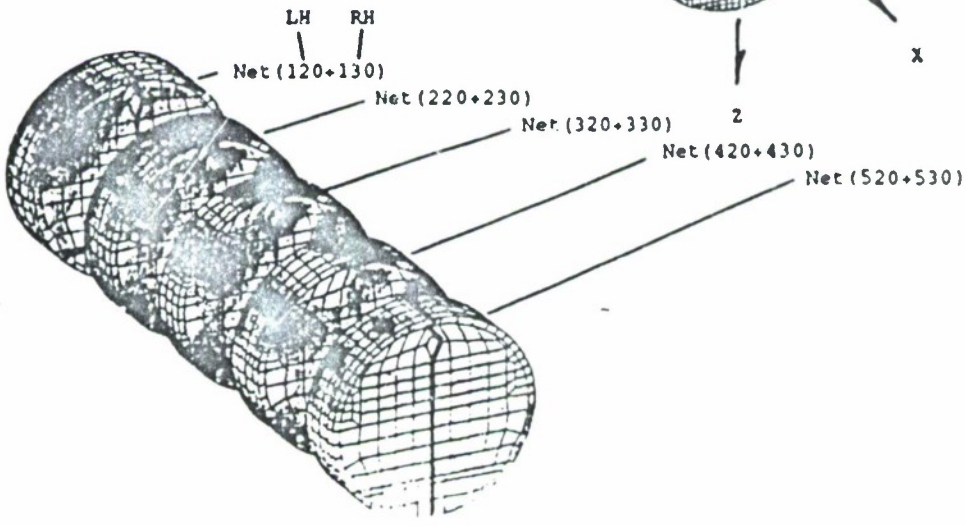

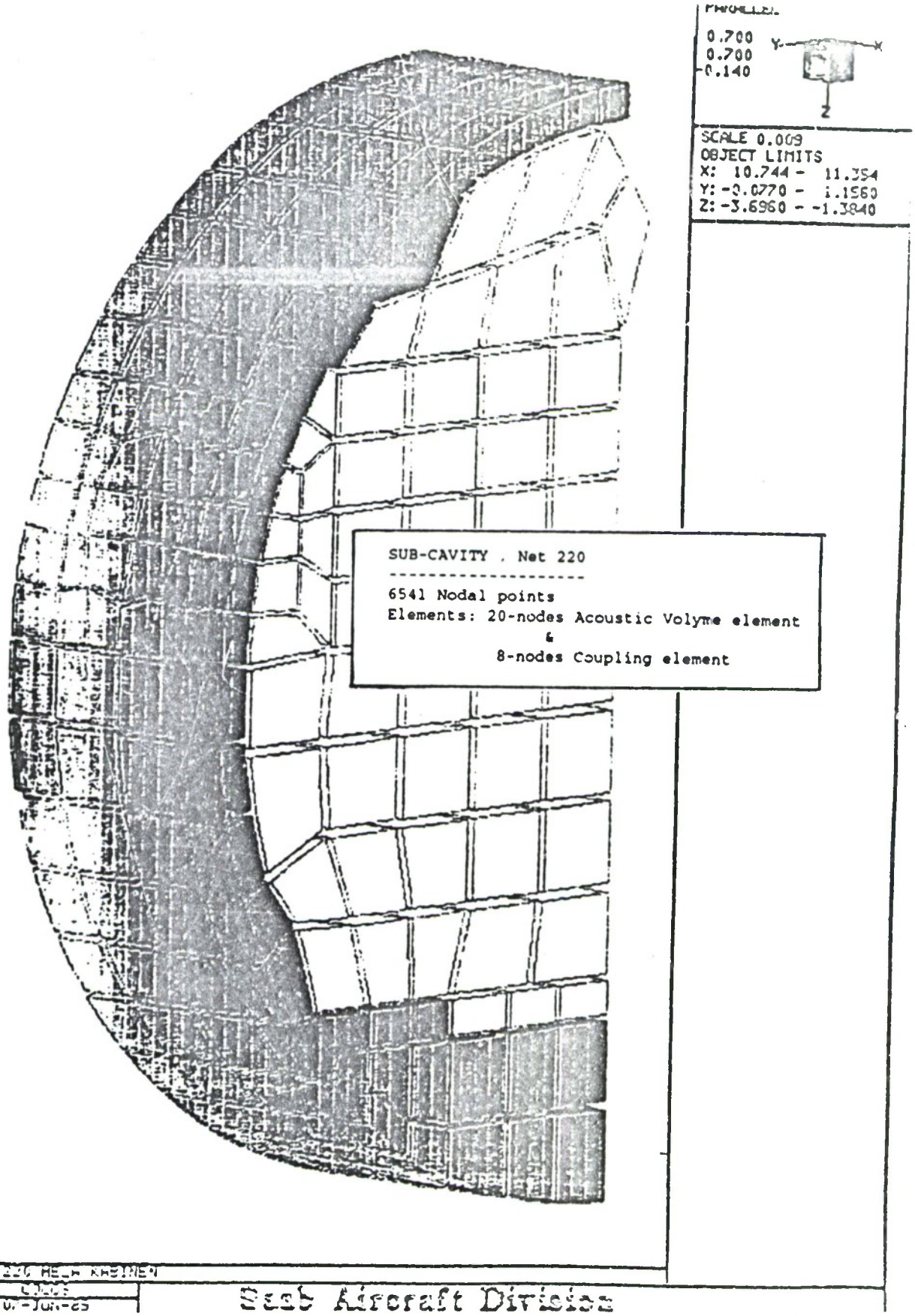
0.700
0.700
0.140
Y
Z
SCALE 0.009
OBJECT LIMITS
X: 10.744 - 11.354
Y: -0.0770 - 1.1560
Z: -3.6960 - -1.3840
SUB-CAVITY . Net 220
6541 Nodal points
Elements: 20-nodes Acoustic Volyme element
&
8-nodes Coupling element
Saab Aircraft Division

SAAB

ACOUSTIC MODEL

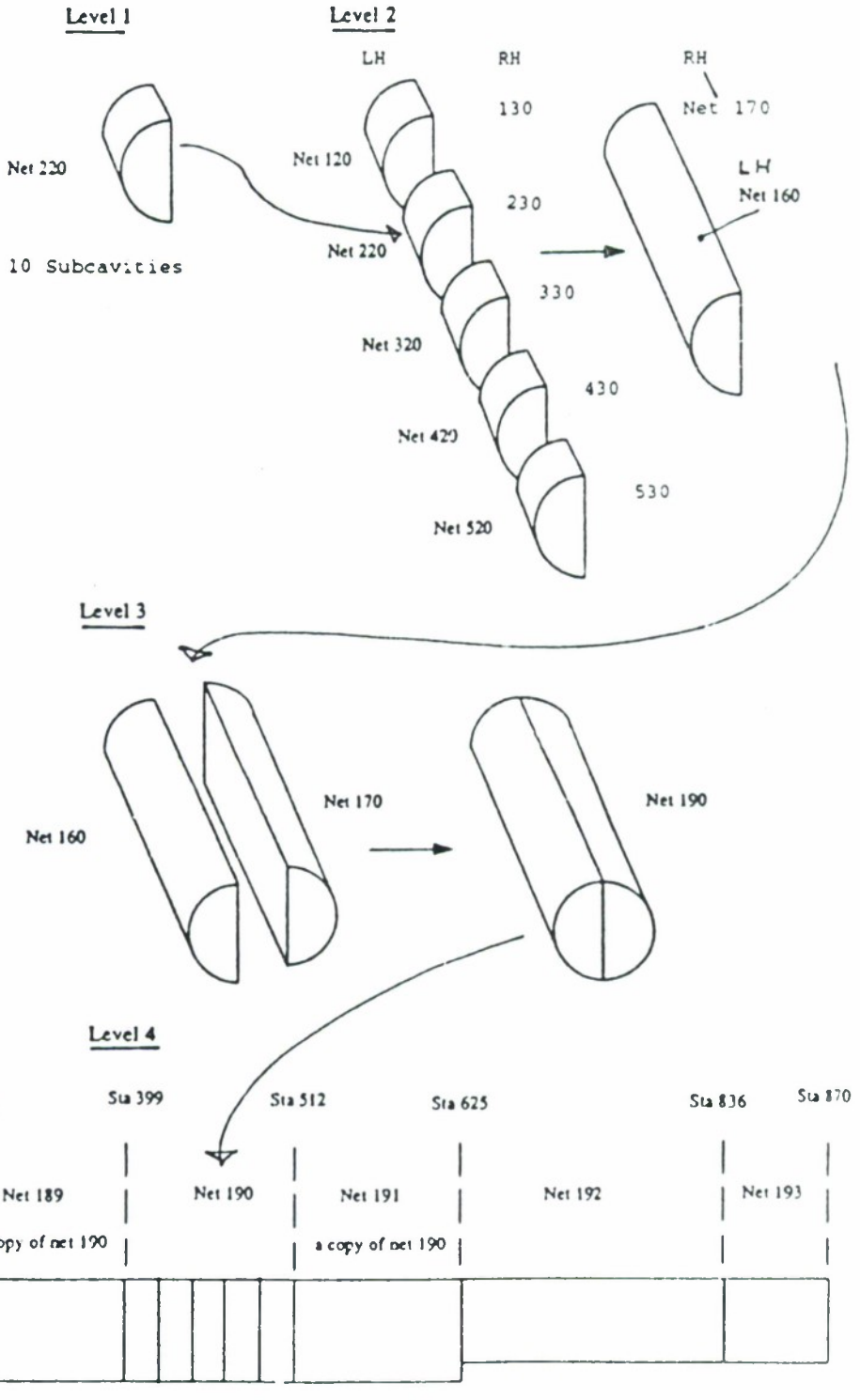

Main net 200

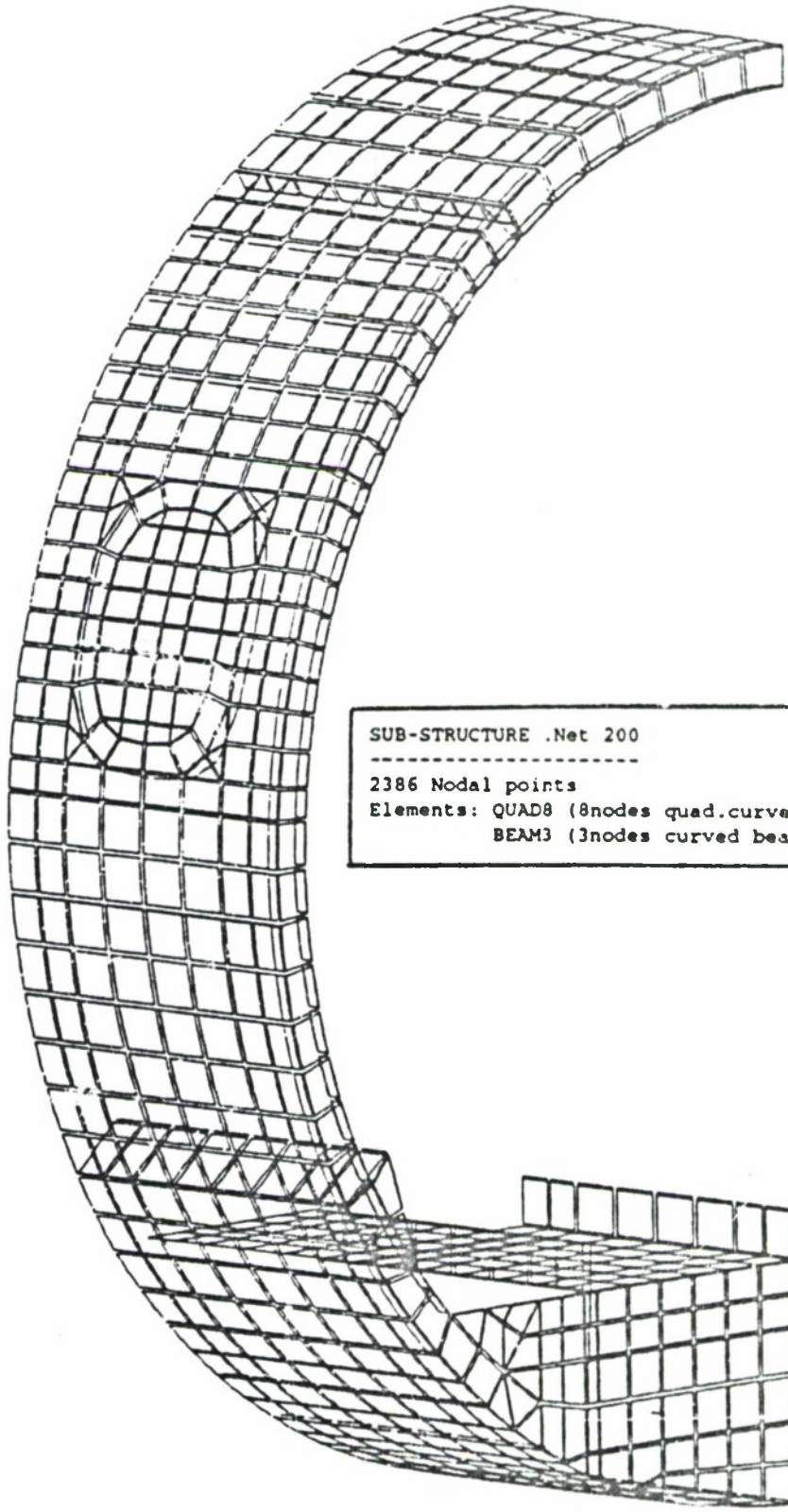
SUB-STRUCTURE .Net 200
2386 Nodal points
Elements: QUAD8 (8nodes quad.curved shell)
BEAM3 (3nodes curved beam)
OBJECT LIMITS
X: 10.7440
11.3690
Y: 0.000000
1.19400
Z: -3.49500
-1.36400
SCALE 1:36.3*3

SAAB

STRUCTURAL MODEL

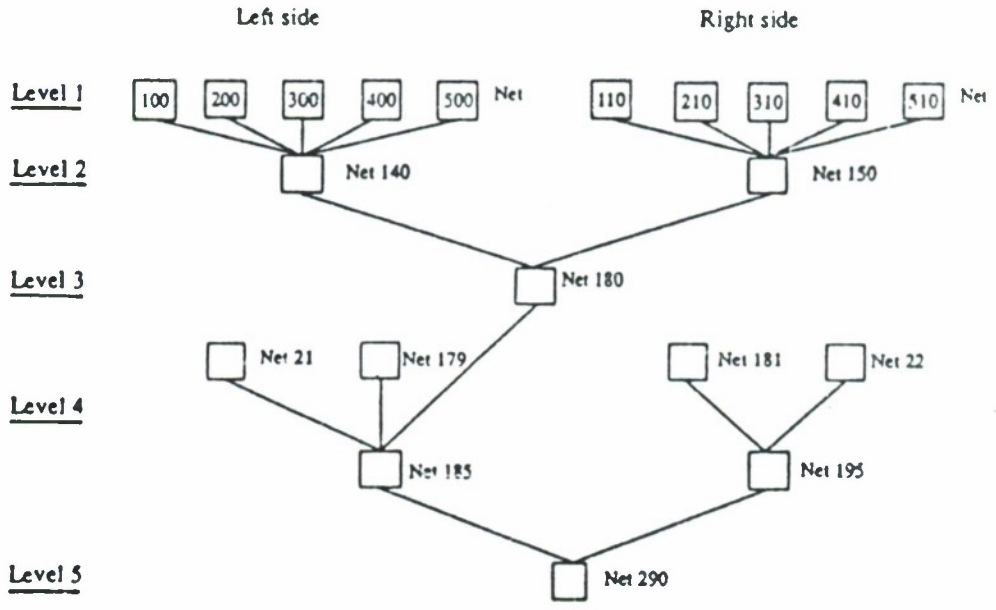

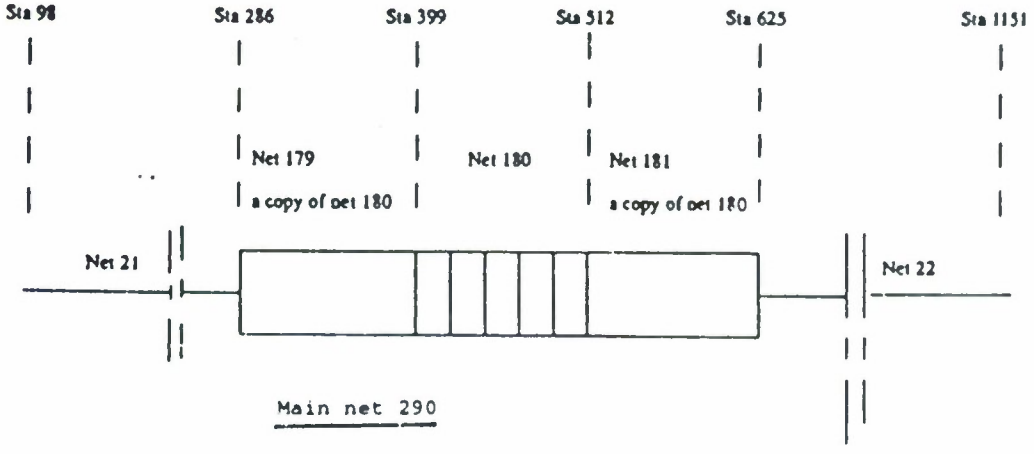

COUPLED ACOUSTIC-STRUCTURAL MODEL

Coupling only for the master sections Sta 399 - Sta 512 :

Acoustic net 190 + Structure net 180

With rest of the models Main nets 300 and 290 uncoupled.

SAAB

2000 ASEM.
CREATION OF THE COUPLED ACOUSTIC-STRUCTURAL MODAL DATABASE.

ASKA analyses on CRAY X-MP/416

Total number of DOF's for the models : > 400000

Analyses performed with substructuring (Sub-,Mid-and Main nets) and modal component synthesis for reduction of the number of DOF's at each level.

- ACOUSTIC MODEL (Master section Sta 399-Sta 512)

LEVEL	TOTAL NUMBER UNCONSTRAINED DOF	TOTAL NUMBER NORMAL MODES	TOTAL CPU-TIME IN CRAY (SEC)
1	30300	268	8000
2	3200	284	5700
3	2100	295	7800
4	4000	596	10500

- STRUCTURAL MODEL (Master section Sta 399-Sta 512)

LEVEL	TOTAL NUMBER UNCONSTRAINED DOF	TOTAL NUMBER NORMAL MODES	TOTAL CPU-TIME IN CRAY (SECS)
1	117000	913	44000
2	6860	776	22800
3	2610	728	16000
4	3524	1029	3700
5	2025	720	7250

- COUPLED ACOUSTIC-STRUCTURAL MODEL (Master sections)

Number of Acoustic normal modes: 596 (10.9 - 400 Hz)
Number of Structural normal modes: 720 (11.2 - 342 Hz)
After the coupled analysis,
Number of coupled normal modes: 700 (9.6 - 288 Hz)

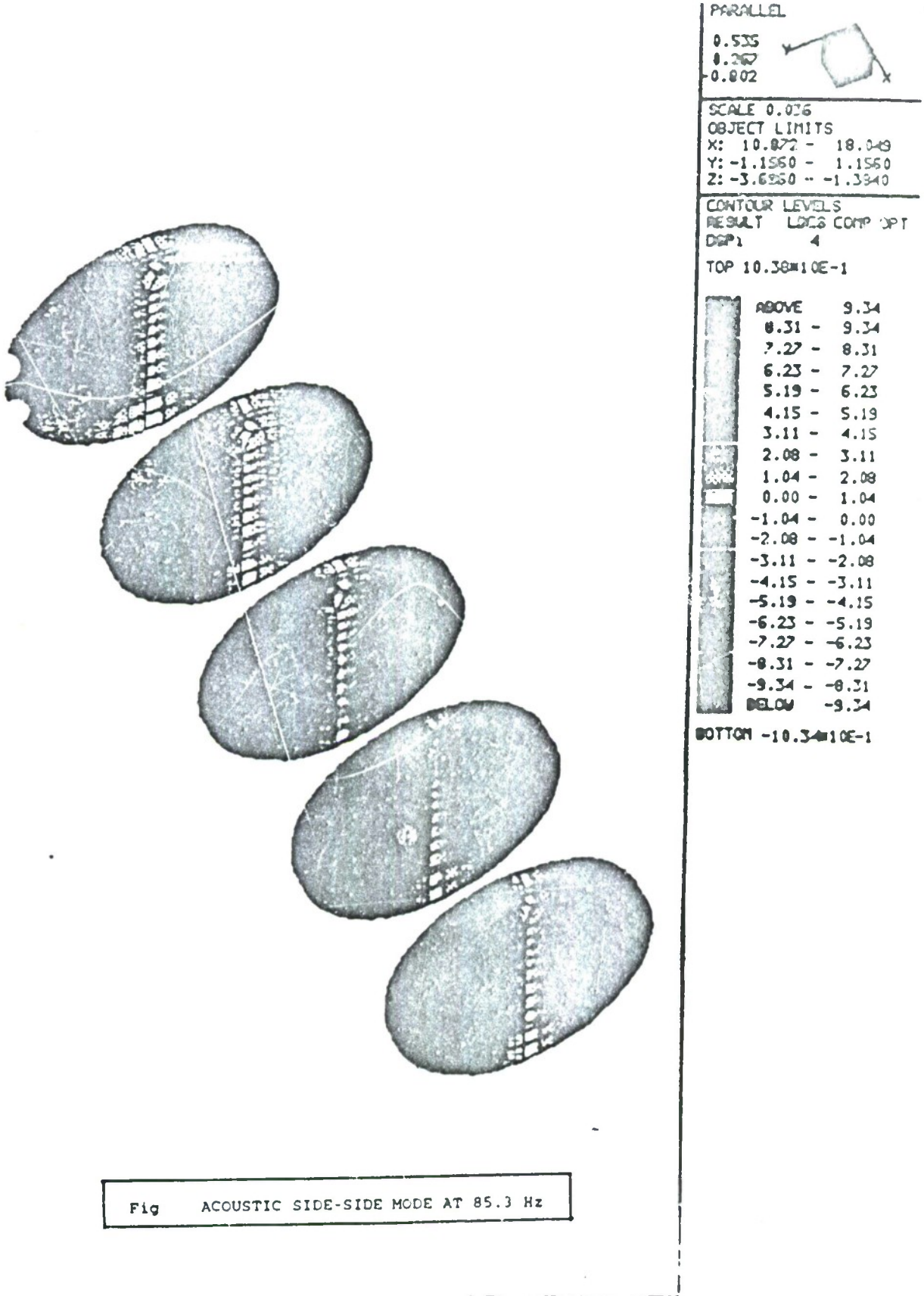

Fig ACOUSTIC SIDE-SIDE MODE AT 85.3 Hz

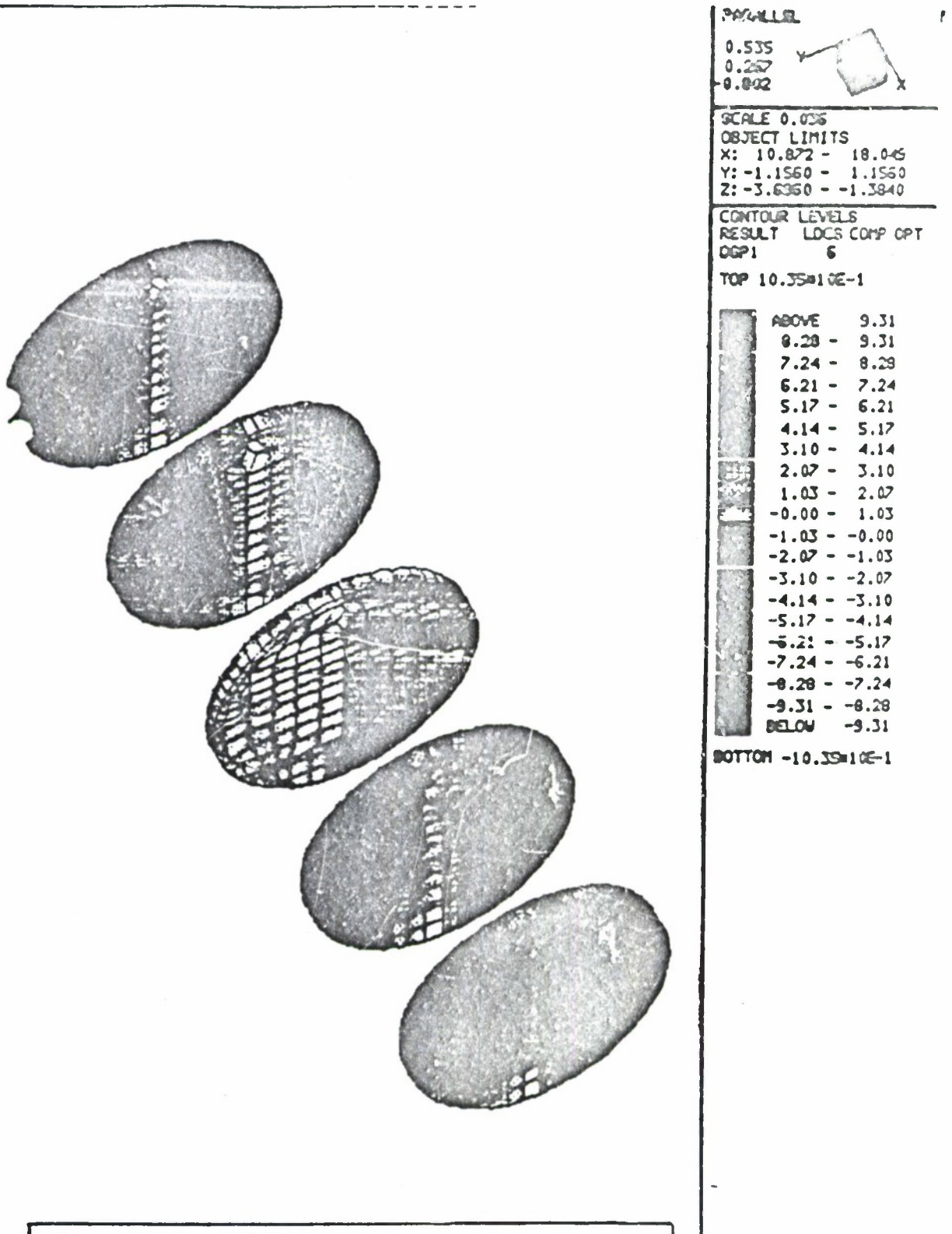

Fig ACOUSTIC SIDE-SIDE MODE with LH/RH shift AT 101.6 Hz

SAAB-SCANIA

Cross-sectional mode shapes (Frames).

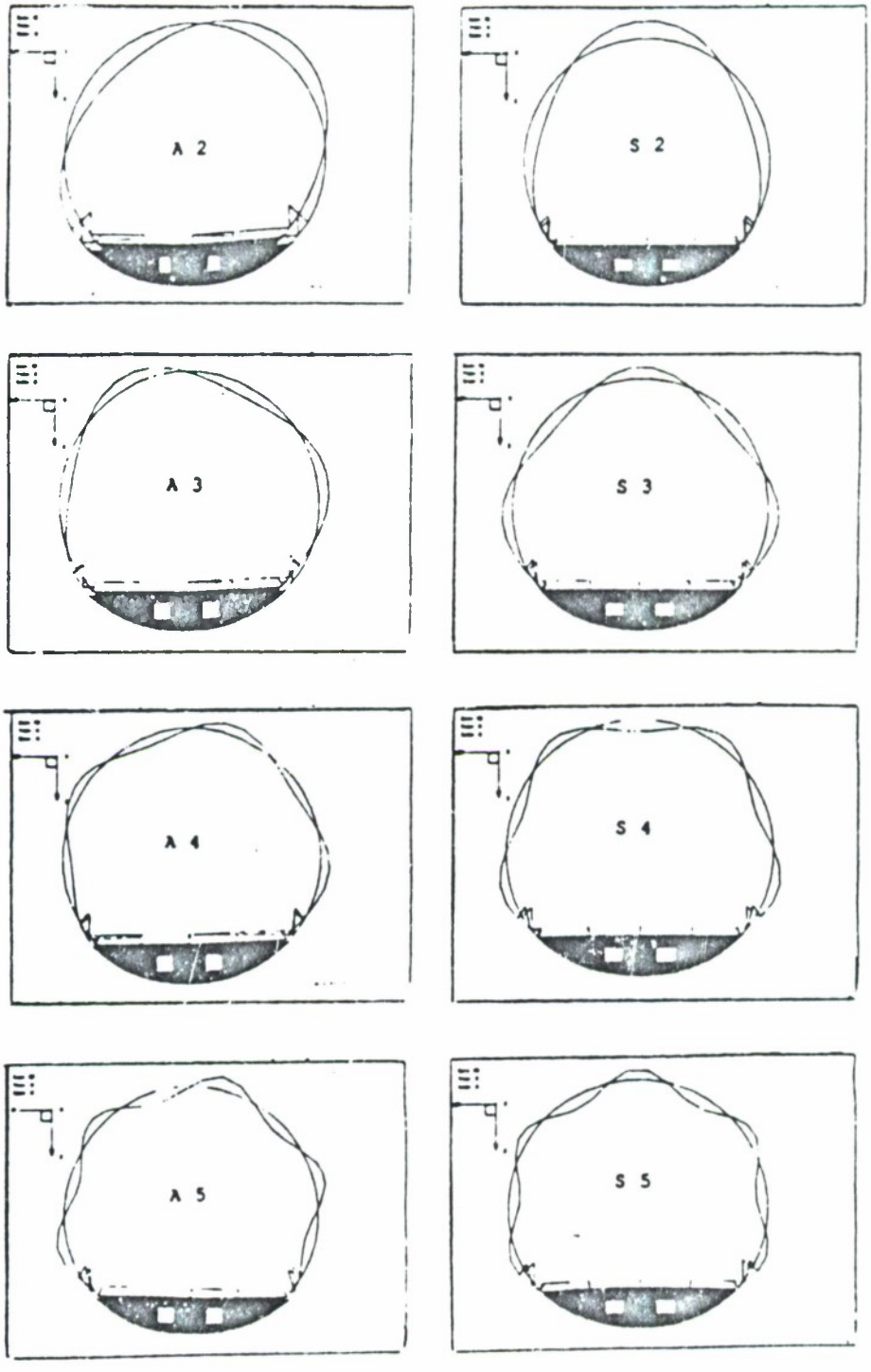

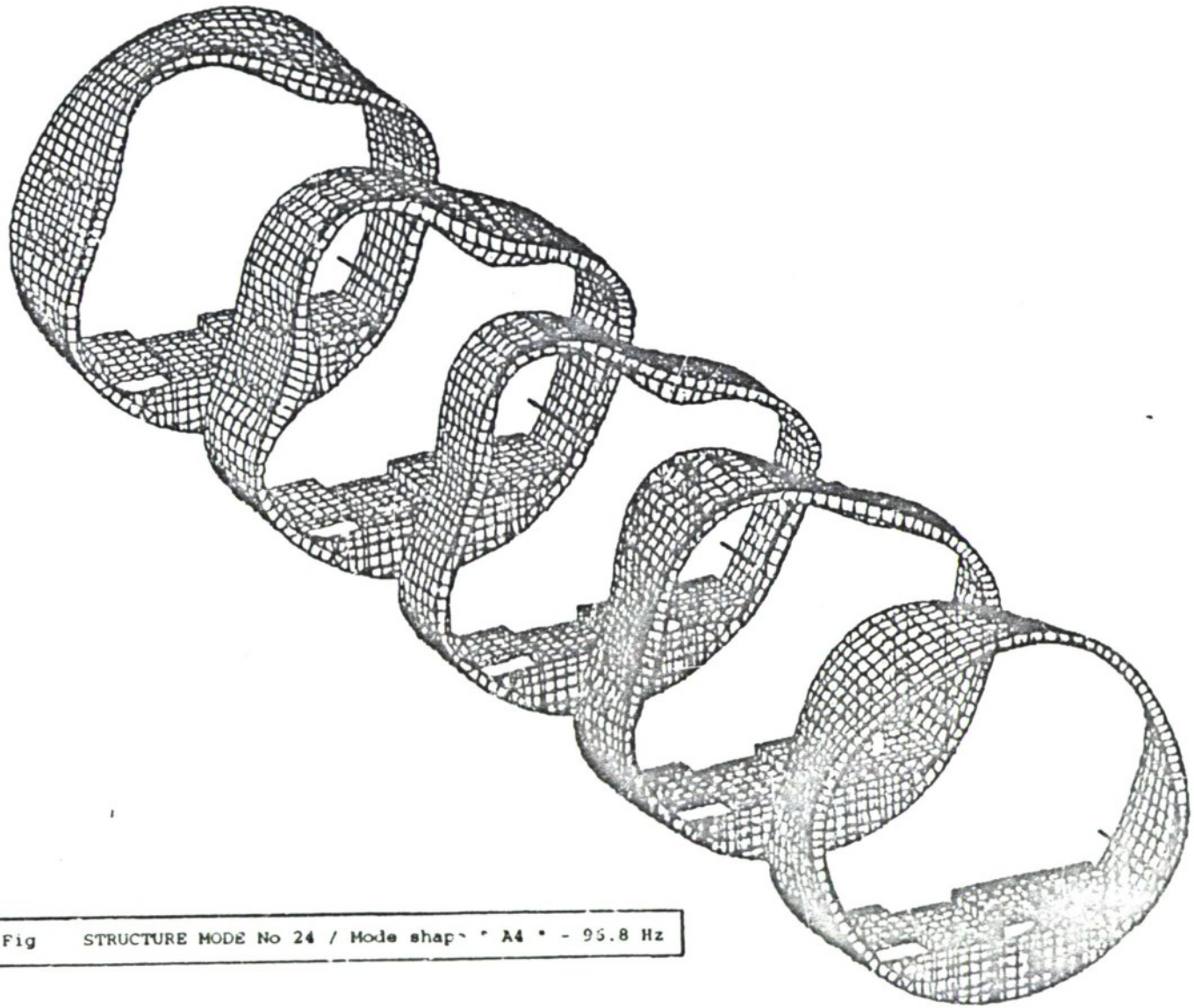

Fig STRUCTURE MODE No 24 / Mode shap* * A4 * - 95.8 Hz

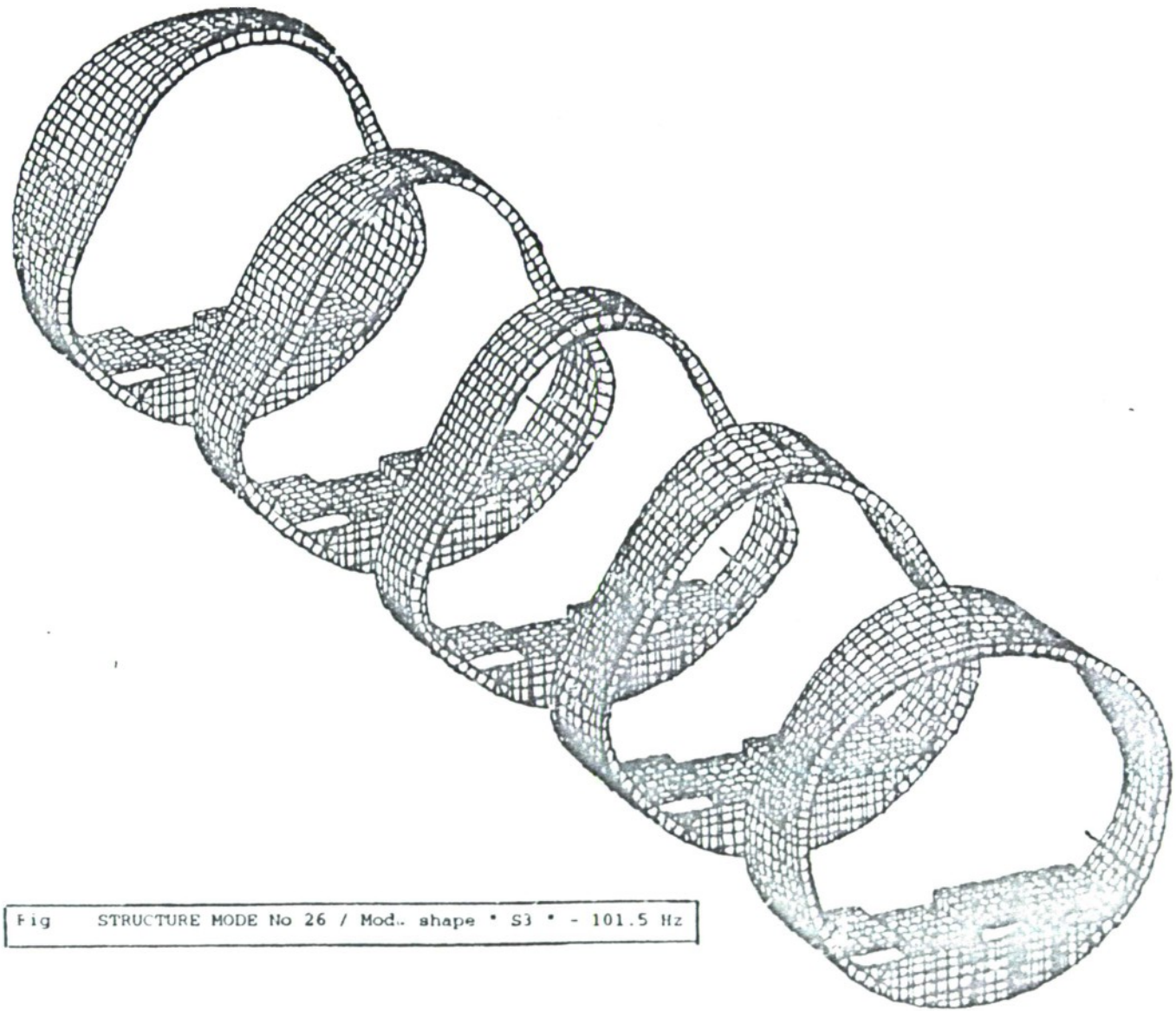

Fig STRUCTURE MODE No 26 / Mod. shape * S3 * - 101.5 Hz

- BPF pressure field excitation
  - Cruise flight nearfield BPF noise prediction
  - Inclusion of fuselage scattering
- Propeller free field prediction program NOISEGEN developed at FFA.
- Program code based on a linearized version of Ffows-Williams-Howkings equation.
- Fuselage scattering and boundary layer effects added.
- Complex pressures converted to Real and Imaginary. pressure fields (Load data).
- Load data applied to Structure Subnets.

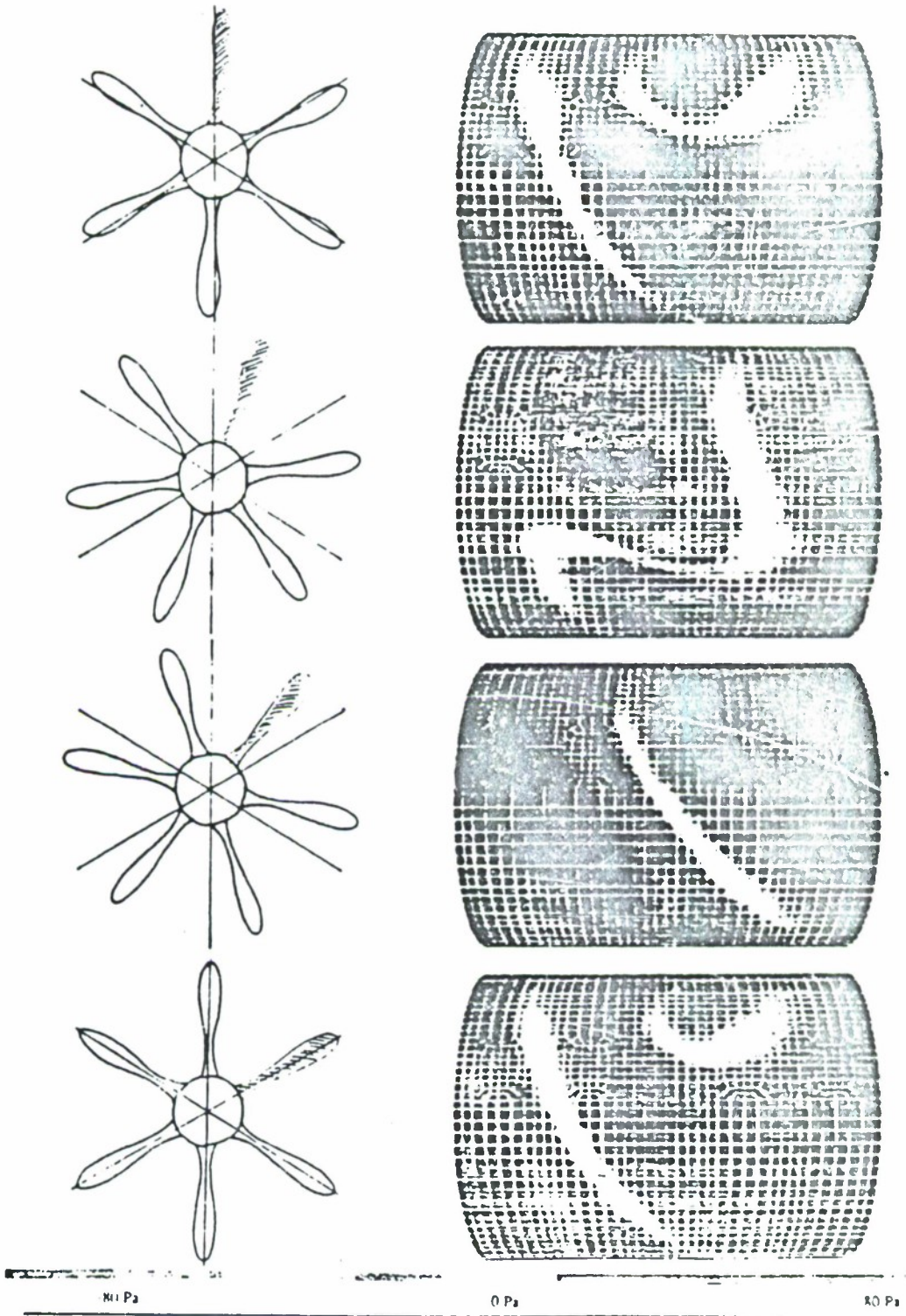

Figure Predicted pressure field on the lefthand side of the Saab 2000 at different time steps

SAAB

- Scheme of computation

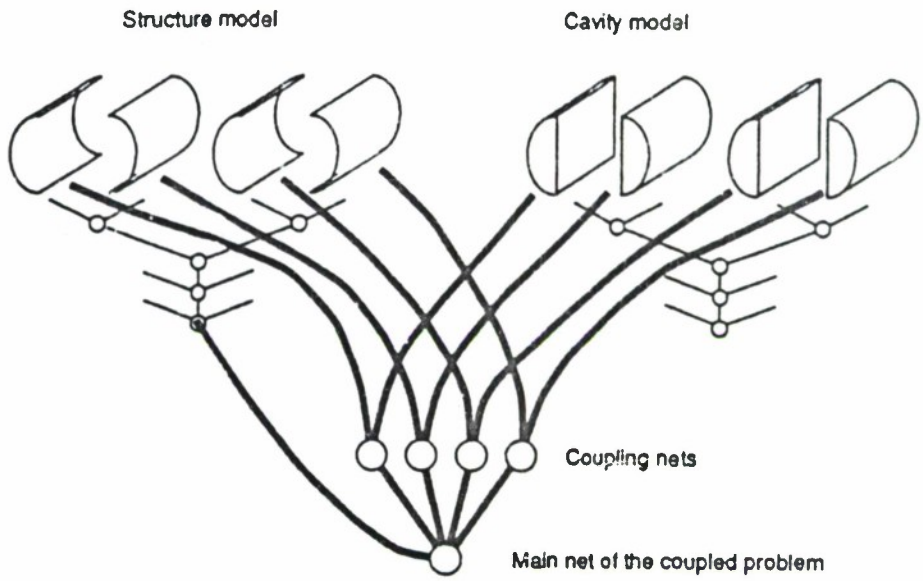

Figure . Natural mode flow of computation

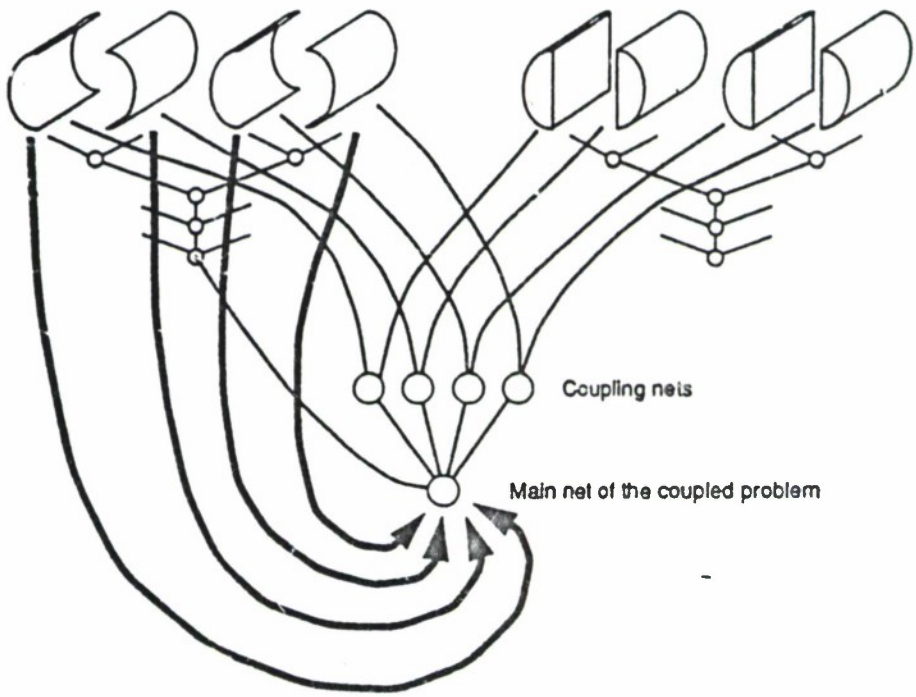

Figure . Frequency response flow of computation

Fig - MODAL CONTRIBUTION TO BPF RESPONSE

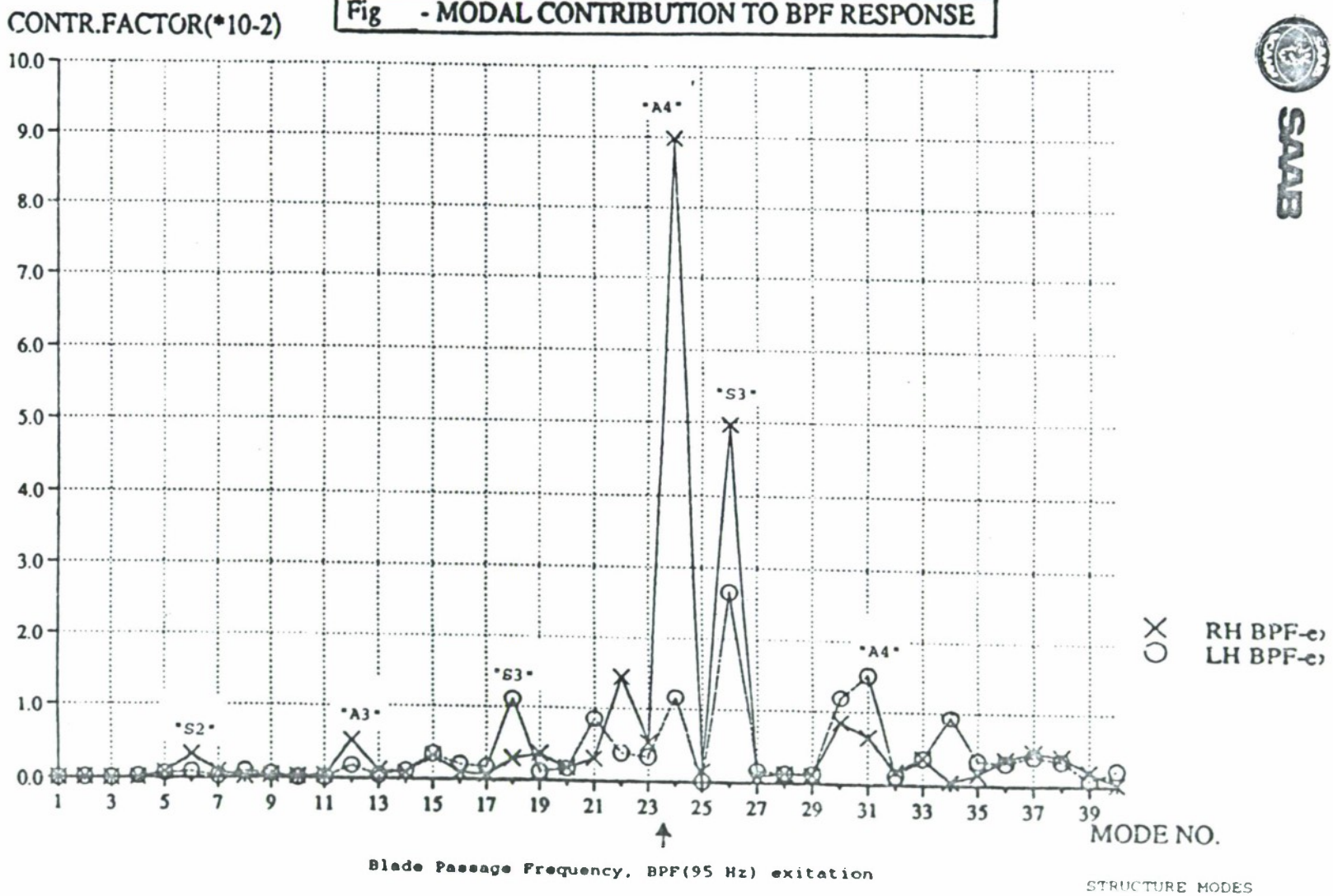

SAAB

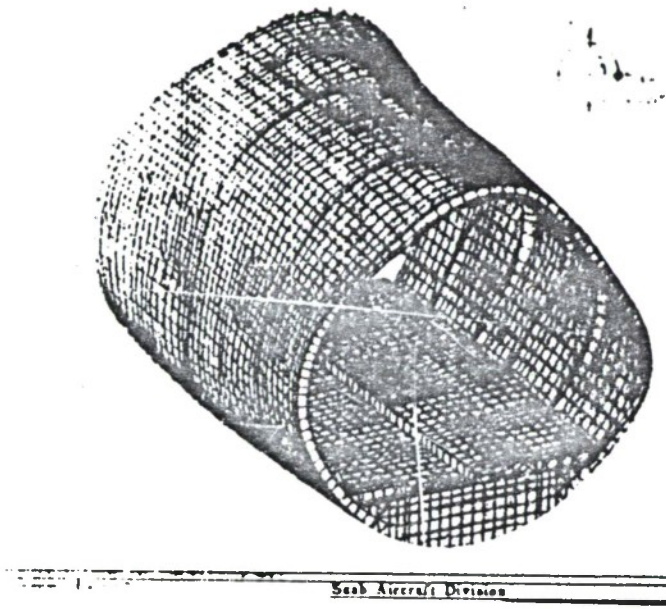

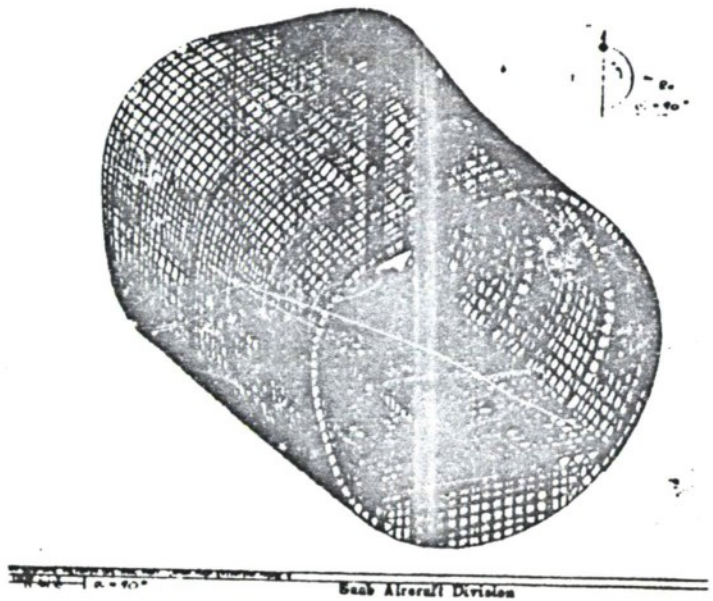

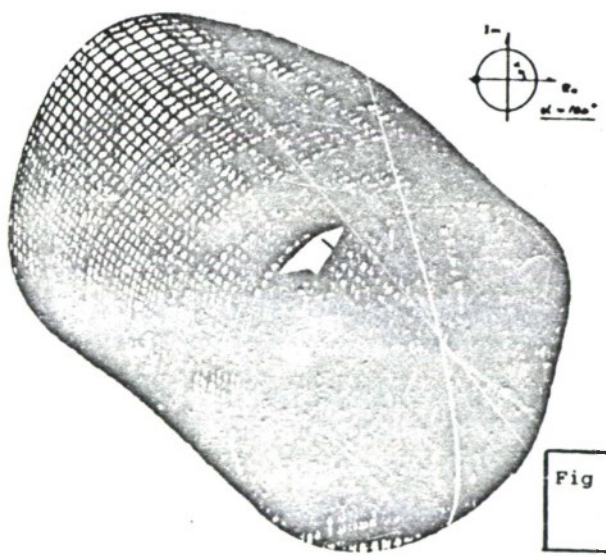

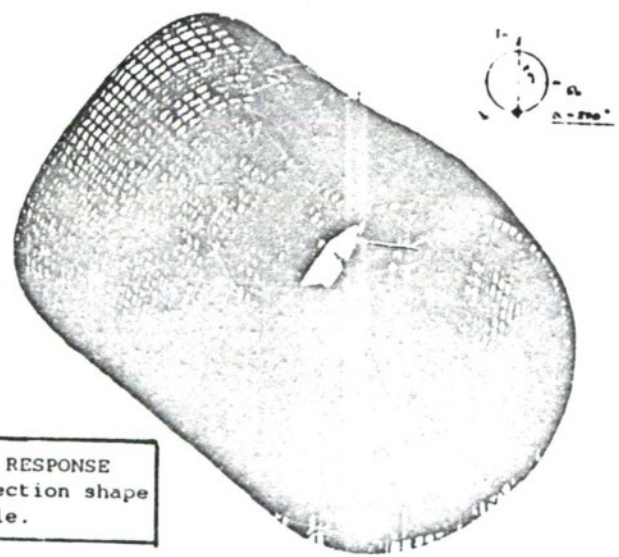

Fig STRUCTURAL BPF RESPONSE
Operating deflection shape during one cycle.

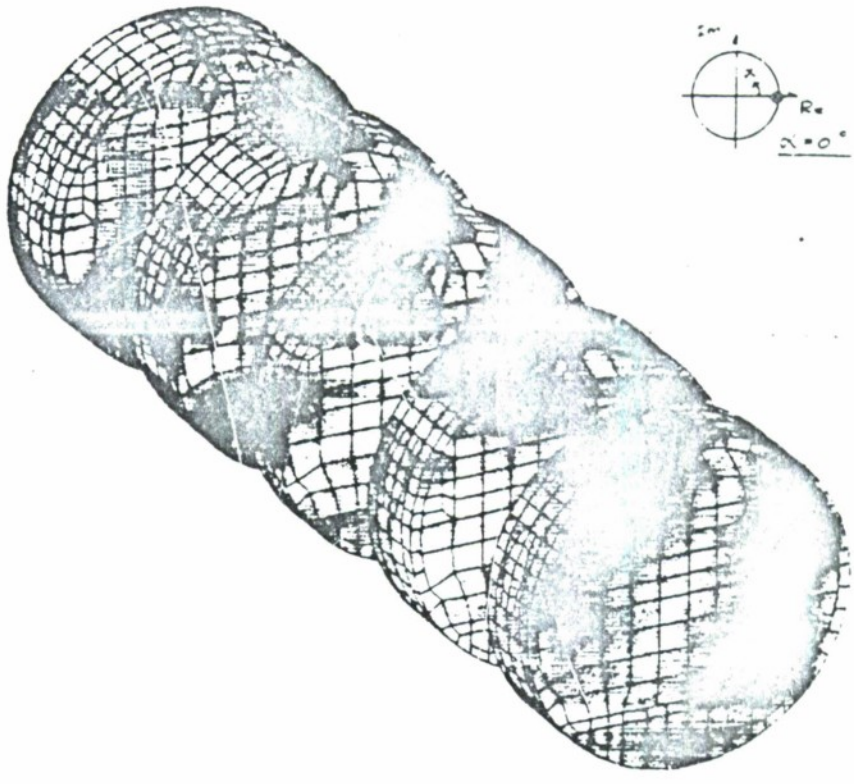

α = 0°

Saab Aircraft Division

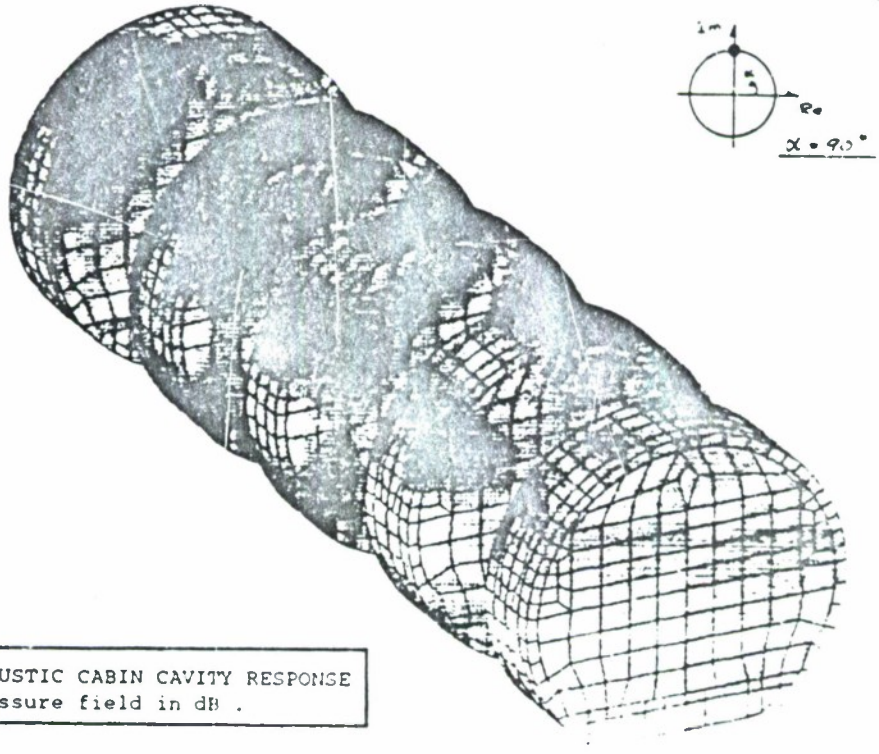

Fig ACOUSTIC CABIN CAVITY RESPONSE
Pressure field in dB .

Saab Aircraft Division

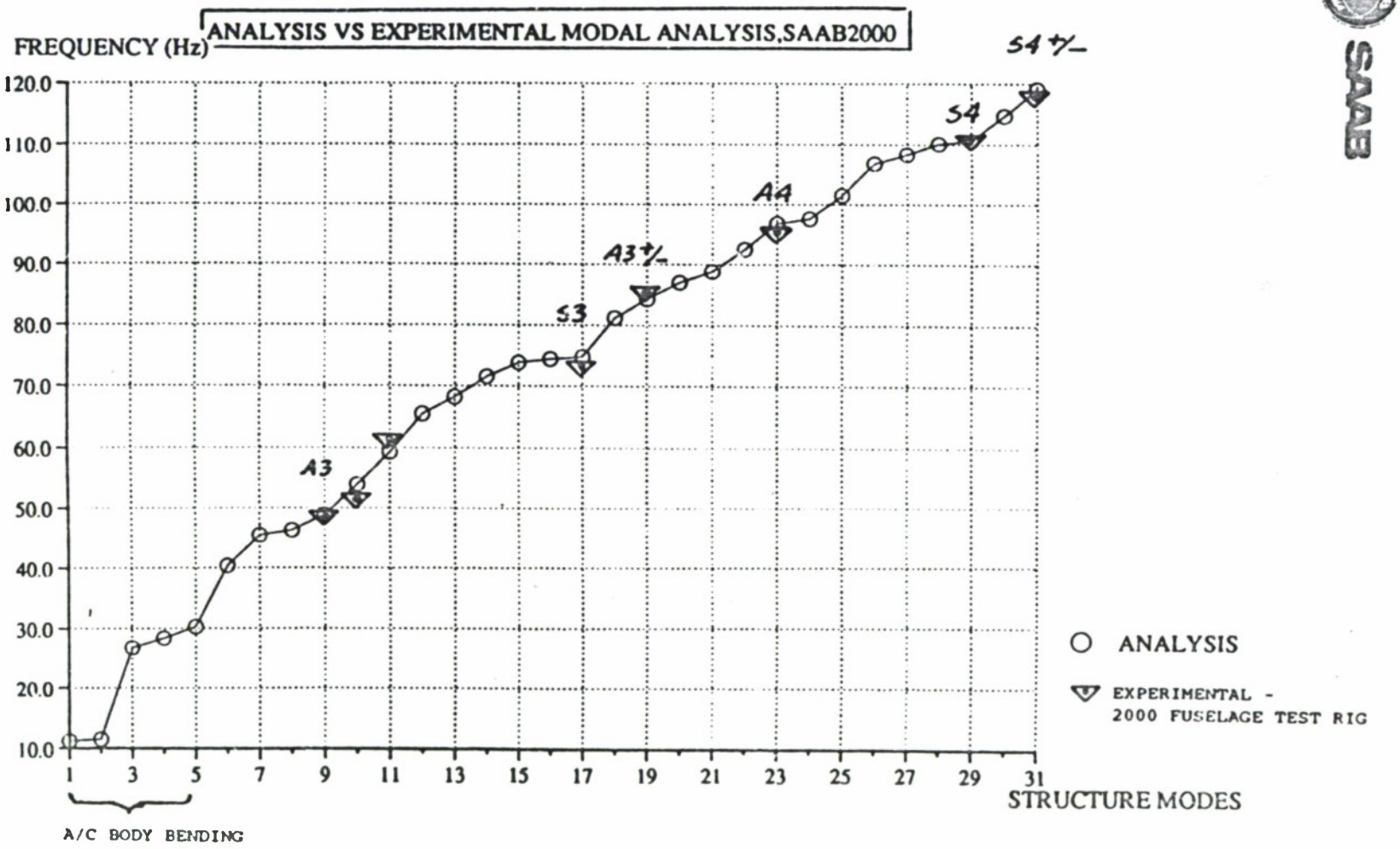
ANALYSIS VS EXPERIMENTAL MODAL ANALYSIS,SAAB2000
FREQUENCY (Hz)
120.0
110.0
100.0
90.0
80.0
70.0
60.0
50.0
40.0
30.0
20.0
10.0
A3
S3
A3+/-
A4
S4
S4 +/-
1
3
5
7
9
11
13
15
17
19
21
23
25
27
29
31
STRUCTURE MODES
A/C BODY BENDING
ANALYSIS
EXPERIMENTAL -
2000 FUSELAGE TEST RIG

SAAB

MODEL VALIDATION ANALYSIS

Acoustic Mockup shaker test simulation

- 16 shakers with simultaneously sinusodial force (95 Hz) excitation.
- Force and phase distribution randomly choosen.

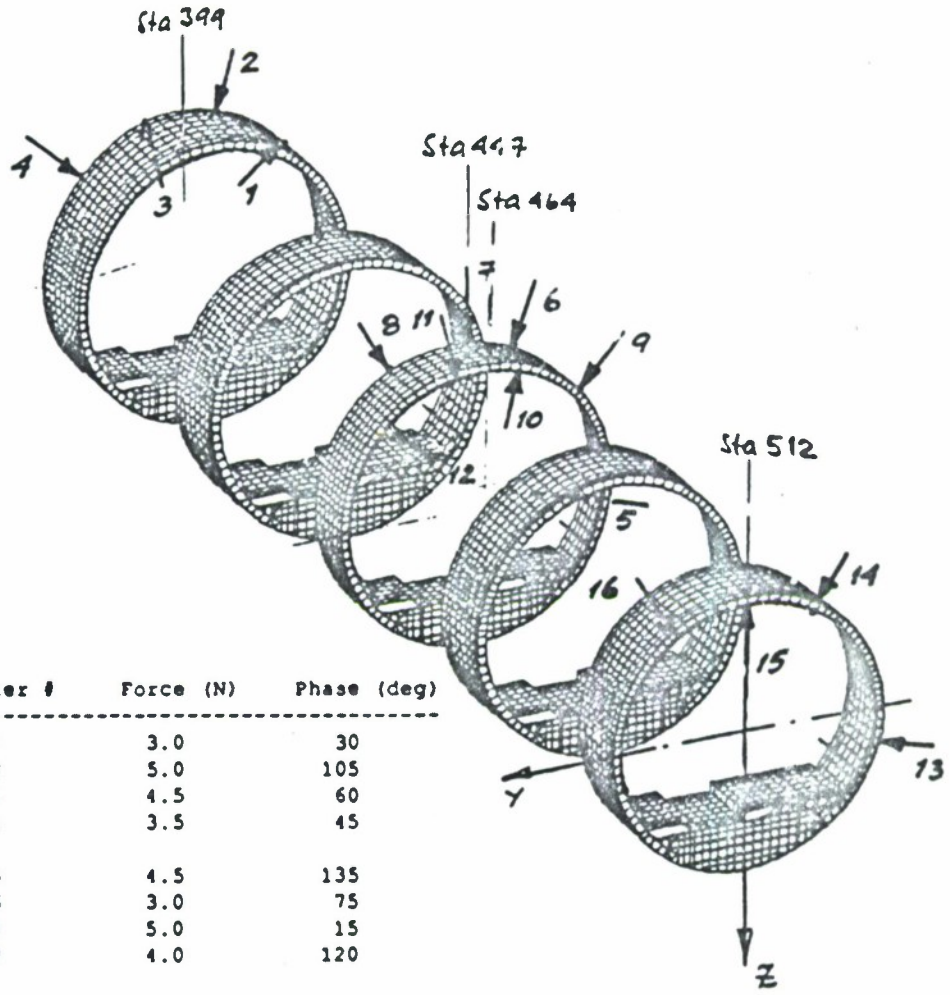

Shaker #	Force (N)	Phase (deg)
1	3.0	30
2	5.0	105
3	4.5	60
4	3.5	45
5	4.5	135
6	3.0	75
7	5.0	15
8	4.0	120
9	3.5	150
10	4.5	120
11	3.5	75
12	5.0	45
13	4.0	15
14	3.5	60
15	5.0	165
16	4.0	105

Saab Aircraft Division

SAAB

Planned analyses

- Tuned dampers

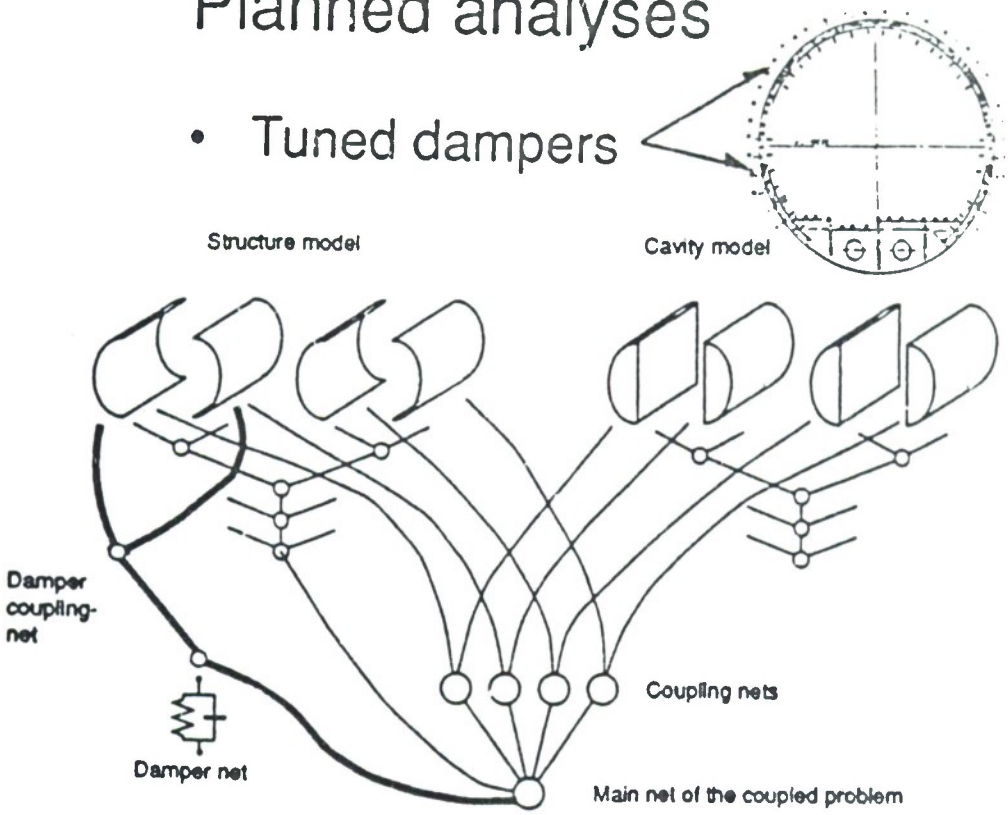

- Structure-borne path identification

- Active Vibration Control

SAAB

- Model development
  - Fuselage sections with interior
  - Active Noise Control analyses

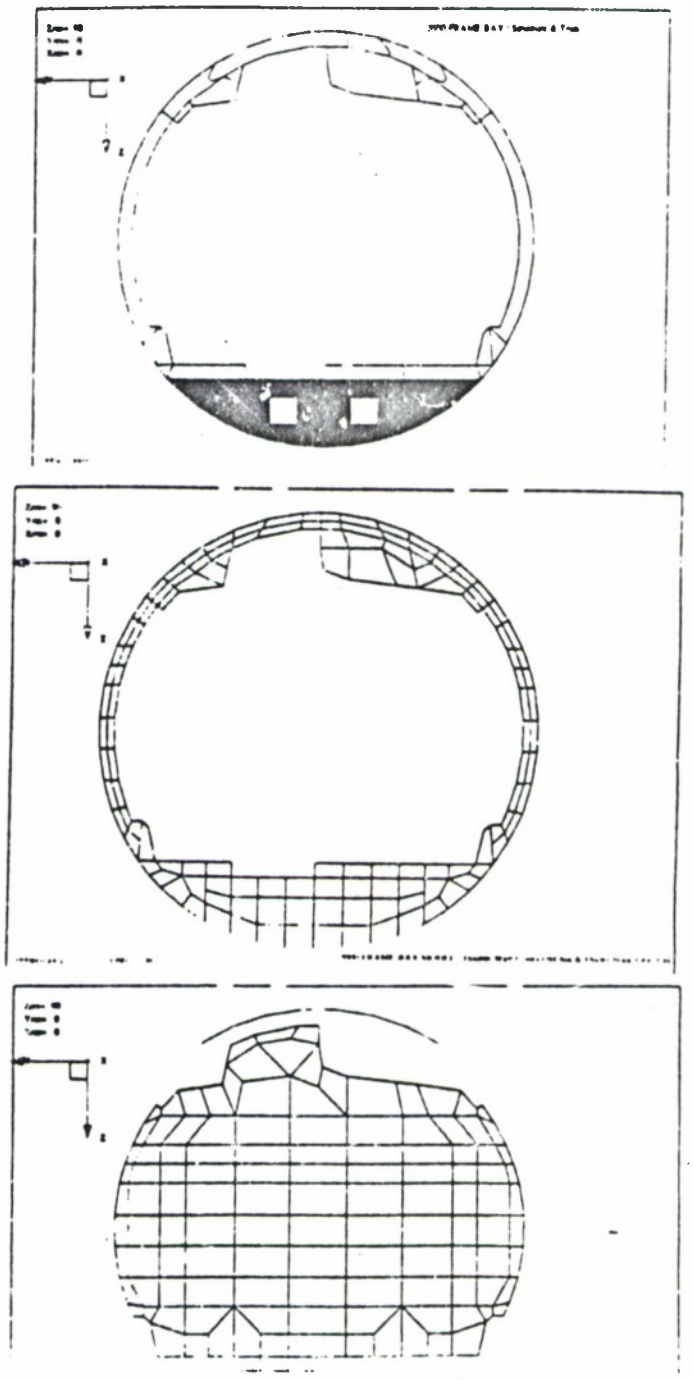

70

SOUND POWER DETERMINATION USING THE SOUND INTENSITY SCANNING TECHNIQUE

G. Krishnappa
Institute for Mechanical Engineering
National Research Council
Ottawa, Canada K1A 0R6

Why sound intensity for determining sound power?

- Sound power from sound pressure measurements leads to:
  - approximations.
  - necessary to specify source characteristics, measurement environment, and positions.
  - requires costly facilities.

- Sound intensity:
  - primary quantity to determine sound power levels.
  - no costly facilities required.
  - measurements can be made in the presence of extraneous noise.

$$\textit{Sound power} = \int_S \vec{I}_n \cdot \vec{ds}$$

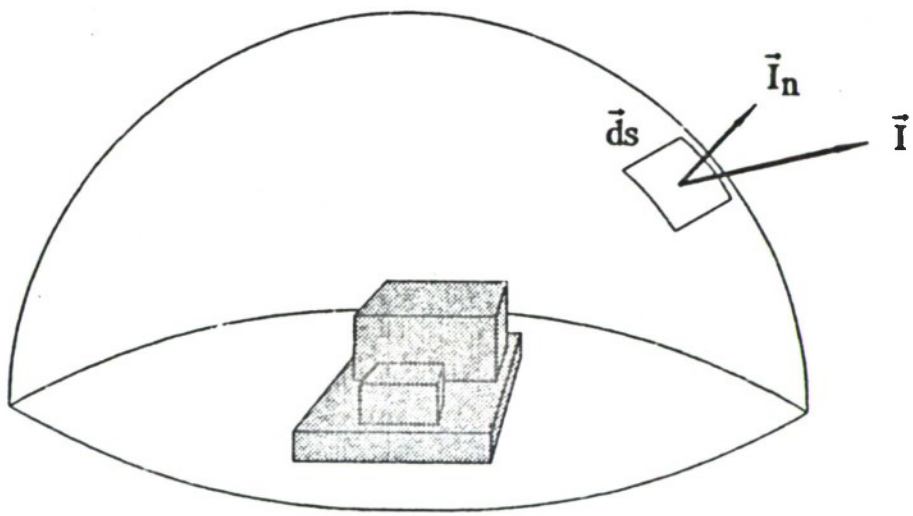

Sound Power from Sound Intensity Measurements

- Sampling of sound field based on:
  - measurements at discrete points distributed on the surface.
  - sound intensity probe scan over the surface.

Discrete Point Method

- Initial measurement surface chosen.
- Sound intensity independently measured at a large number of points.
- Measurement accuracy determined by iterative procedure based on indicator criteria.
- Frequently requires more than one test procedure, requiring changes to measurement parameters:
  - measurement surface.
  - its distance.
  - number of points.
- This method is complex and time consuming.

Sound Intensity Probe Scan

- Initial measurement surface chosen.
- Probe moved continuously along one or more prescribed paths.
- Surface average values of sound intensity obtained in a few scans.
- Relatively quick and easy to perform.
- Gives good engineering grade accuracy.
- Can be done mechanically or manually.

Measurement Accuracy

- Acoustic field conditions:
  - acoustic environment.
  - extraneous noise.
  - measurement surface chosen.

- Scanning parameters:
  - speed of scanning.
  - density of scanning.
  - scanning pattern.

P-I Indicator

- Difference between the level of the surface integrated pressure and the level of the surface integrated normal sound intensity.
- Measurement accuracy is sensitive to the difference between sound pressure level and intensity level.
- Large P-I indicator caused by:
  - intensity vector at a large angle.
  - strong contributions to local sound pressure from outside the measurement surface.
  - reverberant field.
  - presence of nearfield or standing waves.
  - areas of +ve and -ve intensities close to surface.

Important Questions to be Resolved

- How is the accuracy of sound power related to:
  - scanning parameters.
  - P-I indicator.

Diagram of the measurement set-up showing the complex source, extraneous noise source, and measurement plane.

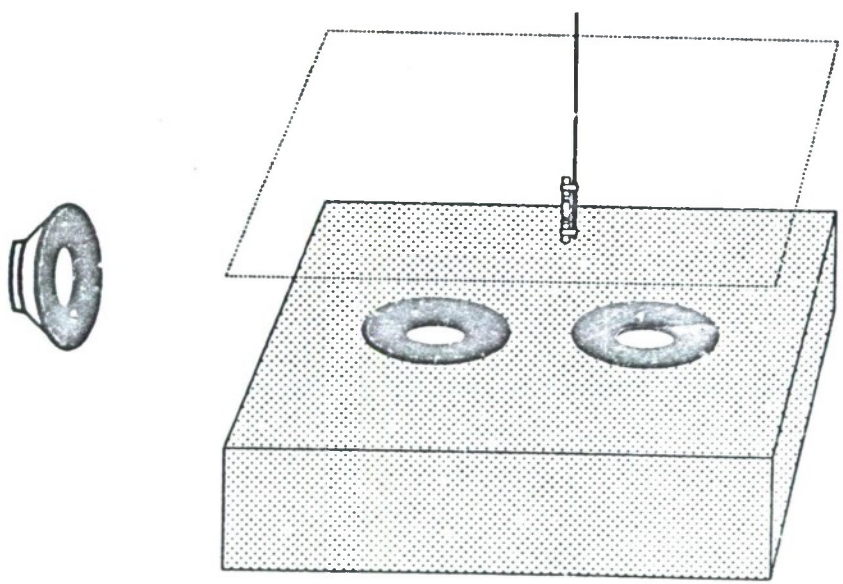

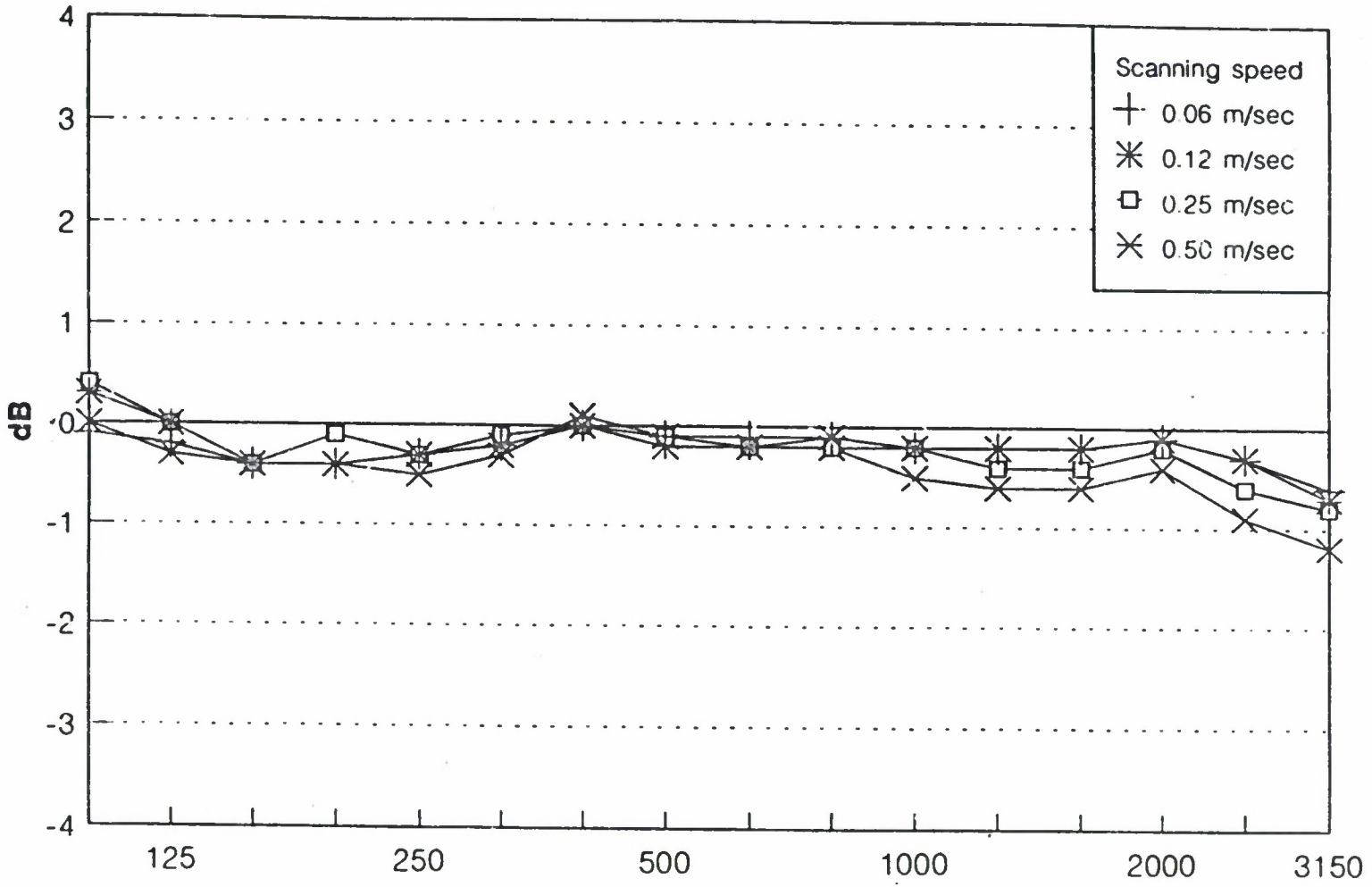

DIFFERENCE IN SOUND POWER LEVELS

between manual scanning and discrete-points methods
measurement surface: 0.5 m

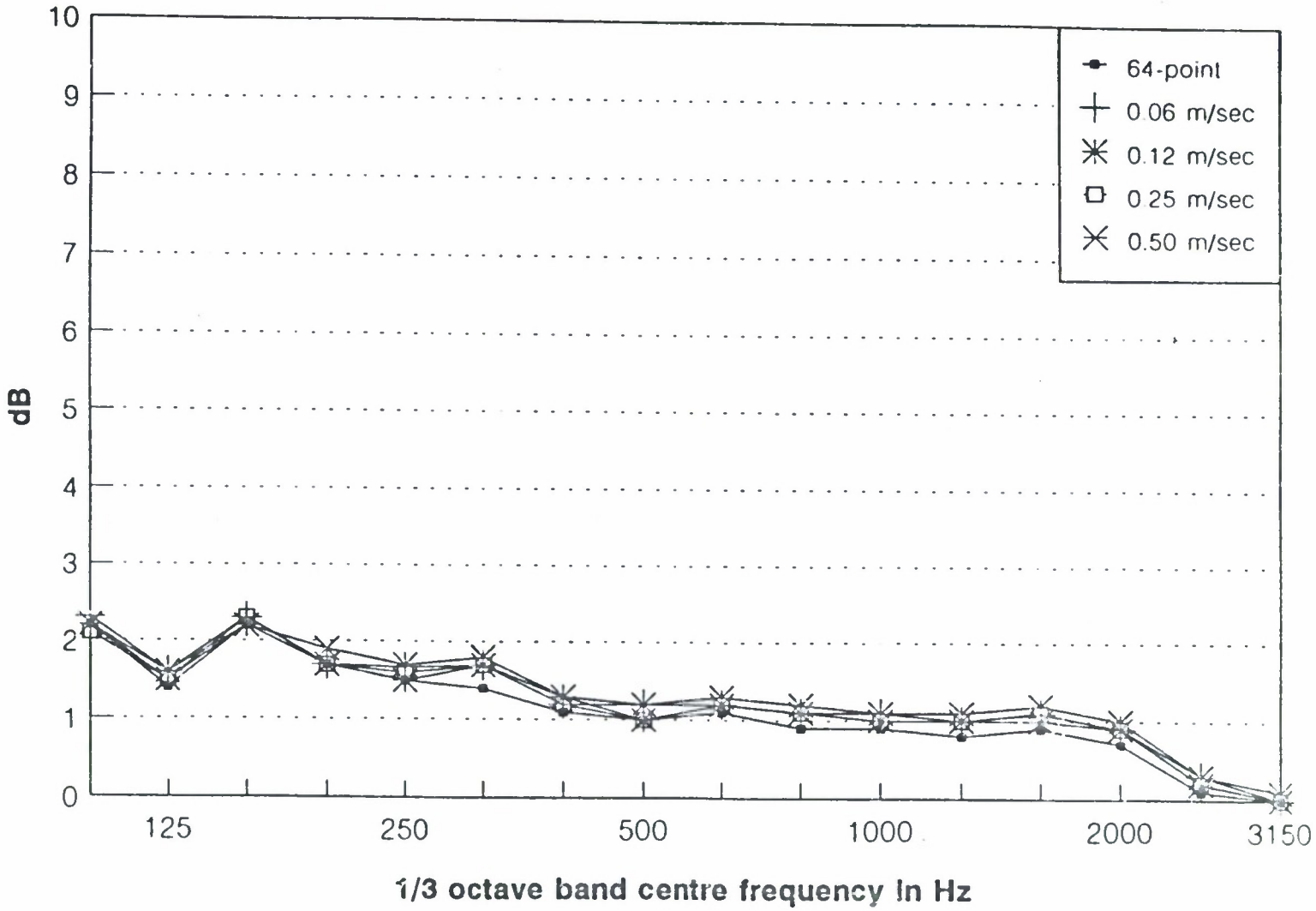

SOUND FIELD PRESSURE-INTENSITY INDICATORS

discrete-point & manual scanning methods
measurement surface: 0.50 m

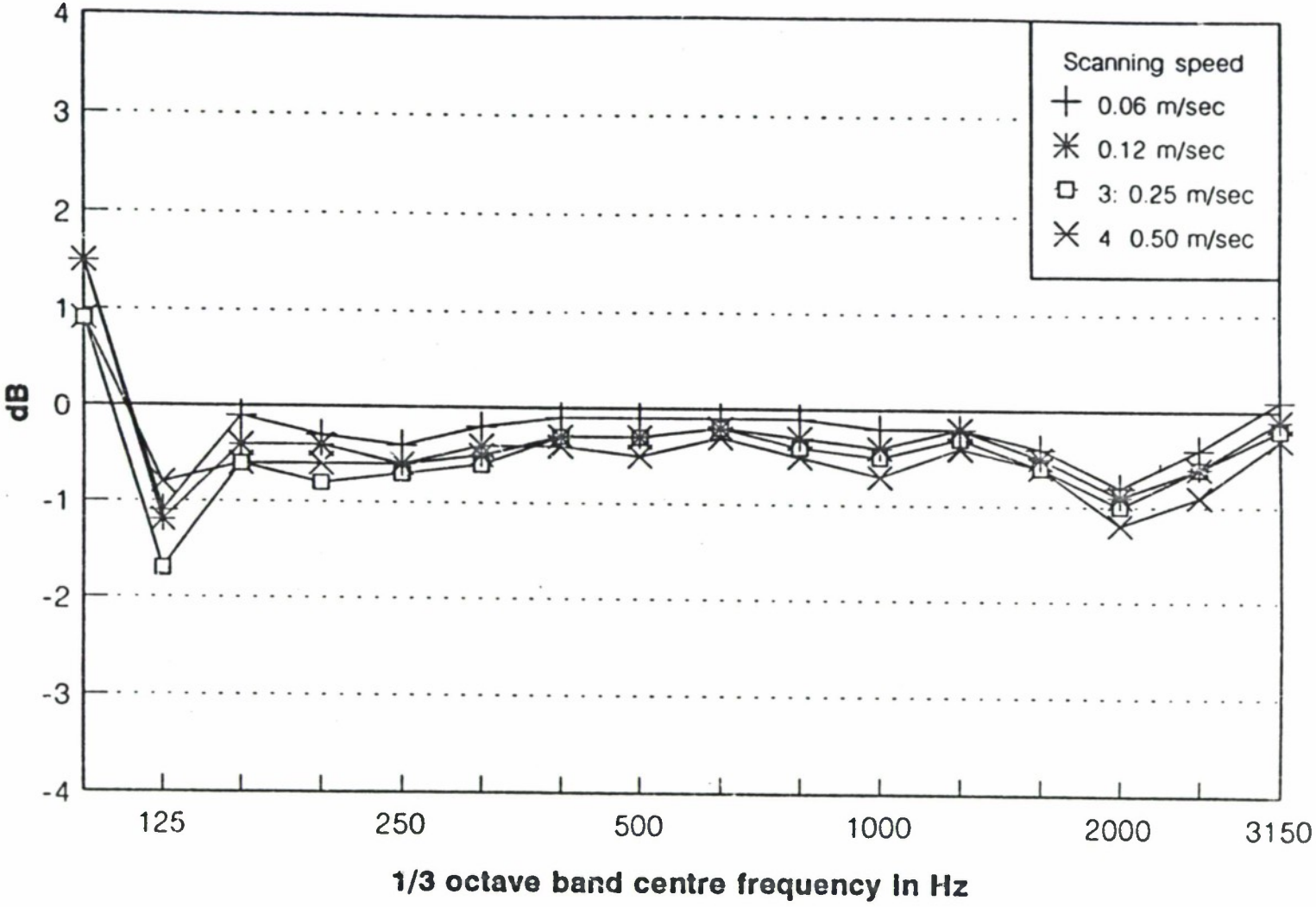

DIFFERENCE IN SOUND POWER LEVELS

between manual scanning & discrete-points methods
measurement surface: 0.25 m

DL125 M.

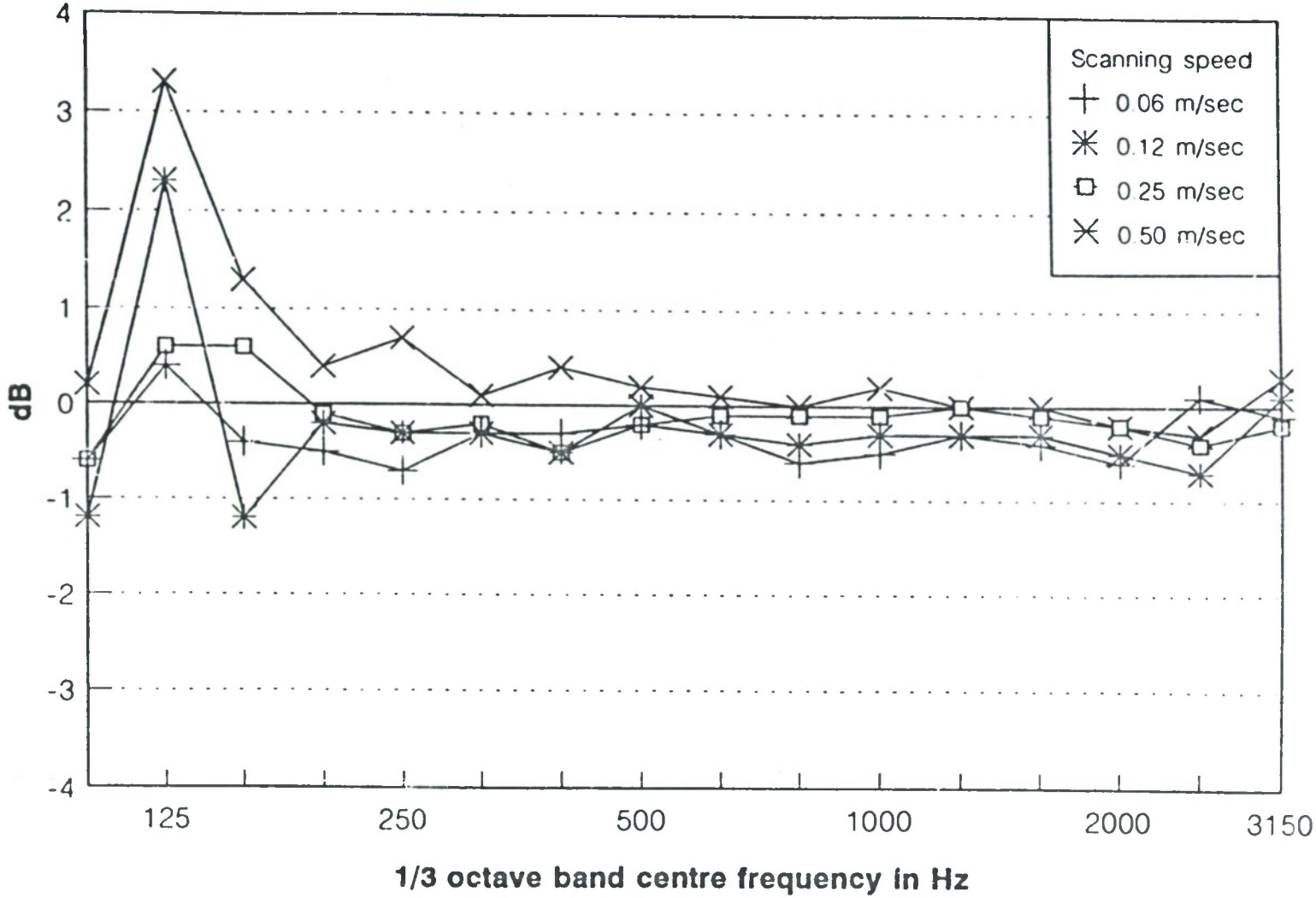

DIFFERENCE IN SOUND POWER LEVELS

between mechanical scanning & discrete-points methods
measurement surface: 0.25 m

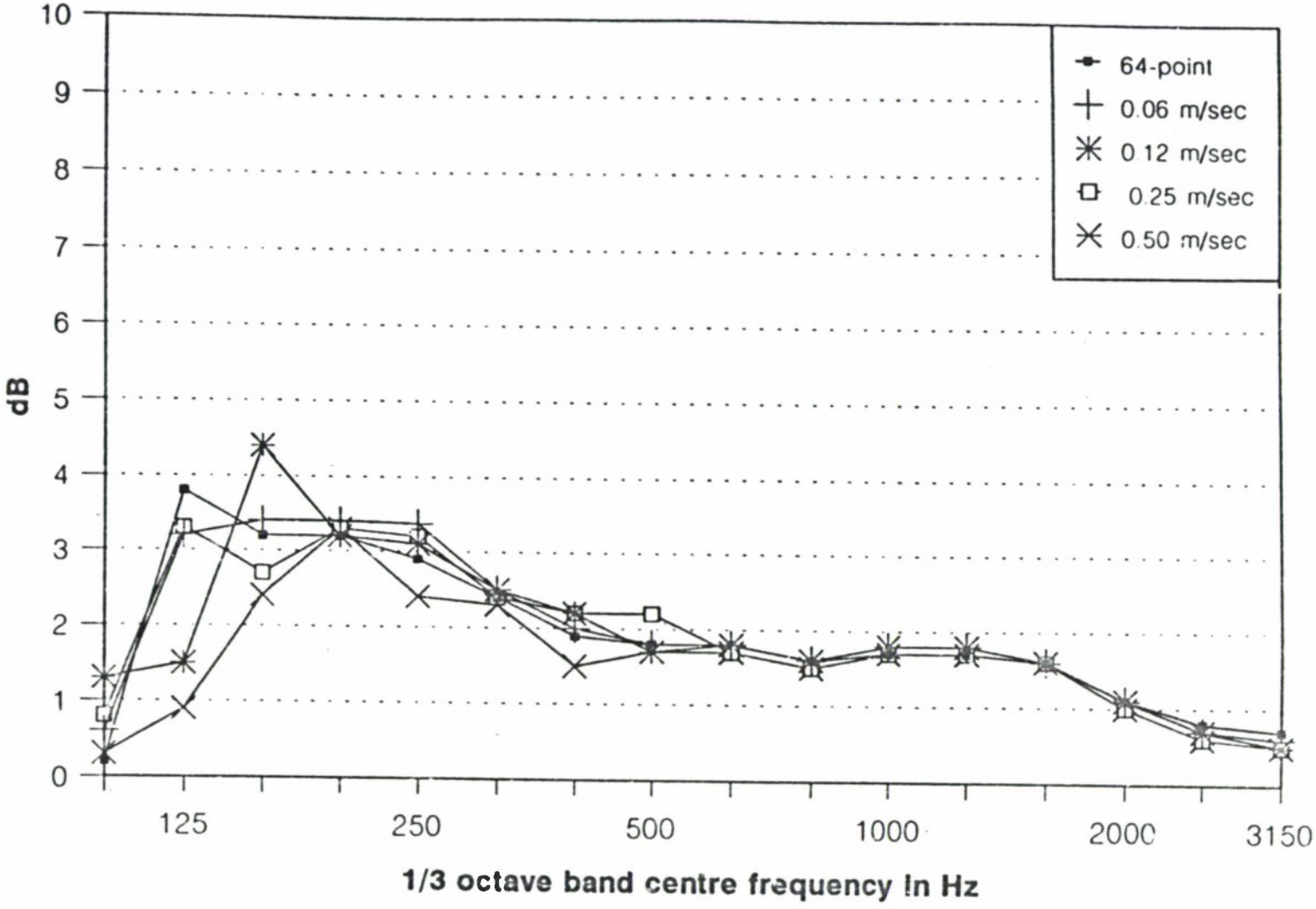

SOUND FIELD PRESSURE-INTENSITY INDICATORS

discrete-point & mechanical scanning methods
measurement surface: 0.25 m

F3A25.013

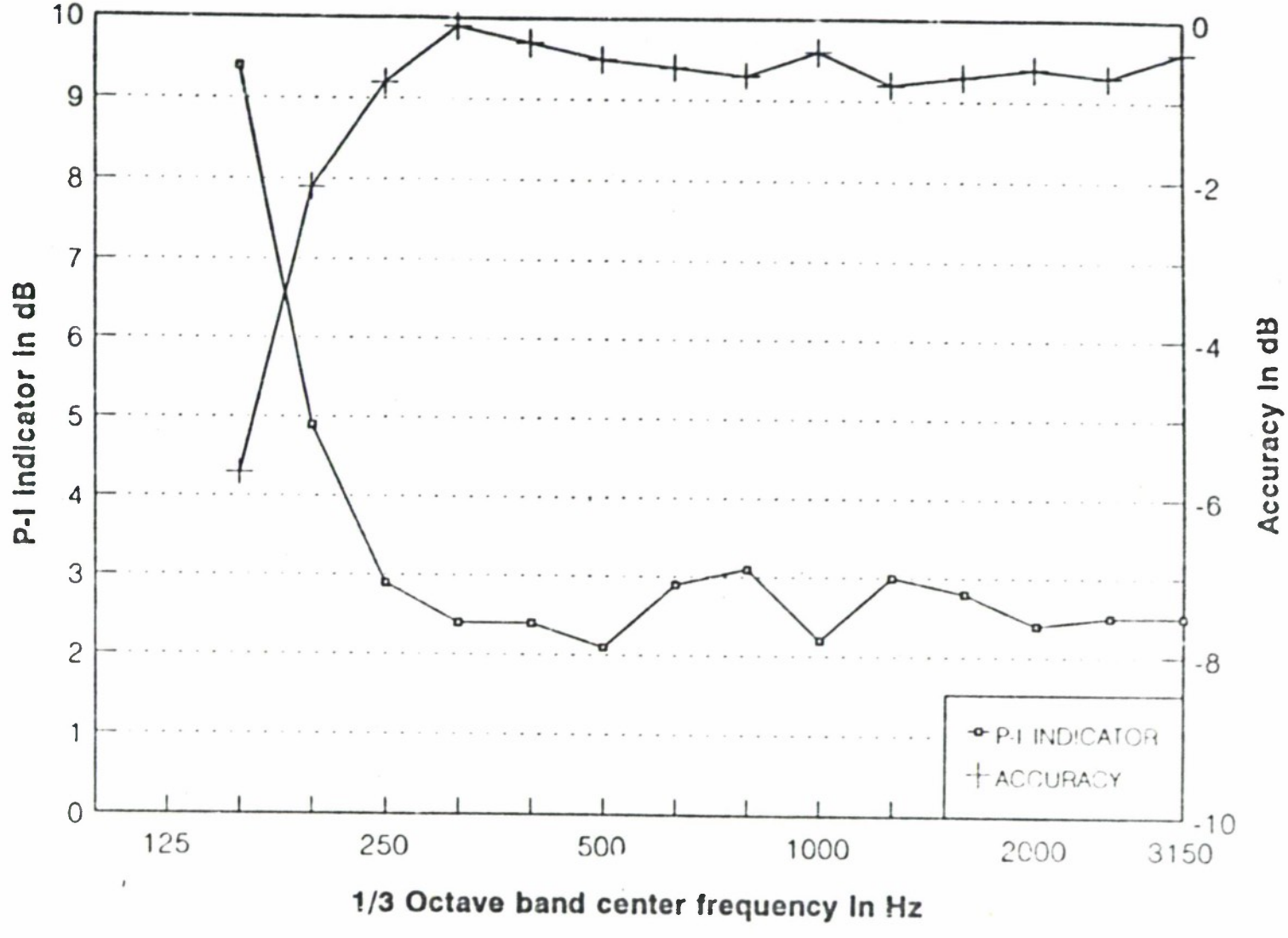

P-I INDICATOR & SOUND POWER LEVEL ACCURACY

ext noise level = source level, meas surface: 0.50 m

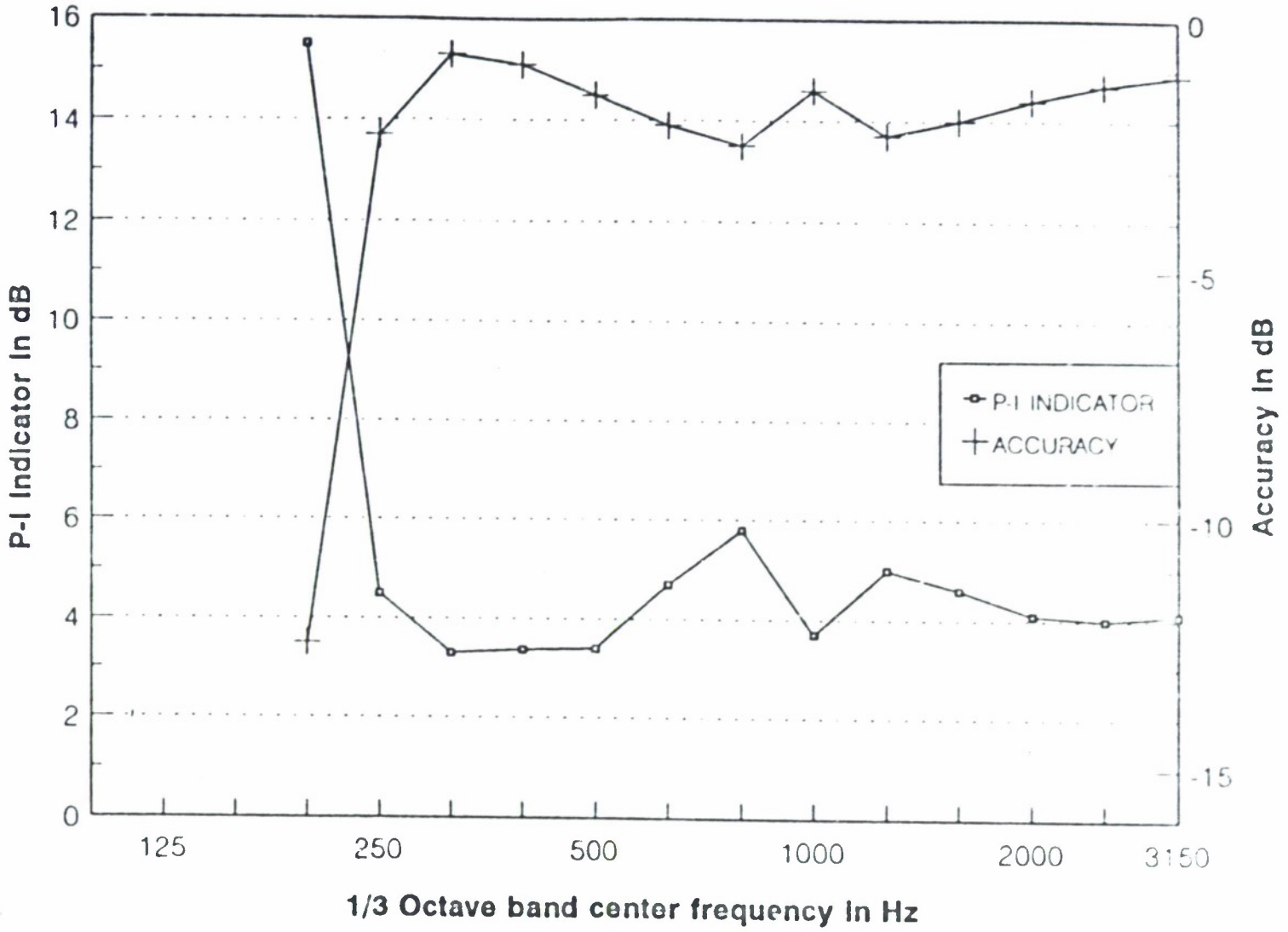

P-I INDICATOR & SOUND POWER LEVEL ACCURACY

ext noise: 3 dB, meas surface: 0.5 m

Scanning Path on the Measurement Surface

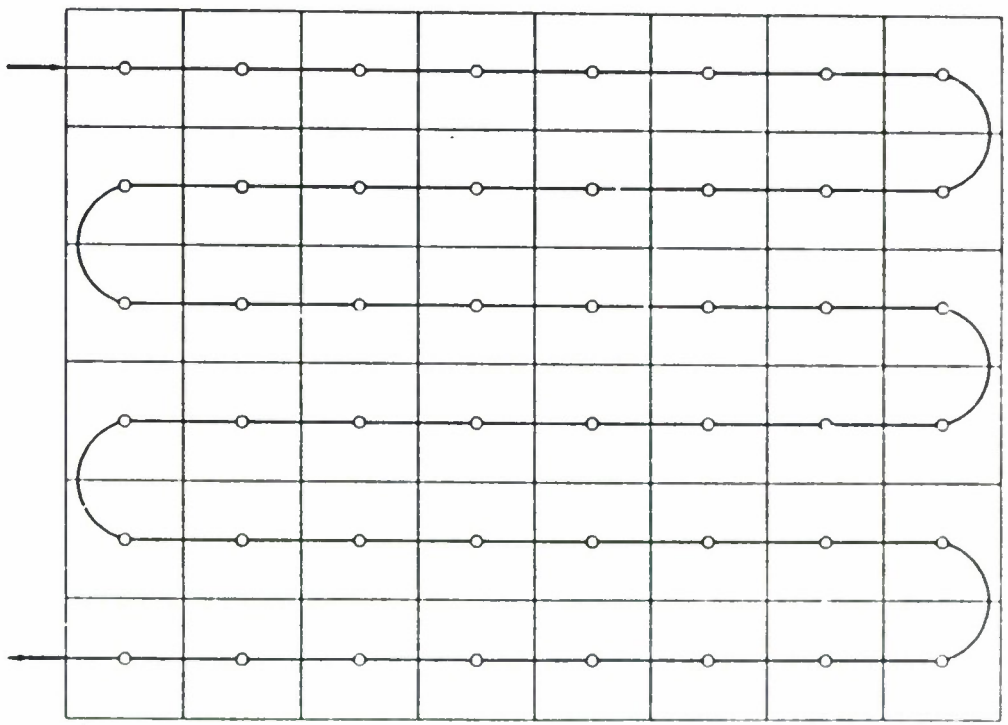

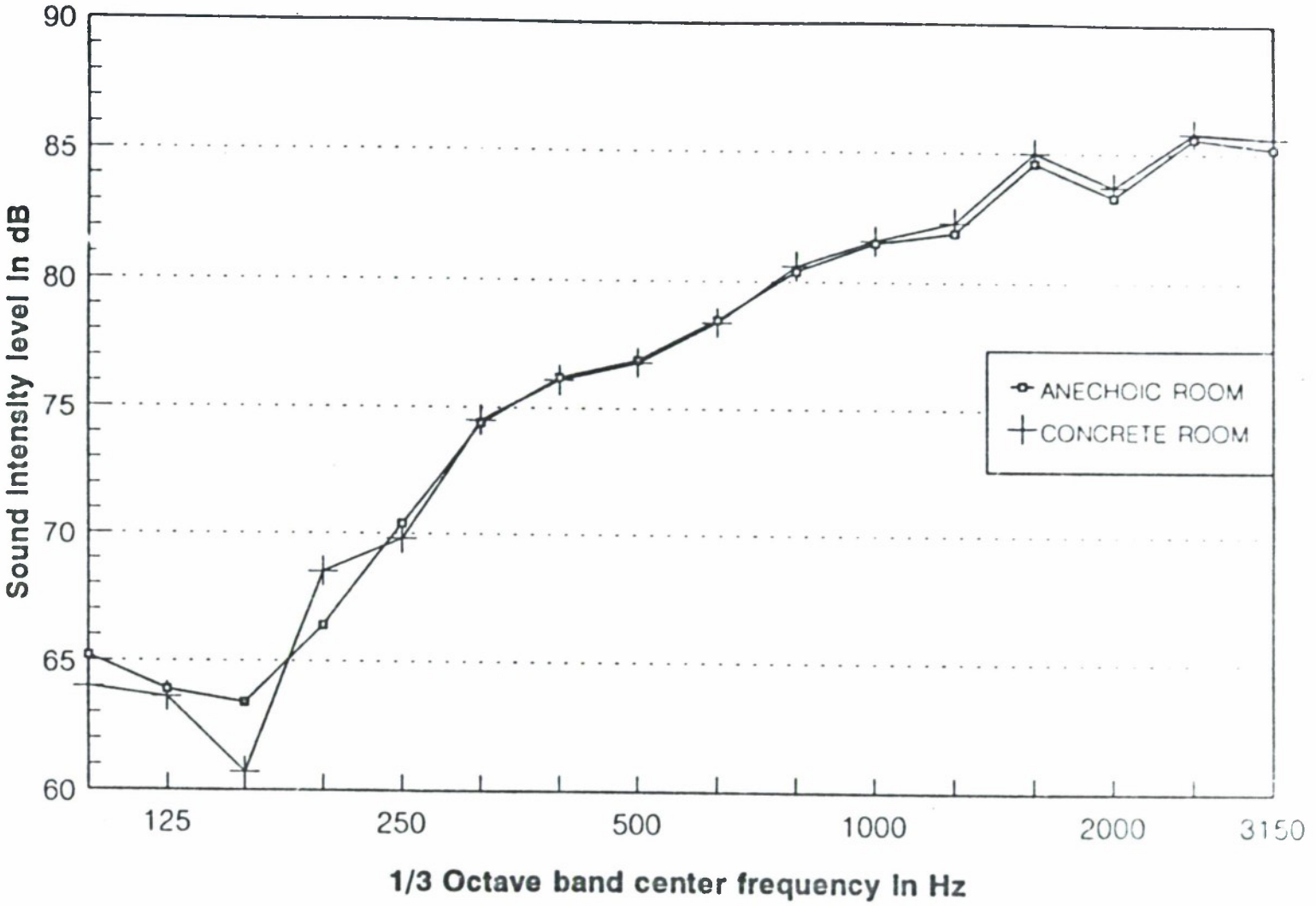

SURFACE AVERAGE VALUE OF SOUND INTENSITY LEVELS

measured in anechoic & concrete-walled rooms
(sound source only, meas surface: 0.5 m)

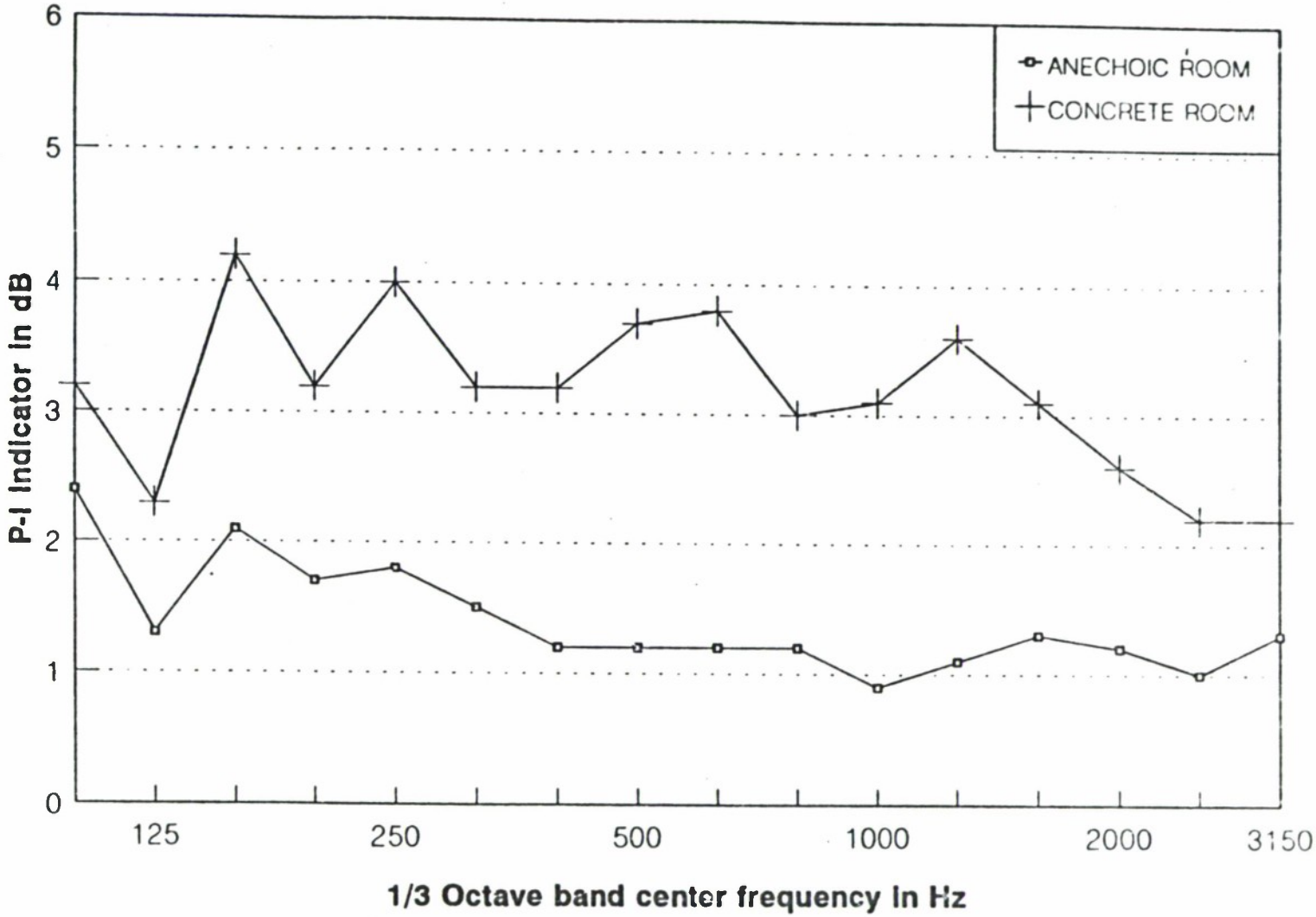

PRESSURE - INTENSITY INDICATORS

measured in anechoic & concrete-walled rooms
(sound source only, meas surface: 0.5 m)

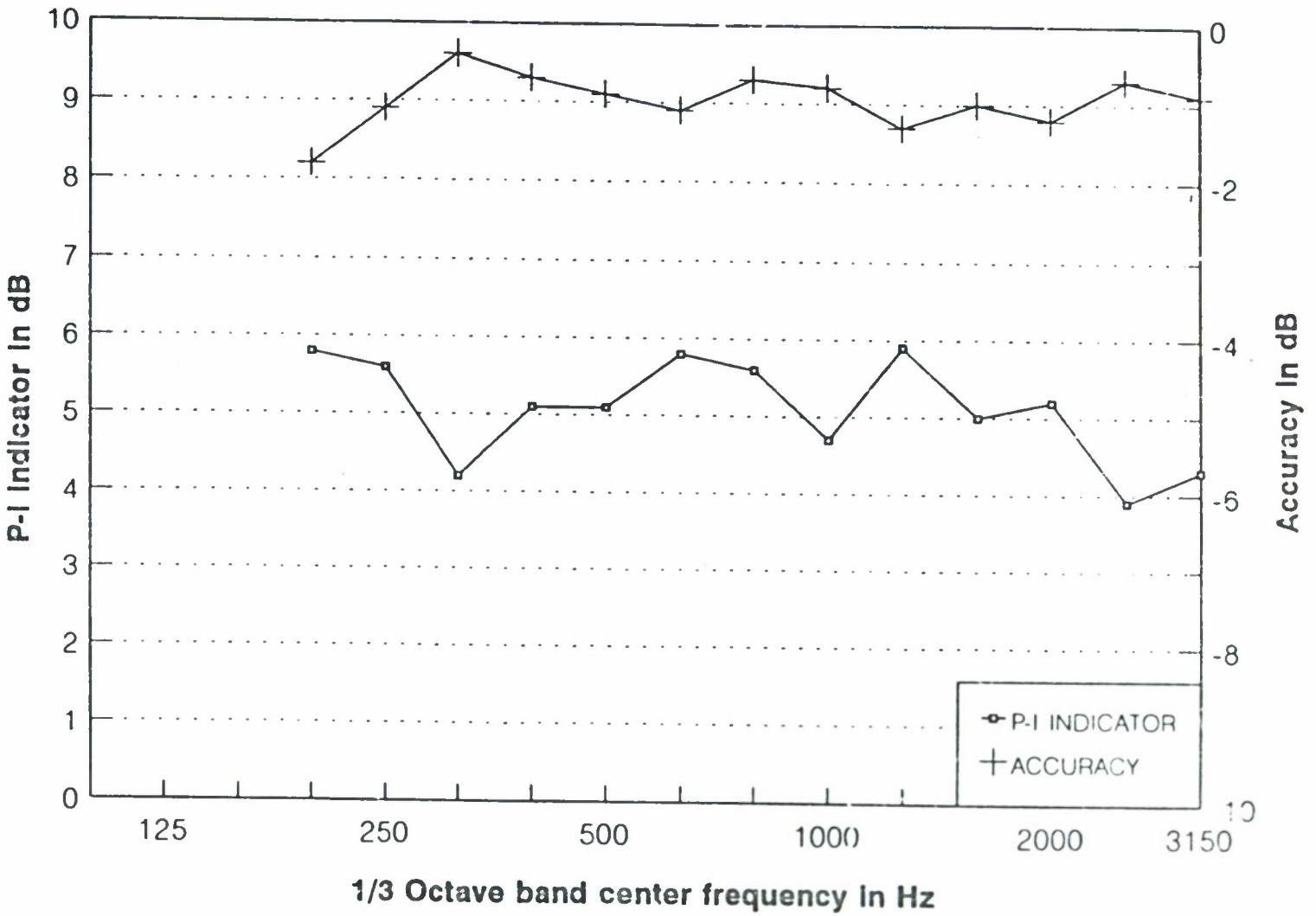

P-I INDICATOR & SOUND POWER LEVEL ACCURACY

ext noise level = source level, meas surface: 0.50 m
(in a 4.7 x 4 x 3 m concrete-walled room)

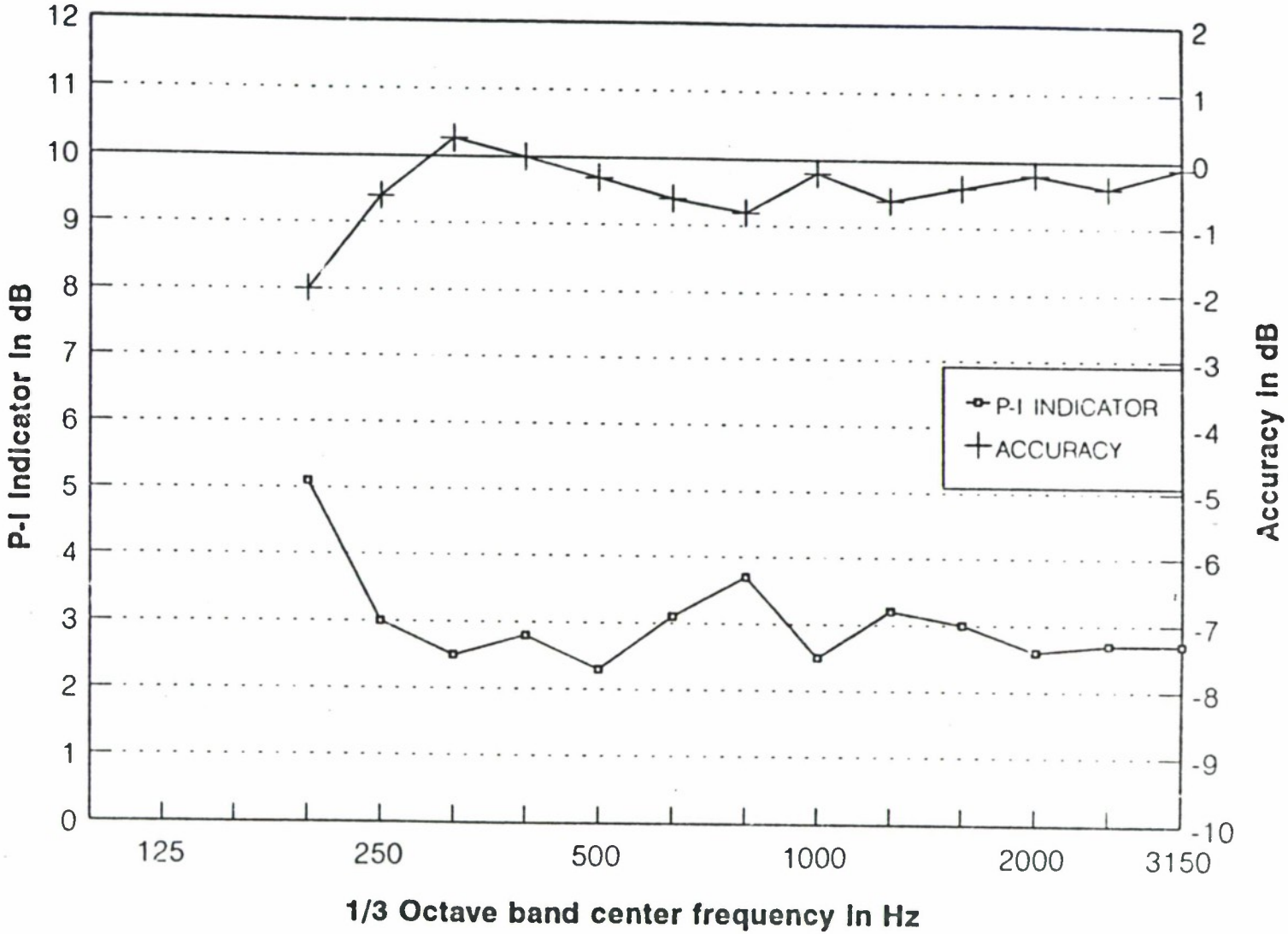

P-I INDICATOR & SOUND POWER LEVEL ACCURACY

ext noise level = source level, meas surface: 0.5 m

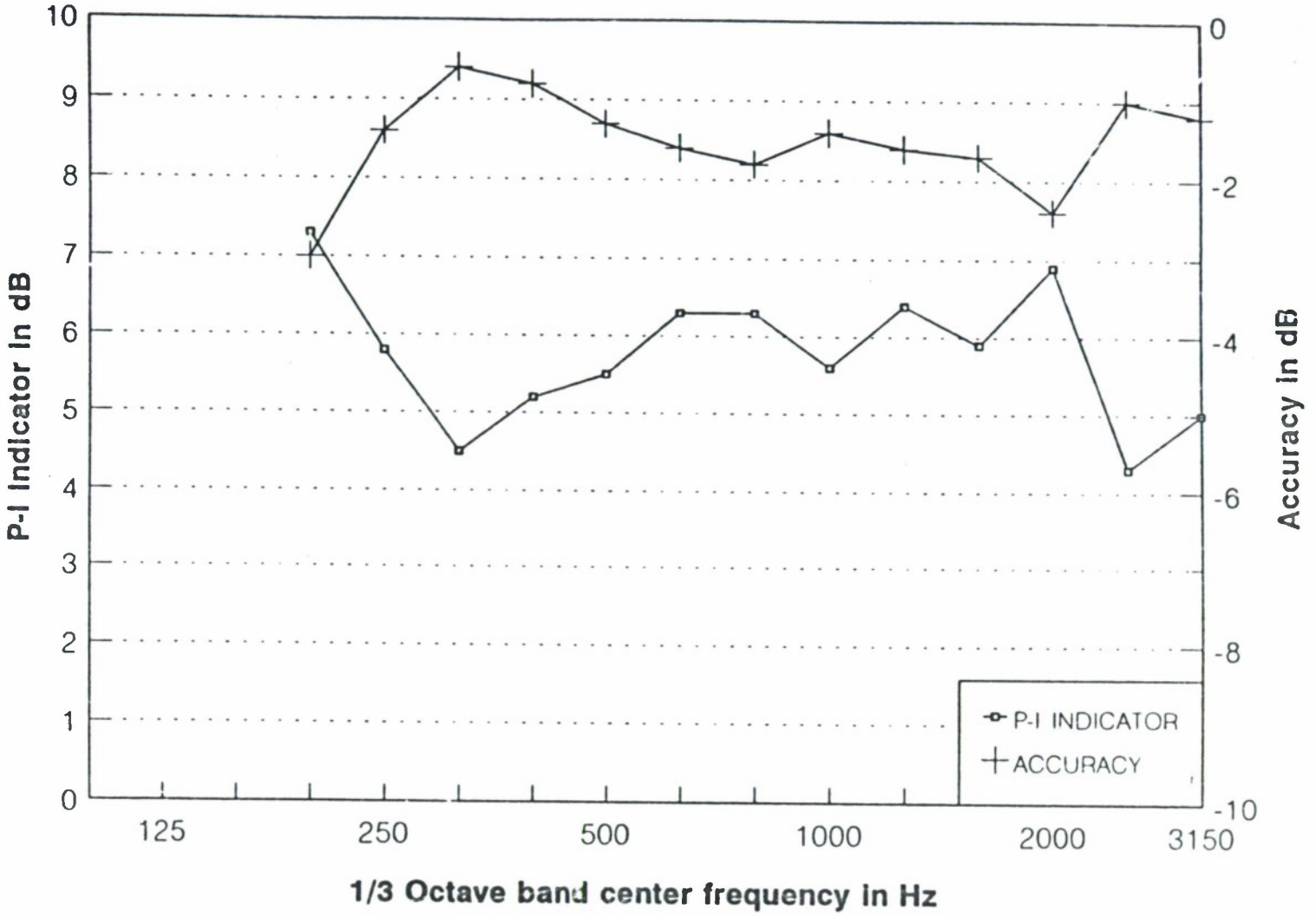

P-I INDICATOR & SOUND POWER LEVEL ACCURACY

ext noise: 1 dB, meas surface: 0.5 m
(in a 4.7 x 4 x 3 m concrete-walled room)

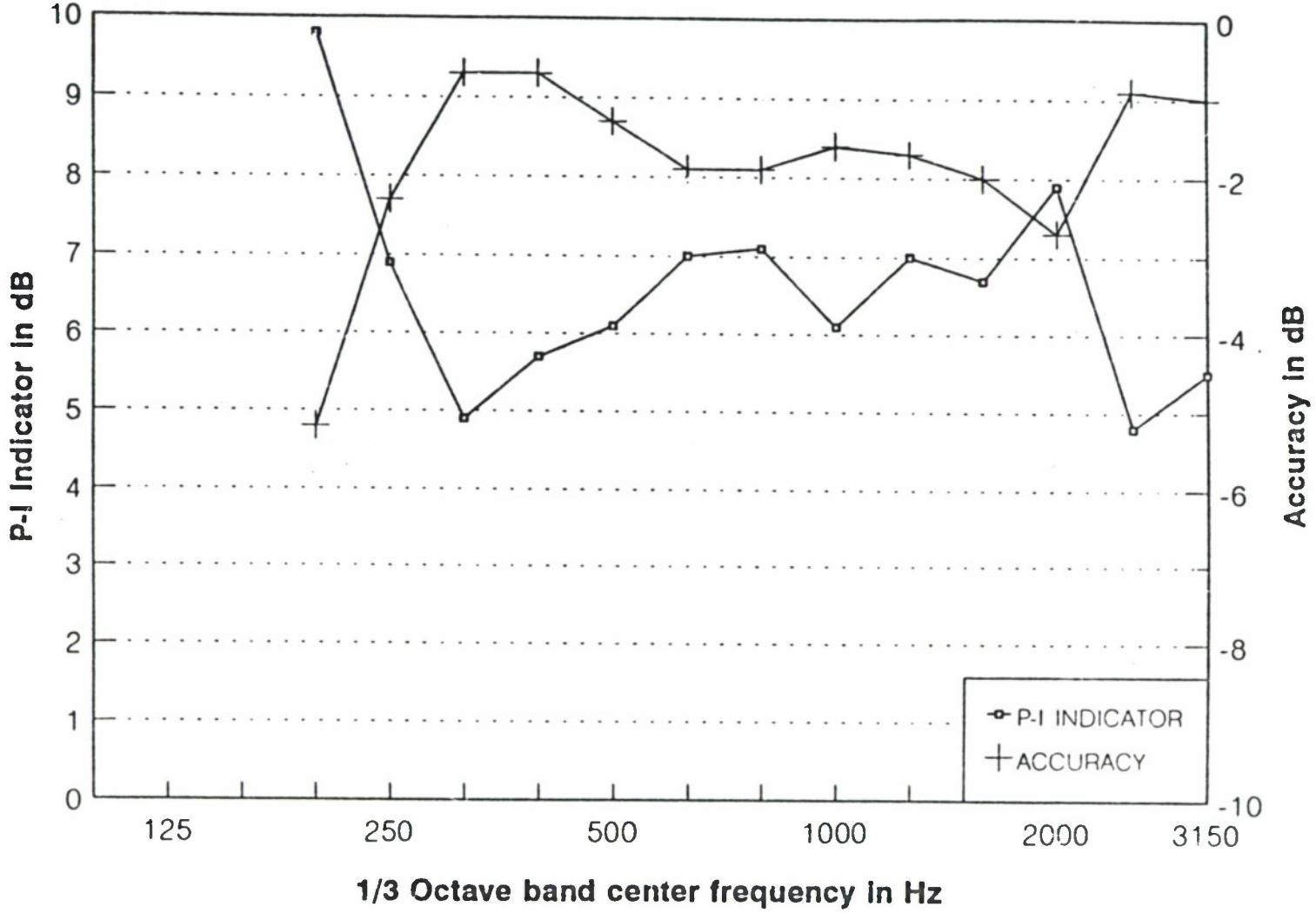

P-I INDICATOR & SOUND POWER LEVEL ACCURACY

ext noise: 2 dB, meas surface: 0.5 m
(in a 4.7 x 4 x 3 m concrete-walled room)

Conclusions

- Mechanical and manual scanning give good accuracy.
- Measurement distance should be greater than 25 cm.
- P-I indicator values should be less than 6 dB for accuracies within 1 dB.
- Accurate measurements can be made in the presence of extraneous noise up to +3 dB (depends on the location of the source).
- Accurate measurements are possible in an environment with severe reflections.

Recent Advances in Statistical Energy Analysis

Dr K H Heron

Defence Research Agency
RAE Farnborough
ENGLAND

NASA SAE DLR
4th Aircraft Interior Noise Workshop
May19-20,1992
Graf Zeppelin Haus
Friedrichshafen, Germany

RECENT ADVANCES IN SEA

Dr K H Heron
DRA, Farnborough,England

Summary

Statistical Energy Analysis has traditionally been developed using a modal summation and averaging approach, and this has led to the need for the many well known and restrictive SEA assumptions. The assumption of 'weak coupling' is particularly unacceptable when attempts are made to apply SEA to structural couplings. Many researchers now believe that this assumption is more a function of the modal formulation rather than a necessary requirement of SEA itself.

This presentation ignores this restriction and describes a wave approach to the calculation of plate-plate coupling loss factors. In this formulation each plate is modelled as three SEA subsystems to take full account of the three plate wavetypes. Accurate infinite transmission coefficients are calculated using line wave impedance techniques, and these are then converted to coupling loss factors in the usual way.

Predictions based on this method are compared with results obtained from experiments using point excitation on one side of an irregular six-sided box structure. This work was sponsored by the CEC under Brite-EuRam contract number AERO-0028 and performed in collaboration with Agusta, MBB, Westland, Brüel & Kjær, CIRA, and Southampton University. The agreement is shown to be very good, both for the structural response and for the internal noise.

This presentation concludes that the use and calculation of infinite transmission coefficients is the way forward for the development of a purely predictive SEA code.

DATA FOR SEA PLATE MODEL (25 October 1991)

Young's Modulus	7.0e10	±1%
Poisson's Ratio	0.345	±1%
material density	2700	±1%
plate length	0.83	±0.001
plate width	0.53	±0.001
plate thickness	0.003	±0.0001
plate energy damping ratio	0.02	±10%
force position	(0.17,0.23)	±0.001
response position	(0.53,0.43)	±0.001

Forced response calculated by including modes within a factor of two from the frequency of interest. Energy damping ratio of 2% is equivalent to a critical damping ratio of 1%. Each realisation was obtained by assuming the above standard errors and a Normal distribution, and simply choosing a value for the eleven variables above using a Monte Carlo approach.

nominal modal density	=	0.04682 modes/Hz
nominal fundamental	=	148 Hz
modal overlap factor = 1	at	1068 Hz

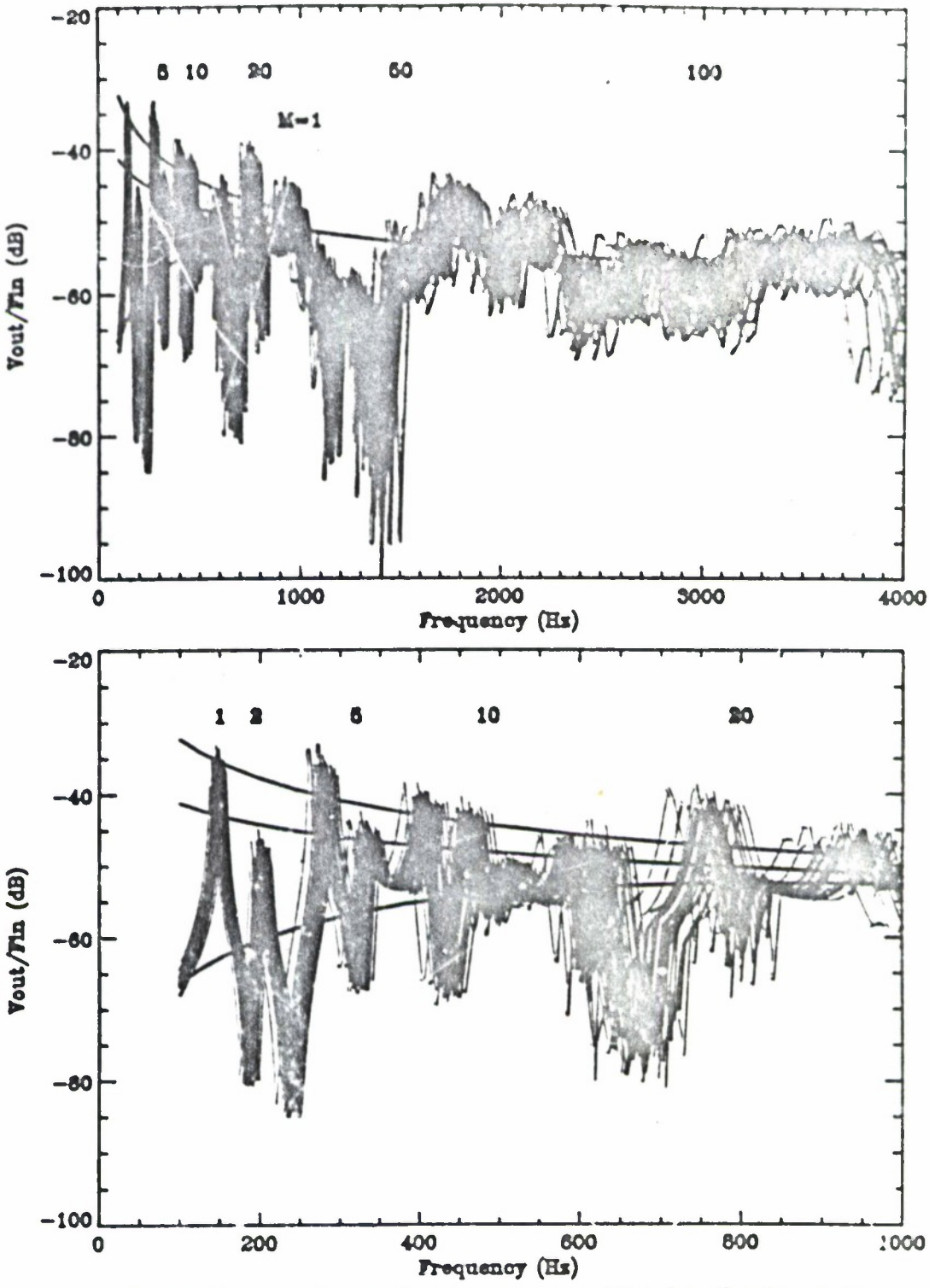

One plate : forced response : Monte Carlo x 20

HERON : 13 November 1991

THE WAVE APPROACH

- Each beam is represented by at least 4 subsystems (longitudinal, torsional and two bending).
- Each plate is represented by at least 3 subsystems (inplane iongitudinal, inplane shear and bending).
- Each cavity is represented by at least 1 subsystem.

PHILOSOPHY

Once all the properites of the equivalent infinite junctions have been calculated we have all the required information about the joints that we need for any predictive method aimed at the high frequencies or aimed at a 'mean' prediction.

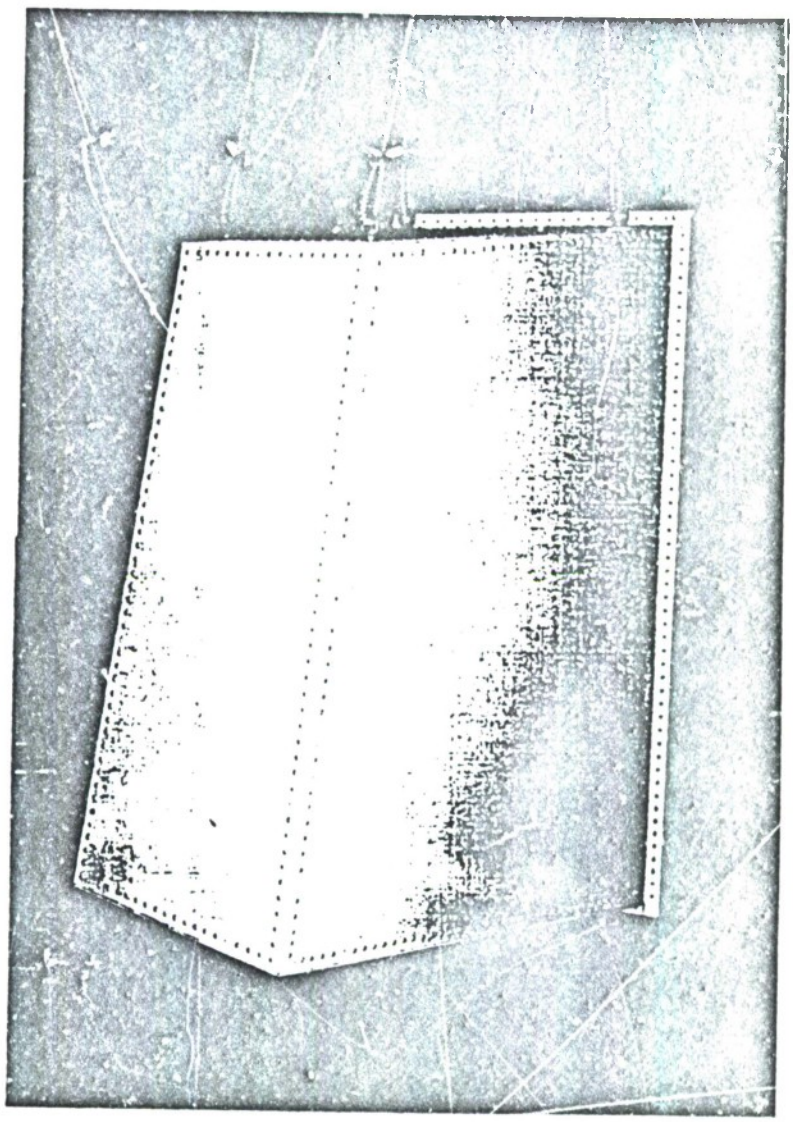

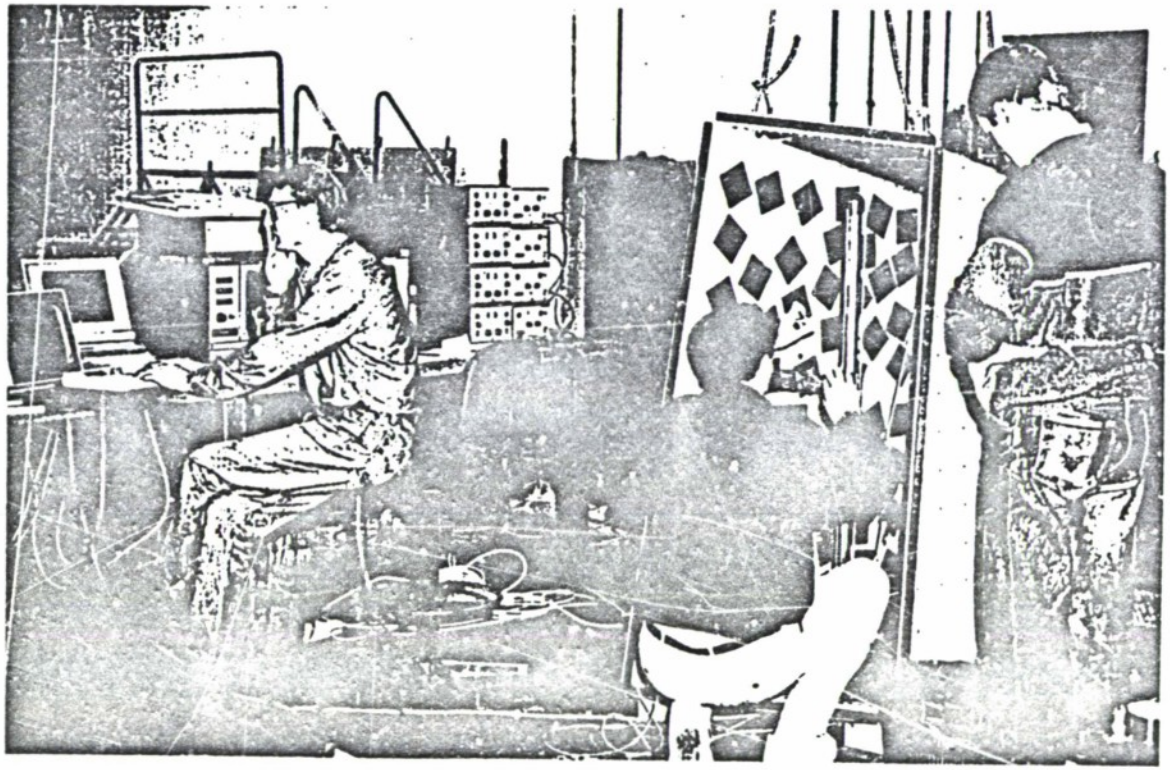

MODEL STRATEGY

1) Each plate is three SEA sub–systems.
2) Calculate 'infinite' random incidence transmission coefficents.
3) Hence via the wave approach calculate the SEA coupling loss factors.
4) Add the acoustics via radiation efficiency and transmission loss calculations.

ASANCA/SEA/17May01/KHH02

ASSUMPTIONS

Standard SEA wave approach assumptions +

1) Beams not included in the SEA model,
   because of equivalent beam problem.
2) All indirect couplings set to zero,
   because no theory exists.
3) Simple acoustic radiation factors,
   because no better theory exists.

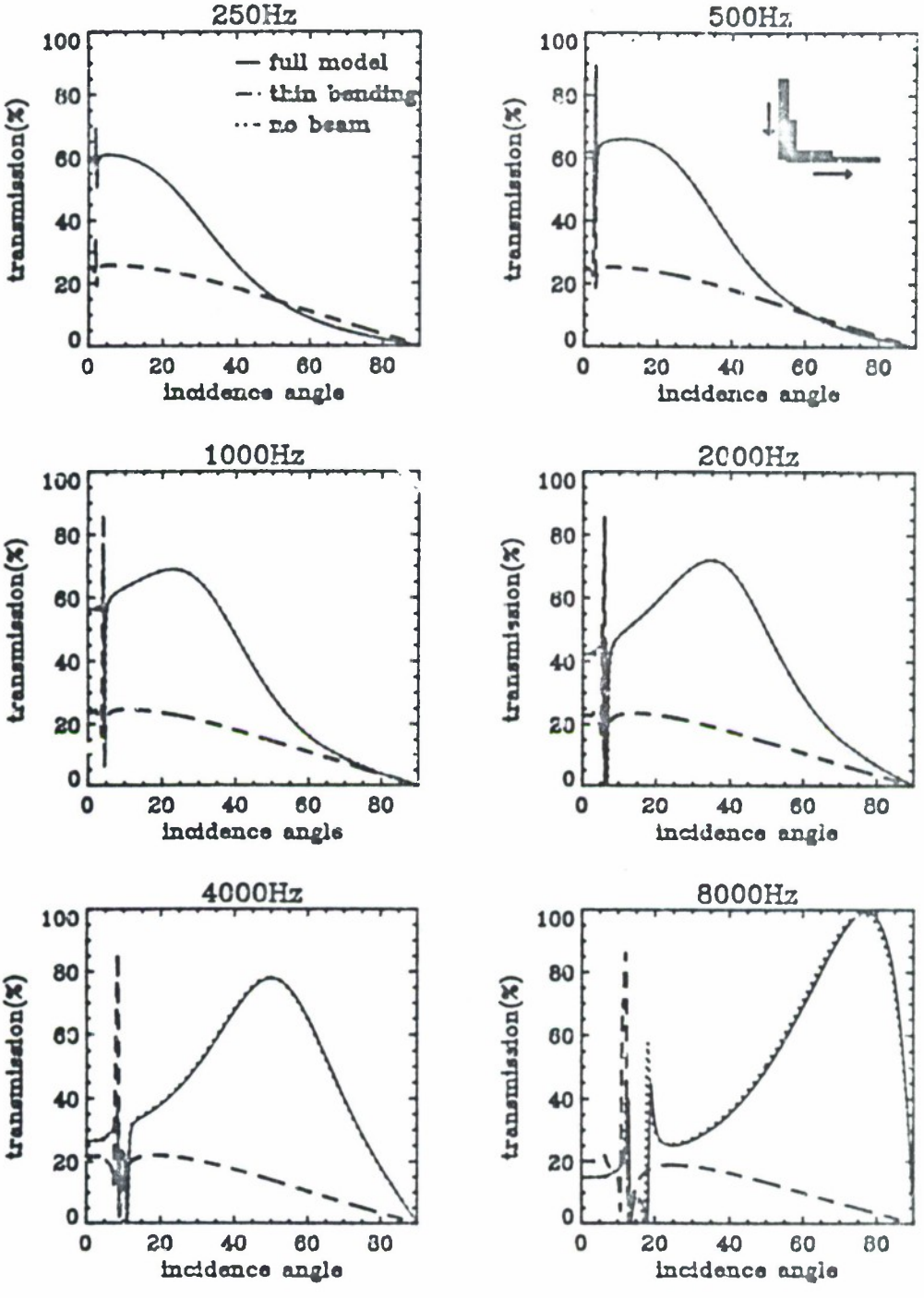

10 May 1991 - A.S.A.N.C.A. Box

Bending transmission coefficients for junction at L09

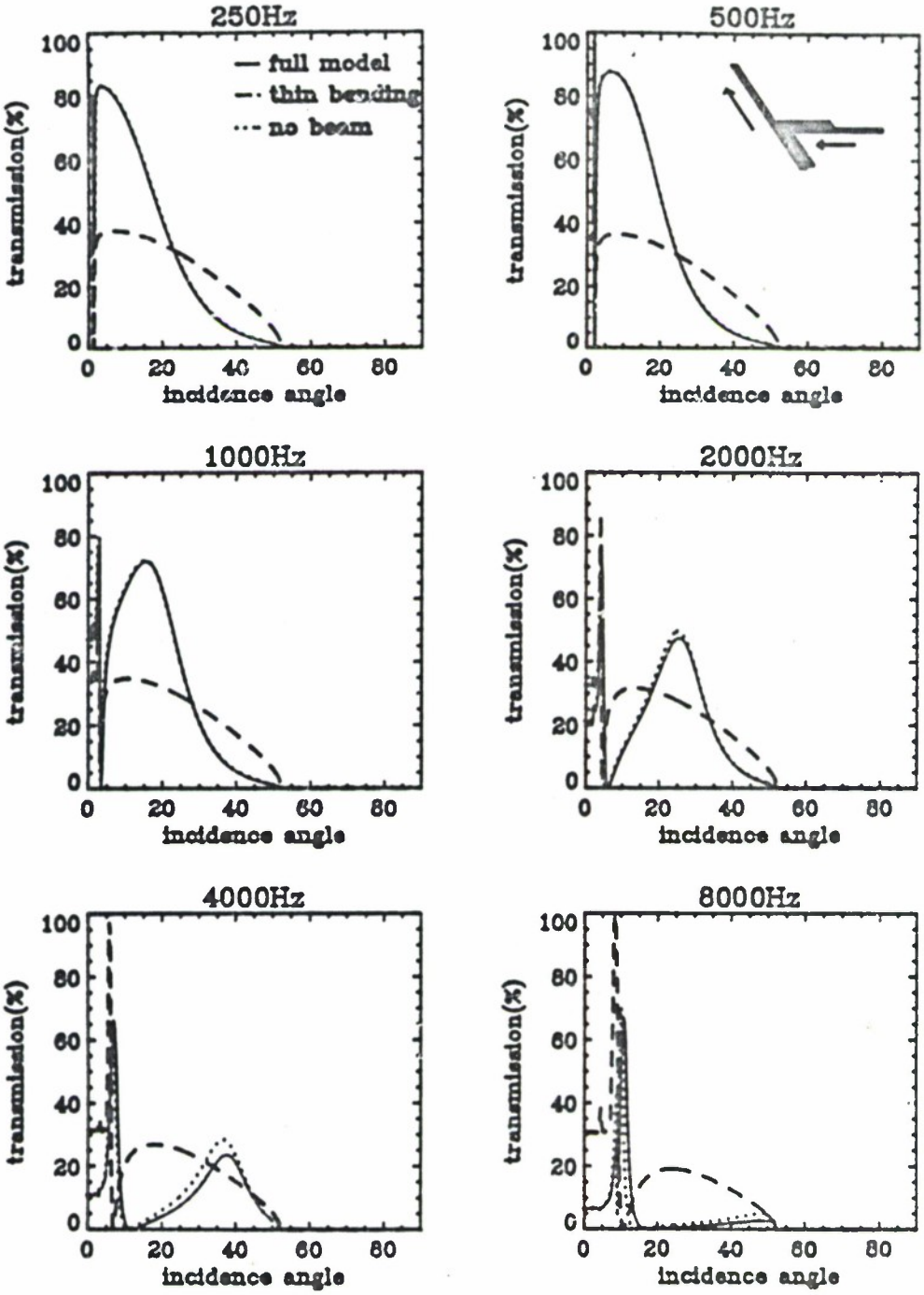

10 May 1991 – A.S.A.N.C.A. Box

Bending transmission coefficients for junction at L13

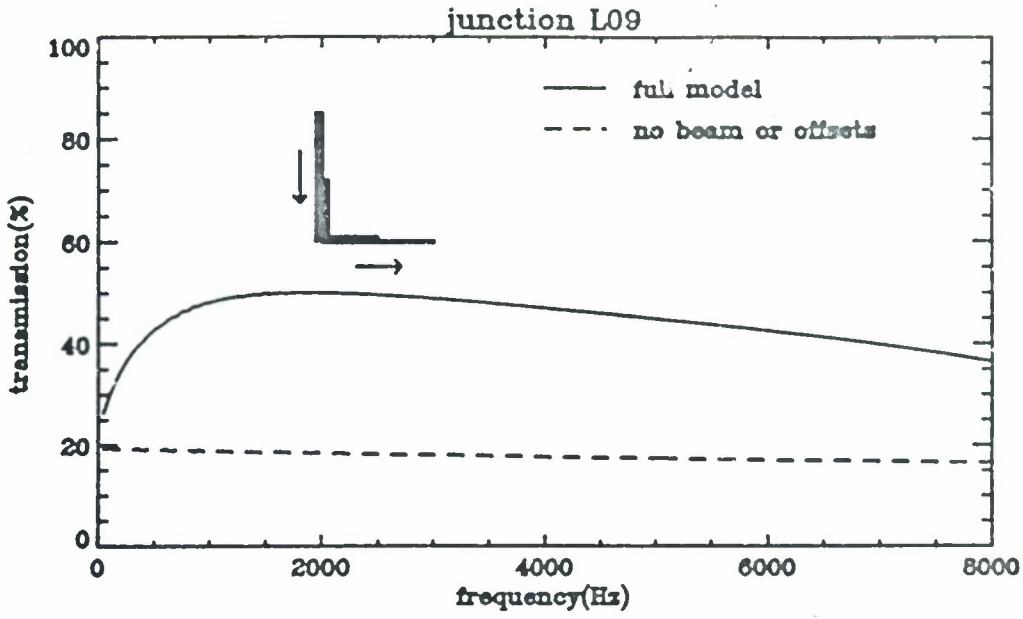

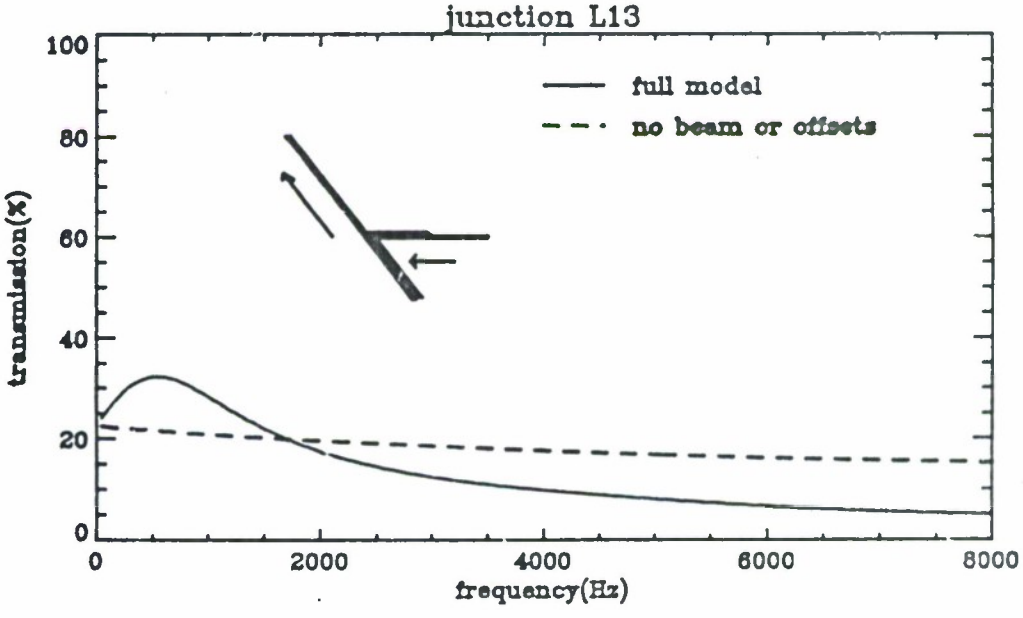

13 May 1991 – A.S.A.N.C.A. Box

Random incidence bending transmission coefficients

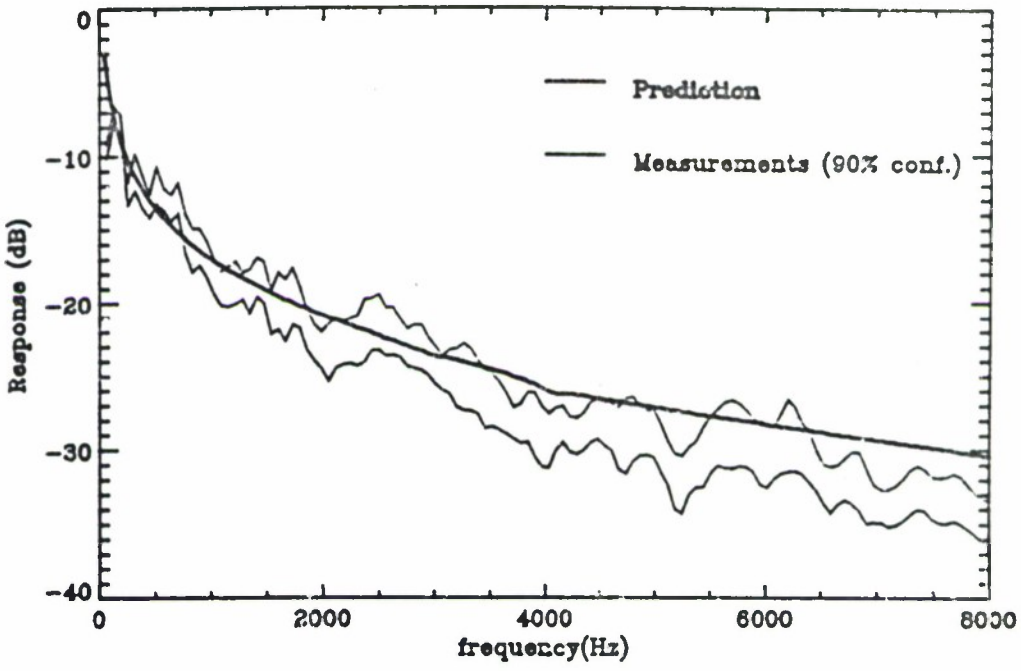

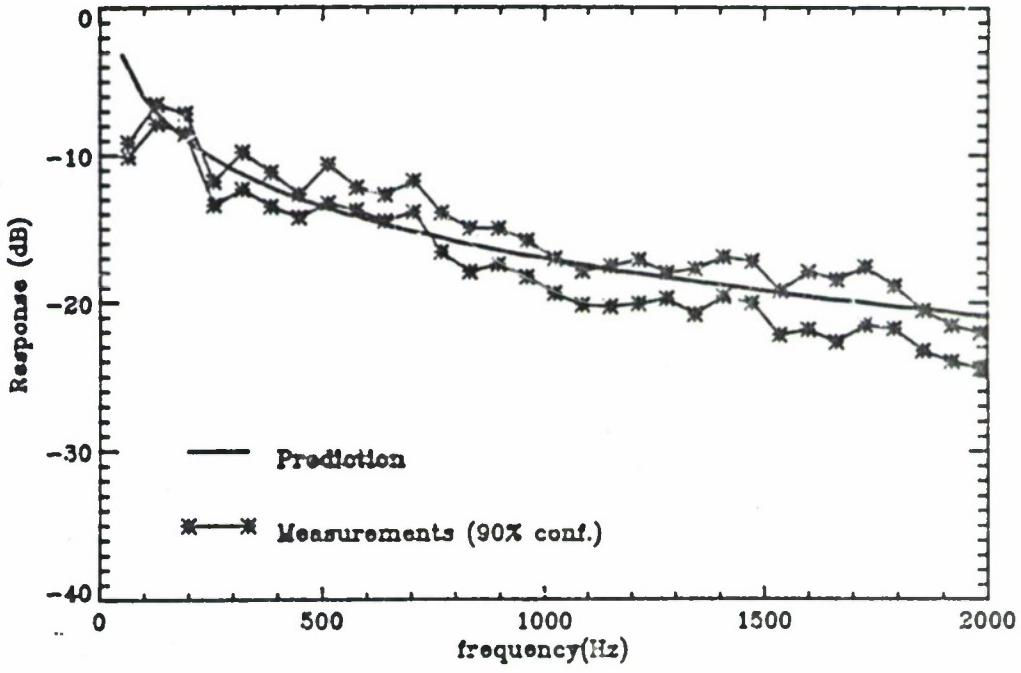

Plate 1 Base 4mm (Vout/Vin)

16 May 1991 – A.S.A.N.C.A. Box

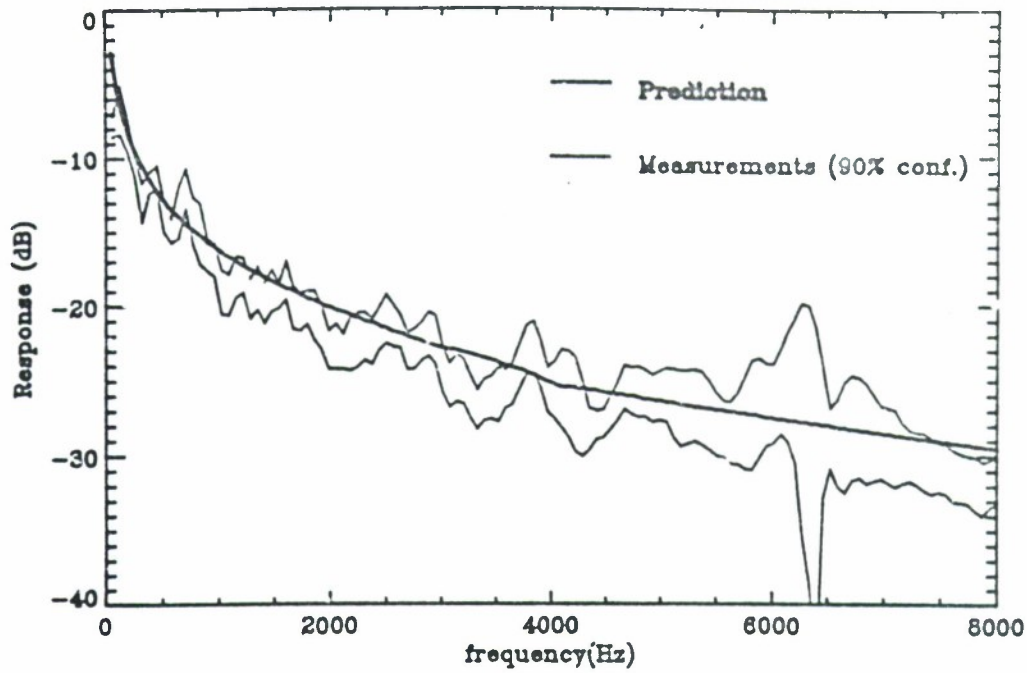

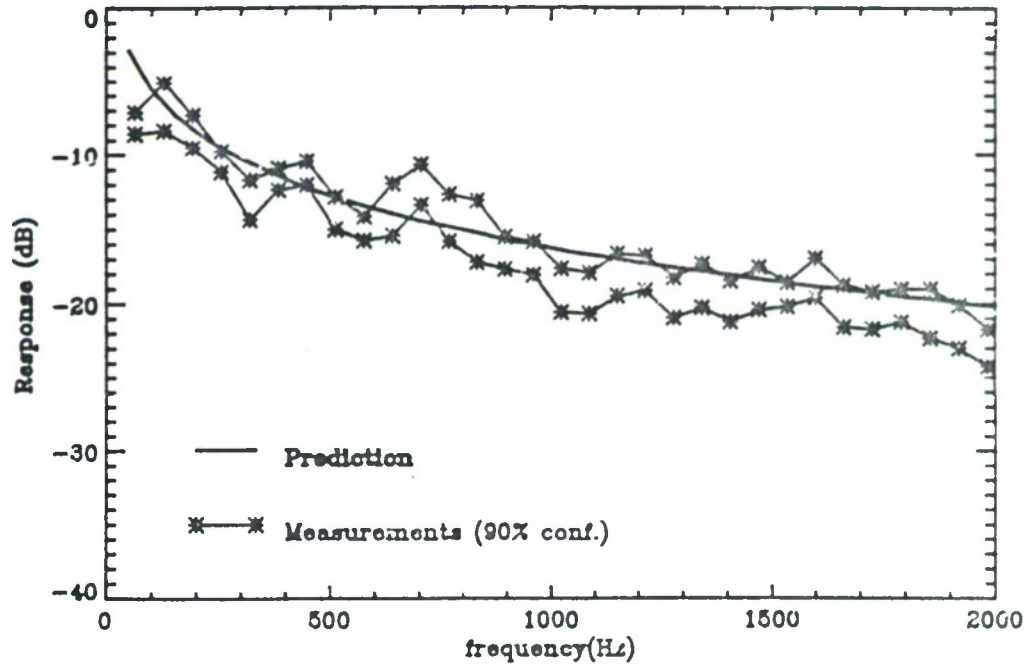

Plate 2 Roof 4mm (Vout/Vin)

16 May 1991 – A.S.A.N.C.A. Box

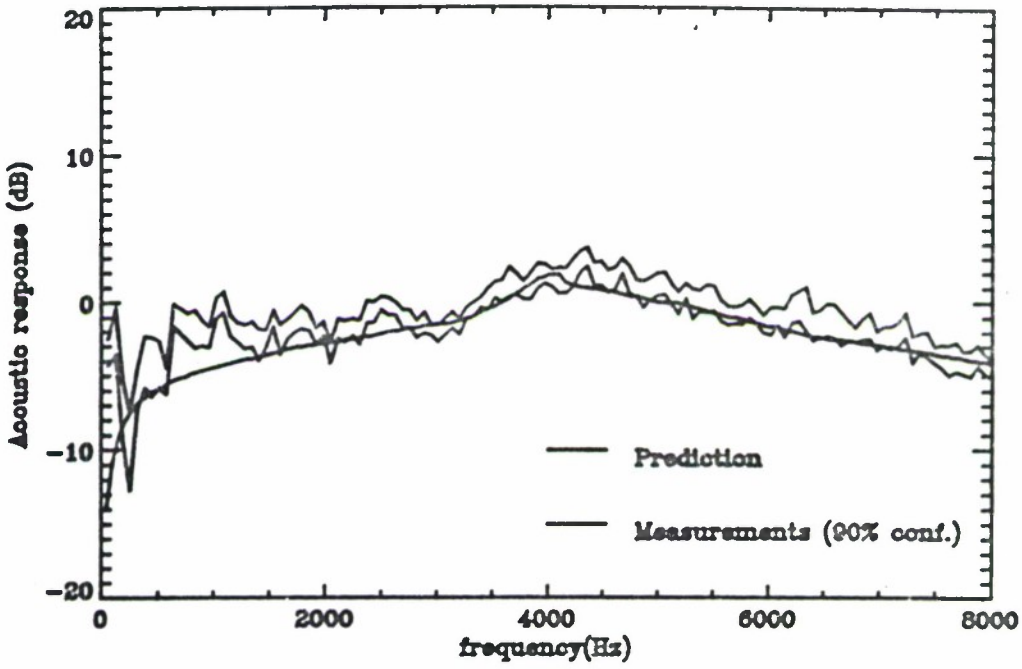

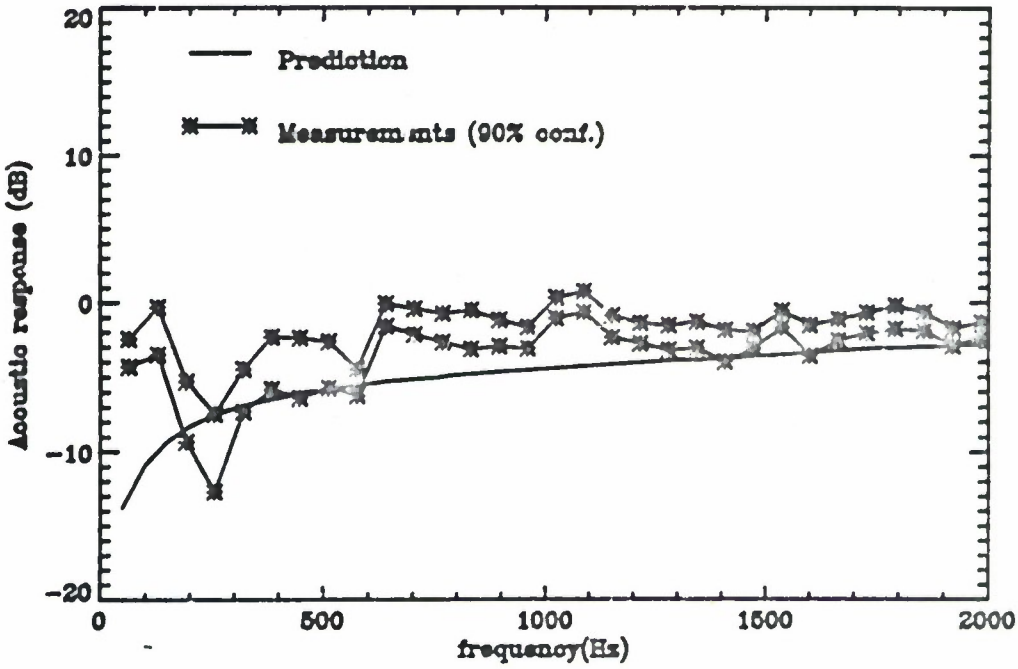

Interior Cavity Pressure (normalised to $\rho c V_{in}$)

22 May 1991 - A.S.A.N.C.A. Box

CONCLUSIONS

- Modern, purely predictive, SEA has been shown to agree well with experimental evidence for the case of an irregular 6 sided box.

- The use and accurate calculation of infinite transmission coefficients is the way forward.

Use of SEA to Predict Structure-borne Noise in Aircraft

Jerome E. Manning
Cambridge Collaborative, Inc.

Presented to
4th NASA/SAE/DLR Aircraft Interior Noise Workshop
Friedrichshafen, Germany

Structure-borne Noise

Structure-borne noise is vibration:

1) generated at one location,

2) transmitted by the structure to other locations, and

3) radiated into the cabin as noise.

Sources of Structure-borne Noise

- Engine vibration
- Mechanical and hydraulic equipment
- Localized excitation by propellor fluctuating pressure fields

Cambridge Collaborative, Inc.

Direct Sound Transmission

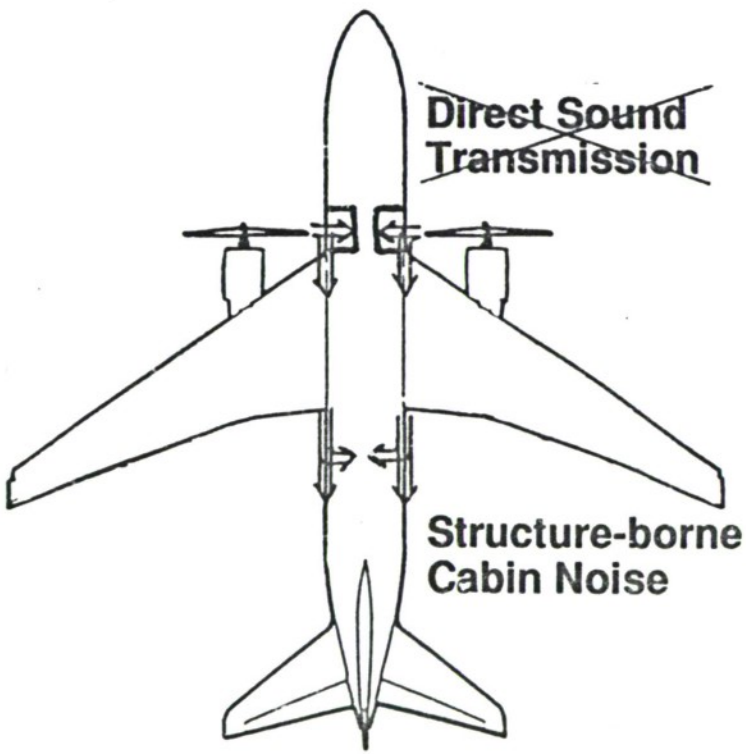

Vibration Containment

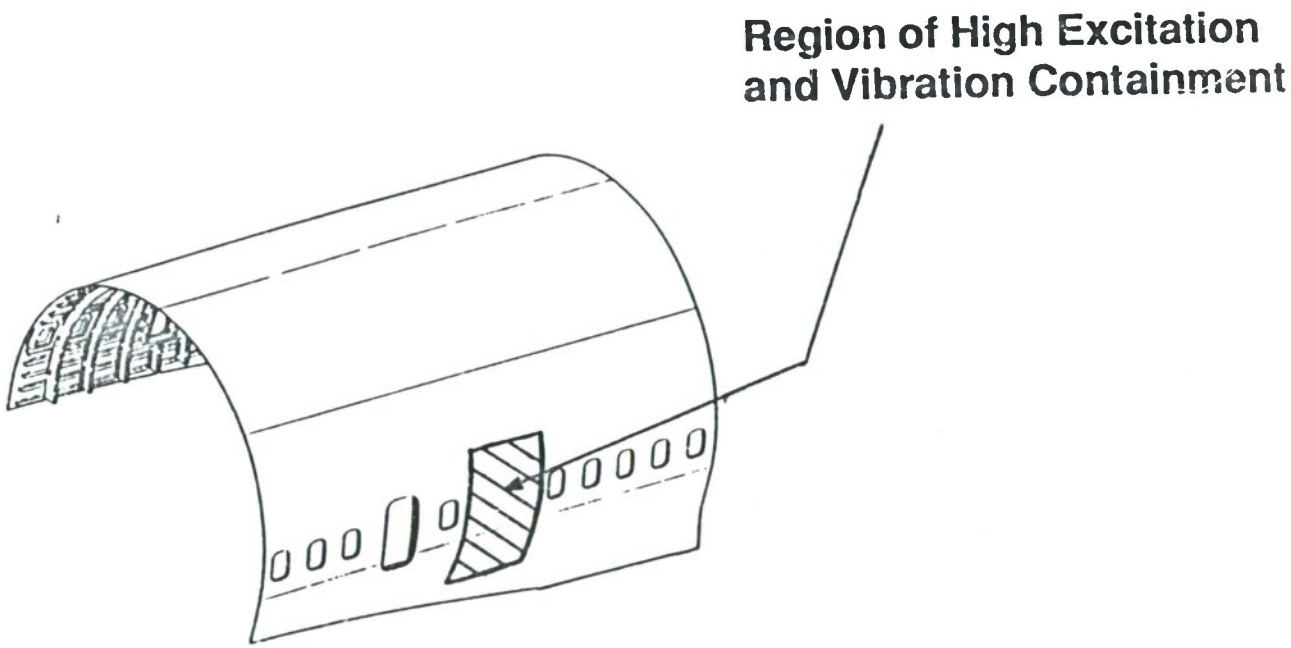

Power Balance

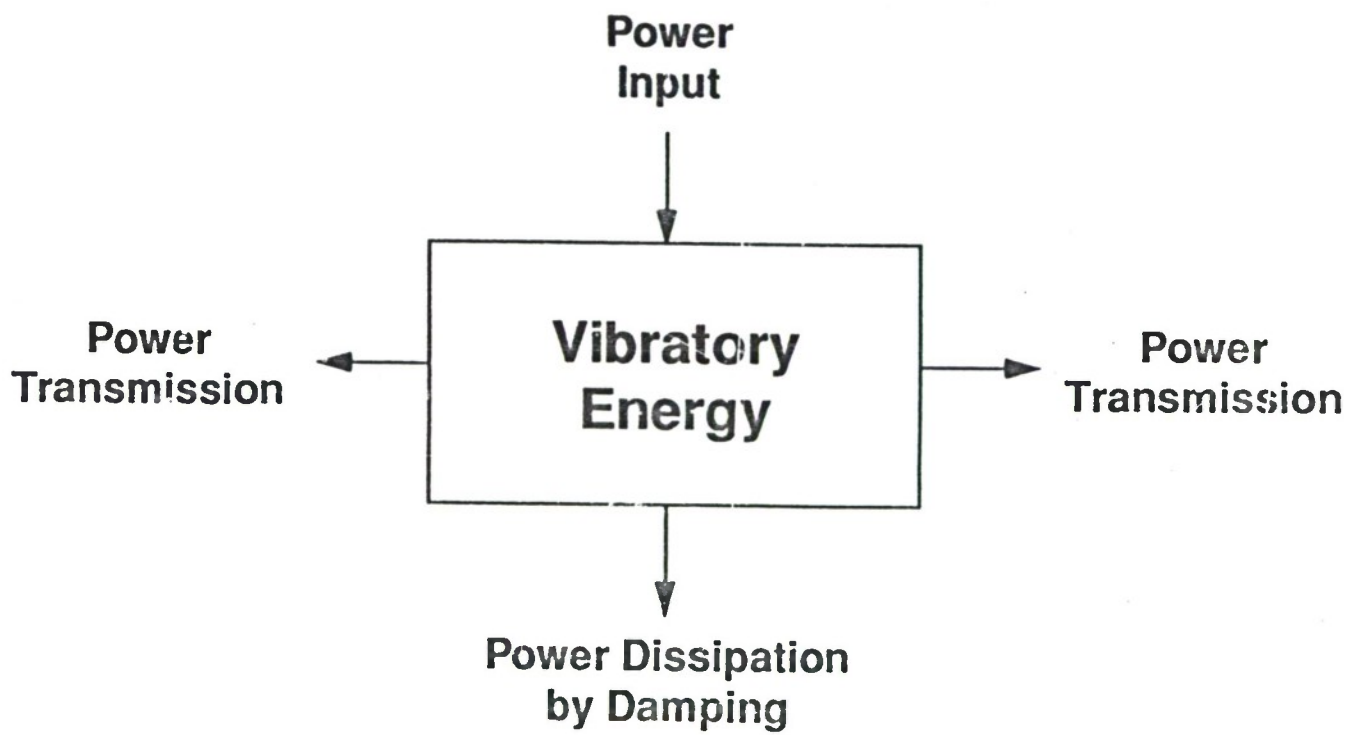

SEA Power Balance Equations

$$W^{trans} + W^{diss} = W^{in}$$

$$W^{diss} = \omega \eta_{diss} E$$

$$W^{trans} = \omega \eta_{coupling} E$$

SEA Energy Flow

$$\frac{W^{trans}}{W^{in}} = \frac{\eta_{coupling}}{\eta_{coupling} + \eta_{diss}}$$

$$W^{trans} \approx W^{in} \quad \text{if} \quad \eta_{coupling} >> \eta_{diss}$$

$$W^{trans} << W^{in} \quad \text{if} \quad \eta_{diss} >> \eta_{coupling}$$

Reducing Structure-borne Noise

Add a damping treatment to increase the damping loss factor of the highly excited region of the fuselage.

Use a vibration blocking treatment to decrease the coupling loss factor between the highly excited region of the fuselage and remaining sections.

Design Considerations

Both damping and vibration blocking treatments add to the aircraft weight.

Options:

1) Design treatments to minimize weight within specified noise reduction goals.

2) Design treatments to maximize noise reduction within specified weight limits.

Coupling Loss Factor

$$\eta_{coupling} = \frac{1}{G_{pt}} \quad \frac{1}{\omega m A} \quad \frac{k_p L_j}{4\pi} \tau_o$$

m = Mass per unit area

A = Containment area

L_j = Perimeter of containment area

τ_o = Power transmission coefficient

Point Conductance

$$G_{pt} = \frac{1}{8} \frac{1}{\sqrt{m}} \frac{1}{\sqrt{EI'}}$$

m = Mass per unit area

EI' = Bending stiffness

Transmission Coefficient

$$\tau_o = \frac{4\,\mathrm{Re}\{Z_s\}\,\mathrm{Re}\{Z_r\}}{|Z_s + Z_r|^2}$$

Z_s = Source subsystem line impedance

Z_r = Receiving subsystem line impedance (including junction impedance)

Cambridge Collaborative, Inc.

Impedance Definitions

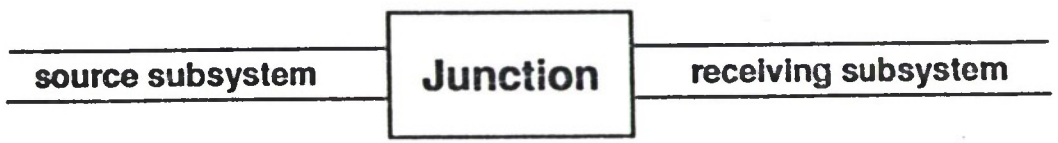

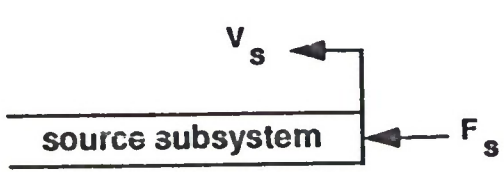

$$Z_s = \frac{F_s}{V_s}$$

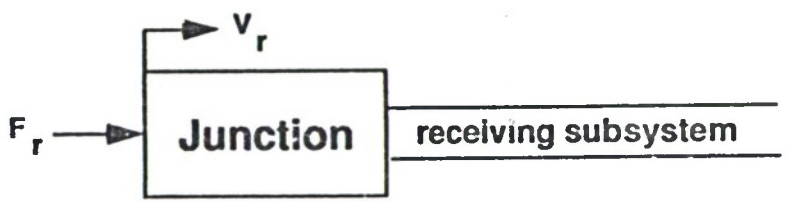

$$Z_r = \frac{F_r}{V_r}$$

Results

Results for the design study were obtained using the computer code SEAM®.

Inputs:

materials
subsystems
junctions
excitations
parameters

Outputs:

vibration levels
acoustic levels
modal energy
power flow

Conclusions

The SEAM® program makes it possible to use SEA to study a wide range of design options and noise control treatments.

Acoustic Design Analysis

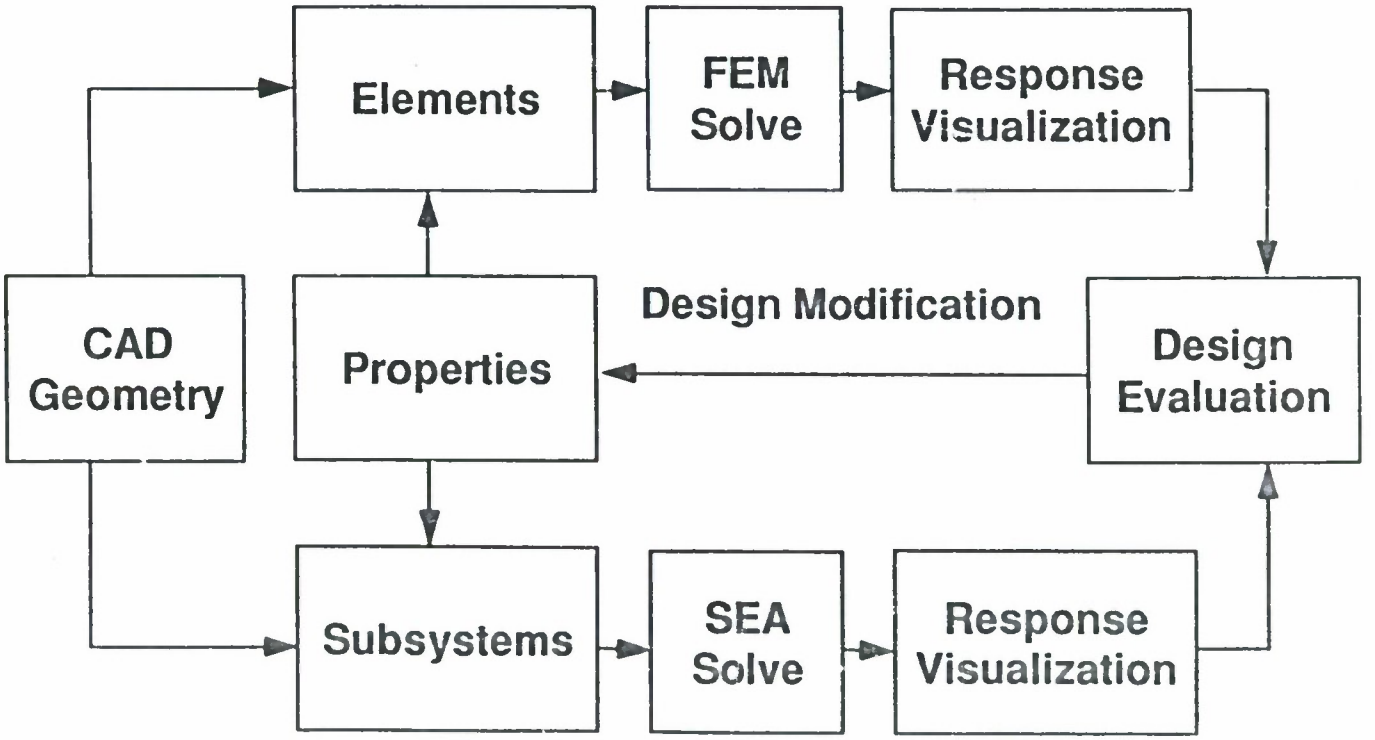

DGLR / AIAA-92-02-092

Advanced Study for Active Noise Control in Aircraft (ASANCA)

I.U. Borchers, Dornier Luftfahrt GmbH
U. Emborg, Saab Aircraft Division
A. Sollo, Alenia
E.H. Waterman, Fokker Aircraft B.V.
J. Paillard. Matra Sep Imagerie et Informatique
P.N. Larsen, Reson System A/S
G. Venet, Metravib, R.D.S.
P. Göransson, FFA
V. Martin, CNRS
et al

DGLR/AIAA 14th Aeroacoustics Conference
May 11-14, 1992 / Aachen, Germany

ADVANCED STUDY FOR ACTIVE NOISE CONTROL IN AIRCRAFT (ASANCA)

Ingo U. Borchers [1]
Urban Emborg [2]
Antonio Sollo [3]
Elly H. Waterman [4]
Jacques Paillard [5]
Petsr N. Larsen [6]
Gerard Venet [7]
Peter Göranseon [8]
Vincent Martin [9]
et al

ABSTRACT

A first broader European study on aircraft interior active noise control is in progress involving 22 organizations located in 11 different European countries. The main tasks and goals of the program are described in this paper and selected preliminary results are presented. The study includes first detailed aircraft interior noise and vibration measurements in flight and on the ground on four different partner aircraft. In addition, related initial noise calculations without and with active noise control are conducted. Furthermore, first development work on advanced actuators and sensors are performed and demonstrator active noise control units for planned initial flight testing are developed. The results obtained so far show that active noise control may be an effective mean for reducing the critical low frequency aircraft interior noise. First full scale data evaluation indicated, for example, possible noise reductions up to 15 to 20 dB. However, for future practical aircraft applications, further detailed research on this topic is required for optimum control system selection as well as system weight and size minimization.

1. INTRODUCTION

Initial assessments indicate that active noise control, the introduction of anti-noise cancelling the original noise, has a promising potential for solving the critical low frequency interior noise problem of fixed wing and rotary wing aircraft. The problem is caused by the intense low frequency noise of, for example, the aircraft propellers or helicopter rotors, which is difficult if not impossible to reduce applying light-weight and standard noise reduction measures.

The use of the active noise control technique is based on an active noise control system. The system consists of different sensors providing synchronous noise source signals and measured residual interior noise data. The main component is a computerized control unit which uses these data as inputs and which derives optimized output control signals. The latter are fed to a set of actuators generating the required anti-noise fields for primary noise field reduction. A scheme of such a possible system is shown in Figure 1. Based on the low frequency content corresponding to large wave lengths and the deterministic character of the exterior source noise, very high noise reductions at the critical low frequencies, above 10 dB, appear possible for aircraft applying this noise control technique.

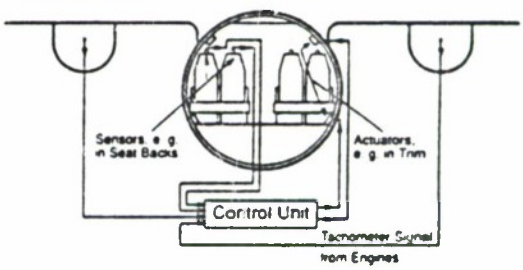

Figure 1: Scheme of possible active noise control system

1) Dornier Luftfahrt GmbH, Friedrichshafen, Germany
2) Saab Aircraft Division, Linköping, Sweden
3) Alenia, Naples, Italy
4) Fokker Aircraft B.V., Schiphol, The Netherlands
5) Matra Sep Imagerie et Informatique, St. Quentin en Yvelines, France
6) Reson System A/S, Slangerup, Denmark
7) Metravib R.D.S., Ecully, France
8) FFA, The Aeronautical Research Institute of Sweden, Bromma, Sweden
9) CNRS, Centre National de la Recherche Scientifique, Marseille, France

In order to meet this goal, however, extensive advanced research is required, for example, in the field of aircraft interior acoustics including vibro/acoustic interactions, for the development of advanced actuators and sensors, and for optimizing control unit algorithms and related hardware components. This is needed to meet the extreme constraints given by the complex aircraft environment, for example, minimum control unit weight and size, minimum number of actuators and sensors, easy implementation of these components into the aircraft interior, adaptability to instationary flight conditions, various safety aspects and others.

The major part of the present program is related to fixed wing aircraft and has the main goal to initiate this required research in greater detail taking the different aircraft constraints into account. In particular first information on feasible optimum active noise control systems for future practical applications shall be identified and demonstrated during first flight testing. Also information on other important topics shall be obtained such as practical noise reduction potential. In addition, detailed baseline information for further improving this technology shall be established. As a second part, a workprogram on rotary wing aircraft interior noise control is included in the project attempting to identify, for example, the most promising research methods that are available for helicopters.

In the following the main tasks of these program parts are briefly described. After this, selected interesting experimental and theoretical result of the fixed wing aircraft work are presented and discussed.

2. PROGRAM MAIN TASKS AND CURRENT STATUS

The program includes first detailed experimental as well as systematic theoretical work. For the fixed wing aircraft, both corresponding full scale aircraft studies and laborstory investigations are considered. The program part on rotary wing aircraft includes related laboratory work, but also some full scale ground testing.

2.1 Fixed Wing Aircraft Related Work

The main tasks of the fixed wing aircraft related work can be described and summarized as follows:

- Summary and continuous evaluation of pertinent active noise control work relevant for this study
- Detailed experimental surveys of interior sound fields and tests for determining optimum control systems in selected partner aircraft
- Theoretical description of interior sound field and performance of supporting active noise control calculations for selected aircraft
- Data evaluation and preselection of optimum control system configurations and development of demonstrator control units including hardware and software realization
- Integration of complete demonstrator control systems and initial testing of these systems in one of the partner aircraft
- Evaluation of results and recommendations for future control system improvements

The testing and the theoretical work are performed on four different partner aircraft, i.e., Dornier 229, Saab 340, ATR 42 and Fokker 100. These aircraft were selected in order to identify general noise control information and to show that active noise control is feasible also in aircraft with large differences in acoustical character. The Dornier 228 is, for example, a propeller aircraft with an unpressurized fuselage with a rectangular cross-section. In contrast, the Saab 340 and the ATR 42 are pressurized propeller aircraft with a circular fuselage and the Fokker 100 is a jet aircraft with aft mounted engines. In all aircraft low frequency tones are present which contribute to the overall noise levels. This makes these and other aircraft especially suitable for the application of active noise control.

The testing task includes also the adaptation and development of special test data processing software and first limited laboratory development on advanced actuators, which may be integrated into the aircraft trim panel with very low weight impact. In addition, laboratory tests on alternative noise control approaches, e.g. noise control in the cavity between fuselage and trim panel and active damping are planned.

The noise control calculations are primarily based on finite element analysis and advanced analytical methods. In addition numerical modeling analyses are conducted based on models with reduced numbers of degrees of freedom. The calculations are performed for the same test aircraft and simplified structures as used in the experiments and shall provide detailed theoretical inputs for selecting optimum active noise control approaches, including optimum number and locations of actuators and sensors for given control systems.

2.2 Rotary Wing Aircraft Related Work

Following a critical review of available relevant knowledge and interior noise source identification, the rotary wing aircraft work covers the following main tasks:

- Design, manufacturing and testing of a model helicopter fuselage
- Assessment of prediction codes and comparison with experimental results
- Laboratory validation of a new noise transmission path identification method
- Review and apprsisal of active noise control methods for helicopters

The model helicopter fuselage has dimensions of approximately 2 m x 1 m x 1.5 m and is excited during the tests by a mechanical shaker and plane acoustic waves. The prediction code assessment considers in particular finite element, boundary element and statistical energy analysis methods.

The experimental validation of the new noise transmission path identifaction method is conducted on a ground based helicopter fuselage and includes the simulation of at least six flight conditions with known ratios of airborne and structureborne components.

2.3 Current Status

The project started July 1, 1990, and since then progressed extremely well. For example, for the fixed wing aircraft related part, all planned tests in the selected partner aircraft and most of the planned theoretical work could be performed and finished as scheduled. In addition, successfull design reviews were held on the developed demonstrator control systems. One of the control systems could be already successfully tested in a full scale aircraft fuselage test section on the ground and will be flight tested very soon as planned. Similar progress has been made for the rotary wing aircraft part. Most of this work could be finished in time including all model helicopter testing and related theoretical work.

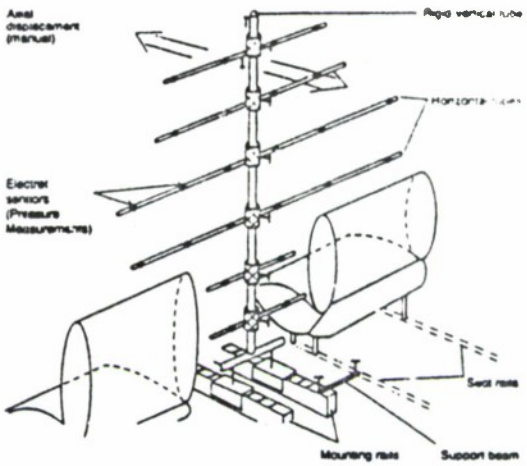

Figure 2: Microphone antenna for in-flight interior noise surveys

3. AIRCRAFT TESTS AND RELATED RESULTS

The experiments on the different partner aircraft mentioned in Section 2 have played an important role in the present project. It was considered as a very direct method to arrive at feasible control system configurations for later flight demonstration.

The measurements consisted of two parts. First, the in-flight primary noise fields in the aircraft were recorded in great detail to clearly identify the noise distributions which need to be controlled. Secondly, extensive ground tests were conducted for various positions of secondary sources to determine an effective secondary sound field for noise cancellation. After the tests, the data were evaluated and related optimum secondary source configurations including source number and source positions were selected.

3.2 Aircraft Flight Tests

For performing these tests, special test equipment was provided including a movable antenna, which could be equiped with up to 25 microphones, see Figure 2. The antenna was adaptable to the size of the four different aircraft and was located at up to about 20 different sections equally spaced in flight direction. With this the noise distribution including amplitude and phase information of the various propeller or engine tones could be in detail measured in the entire passenger cabin (Dornier 228 and Saab 340) or in an extended part of it (ATR 42 and Fokker 100). In addition, a large number of accelerometers, typically 80, were located on different primary structure locations and on the trim panels for identifying operating vibration deflection shapes. Furthermore, several other informations were recorded such as propeller or engine tachometer signals, relative propeller angle variations and external noise distributions. These data were used to separate the recorded data into left and right propeller or engine contributions, for optimizing the control system design and for planned interior noise predictions.

A typical result of the noise measurements is given in Figure 3. The figure shows the interior noise level contour of the Dornier 228 in four vertical cross-sections and in the plane of the passengers heads. In addition, Figure 4 show fuselage vibrational modes as identified from vibration data measured also during this test. These and other data provided first inputs for selecting promising secondary source position tested after the flight measurements on the ground.

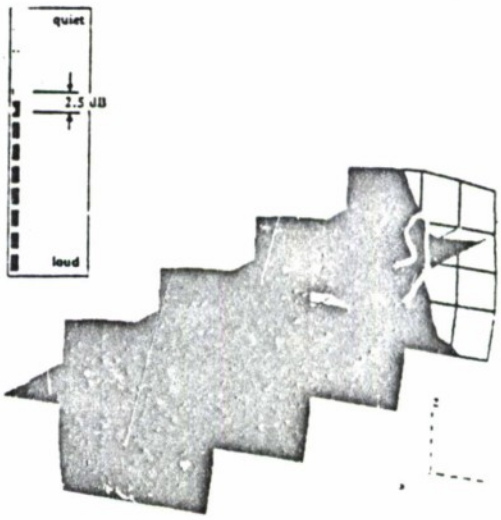

Figure 3: Noise distribution measured in Dornier 228 (1xBPF)

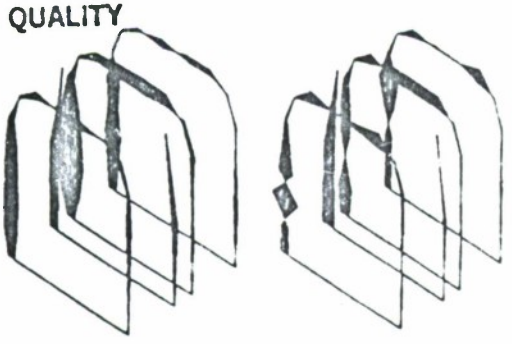

a) f = 102 Hz b) f = 204 Hz

Figure 4: Fuselage vibrational modes of Dornier 228 identified by measurements

3.2 Aircraft Ground Tests

During the ground tasts, in each aircraft typically sround 45 secondary sources positions were tested. As sources essentially loudepeakers but eiso shekers were used ae s first step investigetion. In two eircraft (Dornier 228 snd Fokker 100) the loudspsakers were partially integrated into the trim panels or mounted in closed wooden boxas and then attsched to these pensis. In addition, loudspeaker boxes pieced on the fioor wers teeted. For the shsker, promising positions on the primary structure snd on the trim panels were selected. The noise generatad by theee sources was messured during these tssts in the plsne of the passenger heeds using a specisl horizontai antenne with 25 microphonee. Two eelected photographe of thie teet set-up ere shown in Figures 5 end 6. In the two other eircraft (Saeb 340 and ATR 42) ths reciprocity technique was appiied for the loudspeaker test to study the iargest number of sources end to reduce tssting time. The technique was confirmed by referencs teets snd involved simiier meesurement positions as for the other sircreft.

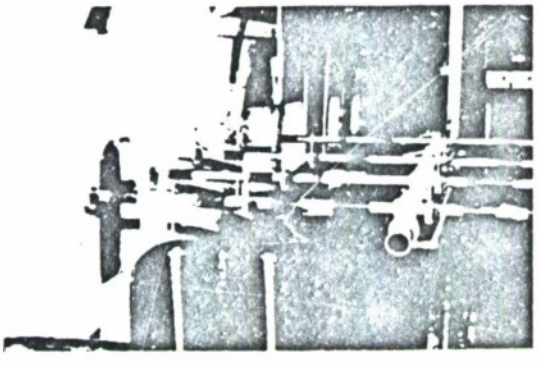

Figurs 5: Horizontal microphone antenna for actuator ground tssts

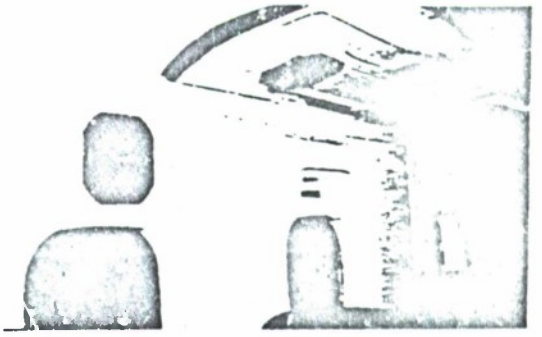

Figure 6: Integrated epeakers for first actuetor testing in Dornier 228

During sil tests the source and microphons signals and the reisted transfer functions were determined. From these data the amplitude and phase distribution of the secondary noise field in the plane of the passenger heads of sach source was sxtracted at the frequencies of interest of the propeliers or engines. Two seiected exampies of these results srs given in Figurss 7 and 8. Figur 7 ahows the secondary sound fieid in the complete paessnger cabin of the Dornier 228 generated by e loudspeeker iocated et the reer weil of the cabin. As may be eeen the sound fieid hes a typicai stending wave behaviour resembiing a iongitudinsl mode. Figure 8 presents the secondary sound field in the rsgion of the six sft seet of the Fokker 100 produced by a loudspesker located below a seat at the right hand cabin side. In this case, a typicel running weve behaviour of the eound fieid may be noted. Thus, as expected, principally differsnt types of secondary sound fields msy be generated end the selection of optimum eecondary source configuratione must be carefully performed.

3.3 Data Evaiuation

In the prssent study the determination of optimum secondary source configurations for the different aircraft was to a iarge extent based on the flight end ground test data deecribed before. For the corresponding evaiuation s special computer program wea deveioped handling effectiveiy tne estabiiehed iarge data base.

The computsr program used en optimization algorithm for the ampiitude and phase optimization of the sscondary sourcse, togethar with the data of the primary fieid and the iarge number of different secondary fieids. For seiected combinations of source positione the most favourable secondary sound fieid generating the highest noise reduction ' s caiculated. During later evaiuations aiso the power consumption of the different sources was considered. Ae the number of poasibiiitiee of combining ail tested secondary source positions was virtuaiiy infinite the real optimum configuration for active noise controi could not be detsrmined. However, severai practical approaches couid be applied to obtain configurstione near thie optimum. In addition, the sensor microphone iocatione could be optimized in ssvsrai ways using tha deveioped computsr program.

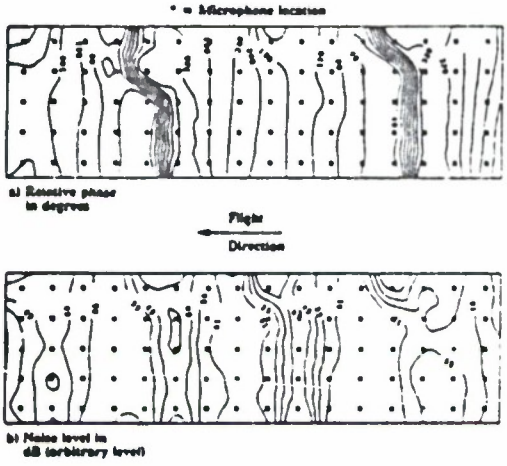

Figure 7: Measured secondary noise field of a speaker at the rear cabin wall of the Dornier 228

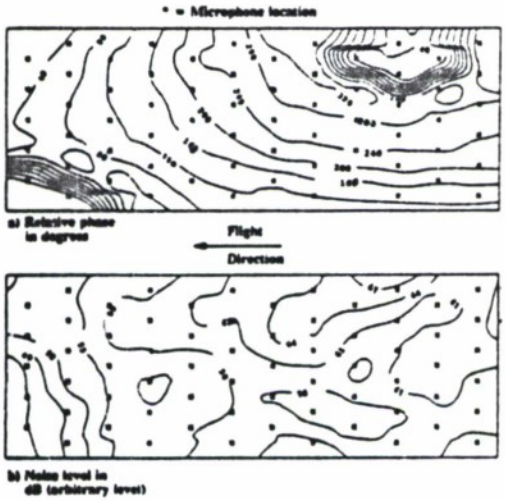

Figure 8: Measured secondary noise field of a speaker below a seat at the right hand cabin side of the Fokker 100

In Figure 9, selected potential noise reductions obtained by applying this evaluation for secondary loudspeaker sources is plotted versus the source number. The data correspond to the fundamental propeller or engine tone and present average values of 48 sensor microphones in the plane of the passenger heads. Additional results corresponding to 32 sources and the total microphone measurement plane are given for the Fokker 100 in Figure 10. It follows from these results that active noise control may be very effective in the various aircraft and may produce noise reductions up to 20 dB. The somewhat lower noise reduction identified for the Dornier 228 may indicate that rectangular fuselages are possibly somewhat less suitable for this technique than typical circular ones. However also for this aircraft interesting noise reductions up to 15 dB were found.

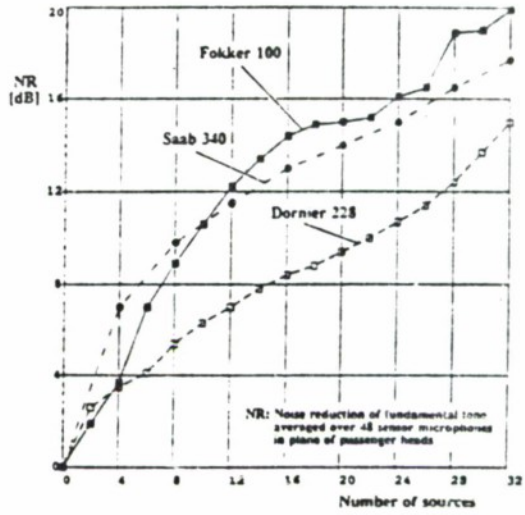

Figure 9: Determined noise reduction (NR) for active noise control based on actuator ground testing

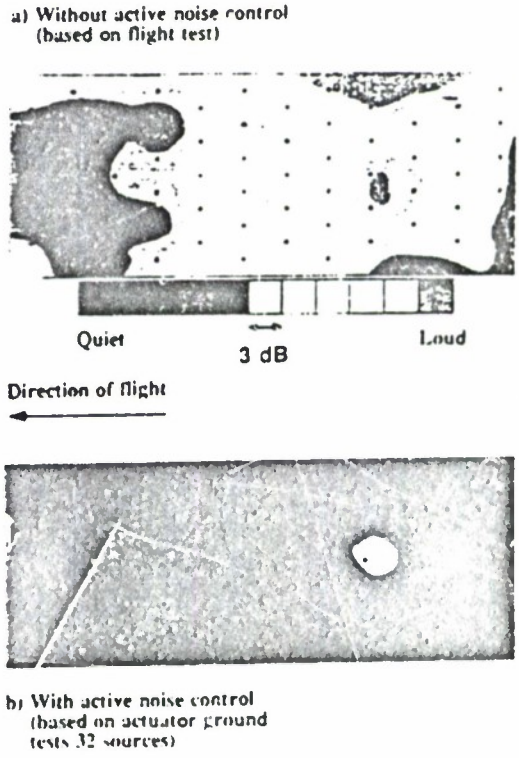

Figure 10: Determined noise levels in the plane of passenger heads of the rear part of the Fokker 100 without and with active noise control

4. FINITE ELEMENT CALCULATIONS AND FIRST RESULTS

The finite element calculations within this program are divided into two different tasks. One task is concerned with primary interior noise predictions (primary response), the other is related with interior active noise control simulations (secondary response). The first part was in detail performed for the Dornier 228 and Saab 340. It provides the required analysis data base for the related second part calculations and has been to a large extent concluded. The second part calculations are still in progress.

The primary response analyses consisted of the following work:

- Description of external excitation field
- Aircraft fuselage and cavity finite element modelling
- Eigenvalue analyses of complete coupled system
- Response calculations for external field excitation

In the following these topics are briefly described and selected results are given.

4.1 External Excitation Fields

For the Dornier 228 the external acoustic pressure was measured during the flight tests with 10 outside microphones at each side of the aircraft for a given favourable synchrophaser setting. Based on these data, which were dominated by propeller noise, related left and right hand side pressure and phase distributions were determined as inputs for the planned response calculation. Figure 11 shows as an example the determined pressure field of the first blade passage frequency tone of 102.0 Hz (1xBPF) at the right side of the aircraft. As can be seen, the pressure has a strong peak near the plane of the propeller. This and the related left hand side pressure field was used together with the corresponding phase distribution as excitation force field for the 1x BPF response calculations. In addition it was used as approximate force field for frequencies below 1xBPF and up to about 1.5xBPF to obtain also for these frequencies first response information.

For the Saab 340 the external acoustic pressure field is also dominated by propeller noise. The pressure field was predicted using an available propeller noise prediction code and taking installation effects into account. The fundamental propeller tone has a frequency of 84.7 Hz. For the first response calculations the pressure field was calculated for the plane of the propellers around the circumference of the aircraft. It was then assumed to be constant in axial direction over a width of about 0.5 m including the propeller plane based on the strong peak of the pressure field around the plane of rotation. Since the pressure field of each propeller is not stationary in space both real and imaginary parts were calculated. The structural responses were analyzed correspondingly and thus consist also of these parts.

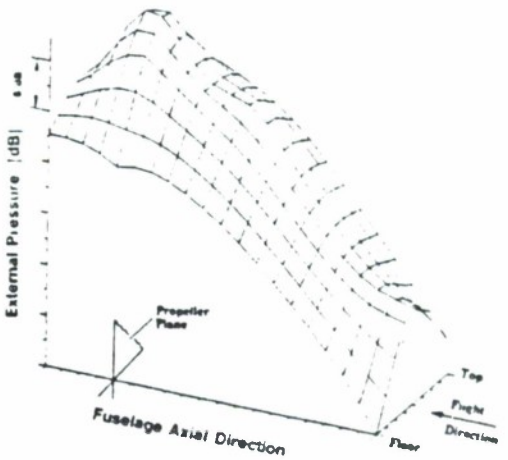

Figure 11: Applied external pressure field of Dornier 228 based on test data (fuselage right side, 1xBPF)

4.2 Finite Element Models

For both aircraft, the finite element idealization consisted of seperate models for the fuselage structure and the enclosed air cavity, which for the analyses were correspondingly coupled.

For the Dornier 228 the full passenger compartment was idealized. For the structural model detailed design influences were taken into account such as local stiffeners wall panels, windows etc., in addition to standard frame, stringer and floor constructions. A view of this model is shown in Figure 12a. The model was set-up to predict structural modes up to 350 Hz. The acoustic cavity was idealized in a way to represent especially the plane of the passenger heads and to get accurate eigenvalue results up to about 400 Hz. A view of this model is shown in Figure 12b.

The structural model of the Saab 340 was built up by two sub-nets each representing one half of a fuselage section of 3 m length located in the main propeller noise excitation region. A picture of this model including similar design details as the model of the Dornier 228 is given in Figure 13a. The model of the acoustic cavity included four sub-nets and covered the entire cabin length. A view of the total cavity model is shown in Figure 13b. Using sub-nets for the structure and cavity the calculation time for each step could be reduced to a reasonable amount.

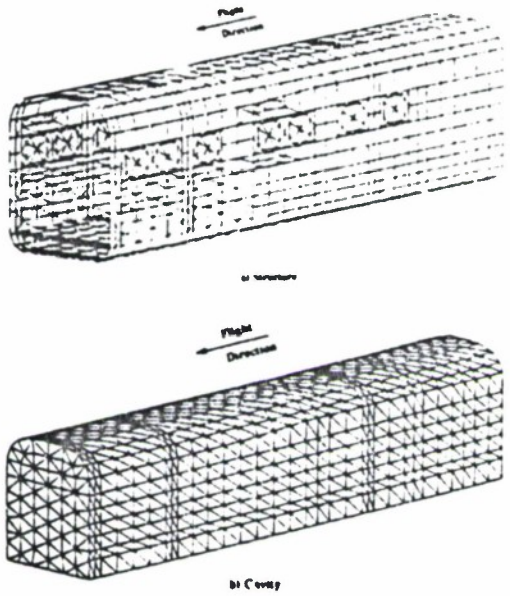

Figure 12: Dornier 228 fuselage and cavity finite element idealization

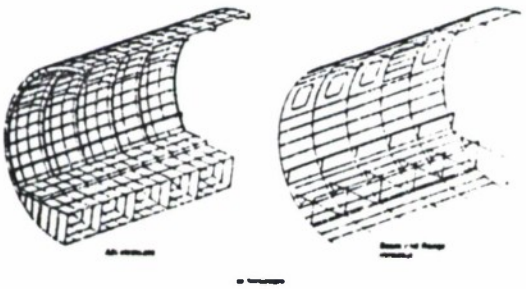

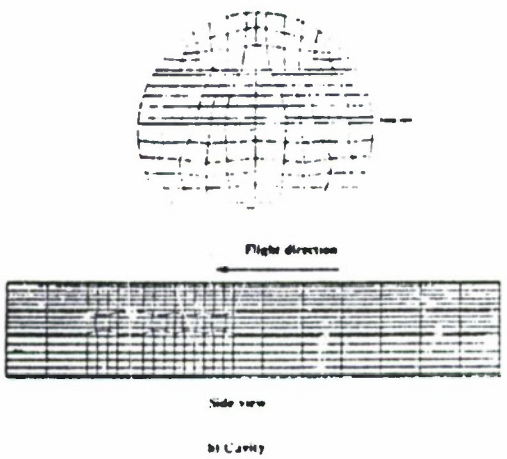

Figure 13: Saab 340 fuselage and cavity finite element idealization

4.3 Eigenvalue Analyses

For the Dornier 228, uncoupled eigenvalue analyses for the structure and cavity were performed. The model for the structure and cavity had about 22000 and 14000 degrees of freedom which were reduced for this analyses to about 2400 and 2100, respectively. The analyses provided the modal basis for the coupling procedure and yielded important uncoupled mode information necessary for interpreting the coupled results. About 300 structural and 250 cavity frequencies were calculated for frequencies up to 409 Hz and 470 Hz, respectively. Two typical results are shown in Figure 14. The used coupling procedure was a modal synthesis of the uncoupled structure and cavity modes. Both systems were connected at their common interface area at 950 points. The related coupled analyses yielded coupled system modes as linear combination of all uncoupled modes with different weighting and covered eigenvalues up to 470 Hz. The resulting mode-shapes were classified as structure-dominated modes, cavity dominated modes or simply as coupled modes if both structure and cavity uncoupled modes were about equally involved.

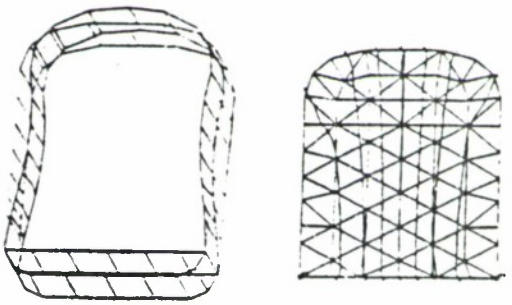

Figure 14: Selected uncoupled structure and cavity modes of Dornier 228

The eigenvalue analyses of the Saab 340 followed similar steps. First the eigenmodes of each of the sub-structures were extracted. Since the frequency considered was up to about 400 Hz, approximately up to about 150 eigenmodes were obtained. These eigenmodes then entered the equations at the next higher level of substructure hierarchy as the degrees of freedom of the substructures. In the last step the problem was solved at the main net level and the lowest 255 coupled system eigenmodes were calculated. With this modal synthesis the total number of degrees of freedom of about 60000 was reduced to about 5000. The obtained eigenmodes were classified similar as described above. The structural part of an identified important coupled mode at the frequency f = 85.5 Hz of the Saab 340 is shown as example in Figure 15.

4.. Response Analyses

The response analyses were performed for the exterior pressure fields as described before.

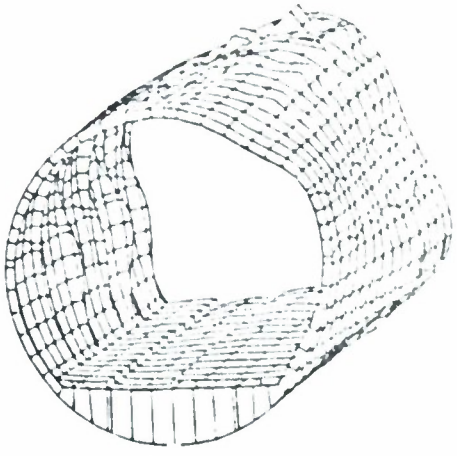

Figure 15: Structural part of coupled Mode 17 of Saab 340 (f = 85.5 Hz)

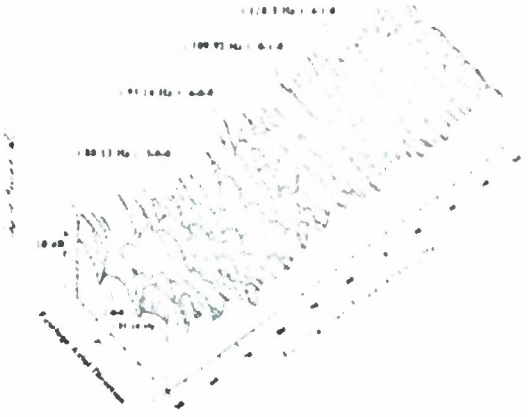

Figure 17: Predicted frequency dependent average noise levels inside Dornier 228 versus fuselage axial direction

For the Dornier 228 corresponding calculations were conducted for frequencies between 50 Hz and 150 Hz to show all critical resonances which may be excited in this frequency range. An example of the obtained results is given in Figure 16. The figure shows predicted interior noise spectra averaged over all points of the whole cavity. Hereby no modal damping or a damping of 0.8%/10% for structure-dominated and of 0.1%/0.2% for cavity-dominated modes was assumed. Figure 17 presents a 3-dimensional plot of individual spectra averaged over all points in different 33 cross-sectional planes in axial direction. Furthermore, in Figure 18 predicted pressure distributions for 102 Hz and 103 Hz excitation are given for the plane of the passenger heads. From these and other results indications were found that the structure may strongly influence the cavity response. Also the tendency was identified that especially transverse mode govern the resulting overall sound pressure level in the front cabin section.

For the Saab 340 generalized responses for the different modes where calculated for 1xBPF and 2xBPF. Furthermore, acoustic and structural responses for these excitation frequencies where predicted in form of sound pressure contours and deflection shapes. Corresponding results are given in Figures 19 to 21. From the generalized response diagram shown in Figure 19 it follows that the 1xBPF response is dominated by only a few modes. Most of these modes were classified as strongly coupled modes with the exception of Mode 20 which was deemed to be a cavity-dominated mode. Since all of the interesting modes showed a more or less clear side-side behaviour, the related response in the cavity can be expected to look also like a side-side pressure variation. The 1xBPF response due to left propeller excitation is dominated by the same modes as the one due to right propeller excitation with one addition, Mode 22. This mode, which is a symmetrical structural mode of the S4 type (4 circumferential wave lengths), gives a local pressure increase close to the top of the cavity which might result in a distortion of the otherwise dominating side-side behavior. Figure 20 confirms that the acoustic response at 1xBPF is clearly one of the side-side type, i.e. high pressure at the sidewalls, with a tendency of a decaying pressure towards the rear of the cabin. The related structural response of the frames in the propeller plane, is a combined A4/S4 response in the real part and a pure A4 (anti-symmetric) in the imaginary part, see Figure 21.

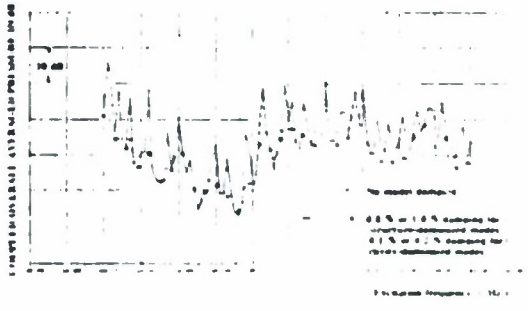

Figure 16: Predicted overall average interior noise of Dornier 228 versus frequency (coupled response)

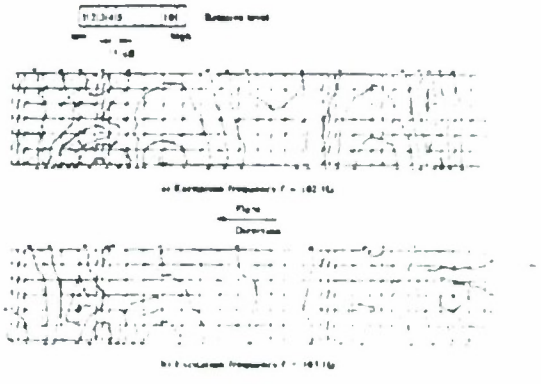

Figure 18: Calculated noise distribution in the plane of the passenger heads of Dornier 228

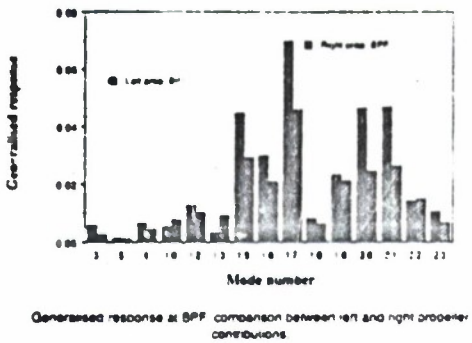

Figure 19: Generalized response diagram of Saab 340 for 1xBPF and left and right propeller

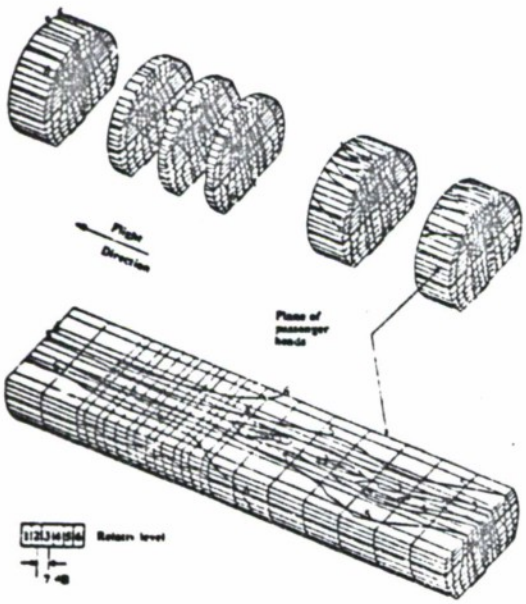

Figure 20: Predicted acoustic part of coupled response of Saab 340 for 1xBPF due to right propeller

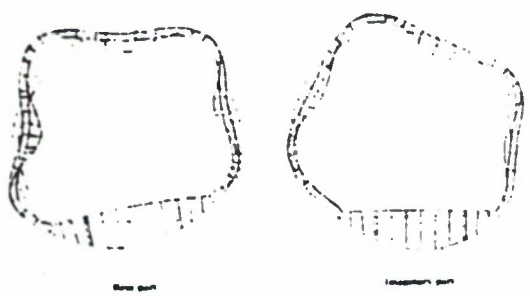

Figure 21: Calculated structural part of coupled response of Saab 340 for 1xBPF due to right propeller

5. DEVELOPMENT WORK ON ADVANCED ACTUATORS

A big problem of applying active noise and/or vibration control to aircraft may be the weight of the actuators (loudspeaker and/or shaker systems), necessary for generating the secondary noise and/or vibration field. The required performance of loudspeakers is, for example, a high acoustic output at frequencies below 500 Hz. Currently, the smallest conventional loudspeakers which will meet this requirement have a weight of more than 1.0 kg. Since a larger number of such sources may be needed for aircraft to obtain a global noise reduction in the cabin, the resulting total weight of the control system could be very large.

In the present study, therefore, initial development work on advanced actuators has been included. By advanced actuators new loadspeaker and shaker systems are meant which are especially designed for meeting the stringent aircraft needs. A basic idea was to develop actuators which are more or less an integrated part of the interior trim and which are restricted to the required low frequency range so that significant weight and space can be saved. In the following an outline of this work and some selected results are given.

5.1 Studied Actuator Designs

The actuators studied in this program are primarily based on the piezo-electric and the electrodynamic principle.

The advantages of the piezo-electric principle are the simple and robust design, the high forces, and the low weight. The major disadvantage is the small displacement. This disadvantage may however be overcome by utilizing the bimorph principle. Here the piezo-electric material is combined to an elastic materiel, which will amplify the displacement. By applying a thin piezo-electric polymer film (PVDF) to a specially designed trim panel the whole panel may be made to radiate sound, thus creating a simple and robust loudspeaker with nearly no additional weight. The principle of such a design is illustrated in Figure 22.

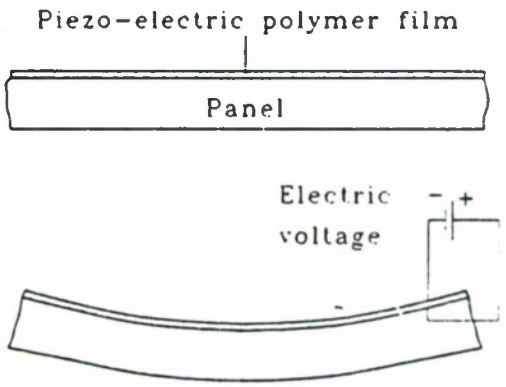

Figure 22: Principle of piezo-electric polymer film attached to a panel

Another configuration studied included a sandwich designe of PVDF layers, which were attached to e Dornier 228 trim panel for testing. Different numbers of PVDF layers were considered. A photograph of this design is shown in Figure 23.

Furthermore, designs using e number of small piezo-electric drive units or e number of small coil/magnet-systsms were evaluated. The units excite in parallel a large stiff noise redieting area, which could be the trim panel or part of it. Speakers with radiation area 0.2 m^2 end with a height of less than 25 mm or 35 mm ere currently undergoing tests for installation in a Dornier 228 ceiling trim panel. The design is shown in Figure 24.

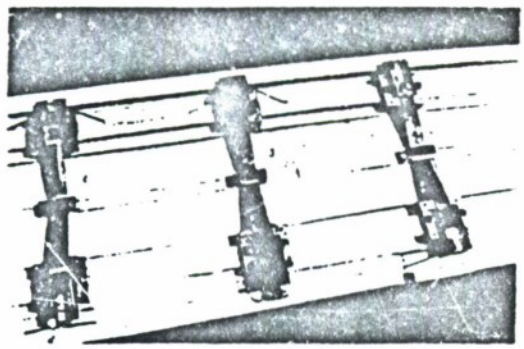

Figure 23: First design of PVDF ectuetors integrated into Dornier 228 trim panel

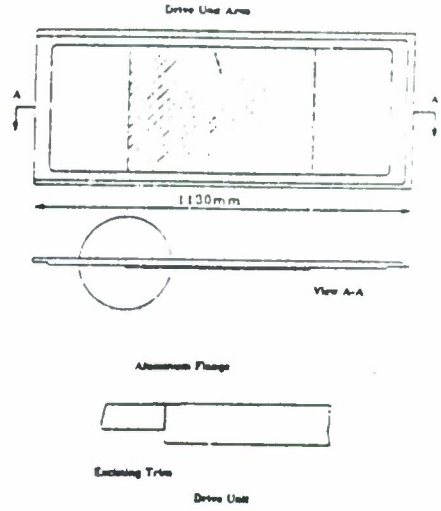

Figure 24: Trim panel design including piezo-electric or electrodynamic drive units

The results available so far thus rhow that advanced actuator designe have a great potsntiel for aircraft ective noise end/or vibration control. However, in order to define and provide feesible configuratione, related additionel detailed research is required.

5.2 Performed Test

The different actuator designs have been firstly tested in the leberatory on stand elone units in order to improve the knowledge on their dynemic behaviour end their parameter seneitivity.

After the selection of most suitable designs, sets of theee ectuetor units have been mounted on reel aircraft trim panels in order to deel directly with the coupling end integration espects. For this integration, large effort hes been devoted to the whole dynamic trim panel behaviour, including global stiffness, damping ratio, boundary conditions etc.. The trim panels were then tested to determine important parameter such as acoustic efficiency, harmonic distortion and others.

An example of the rssults of the trim panel test is given in Figurs 25 together with some theoretical data. The figure shows the sound pressure level at 1 m distance from the panel for e trim panel actuator design es shown in Figure 23 but not with thrse but only with one ectuator. As can be seen, the noise radiation includes as desired rather low frequencies. However, similar as for other first designs ths radiated noise levels are comparatively low, in the shown example only up to about 70 dB. This deficiency could be overcome with later improved designs showing noise levels up to more than 100 dB.

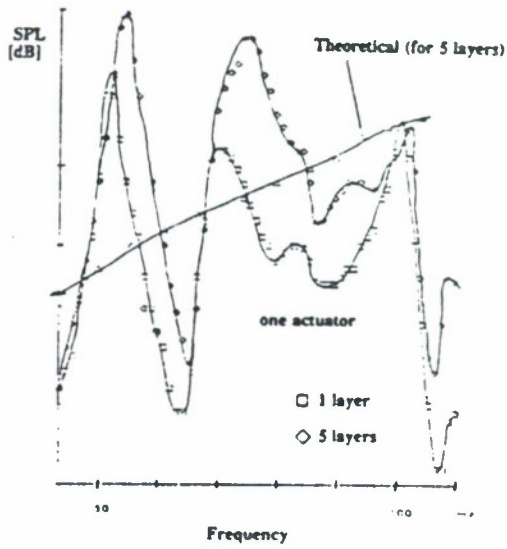

Figure 25: Radiated noise levels of the first trim panel integrated PVDF actuator design

6. DEMONSTRATOR CONTROL SYSTEM DEVELOPMENT AND FIRST RESULTS

In the first course of the program the established experimental and theoretical results were carefully evaluated as soon as they became available. Based on this, a preferable noise control approach was selected, which via the required maximum number of actuators and sensors could strongly influence the demonstrator control unit definition. In addition, other important tasks were performed such as selection of feasible actuators and sensors, simulation of different control algorithms and preliminary selection of control unit architecture. Using the results of these partial studies, the control unit hardware set-ups were defined and required software was realized and tested. Finally, the required hardware boards and components were realized and integrated to the complete demonstrator control units.

6.1 Outline of Overall Control System

As preferable noise control approach loudspeakers and/or advanced actuators both implemented into the trim panels of the selected Dornier 228 test aircraft were chosen. With this first detailed results on this approach could be obtained, important for future control technique improvements. As control sensors, microphones of rather small size, about 6.0 mm diameter, were used. The positions and the number of the actuators and sensors were strongly based on the test data evaluation described in Section 3. In order to achieve highest feasible noise reductions 32 output and 48 input channels were selected. With this also a versatile system for future more detailed investigation was made available.

6.2 Control Unit Description

Until the present time one of the realized demonstrator control units could be preliminary tested under simulated flight conditions on the ground. The tested control unit is partially comprised of available standard boards, especially for the non-critical tasks such as AD and DA converting. In addition, special boards were used for overall system management, main tasks sequencing and data transfer control.

In the control unit both a time-domain and a frequency domain control algorithm are implemented. The time-domain algorithm is based on a multi input/multi output algorithm which was implemented with an asynchronous sampling. The frequency domain control algorithm uses complex amplitudes. It identifies on-line the secondary transfer function of each actuator and each sensor.

6.3 Initial Laboratory Testing

Before flight testing initial laboratory tests were performed on the control system described before, for overall system checks and possible control unit adjustments.

In order to conduct these tests under conditions as realistic as possible, use was made of the Dornier 328 Acoustic Test Cell (ATC). This facility is located in a laboratory and consist of a large Dornier 328 fuselage section extending over the entire aircraft cabin. The propeller noise is simulated by three external and softly attached full circle loudspeaker rings including a total of 60 separately enclosed speakers. The speakers are driven by an advanced 60-channel computer/amplifier system permitting to generate external pressure fields with quite realistic phase distributions.

For performing the tests in the Dornier 328 ATC, loudspeakers enclosed by suitable wooden boxes were used as actuators and attached to the inner fuselage structure at preselected positions. The positions were only approximately chosen as only general system functional tests need to be conducted. As sensors the selected system microphones were used which were placed in the plane of the passenger heads as planned for later flight testing. The required propeller synchronization signals were provided by the exterior noise generation system which was adjusted to propeller frequencies corresponding to the selected test aircraft. A photograph showing this test set-up is given in Figure 26.

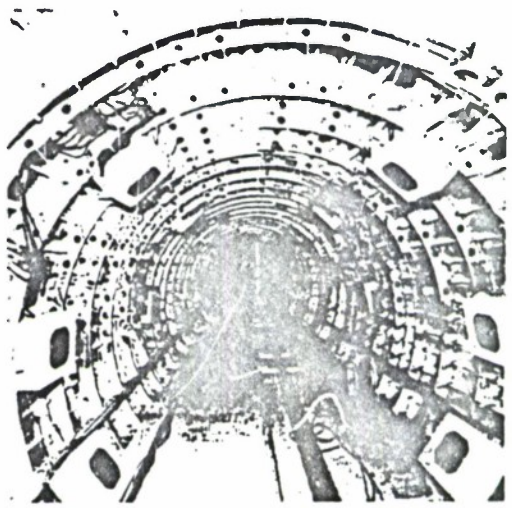

Figure 26: Laboratory active noise control test set-up in Dornier 328 ATC

The laboratory testing in the Dornier 328 ATC was very successfull. A selected preliminary result is shown in Figure 27. The data were obtained for the described control unit with selected time-domain algorithm and correspond to the averaged noise level at the used sensor microphone without and with active noise control. As can be seen, noise reductions of about 15 dB at 1xBPF, 16 dB at 2xBPF, and 10 dB at 3xBPF were measured. In addition and that seems to be of equal importance, walking of several peoples in the ATC during the test seemed to have no large effect on this result and yielded the impression of a rather global noise reduction. Furthermore, the power consumption of all loudspeakers during this test was measured to be only about 40 watts which is relatively low.

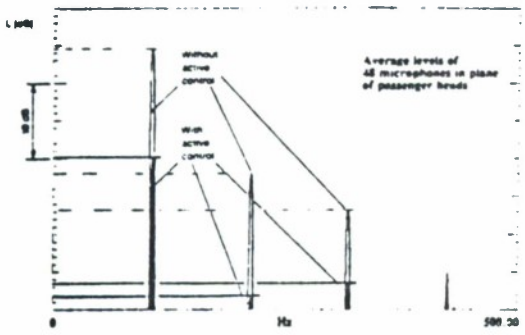

Figure 27: Preliminary active noise control result of Dornier 328 ATC testing

7. CONCLUDING REMARKS

The experimental and theoretical results of the ASANCA program summarized in this paper provided very important information on aircraft interior active noise control.

The evaluation of the performed aircraft flight and ground test indicate, for example, a noise reduction potential of this technique up to about 15 to 20 dB for the first propeller tone (1xBPF) depending on the number of secondary sources used. During the laboratory testing of one of the developed control systems in the Dornier 328 Acoustic Test Cell (ATC) preliminary data evaluation showed noise reductions of about 15 and 16 dB for 1xBPF and 2xBPF and about 10 dB for 3xBPF. This is in good agreement with the results based on the flight and ground tests as probably not optimum actuator positions were used in this experiment. Furthermore important results were obtained from the performed finite element calculations providing a detailed data base for still ongoing or planned future active noise and vibration control predictions.

In addition, the study identified that for future practical aircraft applications further detailed research on this topic is required, for optimum control system definition as well as system weight and size minimization.

ACKNOWLEDGEMENT

The ASANCA project was supported by the Commission of the European Communities (CEC), Directorate-General for Science, Research and Development, DG XII, under contract AERO 0028-C, which is acknowledged by all ASANCA partners. In particular, appreciation is expressed to Mr. J.M. Martin-Hernandez for his review of the research progress and many fruitful technical discussions.

ACTIVE CONTROL OF SOUND TRANSMISSION THROUGH STIFF LIGHTWEIGHT COMPOSITE FUSELAGE CONSTRUCTIONS

D. R. Thomas, P. A. Nelson, R. J. Pinnington and S. J. Elliott

Institute of Sound and Vibration Research
University of Southampton.

SUMMARY

1. Outline a model of a vibrating plate with arbitrary boundary conditions previously used by Berry *etal.*
2. Minimise the far field radiated acoustic power using point secondary force inputs.
3. Use the model for the simple case of freely mounted stiff lightweight panel.
4. Present experimental results for an aluminium honeycomb composite panel.
5. Present experimental results for the combination of a clamped steel plate and an aluminium honeycomb panel with secondary forces acting between the partitions.
6. Present experimental results for the combination of a clamped steel plate with four secondary aluminium honeycomb panels.

ACTIVE CONTROL OF SOUND TRANSMISSION: A NEW APPROACH

- The problem: Propeller noise in aircraft cabin.
- One proposed solution is the use of secondary acoustic sources in the cabin to minimise the internal sound pressure.
- Another approach suggested by Fuller is to use secondary forces acting on the fuselage to minimise the internal sound pressure.
- Secondary forces are more effective than secondary acoustic sources in achieving global reductions in sound pressure.
- the use of secondary forces could however significantly increase fuselage vibration.
- A hybrid approach: Partially replace internal trim with stiff lightweight panels attached to the fuselage by means of secondary force actuators.

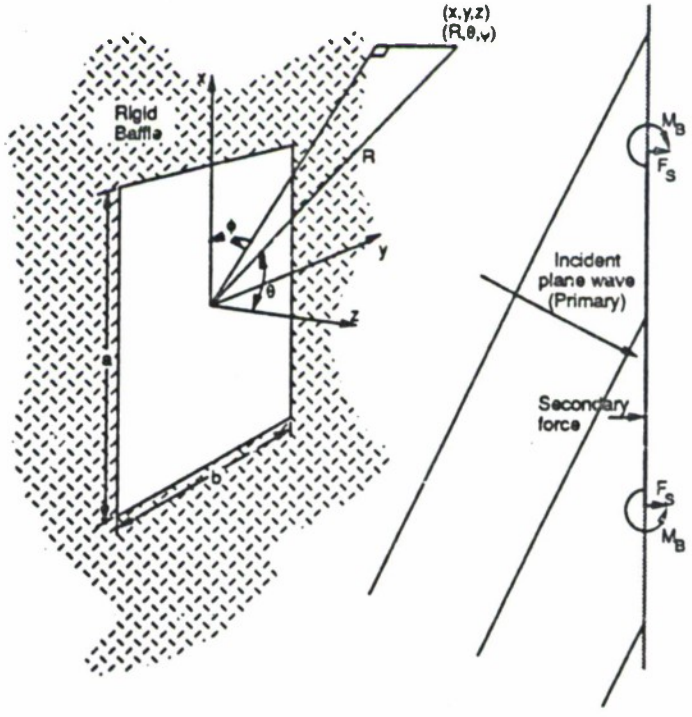

Diagram of the clamped rectangular plate illustrating the co-ordinate system used.

THE EQUATION OF MOTION FOR THE PLATE

The shear force $F_S(P,t)$ and the bending moment $M_B(P,t)$ at point P on the edge of the plate are given by

$$\boldsymbol{F}_S(P,t) = -K(P)w(P,t)\boldsymbol{n}_z, \tag{1}$$

$$\boldsymbol{M}_B(P,t) = C(P)\frac{\partial w}{\partial n_e}(P,t)\boldsymbol{\Gamma}, \tag{2}$$

where $K(P)$ and $C(P)$ are the translational and rotational stiffness per unit length at point P.

Non-dimensional edge parameters $k(P)$ and $c(P)$

$$k(P) = K(P)a^3/D, \tag{3}$$

$$c(P) = C(P)a/D, \tag{4}$$

The Lagrangian for the response of the plate described above to an arbitrary forcing function $f(x, y, t)$ can be expressed as

$$L(w) = T\left(\frac{\partial w}{\partial t}\right) - V(w) + W(w), \tag{5}$$

$$T = \int_{-1}^{+1}\int_{-1}^{+1} \frac{1}{8}\rho h \frac{a^2}{r}\left(\frac{\partial w}{\partial t}\right)^2 d\alpha\, d\beta, \tag{6}$$

where $\alpha = 2x/a$ and $\beta = 2y/b$ and $r = a/b$.

$$V = V_1 + V_2 + V_3, \tag{7}$$

where V_1 is the potential energy of plate bending given by

$$V_1 = \frac{D}{a^2}\left\{\int_{-1}^{+1}\int_{-1}^{+1} \frac{2}{r}\left[\left(\frac{\partial^2 w}{\partial \alpha^2}\right)^2 + r^4\left(\frac{\partial^2 w}{\partial \beta^2}\right)^2 + 2\nu r^2 \frac{\partial^2 w}{\partial \alpha^2}\frac{\partial^2 w}{\partial \beta^2} + 2(1-\nu)r^2\left(\frac{\partial^2 w}{\partial \alpha \partial \beta}\right)^2\right] d\alpha\, d\beta, \tag{8}$$

V_2 is the potential energy associated with the translational stiffness at the edges of the plate given by

$$V_2 = \int_{-1}^{+1} \frac{k}{4}[w^2(\alpha, 1) + w^2(\alpha, -1)]\, d\alpha + \int_{-1}^{+1} \frac{k}{4r}[w^2(1, \beta) + w^2(-1, \beta)]\, d\beta, \tag{9}$$

and V_3 is the potential energy associated with the rotational stiffness at the edges of the plate given by

$$\begin{aligned} V_3 = {} & \int_{-1}^{+1} cr^2\left[\left(\frac{\partial w}{\partial \beta}(\alpha, 1)\right)^2 + \left(\frac{\partial w}{\partial \beta}(\alpha, -1)\right)^2\right] d\alpha \\ & + \int_{-1}^{+1} \frac{c}{r}\left[\left(\frac{\partial w}{\partial \alpha}(1, \beta)\right)^2 + \left(\frac{\partial w}{\partial \alpha}(-1, \beta)\right)^2\right] d\beta\Big\}, \end{aligned} \tag{10}$$

The work done on the plate by external forces, W is given by

$$W(w) = \frac{a^2}{4r}\int_{-1}^{+1}\int_{-1}^{+1} f(\alpha, \beta) w(\alpha, \beta)\, d\alpha\, d\beta \tag{11}$$

Hamilton's principle

$$\delta \int_{t_0}^{t_1} L(w)\, dt = 0. \tag{12}$$

Rayleigh-Ritz:

$$\begin{aligned} w(x,y,t) &= \sum_{m,n} a_{mn}\phi_m(x)\psi_n(y) \\ &= \boldsymbol{a}^T\boldsymbol{\Phi}, \end{aligned} \tag{13}$$

$$\Phi_{mn} = \phi_m(x)\psi_n(y), \tag{14}$$

$$\begin{aligned} \phi_m(x) &= \left(\frac{2}{a}x\right)^m, \quad m = 0,1,2,\ldots M, \\ \psi_n(y) &= \left(\frac{2}{b}y\right)^n, \quad n = 0,1,2,\ldots N, \end{aligned} \tag{15}$$

Equation of motion:

$$\boldsymbol{M}\ddot{\boldsymbol{a}} + \boldsymbol{K}\boldsymbol{a} = \boldsymbol{f}, \tag{16}$$

M is of the form

$$\begin{bmatrix} M_{1111} & M_{1211} & \cdots & M_{mn11} & \cdots & M_{MN11} \\ M_{1112} & M_{1212} & \cdots & & & \\ \vdots & & \ddots & & & \\ M_{11pq} & \cdots & & M_{mnpq} & & \\ \vdots & & & & \ddots & \\ M_{11PQ} & \cdots & & & & M_{MNPQ} \end{bmatrix} \tag{17}$$

with

$$M_{mnpq} = \frac{a^2}{4r} \int_{-1}^{+1} \int_{-1}^{+1} \rho h \phi_m(\alpha) \psi_n(\beta) \phi_p(\alpha) \psi_q(\beta)\, d\alpha\, d\beta. \tag{18}$$

The matrix K is of the same size and form as M with the elements given by

$$K_{mnpq} = K^1_{mnpq} + K^2_{mnpq} + K^3_{mnpq}, \tag{19}$$

where K^1_{mnpq} is the contribution of the plate stiffness to the stiffness matrix given by

$$K^1_{mnpq} = \frac{D}{a^2}\int_{-1}^{+1}\int_{-1}^{+1}\frac{2}{r}\Big(\frac{\partial^2\phi_m}{\partial\alpha^2}\psi_n\frac{\partial^2\phi_p}{\partial\alpha^2} + r^4\phi_m\frac{\partial^2\psi_n}{\partial\beta^2}\phi_p\frac{\partial^2\psi_q}{\partial\beta^2} + \nu r^2\frac{\partial^2\phi_m}{\partial\alpha^2}\psi_n\phi_p\frac{\partial^2\psi_q}{\partial\beta^2}$$
$$+\nu r^2\phi_m\frac{\partial^2\psi_n}{\partial\beta^2}\frac{\partial^2\phi_p}{\partial\alpha^2}\psi_q + 2(1-\nu)r^2\frac{\partial\phi_m}{\partial\alpha}\frac{\partial\psi_n}{\partial\beta}\frac{\partial\phi_p}{\partial\alpha}\frac{\partial\psi_q}{\partial\beta}\Big)\,d\alpha\,d\beta, \qquad (20)$$

K^2_{mnpq} is the contribution of the translational stiffness at the plate edge to the stiffness matrix given by

$$K^2_{mnpq} = \frac{D}{a^2}\Big[\int_{-1}^{+1}\frac{k}{2}[\phi_m(\alpha)\psi_n(1)\phi_p(\alpha)\psi_q(1) + \phi_m(\alpha)\psi_n(-1)\phi_p(\alpha)\psi_q(-1)]\,d\alpha$$
$$+\int_{-1}^{+1}\frac{k}{2r}[\phi_m(1)\psi_n(\beta)\phi_p(1)\psi_q(\beta) + \phi_m(-1)\psi_n(\beta)\phi_p(-1)\psi_q(\beta)]\,d\beta, \qquad (21)$$

and K^3_{mnpq} is the contribution of the rotational stiffness at the plate edge to the stiffness matrix given by

$$K^3_{mnpq} = \int_{-1}^{+1}2cr^2\Big(\phi_m(\alpha)\frac{\partial\psi_n}{\partial\beta}(1)\phi_p\frac{\partial\psi_q}{\partial\beta}(1) + \phi_m(\alpha)\frac{\partial\psi_n}{\partial\beta}(-1)\phi_p\frac{\partial\psi_q}{\partial\beta}(-1)\Big)\,d\alpha$$
$$+\int_{-1}^{+1}2\frac{c}{r}\Big(\frac{\partial\phi_m}{\partial\alpha}(1)\psi_n(\beta)\frac{\partial\phi_p}{\partial\alpha}(1)\psi_q(\beta)\Big)\,d\beta$$
$$+\int_{-1}^{+1}2\frac{c}{r}\Big(\frac{\partial\phi_m}{\partial\alpha}(-1)\psi_n(\beta)\frac{\partial\phi_p}{\partial\alpha}(-1)\psi_q(\beta)\Big)\,d\beta. \qquad (22)$$

Harmonic time dependency

$$(-\omega^2 \boldsymbol{M} + \boldsymbol{K})\boldsymbol{a} = \boldsymbol{f}, \tag{23}$$

where the elements of $\boldsymbol{f}$ are now given by

$$f_{mn}(t) = \frac{a^2}{4r} \int_{-1}^{+1} \int_{-1}^{+1} f(\alpha, \beta)\phi_m(\alpha)\psi_n(\beta)\, d\alpha\, d\beta. \tag{24}$$

$$\boldsymbol{a} = \boldsymbol{B}^{-1}\boldsymbol{f}. \tag{25}$$

THE ACOUSTIC POWER RADIATED BY THE PLATE

The far field acoustic pressure radiated by the plate is calculated by application of the Rayleigh integral:

$$p(R,\theta,\varphi) = -\rho_a \omega^2 \frac{e^{-j(\omega/c)R}}{2\pi R} \tilde{w}(\lambda,\mu), \qquad (26)$$

Assume that $R >> a$ and $R >> b$ can be defined as

$$\tilde{w}(\lambda,\mu) = \frac{a^2}{4\pi} \int_{-1}^{+1} \int_{-1}^{+1} w(\alpha,\beta) \times \exp\left[j\left(\frac{a}{2}\lambda\alpha + \frac{b}{2}\mu\beta\right)\right] d\alpha\, d\beta, \qquad (27)$$

where

$$\lambda = (\omega/c)\sin\theta\cos\varphi; \qquad \mu = (\omega/c)\sin\theta\sin\varphi. \qquad (28)$$

The acoustic power radiated into the far field is given by

$$\Pi = \frac{\rho_a \omega^4}{8c\pi^2} \int_0^{2\pi} \int_0^{\pi/2} |\tilde{w}(\lambda, \mu)|^2 \sin\theta \, d\theta \, d\varphi, \tag{29}$$

$$\Pi = \frac{\rho_a \omega^4}{8c\pi^2} \boldsymbol{f}^H \boldsymbol{B}^{-H} \boldsymbol{\Omega} \boldsymbol{B}^{-1} \boldsymbol{f}, \tag{30}$$

where $\boldsymbol{\Omega}$ is a matrix of the form

$$\begin{bmatrix} \Omega_{1111} & \Omega_{1211} & \cdots & \Omega_{mn11} & \cdots & \Omega_{MN11} \\ \Omega_{1112} & \Omega_{1212} & \cdots & & & \\ \vdots & & \ddots & & & \\ \Omega_{11pq} & \cdots & & \Omega_{mnpq} & & \\ \vdots & & & & \ddots & \\ \Omega_{11PQ} & \cdots & & & & \Omega_{MNPQ} \end{bmatrix} \tag{31}$$

the elements of which are given by

$$\Omega_{mnpq} = \left(\frac{a^2}{4r}\right)^2 \int_0^{2\pi} \int_0^{\pi/2} \left(\int_{-1}^{+1} \alpha^m e^{j\lambda(a/2)\alpha} \, d\alpha \int_{-1}^{+1} \beta^n e^{j\mu(b/2)\beta} \, d\beta \right) \times \left(\int_{-1}^{+1} \alpha^p e^{j\lambda(a/2)\alpha} \, d\alpha \int_{-1}^{+1} \beta^q e^{j\mu(b/2)\beta} \, d\beta \right)^* \sin\theta \, d\theta \, d\varphi. \tag{32}$$

THE MINIMISATION OF THE ACOUSTIC POWER RADIATED BY THE PLATE BY THE USE SECONDARY FORCE INPUTS

$$\boldsymbol{f} = \boldsymbol{f}_p + \boldsymbol{\Phi}\boldsymbol{f}_s, \tag{33}$$

$$\boldsymbol{\Phi} = \frac{a^2}{4\tau}\begin{bmatrix} \phi_1(x_1)\psi_1(y_1) & \dots & \phi_1(x_l)\psi_1(y_l) & \dots & \phi_1(x_L)\psi_1(y_L) \\ \vdots & \ddots & \cdot & & \vdots \\ \phi_m(x_1)\psi_n(y_1) & \dots & \phi_m(x_l)\psi_n(y_l) & & \vdots \\ \vdots & & & \ddots & \vdots \\ \phi_M(x_1)\psi_N(y_1) & \dots & & & \phi_M(x_L)\psi_N(y_L) \end{bmatrix} \tag{34}$$

$$\Pi = \frac{\rho_a \omega^4}{8c\pi^2}(\boldsymbol{f}_p + \boldsymbol{\Phi}\boldsymbol{f}_s)^H \boldsymbol{B}^{-H}\boldsymbol{\Omega}\boldsymbol{B}^{-1}(\boldsymbol{f}_p + \boldsymbol{\Phi}\boldsymbol{f}_s). \tag{35}$$

If we define a matrix A as

$$A = \frac{\rho_a \omega^4}{8c\pi^2} B^{-H} \Omega B^{-1}, \tag{36}$$

$$\Pi = f_p^H \Phi^H A \Phi f_p + f_p^H A \Phi f_s + f_s^H \Phi^H A f_p + f_s^H \Phi^H A \Phi f_s. \tag{37}$$

$$f_{so} = -(\Phi^H A \Phi)^{-1} \Phi^H A f_p. \tag{38}$$

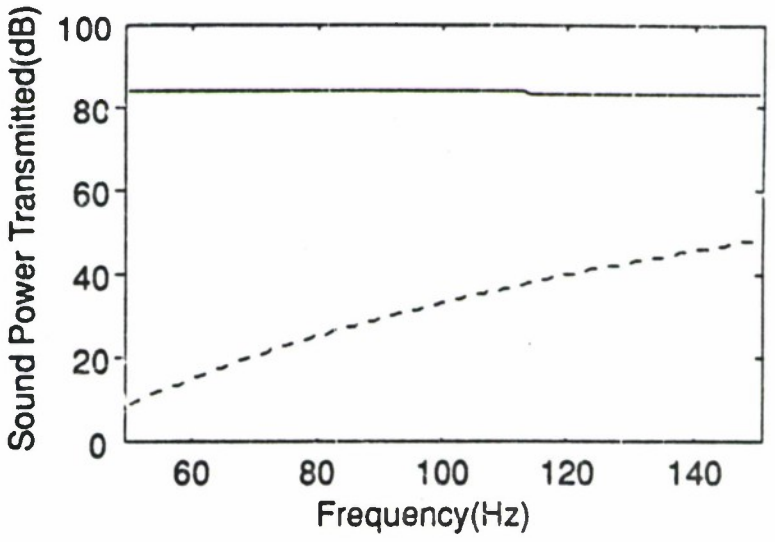

Total radiated acoustic power from a single lightweight stiff panel with a normal incidence primary plane wave and a single secondary force, with control (– – – – –), and without control (——).

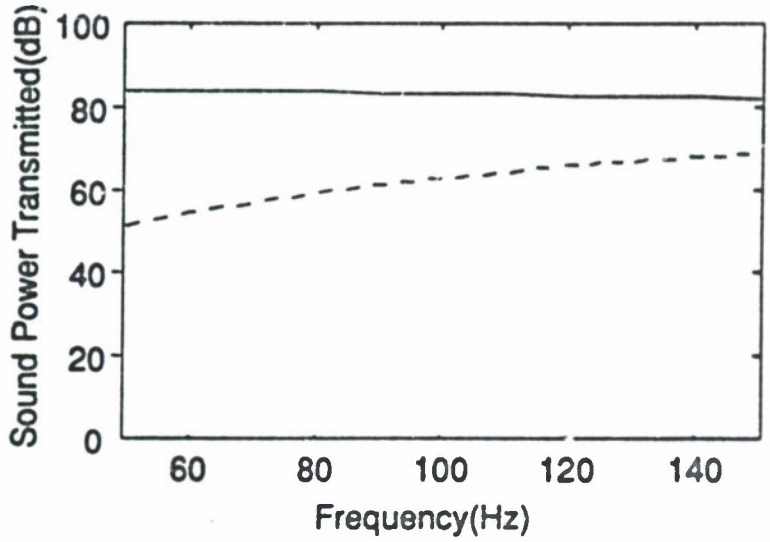

Total radiated acoustic power from a single lightweight stiff panel with a primary plane wave incident at 45° and a single secondary force, with control (– – – – –), and without control (——-).

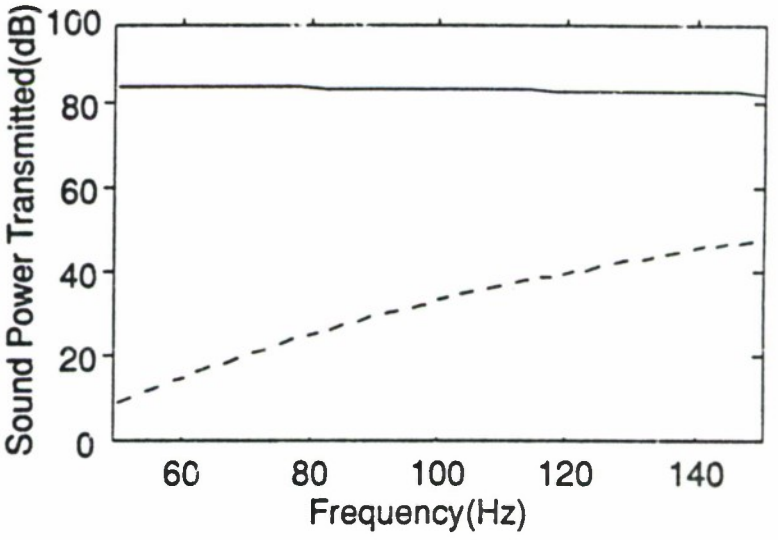

Total radiated acoustic power from a single lightweight stiff panel with a primary plane wave incident at 45° and three secondary forces, with control (– – – – –), and without control (——).

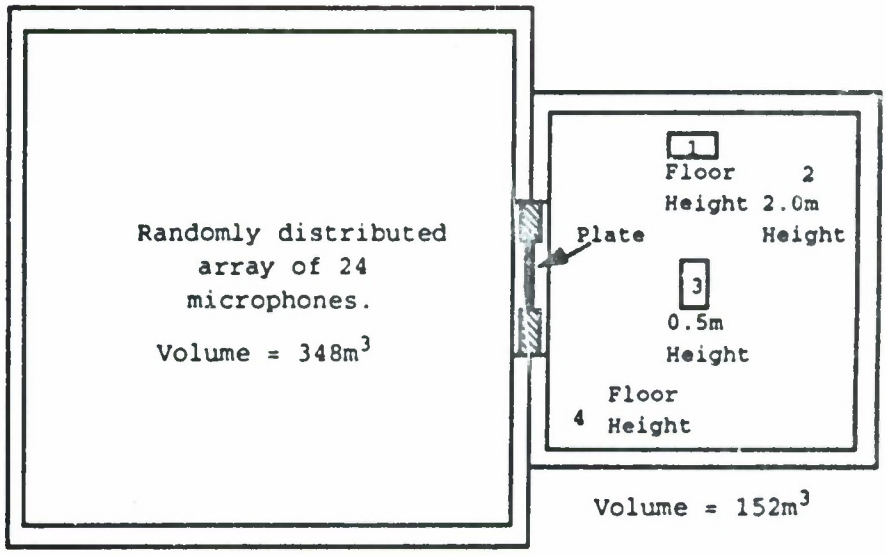

The reverberation suite, showing the clamped steel plate and four primary source positions.

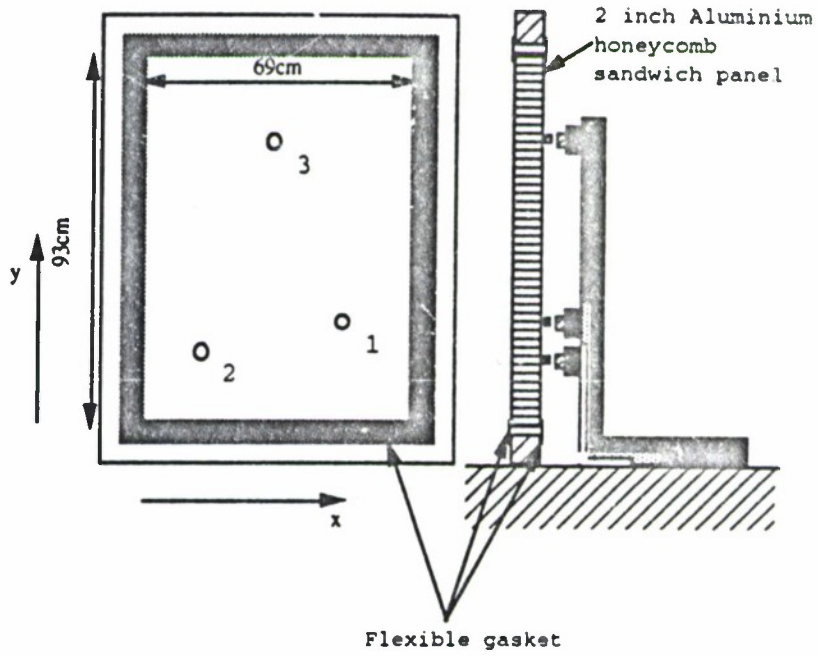

The arrangement of secondary forces and mounting of the aluminium honeycomb panel

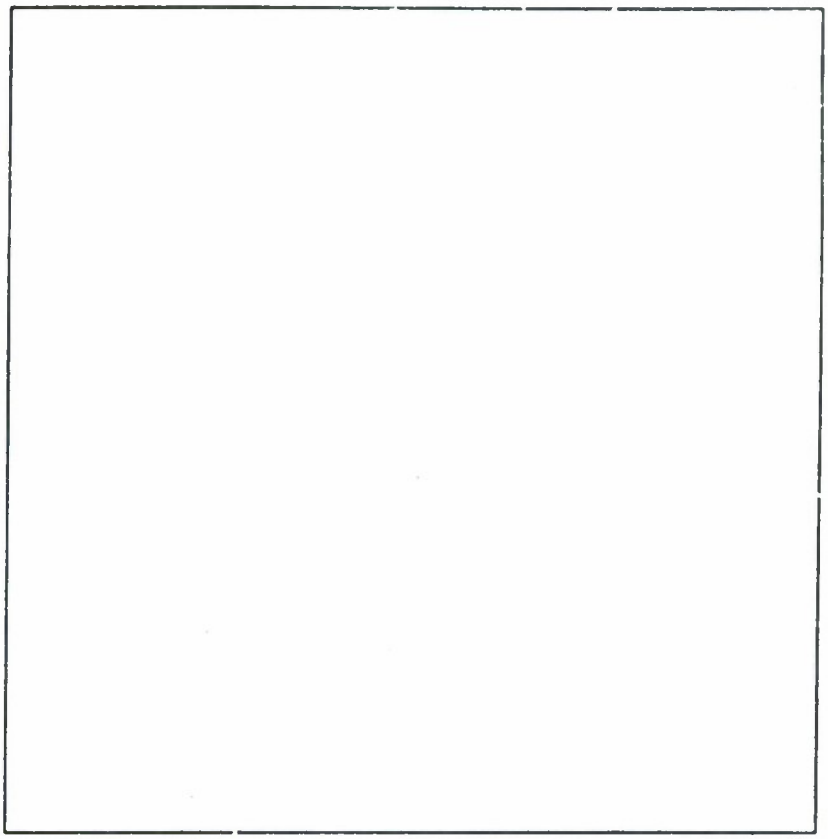

Frequency response of the aluminium honeycomb panel with all edges free

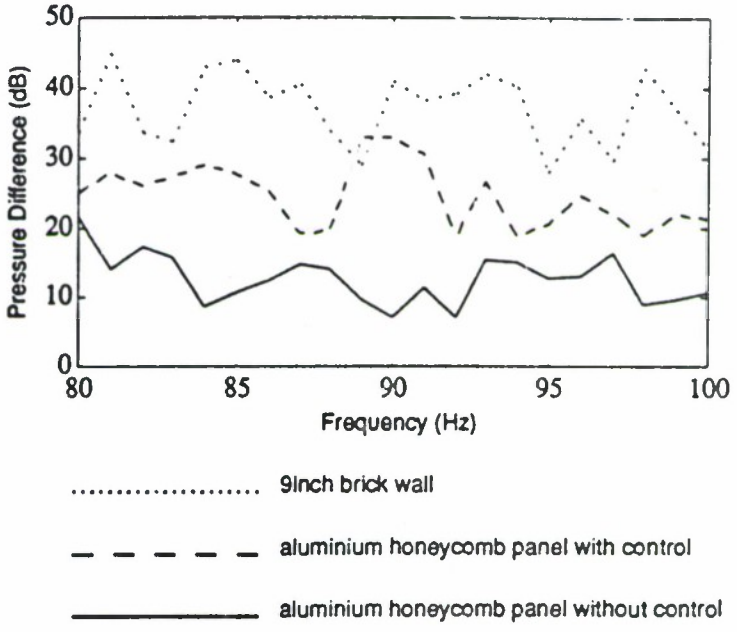

Pressure difference between a single microphone positioned at the centre of the aluminium honeycomb panel (or wall) in the source chamber and the average of the sound pressure at the 24 control microphones in the receiving chamber for the aluminium honeycomb panel with and without control and a 9inch plastered concrete wall.

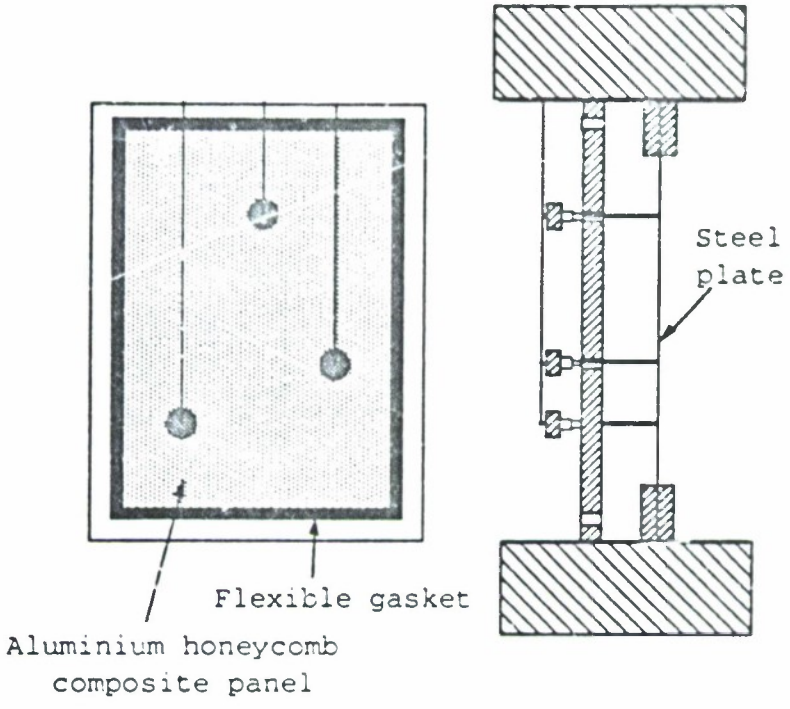

The mounting of the 2 inch aluminium honeycomb panel and clamped steel plate and arrangement of coil and magnet devices.

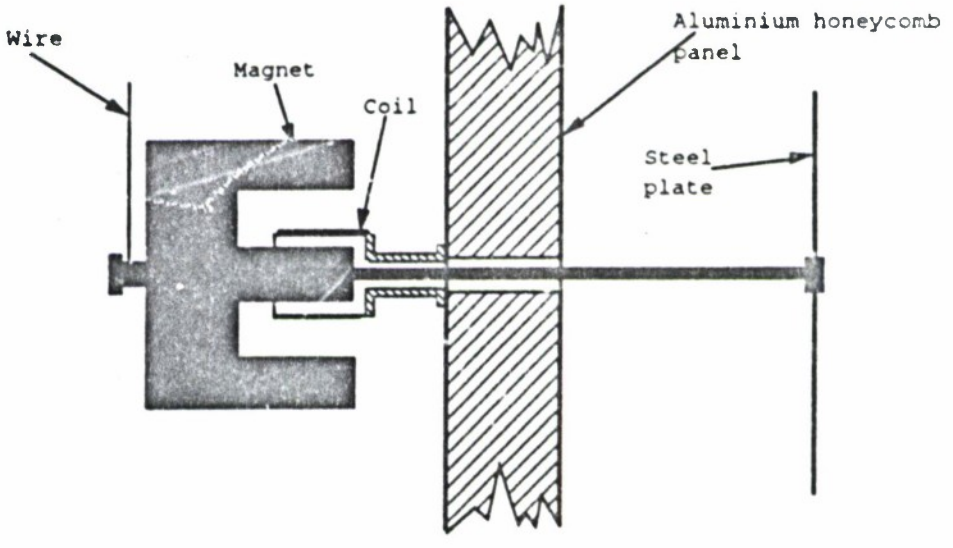

Diagram of the arrangement used for the coil and magnet devices.

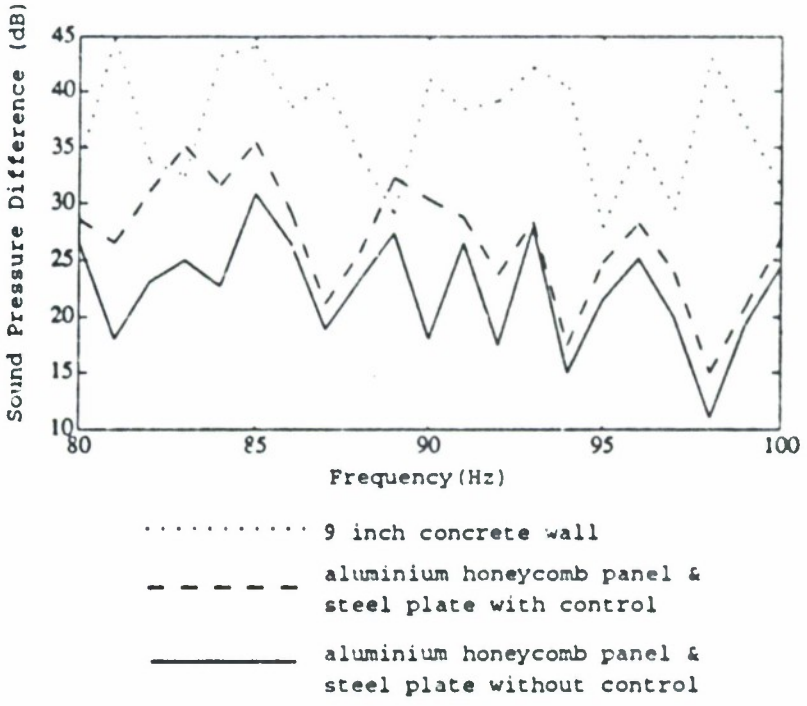

Sound pressure difference between a single microphone positioned at the centre of the steel plate (or wall) in the source chamber and the average of the sound pressure at the 24 control microphones in the receiving chamber for the aluminium honeycomb panel & steel plate combination, with and without control, and for a 9in plastered concrete wall.

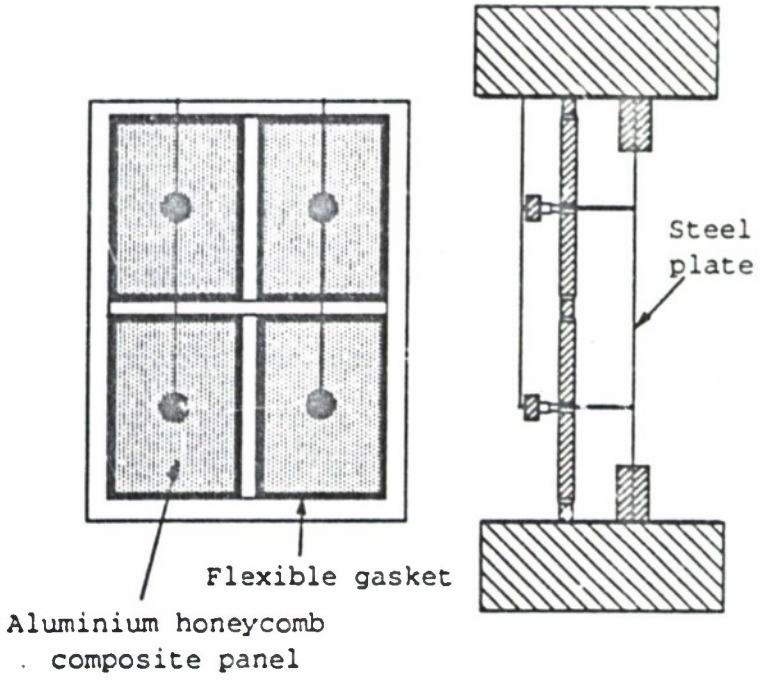

The mounting and arrangement of the 4 1inch aluminium honeycomb panels and the clamped steel plate showing the positions of the coil and magnet devices.

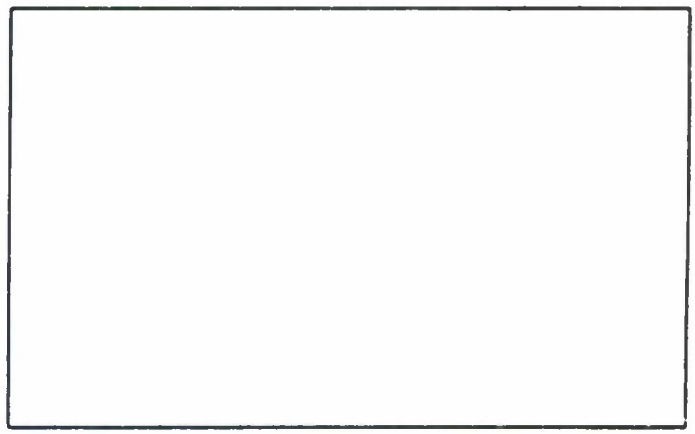

Frequency response of one of the aluminium honeycomb panels with all edges free.

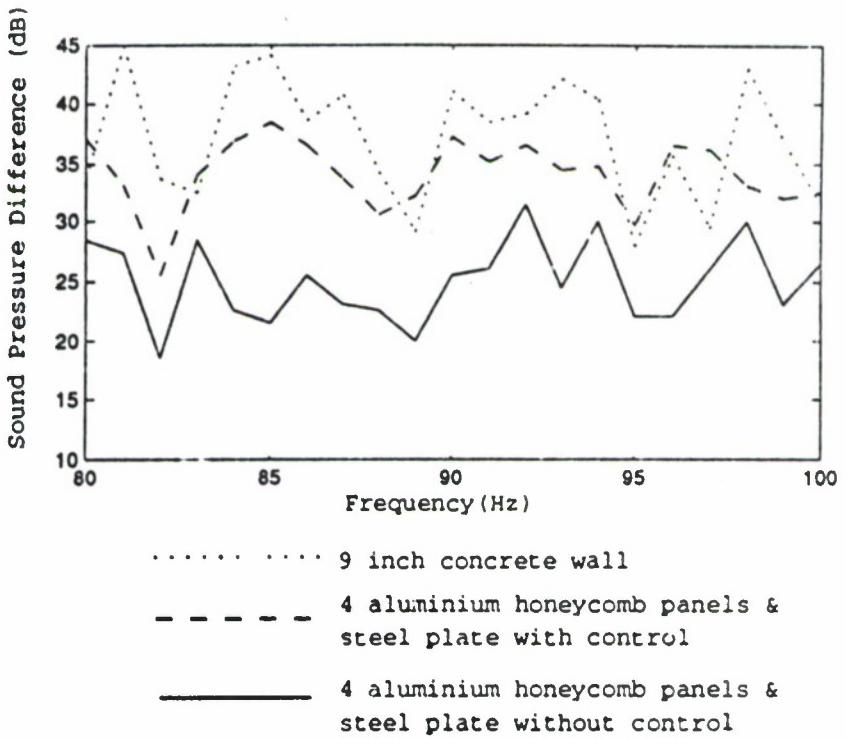

Sound pressure difference for the four aluminium honeycomb panel & steel plate combination, with and without control, and for a 9in plastered concrete wall. The frequency range is from 80Hz to 100Hz.

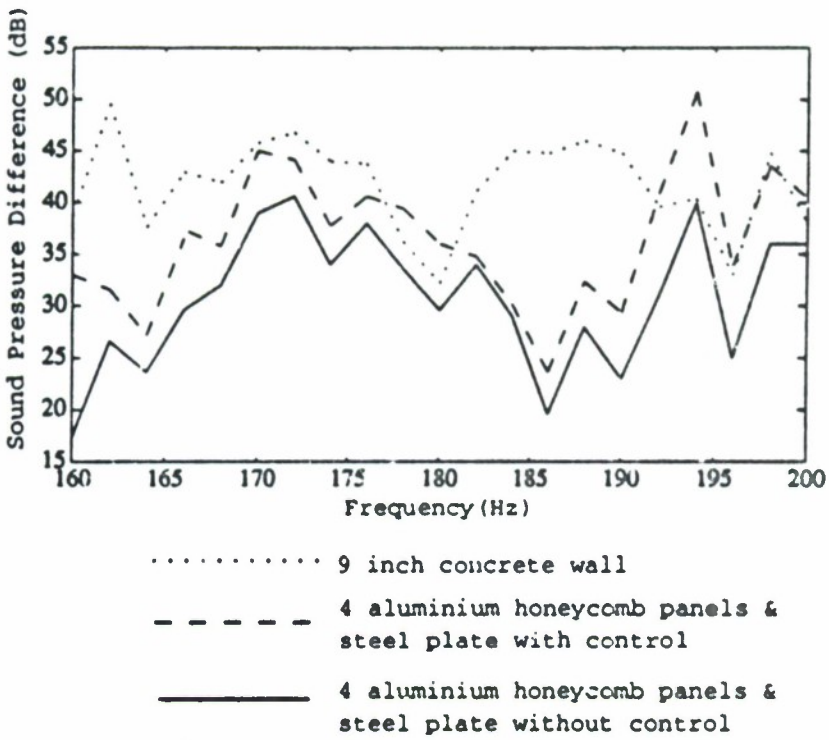

Sound pressure difference for the four aluminium honeycomb panel & steel plate combination, with and without control, and for a 9in plastered concrete wall. The frequency range is from 160Hz to 200Hz.

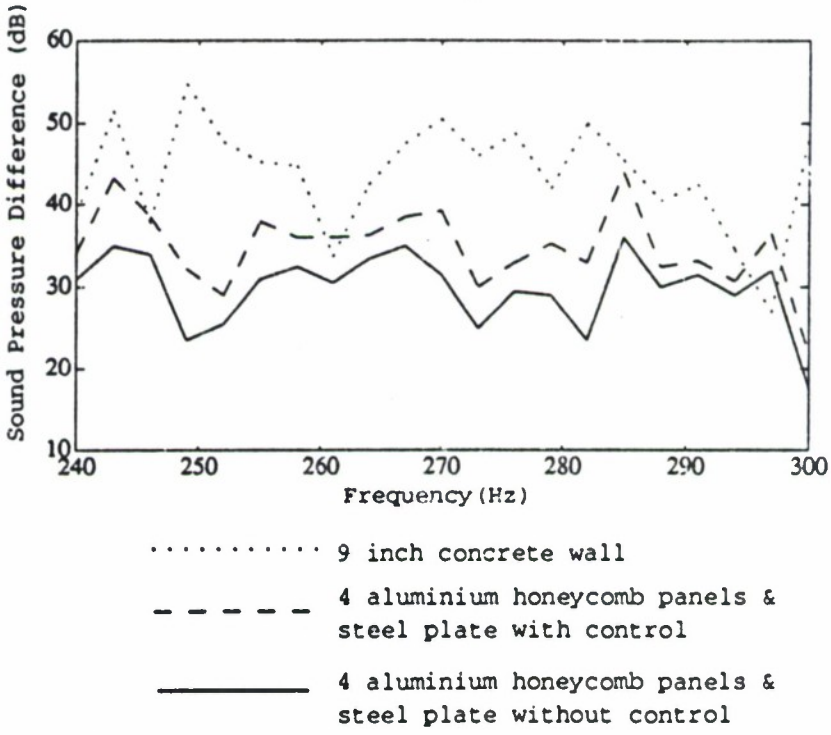

Sound pressure difference for the four aluminium honeycomb panel & steel plate combination, with and without control, and for a 9in plastered concrete wall. The frequency range is from 240Hz to 300Hz.

CONCLUSIONS

1. Large attenuations in sound transmitted through a single freely mounted aluminium honeycomb panel can be achieved with either three secondary forces or a single force if the panel motion is restricted to piston type motion.

2. Global attenuations in transmitted sound pressure can be achieved using secondary forces acting between a clamped steel plate and an aluminium honeycomb panel. (though limits were imposed on the experimental results by flanking transmission paths and the reverberant field).

3. Using four 'secondary panels' with the clamped steel plate produced a partitions with a transmission loss approaching that of a 9 inch thick plastered concrete wall even at frequencies close to 300Hz.

N92-32958

ACTIVE CONTROL OF INTERIOR NOISE IN A LARGE SCALE CYLINDER USING PIEZOELECTRIC ACTUATORS

H. C. Lester and R. J. Silcox
Structural Acoustics Branch
NASA Langley Research Center
Hampton, VA 23665

NASA/SAE/DLR 4th Aircraft Interior Noise Workshop
May 19–20, 1992
Graf Zeppelin Haus
Friedrichshafen, Germany

Abstract

The noise reduction effectiveness of two types of control force actuator models has been analytically investigated: (1) a point actuator and (2) an in-plane, piezoelectric actuator. The actuators were attached to the wall of a simply-supported, elastic cylinder closed with rigid end caps. Control inputs to the actuators were determined such that the integrated square of the pressure over the interior of the vibrating cylinder was a minimum. Significant interior noise reductions were achieved for all actuator configurations, but especially for the the structurally dominated responses. Noise reductions of $9dB$ to $26dB$ were achieved using point force actuators, as well as localized and extended piezoelectric actuators. Control spillover was found to limit overall performance for all cases. However, the use of extended piezoelectric actuators was effective in reducing control spillover, without increasing the number of control degrees of freedom.

Introduction

The reduction of interior noise in the cabins of a wide class of rotorcraft and propeller aircraft has been a continuing problem. Interior noise is particularly intense in smaller propeller aircraft and helicopters, whereas the cabin noise of high-bypass turbofan powered commercial aircraft has been maintained at acceptable levels. However, in recent years, due mainly to the development of advanced turboprop powered aircraft[1], considerable attention has turned to developing more efficient technology to reduce the low frequency noise in aircraft interiors. Passive techniques have been studied, but found generally to be unacceptable due to the adverse effects of added weight on aircraft performance.

Active control of interior noise has therefore received increased emphasis as an effective, lightweight, noise reduction method. Flight tests in propeller aircraft ha[ve] demonstrated 10 to 15 dB of noise reduction using distributions of interior acoustic cont[rol] sources. However, to achieve control over multiple harmonics, actuator numbers rang[e]

from 16 to 32 or more have been required[2,3]. In addition, the optimum distribution of control actuators has been found to be dependent upon the harmonic content of the interior noise[4]. That is, an actuator configuration effective for the first few lower harmonics may lose its effectiveness if higher-order harmonics are to be controlled[4]. Thus, in order to adapt this noise control technology to helicopters, the range of frequencies impacted needs to be expanded to include the higher frequencies typical of gearbox whine, for example, which can range to several kilohertz. Over this higher frequency range, an excessive number of acoustic control sources would probably be required in order to attain the required matching between the primary noise field and the control field, while minimizing control spillover.

Active Structural Acoustic Control (ASAC) is a new technique in which the control inputs, for reducing interior noise, are applied directly to the vibrating structural acoustic system. This approach has been demonstrated to be more efficient for controlling low to mid-frequency structural sound radiation[5]. In contrast to using acoustic control transducers, ASAC applies control forces directly to the structure such that some measure of the resulting interior noise field is minimized. The advantage of this approach is that effective control can be implemented with fewer control actuators, while generating less control spillover. Other advantages are related to the physical implementation of the control hardware in that the transducers can be designed to be reasonably compact.

One particularly attractive active control concept, recently tested at NASA Langley[5], was based on using piezoceramic patches bonded to the vibrating surface of a fuselage model. These piezoelectric actuators were used to apply bending (out-of-plane) forces to the vibrating fuselage. Preliminary results showed 8 to 15 dB of global interior noise reduction, using a least mean square algorithm, over a wide range of test conditions.

A parallel analytical effort to model the transmission and control of interior noise, due to external noise and vibration sources, has also been undertaken at NASA Langley. The analysis[6] models a fuselage as a finite length, elastic cylinder with hard (rigid) end caps. Two types of piezoelectric actuator were used to apply force inputs directly to the cylinder wall: (1) a bending (out-of-plane) model and (2) an in-plane model. The cylinder and interior acoustic response due to each actuator type was computed and the resulting mode spectra studied. In general, the in-plane piezoelectric actuator was found to provide better excitation of the lower-order acoustic cavity modes and, hence, was thought to be the superior actuator model for active noise control applications.

In this paper, the effectiveness of the in-plane piezoelectric actuator model[6] mentioned previously is analytically investigated and compared to a point force actuator model. An acoustic monopole, located very close to the outside wall of the cylinder, was used as the primary offending noise source. The input amplitudes to the control actuators were determined such that a quadratic cost function, defined on the interior acoustic pressure, was minimized. The control actuator configurations required to reduce the interior noise, without excessive spillover, were examined for two dominant, low frequency noise transmission cases. The first case considered is for a cylinder resonance (100 Hz), where the interior acoustic field is driven in multiple, off-resonance cavity modes. The second case is for an acoustic cavity resonance (200 Hz) characterized by both near and

off-resonance cylinder vibration modes which couple effectively with a single, dominant, low-order acoustic cavity mode at resonance.

Analysis

In this paper, the interior noise reduction characteristics of two types of control force actuators, attached to the wall of a vibrating cylinder, are analytically investigated. The two types of force actuators are: (1) a point force model, which simulates the force inputs from an electromechanical shaker, and (2) an in-plane piezoelectric force actuator model. The control inputs to these force actuators are uniquely determined such that a quadratic cost function, defined on the interior acoustic pressure, is a minimum.

Configurational details of the cylinder and force actuator models are shown in Figure 1. A single piezoelectric patch, with dimensions $(\Delta x,\ a\Delta\theta)$, is shown centered at coordinates (x_j, θ_j) on a uniform, elastic, simply-supported cylinder of length L, radius a, and thickness h. A normally directed point control force is also shown applied at coordinates (x_j, θ_j) for illustrative purposes. The cylinder is assumed to have rigid end caps, so that the interior acoustic field is produced by the wall vibration induced by the superposition of the primary acoustic loading and the actuator control forces. Herein, a single acoustic monopole, located at $(x = L/2, r = 1.2a, \theta = 0)$, was used as the primary noise source, although the generalized modal analysis outlined in this paper can readily accomodate the loading produced by more realistic noise sources.

Response To Primary And Secondary Loadings The total interior acoustic pressure field inside the vibrating cylinder can be expressed as[6,7]:

$$p(x, r, \theta) = \sum_{j=1}^{N_c} V_{c,j}\, p_{2,j}(x, r, \theta) + p_1(x, r, \theta) \tag{1}$$

in which $p_1(x, r, \theta)$ is the primary interior acoustic field (produced, for example, by the external monopole shown in Figure 1) which can be expressed by the equations:

$$p_1(x, r, \theta) = \sum_{n=0}\sum_{m=0} J_n(\alpha_m r)\cos\left(\frac{m\pi x}{L}\right)\left[P^c_{1,mn}\cos(n\theta) + P^s_{1,mn}\sin(n\theta)\right] \tag{2a}$$

$$\alpha_m^2 = k^2 - \left(\frac{m\pi}{L}\right)^2 \tag{2b}$$

The modal coefficients $P^c_{1,mn}$ and $P^s_{1,mn}$ define the primary interior acoustic field and can be expressed in terms of the primary cylinder displacement. The first term in equation (1) is due to the control inputs applied to the cylinder by the N_c force actuators. The complex amplitudes $V_{c,j}$ of the actuators are unknown and will be determined by a minimization process. The distributions $p_{2,j}(x, r, \theta)$ define the interior acoustic response produced by a single actuator located at coordinates (x_j, θ_j) with unit amplitude $V_{c,j} = 1.0$. These distributions are given by the following equation[6]:

$$p_{2,j}(x, r, \theta) = \sum_{n=0}\sum_{m=0} J_n(\alpha_m r)\cos\left(\frac{m\pi x}{L}\right)\left[P^c_{2,jmn}\cos(n\theta) + P^s_{2,jmn}\sin(n\theta)\right] \tag{3}$$

The modal coefficients $P^c_{2,jmn}$ and $P^s_{2,jmn}$ appearing in equation (3) are defined by the relations:

$$P^c_{2,jmn} = P_{mn}(\omega) \sum_{m'=1} \hat{C}_{m'm} W^c_{2,jm'n} \tag{4a}$$

$$P^s_{2,jmn} = P_{mn}(\omega) \sum_{m'=1} \hat{C}_{m'm} W^s_{2,jm'n} \tag{4b}$$

in which the modal coupling coefficients $\hat{C}_{m'm}$ account for the coupling of the sin $\left(\frac{m\pi x}{L}\right)$ functions of the cylinder radial displacement to the cos $\left(\frac{m\pi x}{L}\right)$ functions for the interior acoustic pressure. Expressions for these coefficients and the pressure modal transfer functions $P_{mn}(\omega)$ are available in the literature[5]. The shell displacement coefficients $W^c_{2,jmn}$ and $W^s_{2,jmn}$ can be related to the actuator loading coefficients, which will be introduced subsequently for both the point force and in-plane actuator models. Essentially, $W^c_{2,jmn}$ and $W^s_{2,jmn}$ are the shell displacement modal coefficients produced by a unit amplitude input ($V_{2,j} = 1.0$) to a force actuator located at coordinates (x_j, θ_j). It should be noted that the locations (x_j, θ_j) of the N_c actuators must be specified a priori. Then the distribution functions $p_{2,j}(x, r, \theta)$ defined by equation (3) are completely determined. This leaves the complex amplitudes $V_{2,j}$ as the solitary unknowns to be determined by the minimization process.

Cost Function and Optimization Procedure In order to find the optimun input $V_{2,j}$ for each force actuator, consider the following cost function defined on the acoustic pressure inside the vibrating cylinder:

$$\Lambda(V_{2,j}) = \int_0^L \int_0^a \int_0^{2\pi} r|p(x, r, \theta)|^2 d\theta dr dx \tag{5}$$

which, using equations (1) - (3) can be expanded to:

$$\Lambda(V_{2,j}) = \sum_{i=1}^{N_c} \sum_{j=1}^{N_c} K_{i,j} V_{2,i} V^*_{2,j} + \sum_{i=1}^{N_c} C_{2,i} V^*_{2,i} + \sum_{i=1}^{N_c} C^*_{2,i} V_{2,i} + \Lambda_1 \tag{6}$$

The N_c unknown amplitudes $V_{2,j}$ for the actuator forces will be determined such that $\Lambda(V_{2,j})$ takes on a minimum value. Differentiating equation (6) with respect to $V_{2,j}$ and setting the results to zero yields the following matrix equation for the N_c unknown control force amplitudes[6,8]:

$$V_{2,i} = -\left[K^*_{i,j}\right]^{-1} C_{2,j} \tag{7}$$

The minimun value for the cost function is given by:

$$\Lambda(V_{2,i})_{min} = C_{2,i} V^*_{2,i} + \Lambda_1 \tag{8}$$

The system stiffness matrix $K_{i,j}$, force vector $C_{2,i}$, and primary state cost function, Λ_1, can be expressed in the following form:

$$K_{i,j} = \sum_{n=0} \sum_{m=0} \frac{\pi \epsilon_m L}{2} \left[\epsilon_n P^c_{2,imn} P^{c*}_{2,jmn} + P^s_{2,imn} P^{s*}_{2,jmn}\right] D_{mn} \tag{9a}$$

$$C_{2,i} = \sum_{n=0}\sum_{m=0} \frac{\pi \epsilon_m L}{2} \left[\epsilon_n P^{c*}_{2,imn} F^{c}_{1,mn} + P^{s*}_{2,imn} P^{s}_{1,mn} \right] D_{mn} \tag{9b}$$

$$\Lambda_i = \sum_{n=0}\sum_{m=0} \frac{\pi \epsilon_m L}{2} \left[\epsilon_n P^{c}_{1,mn} P^{c*}_{1,mn} + P^{s}_{1,mn} P^{s*}_{1,mn} \right] D_{mn} \tag{9c}$$

In the above equations, the coefficient D_{mn} is given by:

$$D_{mn} = \frac{1}{2\alpha_m^2} \left[(\alpha_m^2 a^2 - n^2) J_n^2(\alpha_m a) + a^2 \frac{dJ_n^2(\alpha_m a)}{dr} \right] \tag{10}$$

It should be recalled that the primary cylinder loading and response is assumed to be known. Hence, the modal coefficients $P^{c}_{1,mn}$ and $P^{s}_{1,mn}$ (eq. 2a) for the primary interior acoustic field can be expressed in terms of the primary cylinder displacement modal coefficients[6]. In a similar manner, the modal coefficients $P^{c}_{2,imn}$ and $P^{s}_{2,imn}$ can also be related to cylinder displacement coefficients $W^{c}_{2,imn}$ and $W^{s}_{2,imn}$ (see eqs. 4). However, the cylinder displacement coefficients $W^{c}_{2,imn}$ and $W^{s}_{2,imn}$ are dependent upon the actuator type, that is, whether the actuator exerts normal forces (point force model) or in-plane stretching forces (piezoelectric model) on the cylinder. These modal displacement coefficients are defined in the following sections.

Point Force Actuator Model The response of a cylinder to an harmonically varying point force can be derived in a straightforward manner[7,9]. The generalized cylinder modal displacements coefficients required in equations (4) can be expressed as

$$W^{c}_{2,jmn} = H_{mn}(\omega) F^{c}_{2,jmn} \tag{11a}$$

$$W^{s}_{2,jmn} = H_{mn}(\omega) F^{s}_{2,jmn} \tag{11b}$$

in which the modal frequency response function $H_{mn}(\omega)$ accounts for the radial response of the cylinder due to a normal (radial) harmonically varying loading. The modal coefficients $F^{c}_{2,jmn}$ and $F^{s}_{2,jmn}$ appearing in equations (11) for a point force are as follows:

$$F^{c}_{2,jmn} = \left(\frac{2}{\pi \epsilon_n L} \right) \sin\left(\frac{m\pi x_{2,j}}{L} \right) \cos(n\theta_{2,j}) \tag{12a}$$

$$F^{s}_{2,jmn} = \left(\frac{2}{\pi \epsilon_n L} \right) \sin\left(\frac{m\pi x_{2,j}}{L} \right) \sin(n\theta_{2,j}) \tag{12b}$$

C-3

In-plane Piezoelectric Actuator Model In order to simulate in-plane actuator loading, the effect of the piezoelectric material on the cylinder is replaced by a line force distribution (f_x and f_θ) acting on the perimeter of the patch area as illustrated in Figure 2. With this actuator model, two piezoelectric patches bonded to opposite surfaces are driven in-phase. This model[10], when utilized on a flat plate, produces a uniform stress distribution through the plate's thickness. It should be noted that only in-plane displacements will be produced in a flat plate. However, in a shell the in-plane and out-of-plane (bending) deformations are coupled due to curvature effects. Therefore, the in-plane piezoelectric actuator will induce out-of-plane cylinder displacements.

Hence, because the in-plane actuator exerts a direct in-plane force on the middle surface of the cylinder and produces an out-of-plane displacement, the in-plane analysis must consider the coupled (axial, tangential and radial) cylinder displacements and is therefore slightly more complicated than the point force analysis outlined previously. The cylinder displacement coefficients $W^c_{2,jmn}$ and $W^s_{2,jmn}$ for the in-plane actuator model have the form

$$W^c_{2,jmn} = H^{(1)}_{mn}(\omega)A^c_{jmn} - H^{(2)}_{mn}(\omega)T^s_{jmn} \tag{13a}$$

$$W^s_{2,jmn} = H^{(1)}_{mn}(\omega)A^s_{jmn} + H^{(2)}_{mn}(\omega)T^c_{jmn} \tag{13b}$$

in which the frequency response functions $H^{(1)}_{mn}(\omega)$ and $H^{(2)}_{mn}(\omega)$ can be developed from the governing shell equations[6]. These transfer functions account for the coupling between the out-of-plane displacements of the cylinder and the in-plane force inputs produced by the piezoelectric actuator.

The axial loading coefficients A^c_{jmn} and A^s_{jmn} appearing in equations (13) are defined as follows[6]:

$$A^c_{jmn} = \frac{-S}{\pi L}\sin\left(\frac{m\pi\Delta x}{2L}\right)\sin\left(\frac{m\pi x_j}{L}\right)\begin{cases}\frac{\Delta\theta}{4} & \text{if } n = 0\\ \frac{1}{n}\sin\left(\frac{n\Delta\theta}{2}\right)\cos(n\theta_j) & \text{otherwise}\end{cases} \tag{14a}$$

$$A^s_{jmn} = \frac{-S}{\pi L}\sin\left(\frac{m\pi\Delta x}{2L}\right)\sin\left(\frac{m\pi x_j}{L}\right)\begin{cases}0 & \text{if } n = 0\\ \frac{1}{n}\sin\left(\frac{n\Delta\theta}{2}\right)\sin(n\theta_j) & \text{otherwise}\end{cases} \tag{14b}$$

and the circumferential (twisting) loading coefficients, T^c_{jmn} and T^s_{jmn} are:

$$T^c_{jmn} = \frac{-S}{\pi a}\sin\left(\frac{m\pi\Delta x}{2L}\right)\sin\left(\frac{m\pi x_j}{L}\right)\begin{cases}0 & \text{if } n = 0\\ \frac{1}{m}\sin\left(\frac{n\Delta\theta}{2}\right)\sin(n\theta_j) & \text{otherwise}\end{cases} \tag{15a}$$

$$T^s_{jmn} = \frac{S}{\pi a}\sin\left(\frac{m\pi\Delta x}{2L}\right)\sin\left(\frac{m\pi x_j}{L}\right)\begin{cases}0 & \text{if } n = 0\\ \frac{1}{m}\sin\left(\frac{n\Delta\theta}{2}\right)\cos(n\theta_j) & \text{otherwise}\end{cases} \tag{15b}$$

Discussion of Results

Results are presented for a large-scale, simply-supported, aluminum cylinder which is $1.68m$ in diameter, $3.66m$ long, and has a thickness of $1.7mm$. The cylinder is closed with hard (rigid) end caps. It is assumed that the interior acoustic field is due solely to the vibration of the cylinder walls. The primary field is harmonic ($e^{-j\omega t}$) and is produced by an exterior acoustic monopole $0.2a$ from the cylinder wall at ($x = L/2, r = 1.2a, \theta = 0°$), as shown in figure 1. This source configuration produces only symmetric axial modes and circumferential $\cos(n\theta)$ modal variations. This simplifies the control problem and makes the data easier to interpret. Generalizations to a realistic aircraft fuselage structure will necessarily be more complicated, but the physical mechanisms and understanding arising from this simpler structural model will aid in understanding more complicated structural acoustic configurations.

All control forces in this study are confined to act in the source plane ($x = L/2$). Two types of control actuators are considered in this paper: (1) normal point forces (shaker inputs) and (2) in-plane piezoelectric force actuators. It should be recalled that a single piezoelectric actuator consists of two congruent patches bonded to opposite sides of the cylinder wall. For all calculations presented herein, the patch dimension in the axial direction is $\Delta x = 3.8cm$ ($1.5in.$). The circumferential dimension ($a\Delta\theta$) varies on a case by case basis depending on the number of piezoelectric actuators used ($N_c = 1, 2, ..., 18$) for a particular configuration. The control inputs (amplitudes) to the actuators were determined so that the integrated square of the acoustic pressure over the interior volume was a minimum.

Various actuator configurations are studied and the effect on overall attenuation and control spillover is examined both for the acoustic cavity response as well as for the vibration response of the cylinder. Results are presented in terms of reductions of the interior sound pressure levels. All sound pressure levels (SPL) are referenced to the maximum SPL for the no control case at that particular frequency. These are shown by comparisons of the pressure distributions in the source cross section ($x = L/2$) for the various control conditions. In addition, comparisons of the pressure response are presented in terms of the axial and circumferential wavenumber spectra, which clearly illustrate the effect of control on the modal content of the interior pressure field. All modal amplitudes for a particular frequency are referenced to the maximum amplitude mode for the no control case.

Results are presented for two frequencies: (1) a cylinder resonance ($100Hz$) and (2) an acoustic cavity resonance ($200Hz$). For a monopole excitation of $100Hz$, the structural acoustic response is dominated by a resonance of the ($m = 1; n = 2$) cylinder mode, which drives an off-resonant acoustic cavity response. The second frequency considered is $200Hz$, which excites an acoustic resonance of the ($m = 0; n = 2$) cavity mode. This response is driven by a number of $n = 2$ cylinder modes. In addition, control spillover effects are present for both of these frequencies and variations in the size and number of the control actuators, for minimizing these effects, are investigated.

Structural Resonance The interior acoustic response, due to the exterior monopole oscillating at $100Hz$, is shown in figure 3a. This response is dominated by the $(m = 0, 2; n = 2)$ cavity modes as shown in the wavenumber distribution of figure 4a. Both of these modes are excited by the $(m = 1; n = 2)$ cylinder mode, which has a resonant frequency of $99Hz$. Due to the circular nature of the cross section, the $\sin\left(\frac{m\pi x}{L}\right)\cos(2\theta)$ cylinder modes couple only with the $\cos\left(\frac{m\pi x}{L}\right)\cos(2\theta)$ cavity modes. However, multiple axial modes are excited due to the coupling of the $\sin\left(\frac{\pi x}{L}\right)$ function to a range of $\cos\left(\frac{m\pi x}{L}\right)$ functions. Due to symmetry, which does not permit even $(m = 0, 2, \ldots)$ order cylinder modes or odd $(m = 1, 3, \ldots)$ order cavity modes, the dominant modes in the primary pressure field are the $m = 0, 2$ modes. All of the other modes are greater than $20dB$ down in the pressure response.

Due to the relatively uniform distribution of the external monopole loading, only low-order cylinder and acoustic modes are excited. Also, the implicitly higher damping that is associated with the higher-order cylinder modes, as well as the reduced structural acoustic coupling of these modes tends to further enhance the importance of the lower-order modes.

Localized Control Actuators Figure 3b shows the optimized interior pressure distribution using two point forces as the control actuators. The two forces are placed at $\theta = 0°, 180°$. The average SPL reduction throughout the interior volume is $17.1dB$. The maximum SPL for this condition is $10.3dB$ less than the maximum amplitude for the no control case. The effect of the controller is to reduce the response of the resonant $(m = 1; n = 2)$ cylinder mode by about $37dB$. The physical mechanism at work here is an increase in the input impedance of the cylinder for this mode, which occurs due to the interaction of the primary and secondary forces. The residual field shown in figure 3b is dominated by higher-order modes $(m = 2, 4; n = 12)$ and $(m = 2; n = 6, 8, 10)$. These modes are generated by the control forces and are collectively referred to as a control spillover effect. That is, the controller produces extraneous modal responses that are not present in the primary structural acoustic response. These arise from the localized response generated by the point control forces. The net effect is to increase the peak vibration response of the cylinder. Peak cylinder vibrations levels increased $4.6dB$ for the composite case of figure 3b over the peak level of figure 3a.

This spillover effect, which arises from the discrete nature of the point control force actuators, tends to excite a wide range of modes in the cylinder. In order to repress these control spillover effects, piezoelectric actuators are often cited as an effective control alternative. However, discrete piezoelectric actuators also tend to excite similar spillover responses. This is shown in figure 3c and 4b. Here, two piezoelectric actuators, 6.35 cm by 3.8 cm in circumferential and axial dimensions, respectively, are used as control actuators. Each actuator subtends a circumferential angle of 4.3°. The composite field, due to the action of these control actuators, is shown to be not discernably different from that for the point force actuators. The volume integrated reduction in interior SPL is $16.9dB$. The wavenumber distribution for the optimized point force actuators are similar to that shown in figure 4b for the optimized piezoelectric actuators. The higher-order

modes dominate the composite pressure response, providing an interior noise floor, which limits the overall reduction. Finally, the peak vibration level of the cylinder for the control case increased $4.7dB$, similar to the previous case.

Extended Control Actuators One method found to be effective in controlling modal spillover is to increase the patch size of the piezoelectric actuators. This effect is displayed in parts (b) and (c) of figure 5, for single piezoelectric actuators with the same axial dimension as considered previously ($3.8cm$). Here, however, the circumferential length has been increased to subtend an angle of 30° in one case and 90° in the second case. The wavenumber distribution is presented for both control cases, as well as for the no control case, figure 5a. The controller with the 30° actuator achieved an volume integrated SPL reduction of $19.6dB$. Comparing figure 5b to figure 4b shows this reduction was achieved by significantly reducing the excitation of higher-order modes by the control input. In this case, the strongest residual mode is the $(m = 2; n = 7)$ mode. This improvement was achieved with a single actuator (one control degree of freedom) as compared to the cases of figures 3 and 4, where two control inputs (two control degrees of freedom) were used. Also, the peak cylinder vibration level was reduced by $2dB$ over the no control case. The case shown in figure 5c reduces the control spillover effects even further, particularly for the lower-order $m = 0$ modes and for the mid-range $n = 2$ modes. This is due to the single piezoelectric actuator not coupling as effectively to those modes with phase reversals over the 90° actuator length. The volume integrated SPL reduction for this case is $22.5dB$ and the peak cylinder vibration was reduced by $7.9dB$.

These reductions were achieved as a result of the uniform distribution of axial (in-plane, see fig. 2) control forces over the circumferential length of the 30° or 90° actuators. Both of these actuator cases utilized a single control degree of freedom, the simplest possible controller implementation. However, such a simple actuator configuration yields a much less flexible control system. In practice, it would be expected that different frequencies (i.e. harmonics) will require different arrangements of actuators. By fixing the actuators in such large increments, compromises across a range of frequencies might be expected to result in substantially reduced performance. However, both of the extended actuator arrangements considered previously resulted in reduced vibration levels in the cylinder. This effect will be important to the structural acoustic designer when loads and fatigue life are considered.

As a final case, a more versatile arrangement of the single 90° actuator is considered. Again, the primary field is that presented in figure 5a, the frequency is $100Hz$ with a dominant cylinder mode driving two dominant acoustic cavity modes. In this configuration, the 90° actuator is broken up into 18 individual actuators, each subtending 5°. This is nearly the same size as the dual actuators of figure 3c. The result of optimizing this 18 degree-of-freedom system is compared in figure 6 to that of the single control actuator of the same overall size. The wavenumber spectra is shown for each case. For this case only 4 modes are evident in the $42dB$ dynamic range of the plot of figure 6b, compared to 10 modes in figure 6a. The $(m = 0; n = 1)$ mode is the strongest residual mode and this mode is nearly $7dB$ higher for the case of figure 6b compare to figure 6a. However,

the integrated volume reduction is $26.1dB$ compared to $22.5dB$ for the single degree of freedom actuator shown in figure 6a. The peak cylinder vibration level is reduced by $8.6dB$ relative to the no control case, only an incremental improvement over the $7.9dB$ reduction obtained with the single actuator of figure 6a.

Therefore, for this excitation frequency ($100Hz$), for a single dominant cylinder mode, the multi-degree of freedom optimization yields only a marginal improvement over the single degree of freedom system. When controller complexity is considered, the single degree of freedom system is more attractive. However, the multi-degree of freedom system adds the element of configurability for different conditions and frequencies. This versatility would be a very desirable characteristic in any implementation of a control system in a real aircraft structure.

Acoustic Cavity Resonance The interior cavity response at $x = L/2$ is shown in figure 7a for an exterior monopole frequency of $200Hz$. The external acoustic monopole remains at location ($x = L/2, r = 1.2a, \theta = 0°$). The interior acoustic response is again seen to be dominanted by a $\cos(2\theta)$ variation in the crossection. The ($m = 0; n = 2$) acoustic cavity mode has a resonance at $199Hz$ and the ($m = 2; n = 2$) mode has a resonance at $220Hz$. The odd order ($m = 1, 3, ...$) acoustic modes cannot be driven due to the symmetry of the excitation. In a more generalized configuration this would not be the case. The structural response is dominanted by the ($m = 3; n = 4$) mode, which has a resonant frequency of $213Hz$. Other modes contributing strongly to the structural response are the ($m = 1; n = 3$) and ($m = 1; n = 1$) modes, both at about $-8.7dB$ and the ($m = 1; n = 2$) mode at $-9.3dB$. The latter cylinder mode is the most significant in this case as it excites the dominant resonant cavity mode. In addition, due to the cross coupling of all the $\sin\left(\frac{m\pi x}{L}\right)\cos(2\theta)$ modes of the cylinder with the $\cos\left(\frac{m\pi x}{L}\right)\cos(2\theta)$ acoustic cavity modes, each of the $n = 2$ cylinder modes may drive this cavity resonance. Therefore, it is not sufficient to control just one cylinder mode; all of these modes ($m = 1, 3, ...; n = 2$) must be controlled.

The wavenumber spectra of figure 8a illustrates the distribution of acoustic cavity modes for the primary response shown in figure 7a. The ($m = 0, 2, 4; n = 2$) cavity modes have relative levels of $0.0dB$, $-14.3dB$, and $-27dB$, respectively, with all modes normalized to the dominant ($m = 0; n = 2$) acoustic cavity mode. The dominant cylinder mode drives the ($m = 0, 2, 4; n = 4$) acoustic modes with relative levels of $-16.6dB$, $-12.7dB$, and $-15.3dB$, respectively. The ($m = 0; n = 3$) cavity mode is also driven at a $-14.5dB$ level. The resonant frequencies of all the $n = 4$ cavity modes are greater than $346Hz$ and the $n = 3$ cavity modes are above $273Hz$. Therefore, these modes are forced by the cylinder vibration and are non-resonant responses. It can be seen that this is a more complicated interior noise field to control than was the case for the previous structural resonance case. The driven modes will impose a noise floor that will limit the control achieveable. It is expected that a sufficient number of degrees of freedom in the control optimization will be required to exercise control over a broad range of modes.

Localized Control Actuators Figure 7b illustrates the control attained using two point control forces at $\theta = 0°$ and $150°$. An integrated volume SPL reduction of $8.7dB$ was attained. The response is now dominated by a higher-order circumferential variation in the source plane. The wavenumber spectra for this case, shown in figure 8b, shows that effective control of the $(m = 0, 2; n = 2)$ cavity modes was attained with reductions of $20.3dB$ and $9.8dB$, respectively. However, considerable control spillover has been generated for a wide range of higher-order modes. The $(m = 2, 4; n = 4)$ cavity modes are now dominant with levels of $-6.2dB$ and $-9.4dB$, respectively, relative to the uncontrolled $(m = 0; n = 2)$ mode. The action of the actuator control forces has contributed to these modes significantly.

Extended Control Actuators Replacing the point control forces with piezoelectric actuators, with the same dimensions as for the case discussed in figure 3c, yields similar results to the point force case just discussed (figure 7b). Therefore, the point force results are compared with a single piezoelectric actuator centered at $\theta = 0°$, having an axial length of $3.8cm$ and a circumferential length subtending an angle of $60°$. The results for this actuator configuration are shown in figure 7c with the wavenumber distribution shown in figure 8c. The circumferential length of this actuator was chosen in order to subtend an angle large enough to avoid exciting higher-order circumferential modes. A piezoelectric actuator extending from $\theta = 45°$ to $\theta = -45°$ with a $\cos(2\theta)$ weighted voltage input would be ideal. However, since the actuator model is defined with a step function at each edge, the actuator length was selected to extend only over $60°$ in order to mitigate some of this effect. Its length still subtends an angle that spans a phase reversal of the $\cos(4\theta)$ mode and all higher-order modes.

The results presented in the wavenumber plot of figure 8c supports this supposition. Most of the higher-order modes have been significantly reduced. The $(m = 0, 2, 4; n = 4)$ cavity modes have all been reduced by $3.2dB$. This reduction is due to $3.2dB$ less controller excitation of the $(m = 3; n = 4)$ cylinder mode for the extended actuator compared to the two point forces. The integrated volume SPL reduction is $17.3dB$, compared to the no control case of figure 7a. Finally, the peak vibration level for this actuator arrangement increased $2.5dB$, significantly less than the $15dB$ increase found for the point force actuators.

Finally, an evaluation of a multi-degree of freedom piezoelectric actuator is examined in figure 9. In this configuration, the actuator elements each subtend a $5°$ angle as before. Twelve actuators, centered at $\theta = 0°$ and subtending $60°$ around the circumference of the cylinder make up the array. The volume integrated SPL reduction remained about the same as for the single actuator, $17.8dB$. The peak vibration response increases by $5.7dB$ over the uncontrolled case, a $3.2dB$ increase over the single actuator case. Comparing the wavenumber spectra of figures 9a and 9b, the optimization of this actuator configuration, with 12 control degrees of freedom, has reduced all of the $(n = 4)$ acoustic cavity modes by an average of $12dB$. This is directly related to a reduction of the $(m = 3, n = 4)$ cylinder mode by $20dB$ over the uncontrolled case. However, a range of higher-order

modes are excited by the 12 degree of freedom optimization. These contribute to the residual acoustic field in such a way as to limit overall interior noise suppression.

In this case, the multi-degree of freedom controller has again not significantly realized increased control performance. In fact, the peak vibration level in the cylinder has increased. Since cylinder vibration effects are not included in the cost function, this is not atypical, especially for an acoustic response dominated by a cavity resonance. In the previous case, the acoustic response was dominated by a cylinder resonance and the vibration response might be expected to be reduced consistently. For the cases considered in this paper, one may argue that the performance does not justify the added complexity of additional controller degrees of freedom, that is, multiple actuators. Again, however, the adaptability of this configuration to a range of operating conditions and broadband frequency control may ultimately justify such an implementation.

Concluding Remarks

The interior noise reduction effectiveness for two types of control force actuator models has been investigated. The two types of force actuators were: (1) a point force model and (2) an in-plane piezoelectric model. The actuators were mounted on the wall of a simply-supported, elastic cylinder closed with rigid end caps. The in-plane piezoelectric actuator model consisted of two congruent, rectangular patches of piezoelectric material bonded to opposite sides of the cylinder wall. The two patches were driven in-phase so as to exert in-plane control forces on the cylinder. The primary, offending noise field inside the cylinder was produced by the cylinder wall vibrations excited by a harmonically varying, external acoustic monopole. Generally, a number of force actuators were employed and the force inputs (amplitudes) to the actuators were determined so that the integration of the square of the interior pressure over the cavity volume was a minimun.

Results were presented for two low frequency response regimes. The first case was for a frequency of 100.0 Hz, where the cylinder response was characterized by a single, resonant (dominant), vibration mode of low order and the interior acoustic response was essentially forced in a number of off-resonant acoustic cavity modes. The second, higher frequency case at 200.0 Hz was typical of situations where the cylinder vibration response consisted of both near- resonant and off-resonant modes. However, the acoustic cavity response was dominated by a single, low-order, cavity mode.

Significant interior noise reductions were achieved for all actuator configurations, but especially for the structurally dominated responses. Reductions of $9dB$ to $26dB$ were achieved using normal point force actuators as well as localized and extended piezoelectric actuators. Comparisons of point force control models to small piezoelectric models indicate no significant advantage of one type over the other in terms of control performance. However, ease of mounting, placement versatility and cost would all tend to favor the piezoelectric actuator.

These results illustrate the power of the Active Structural Acoustic Control methodology for achieving effective noise reduction using only a limited number of actuators.

However, control spillover was found to limit overall performance for all cases. The use of extended piezoelectric actuators was effective in reducing the control spillover without increasing the controller degrees of freedom. However, it is expected that fixed arrangements of extended transducers will inhibit the application of this technology to wideband frequency control. This is especially important in rotorcraft where gearbox noise is dominant.

It was also shown that larger, multi-degree of freedom transducer configurations were effective in controlling interior noise. These configurations tended to excite less vibration in the cylinder than did the localized actuators. A real control system may be expected to add structural response inputs to the cost function in order to insure that the structure is not overly excited. However, this is expected to degrade the acoustic performance.

Finally, the use of multi-degree of freedom control systems may be expected to contribute significantly to overall controller complexity. This study has shown that effective control may be achieved with limited control "channels". However, this conflicts with the requirement for wideband multi-modal control. It is envisioned that reductions in the controller channels may be obtained by driving multiple control elements with a single controller output. By implementing this with broadband filters, an effective, lightweight, limited degree of freedom controller may be feasible.

References

1. Facey, J.R.:"Return of the Turboprops", *Aerospace America*, October, 1988, pp. 14-15.
2. Elliott, S.J. et al: "Preliminary Results of an In flight Experiment on the Active Control of Propeller-induced Cabin Noise", *Journal of Sound and Vibration*, No. 128(2), pp. 355-357, 1989.
3. Dorling, C.M. et al: "A Demonstration of Active Noise Reduction in an Aircraft Cabin", *Journal of Sound and Vibration*, No. 128(2), pp. 358-360, 1989.
4. Elliott, S.J. et al: "In-flight Experiments on the Active Control of Propeller-induced Cabin Noise", *Journal of Sound and Vibration*, No. 140(2), pp. 219-238, 1990.
5. Fuller, C.R. et al: "Active Control of Interior Noise in Model Aircraft Fuselages Using Piezoceramic Actuators", AIAA 13th Aeroacoustics Conference, Paper No. 90-3922, October 22-24, 1990, Tallahassee, FL.
6. Lester, H. C. and Lefebvre, S.: "Piezoelectric Actuator Models for Active Sound and Vibration Control of Cylinders", Proceedings of the Conference on Recent Advances in Active Control of Sound and Vibration, Virginia Polytechnic Institute and State University, Blacksburg, Virginia, April 15-17, 1991, Technomic Publishing Co., Inc.
7. Junger, M. C. and Feit, D.: *Sound, Structures, and Their Interaction*, 2nd ed., The MIT Press, Cambridge, 1986.
8. Noble, B.: "Applied Linear Algebra", Prentice-Hall, Inc., Inglewood Cliff, New Jersey, 1977.

9. Silcox, R. J. and Lester, H. C.: "Propeller Modelling Effects on Interior Noise in Cylindrical Cavities with Application to Active Control", Paper No. 89-1123, AIAA 12th Aeroacoustics Conference, April 10-12, 1989, San Antonio, TX.
10. Dimitriadis, E. K.; Fuller, C. R.; and Rogers, C. A.: "Piezoelectric Actuators for Distributed Noise and Vibration Excitation of Thin Plates", ASME Journal of Vibration and Acoustics, Vol. 113, 1991, pp 100-107.

Nomenclature

A_{mn}	modal coefficients for axial actuator loads
a	radius of cylinder
C_f	speed of sound in air
$C_{2,j}$	system force vector
$\hat{C}_{m'm}$	modal coupling coefficients
F_{mn}	modal coefficients for radial (out-of plane) actuator loads
$H_{mn}(\omega)$	cylinder modal frequency response function
h	cylinder thickness
J_n	complex Bessel function of order n
$K_{1,j}$	system stiffness matrix
k	free space wavenumber, $k = \omega/C_f$
L	length of cylinder
m	axial wavenumber
N_c	number of force actuators
n	circumferential wavenumber
P_{mn}	modal coefficients for acoustic pressure inside cylinder
$P_{mn}(\omega)$	pressure modal frequency response function
p	acoustic pressure inside cylinder
T_{mn}	modal coefficients for tangential actuator loads
V_j	actuator complex amplitude
W_{mn}	modal amplitudes for radial (out-of-plane) cylinder displacement
x, r, θ	cylindrical coordinates
x_j, θ_j	actuator center coordinates
α_m	radial wavenumber
$\Delta x, \Delta\theta$	dimensions of piezoelectric actuator
ϵ_k	equals 2 if k=0, equals 1 otherwise
Λ	cost function
ω	steady state circular frequency
Subscripts	
j	actuator index, $j = 1, 2, \ldots, N_c$
m	axial mode number
n	circumferential mode number
1	primary field variable
2	control field variable

Superscripts

c	denotes $\cos(n\theta)$ component
s	denotes $\sin(n\theta)$component

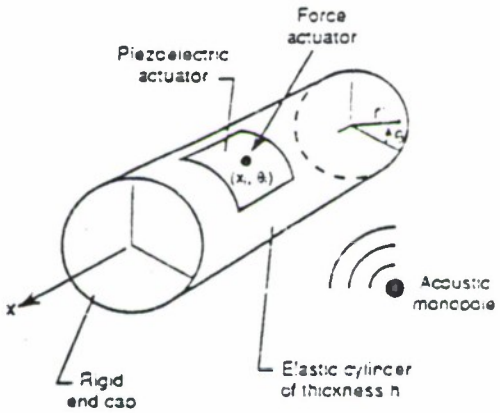

Figure 1. Schematic of fuselage model

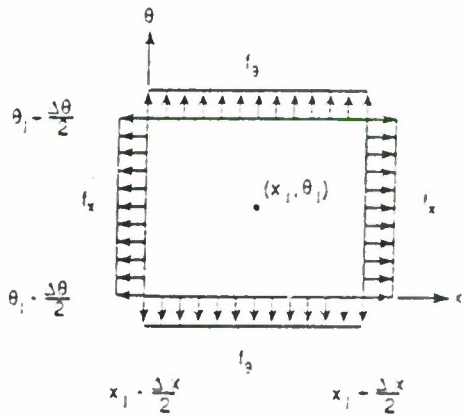

Figure 2. Piezo actuator force model

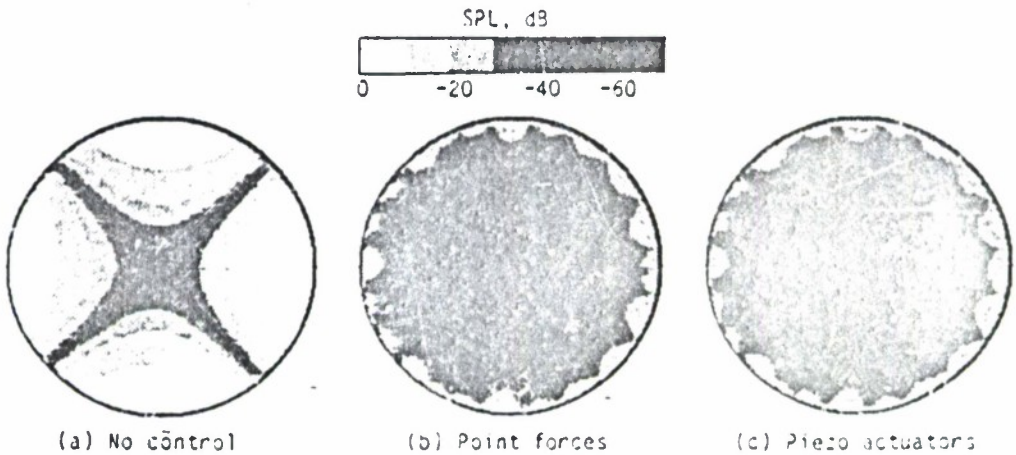

Figure 3. Effect of control actuators on interior pressure. f=100 Hz, x=L/2

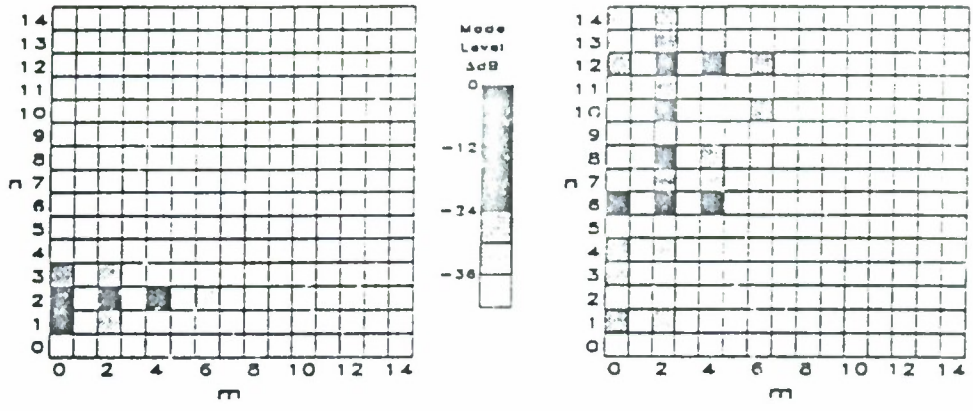

(a) No control (b) Two piezo actuators, $\Delta\theta_2 = 5°$

Figure 4. Effect of two control actuators on wavenumber spectra, f=100 Hz.

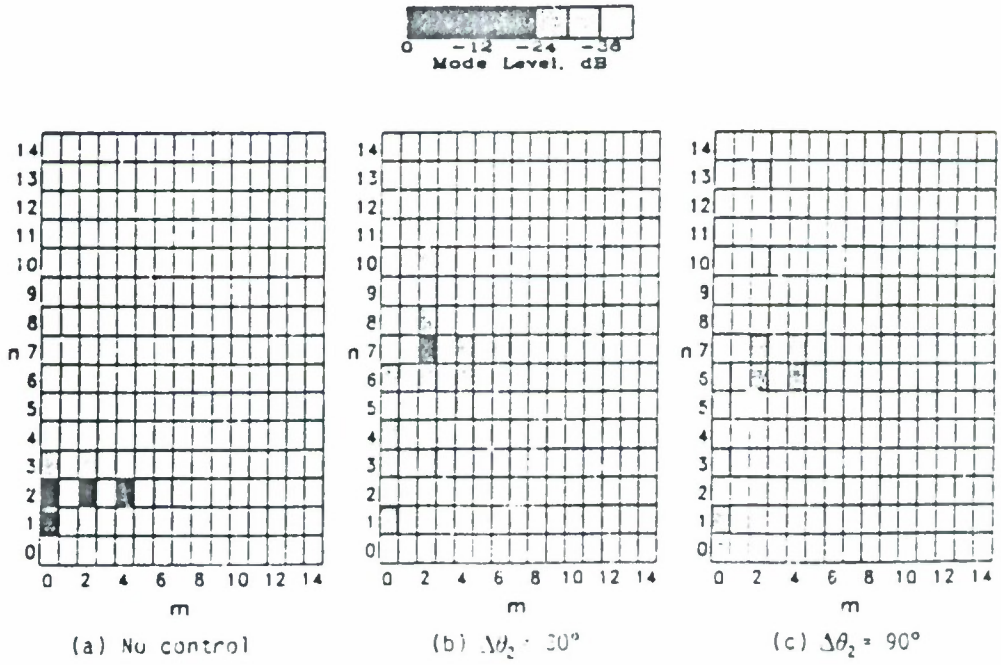

(a) No control (b) $\Delta\theta_2 = 30°$ (c) $\Delta\theta_2 = 90°$

Figure 5. Effect of piezo actuator size on wavenumber spectra, f=100 Hz.

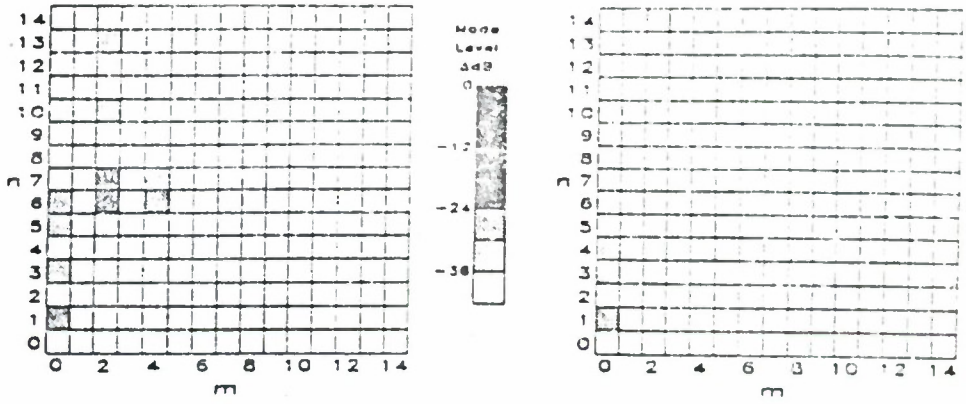

(a) Single piezoactuator, $\Delta\theta_2 = 90°$ (b) 18 piezo actuators, $\Delta\theta_2 = 5°$

Figure 6. Effect of actuator degrees-of-freedom on wavenumber spectra, f=100 Hz.

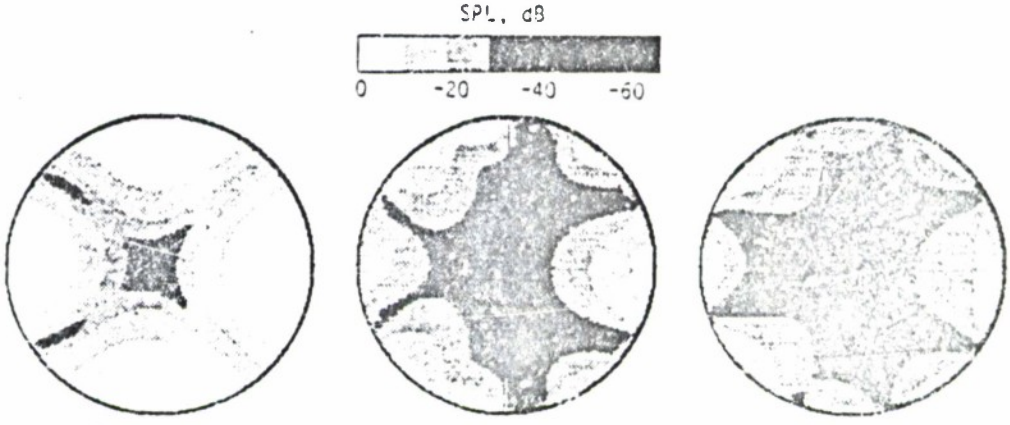

(a) No control (b) Point forces (c) Piezo actuator, $\Delta\theta_2 = 60°$

Figure 7. Effect of two control actuator configurations on interior pressure, f=200 Hz, x=L/2.

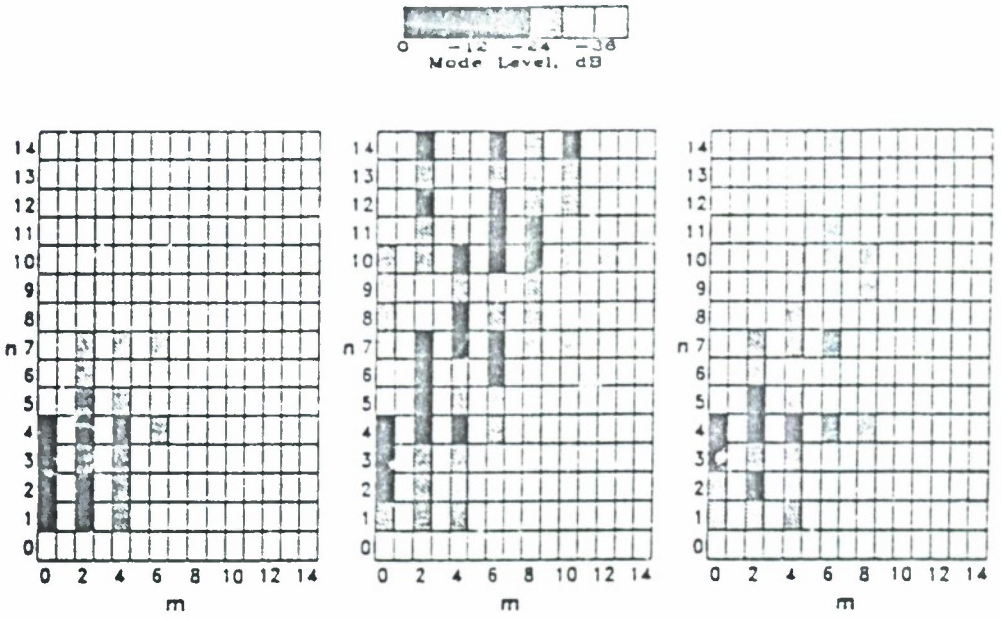

(a) No control (b) Two point forces (c) Piezo actuator, $\Delta\theta_2$ =60°

Figure 8. Effect of two control actuator configurations on wavenumber spectra, f=200 Hz.

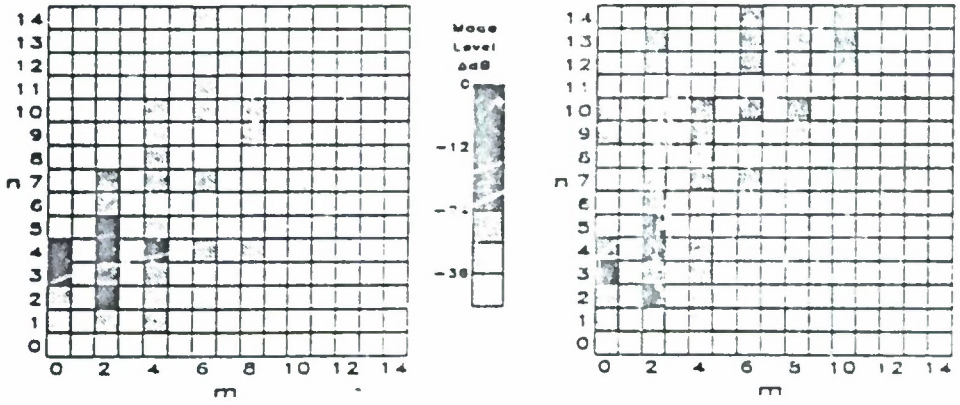

(a) Single piezo actuator, $\Delta\theta_2$ =60° (b) 12 piezo actuators, $\Delta\theta_2$ =5°

Figure 9. Effect of actuator degrees-of-freedom on wavenumber spectra, f=200 Hz.

N92-32959

Sound Transmission Reduction with "Intelligent" Panel Systems

by

Chris R. Fuller and Robert L. Clark
Mechanical Engineering Department
Virginia Polytechnic Institute and State University
Blacksburg, Virginia 24061-0238

This presentation is concerned with an experimental and theoretical investigation of the use of "intelligent" panel systems to control sound transmission and radiation. An "intelligent" panel is defined as a structural system with integrated actuators and sensors under the guidance of an adaptive, learning type controller. The system configuration is based on the Active Structural Acoustic Control (ASAC) concept where control inputs are applied directly to the structure to minimize an error quantity related to the radiated sound field. In this case multiple piezoceramic elements are used as actuators while optimally shaped PVDF piezoelectric elements are employed as sensors. The control approach is a multi-channel Filtered X algorithm implemented on a TMS320C25 DSP. The PVDF sensors are shaped so as to observe that part of the structural motion associated with sound radiation. In essence, the sensors act as distributed wavenumber filters. The importance of optimal shape and location is demonstrated to be of the same order of influence as increasing the number of channels of control. The work demonstrates the large potential of such systems to control sound transmission through distributed structural systems.

Sound Transmission Reduction with "Intelligent" Panel Systems

by

Chris R. Fuller
and
Robert L. Clark

Mechanical Engineering Department
Virginia Polytechnic Institute and State University
Blacksburg, VA 24060

Presentation at NASA/SAE/DLR 4th Interior Noise Workshop
Freidrich Schafen, Germany
May 19-20, 1992

Vibration and Acoustics Laboratory

Outline

- ASAC concepts
- Intelligent panel definitions
- Multiple piezoelectric actuators
- Design optimization of piezoelectric actuators and sensors
- Modal Sensors
- Conclusions

Active Structural Acoustic Control (ASAC) - Concepts

- apply control inputs to the structure while minimizing a sound radiated related variable.
- modal suppression - only control those structural modes well coupled to the acoustic field.
- modal restructuring - little change in amplitude of residual response of structure however has lower overall radiation efficiency.

Radiation Efficiency of Selected Structural Plate Modes

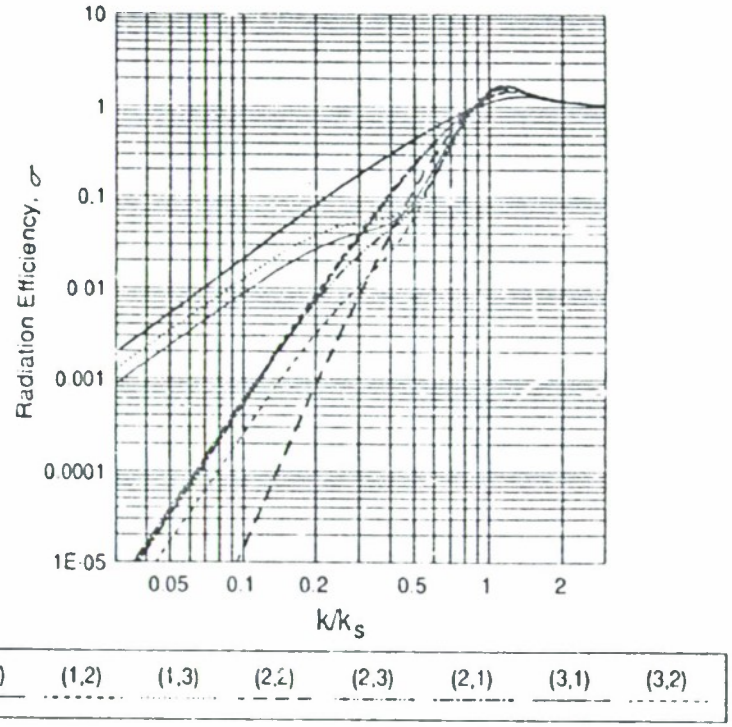

Modes of Radiation

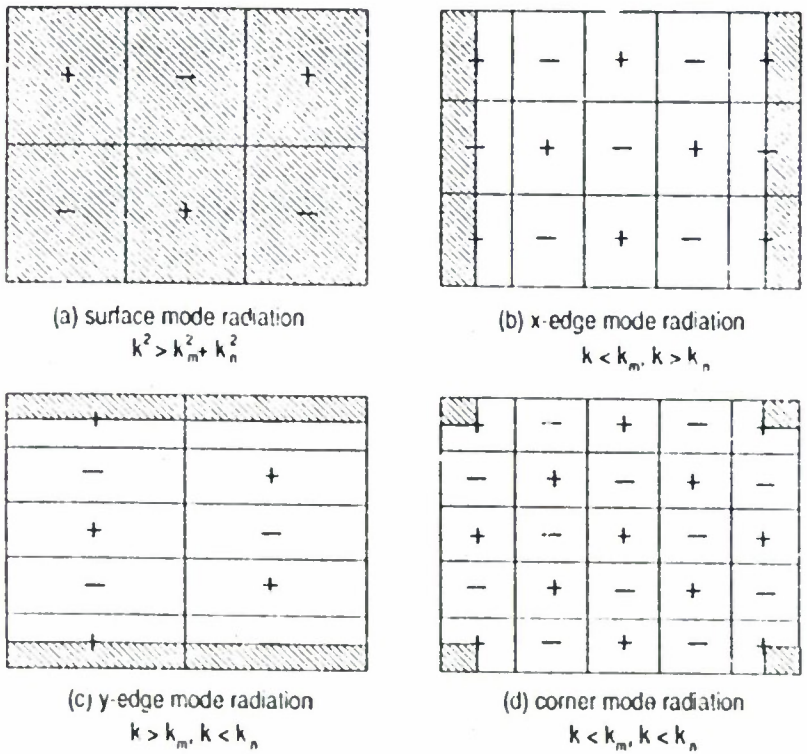

(a) surface mode radiation
$k^2 > k_m^2 + k_n^2$

(b) x-edge mode radiation
$k < k_m, k > k_n$

(c) y-edge mode radiation
$k > k_m, k < k_n$

(d) corner mode radiation
$k < k_m, k < k_n$

The Wavenumber Transform

$$\bar{V}(k_x, k_y) = \frac{1}{\sqrt{2\pi}} \int_{-\infty}^{+\infty} \int_{-\infty}^{+\infty} v(x,y) \exp(-ik_x x) \exp(-ik_y y) dx dy.$$

- only supersonic waves radiate ($k_o \leq \sqrt{k_x^2 + k_y^2}$)
- modal suppression corresponds to a fall of $\bar{V}$ across the spectrum
- modal rearrangement corresponds to a fall **only in supersonic components**, subsonic may even increase

Example of 1-D Wavenumber Spectrum

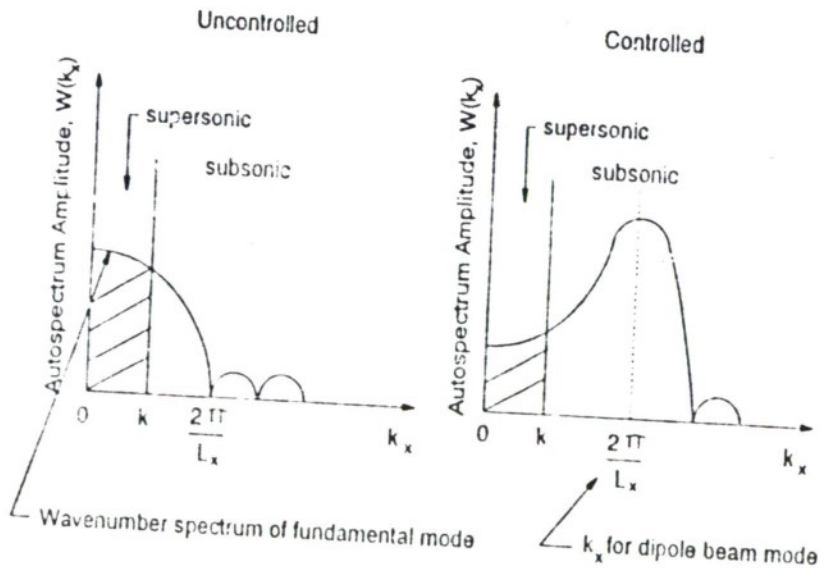

"Intelligent", "Smart" or "Adaptive" Structure

- piezoceramic actuators bonded or embedded in the structure
- PVDF optimized or shaped sensors
- adaptive, learning type controller (non model based)

Block Diagram of LMS Controller

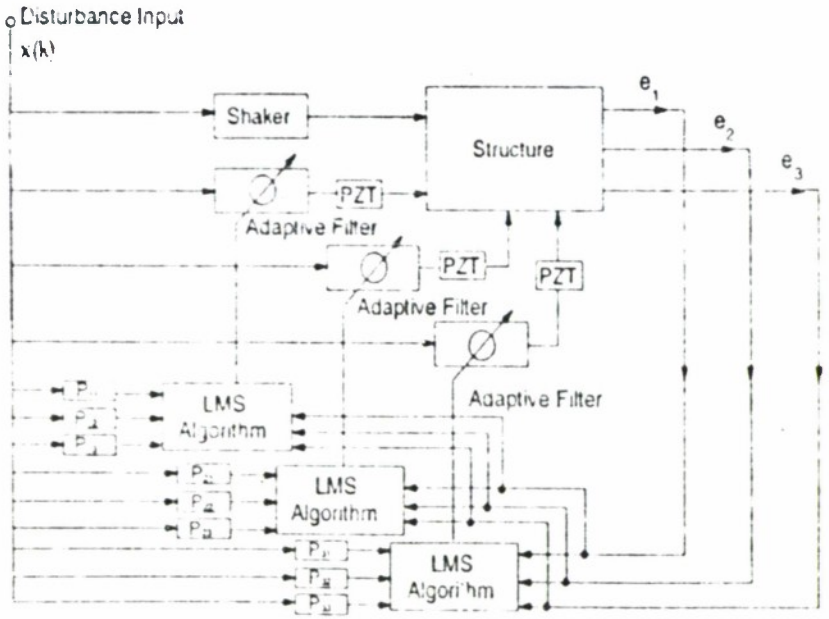

Non-Optimal Multi-Actuator Configuration

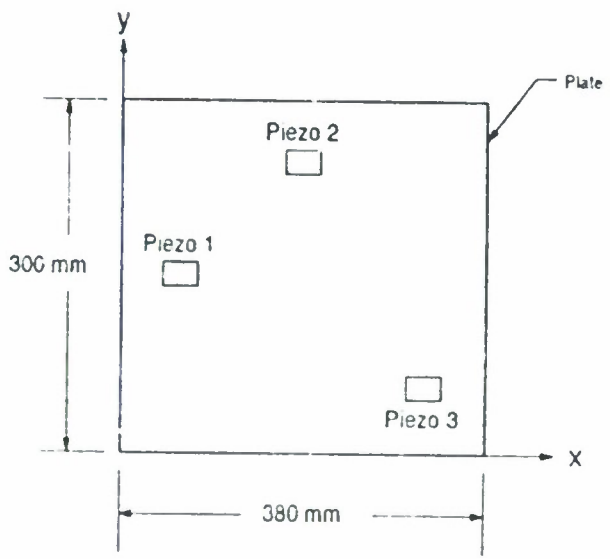

Results from Non-Optimal Multi-Actuator Control Case (400 Hz)

Experimental

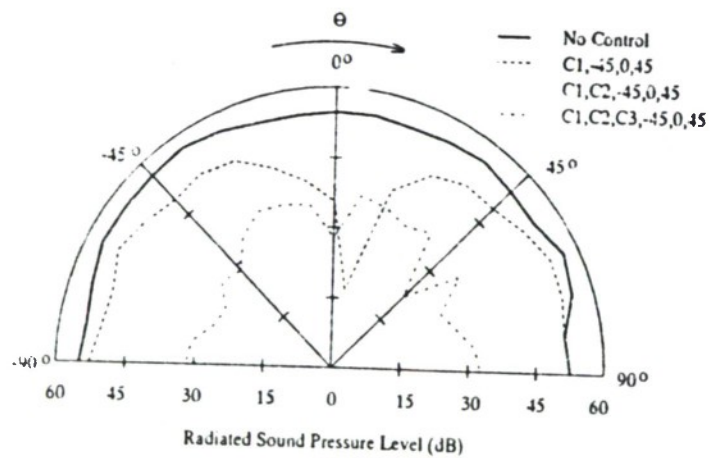

Theoretical

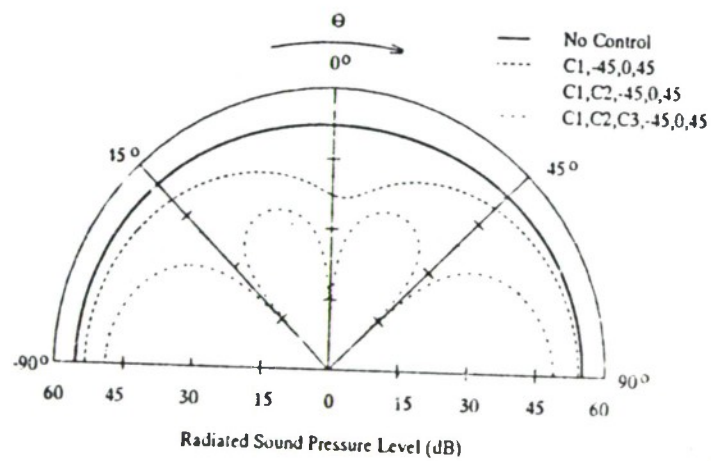

Flow Chart for Optimization

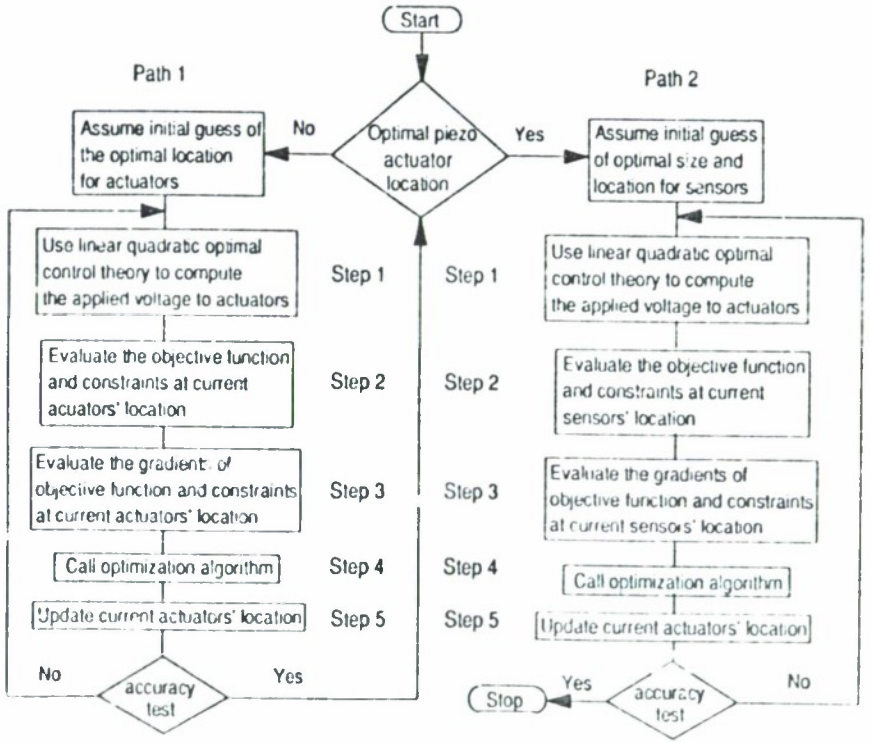

Optimal Actuator/Sensor Location

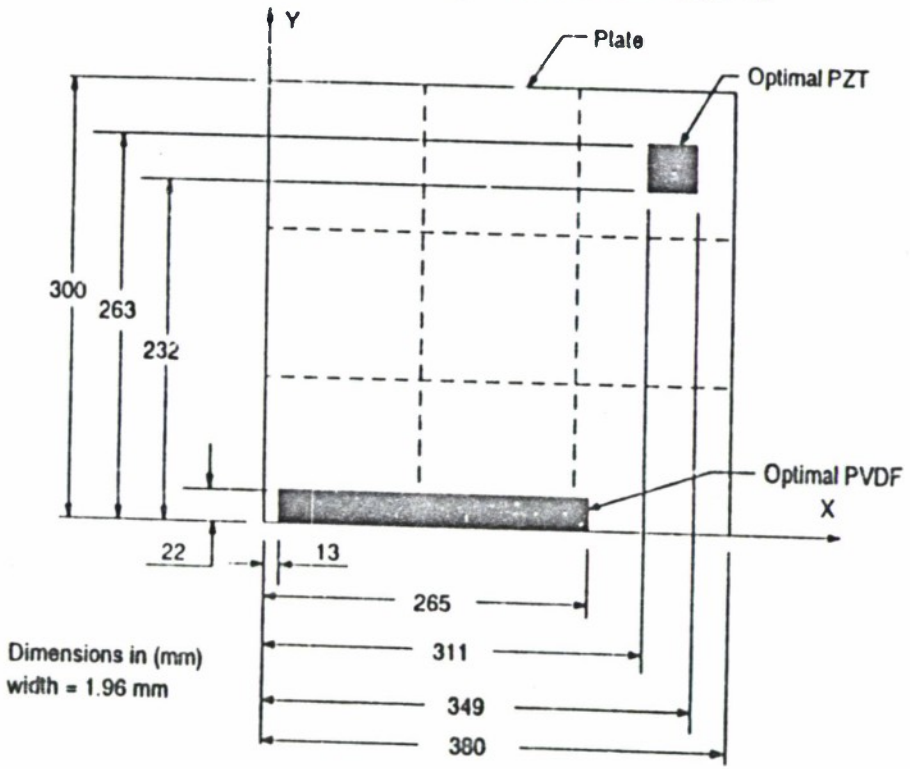

Plate Response Off-Resonance at 550 Hz

Experimental

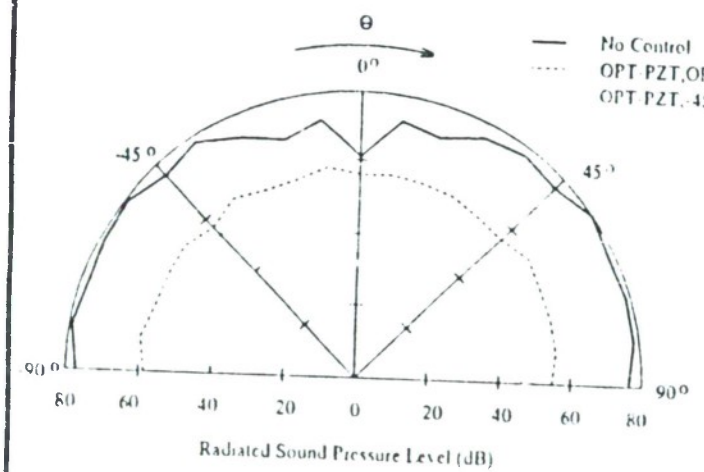

Theoretical

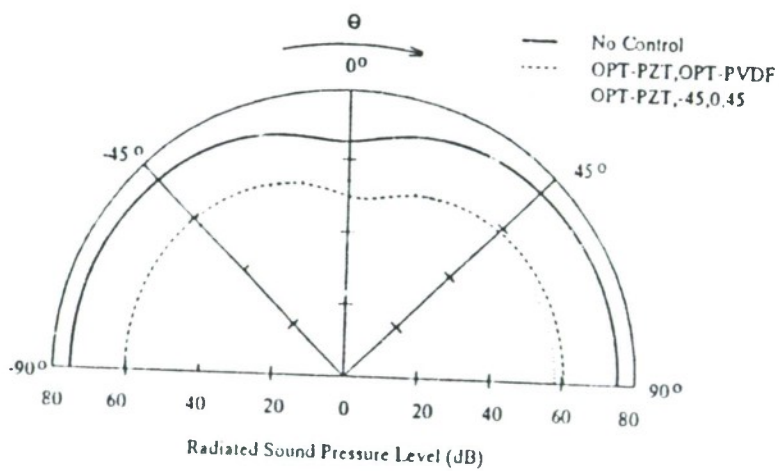

Approximately 15 dB of Attenuation

Structural Response of Plate (550 Hz)

Modal Response

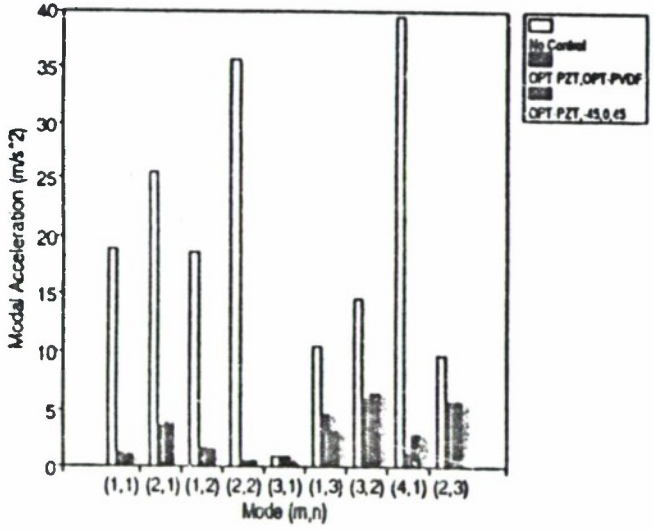

Wavenumber Transform

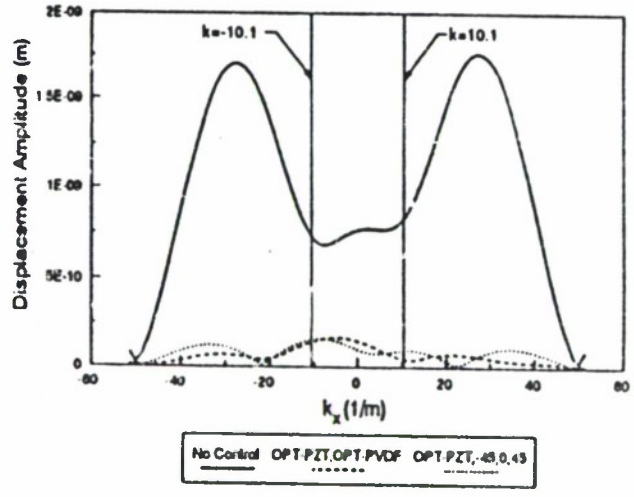

Vibration and Acoustics Laboratory

VAL

Time Averaged Acoustic Intensity (550 Hz)

Before Control

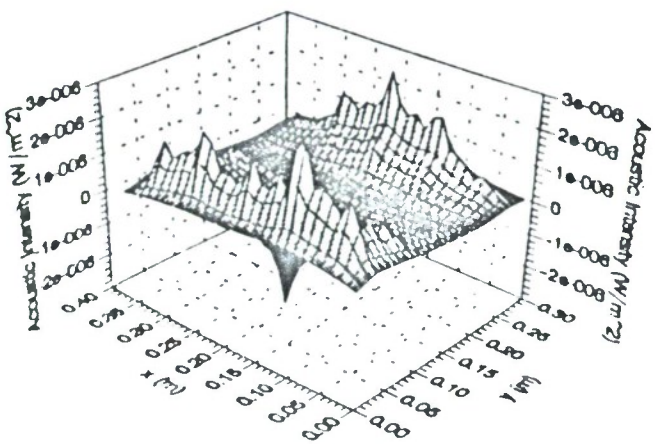

After Control

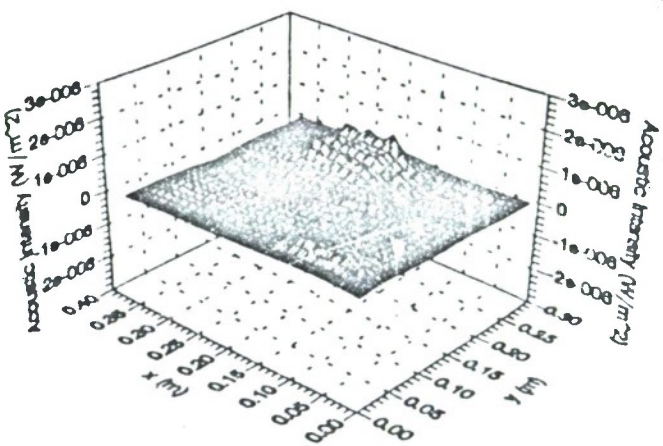

Shaped "Modal" Sensor

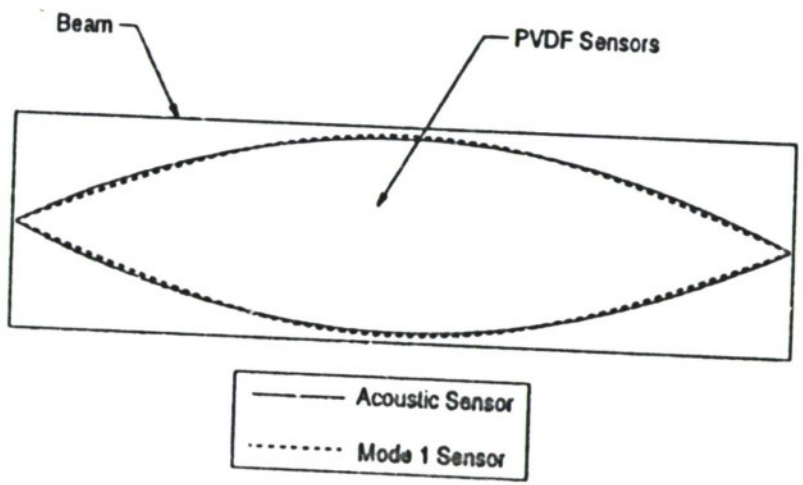

$$q(x,t) = \exp(j\omega t)\frac{(h_b + h_p)e_{31}}{2}\sum_{m=1}^{M}\sum_{k=1}^{K}(\frac{m\pi}{L_x})^2 S_k W_m \int_0^{L_x} \sin\frac{m\pi x}{L_x}\sin\frac{k\pi x}{L_x}dx. \qquad (1)$$

Beam Radiation Response Off-Resonance at 660 Hz

Experimental

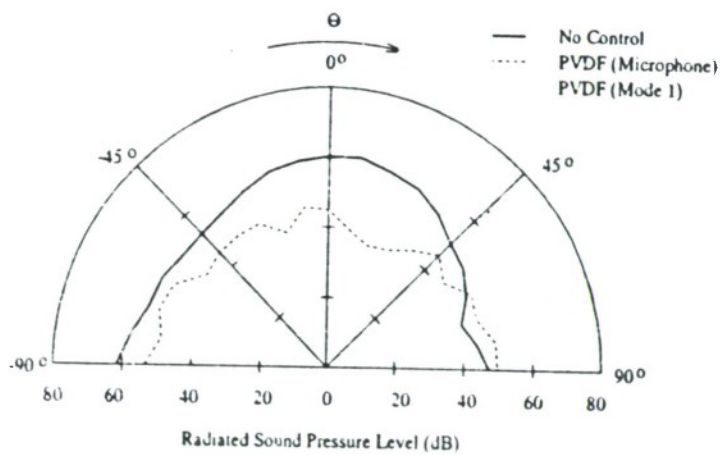

Theoretical

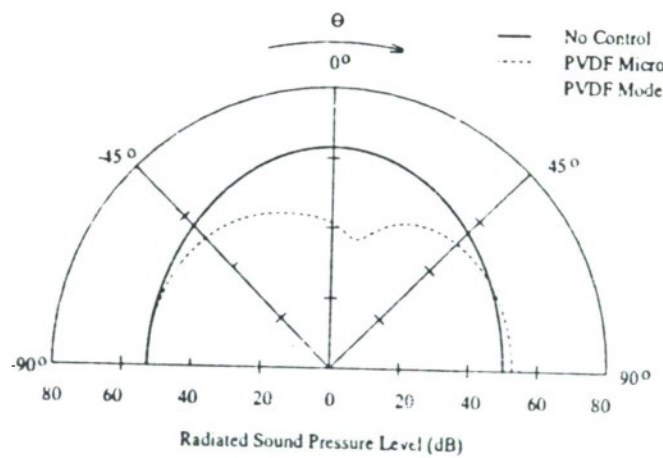

Conclusions

- "Intelligent" panel systems show much promise for control of sound transmission/radiation.
- Increasing channels of control leads to better control for off-resonance cases.
- Important to optimize shape, location and number of transducers (influence is of the same order as increasing the number of control channels).
- Different sensing strategies can be undertaken to observe the radiated pressure variables.

Pilots Noise Exposure During a Boeing 747-400 Round Trip—

Ambient Noise and Acoustic-Head Recording and Analysis of Data

Knut Hoffman
Deutsche Lufthansa AG

Presented at

NASA/SAE/DLR 4th Aircraft Interior Noise Workshop
Friedrichshafen, Germany
May 19-20, 1992

Pilots Noise Exposure during a B747-400 Round Trip

Ambient noise and acoustic head recording and analysis of data.

Judgement of noise analysis in respect to hearing impairment of pilots and discussion of possible measures.

Introduction

Noise, physically is no problem, as long as no humans will be effected. Even the loudest aircraft would be accepted as long as the airborn soundpower may not damage any material and humans are not in the reach of the noise. Consequenily, the reference of all judgement must be the human affected.

Though the soundpower origin is the aircraft, the effect to the humans inside the aircraft is the topic of our presentation. Though the paying passenger is the most important individual, we will deal to day with the well paid pilots - an ambivalent approach from the airlines sales standpoint. But you will learn from our presentation that the pilots are by far the most noise affected human in an modern commercial jet aircraft.

As we all know, there are big differences between the ambient noise and the noise at the outer ear of the active pilot. Aircraft manufacturers, authorities and also the airlines talk about A-levels during specific level flights if they mean cockpit noise.

This A-Level figure is specified and measured according to the ISO 5129 and the APR 4245 1322. There is no doubt that those regulations are of great value for aircraft specifications, comparisions and as a baseline for engineering people.

The actual noise exposure of the pilots ears during normal routine operation is a figure that must be higher than that baseline of ambient noise. A lot of variables and influences must be added to get at least one trips actual pilot exposure.

History

Already in 1980 our occupational insurance authority (Berufsgenossenschaft fur Fahrzeughaltung) (I call it BGF from now on) was confronted with noise impaired pilots claiming for compensation. According to the regulation it has to be studied whether the impairment was of occupational origin. Together BGF and LH started a study that is still in progress and will hold us on the scene for some more years. We summed up more than 100 commercial jet flights accompanied by tape recorders and this KEMAR--acoustic head who or which still got no name.

I will base my presentation on a roundtrip made nealy 1 year ago with a B747. Though both legs of this tour has been recorded in a similar manner I will mainly base the analysis on the first leg of this flight compiling a block or recording time of about 12 Hrs 20 Min. Mr. Hoormann thereafter will take some of the results to make up a judgement of the noise exposure of pilots in modern jet planes.

Measurement Equipment and Recording

3 Transducers or microphones were involved. (Graph)

- One open microphone BK 4166 a pressure capsule placed near the outer ear of the left pilots seat about 40 cm from the outer window. (ISO 5129).

- One open 1/2 inch microphone for a noise dosimeter Metrosonics dB 308 with a formidable A-rated storing capability

- One microcapsule (BK 4134) combined with the modified Swislockycoupler in the right ear of our acoustic head from kemar equipped with a male rubber ear

Both BK-Micros were directly plugged in a NOR 112 attached to a Sony DAT-Recorder TCD D10. The recording chain ended here in a DAT cassette of 2 channel 120 minutes recording time.

This equipment is standard, relatively inexpensive, light and gives you an outstanding quality and reliability. Together with the aluminium case and some straps it is ready to stand the 10 g requirement in the cockpit and gives you no EM -problems in a modern digitalized environment. Electricity we got from a transformer, that took 28 V, 400 Hz from the aircraft and delivered 9 V DC to the tape recorder for the whole flight.

For calibration we used a BK 4230 1000 Hz, 94 dB unit with volume correction of - 0,2 dB for the microphone and minus 0,5 dB for the Kemar. Air pressure correction is not necessary for this calibrator.

ATC-Signal Recording

To get a real objective transcript of a pilots ear impression you have to do some manipulation, switching and you should watch the flight operation from the behind. The flight crew consist of 4 pilots, who are changing their seats and their task like children in the Kindergarten playing "go-around in circles".

Normally one of the guys (sometimes there are ladies involved) is flying the controls and the other is doing the ATC-Radio Communication with an open Sennheiser head-set.

With four pilots involved the individual noise exposure can be quite different during one leg. Instead of following one pilot for 12 hours through the tour (including his resttime in the noisy area behind the cockpit) we tried to connect the Kemar to the active headset pilot for all the available time independent which of the four is doing the job. This gave us a full time ATC- recording of a virtual pilot for one leg.

To get the ATC radio signal on the recorder we had a third headset of the same kind on the Kemar that was directly cabled to the headset of the active pilots headset.

It should clearly be understood that the flight crew must be cooperative and honest enough not to manipulate their individual procedure and show a normal standard operation.

Beside other variables it was not possible to simulate the pilots habit to wear the headset on his ears. The headset deliver one signal likewise to both earpieces. The pilot can use it in very different manners. Standard is to use both cups on the center of both auricles. For this kind of operation you would need the lowest volume on the radio panel for a maximum of signal understanding. Any variation from this manner would require higher volume for the same signal level.

Mainly because the earcups tends to warm up the pilots ears they are used to wear only the outer-earcup directly on the ear and have the inner cup somewhere beside the auricles. This eases the acoustic direct communication with the collegue on the other side of the cockpit in about 1 m in distance. In all these situations the radio volume must be increased, showing a higher signal level on the Kemar recording.

On the other hand I should mention that also the position of the headset on the rubber ear of the Kemar was not always in the maximum. The cup is posed on the ear more or less statistical without objective marks on the head or controls on the recorder. A displacement of the headset by forces from the aircraft is possible and would effect the recording level as well.

Collected Data Analysis

6 tapes were comprising both channels of 12.20 hours blocktime recording. Verbal comments, calibrations, tape changes and not directly cockpit noise related activities reduced the netto recording to 8.20 hours summed up for analysis.

The parallel measurement of the dosimeter gave an Leq over 5 min periods for the total blocktime with an accuracy of within ± 1 dB(A) as cross-checked with the open BK-microphone recording.

While the open microphone and the dosimeter could be used for an analysis without manipulation the Kemar recording of the ATC-radio communication is much more complicated to understand.

The Kemar recording had to be corrected by two different influences:

1. The Kemar sits about 100 cm behind the left pilots seat where the ambient noise is about 3 dB lower. (Graph)

2. Despite the coupler upstreams the Kemar microphone must be corrected for the freefield with a known frequency band as shown in this graph.

To place the Kemar acoustically in the pilots situation you have to add energy for the local displacement and to substract energy for the freefield correction. (Graph)

This calculation would be right only for the ambient noise recording because the radio signal comes directly from the headset and needs no local displacement correction.

If you just analyse the Kemar recording for pilots exposure you have to correct Kemar freefield while radio signals are on and correct both factors while no radio signal is present..

An alterate could be to take the open ambient recording near the left ear on the left seat as a baseline and add the freefield corrected Kemar recording only while radio communication is going on and a signal is on the headset.

The final analysis taking into account the main variables can be done by this Nomegram (Graph).

To the ambient noise you can add simply the signal to noise level to get the signal level. The short term signal level will be reduced by its duration in relation to the total time fragment shown in percentages.

The result of the calculation is the exposure level for the pilot during one time fragment, most useful one flight leg.

According to the german regulations those dB's are impulse-weightened.

The calculation is true for all period lengths and can of course be done the other way round on this nomogramm.

You can learn from this graph that the overall exposure level is strongly dependant on the three variables (Graph)

- Ambient noise - 79.6 dB(A)
- Signal to noise level - 13.7 dB
- Rel. duration of signal - 26 %

Resulting in an overall noise exposure of above 85 dB(A)

The problem of noise exposure for pilots is simply not the cockpit surrounding but the radio communication. You can operate jet aircraft for years without hearing impairment, if there is no radio necessary. But even nice quite aircraft will give you trouble if bad noisy radios are installed and HF-communication is often necessary.

B 747 - 400 NOISE MEASUREMENT AND RECORDING

COCKPIT + LAB SCHEMANICS

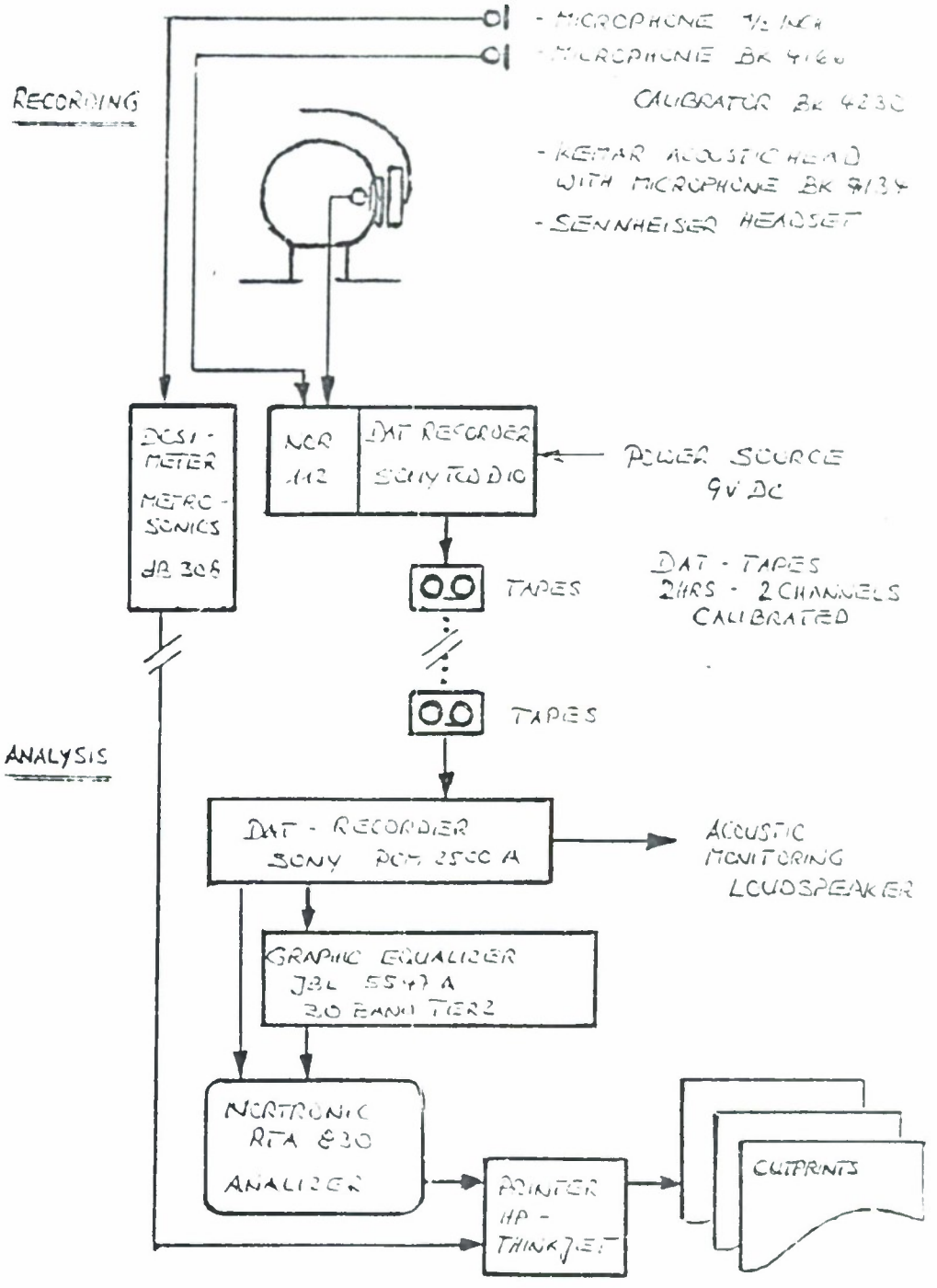

DY / Ho
6 5 92

B747-400 NOISE MEASUREMENT LOCATIONS

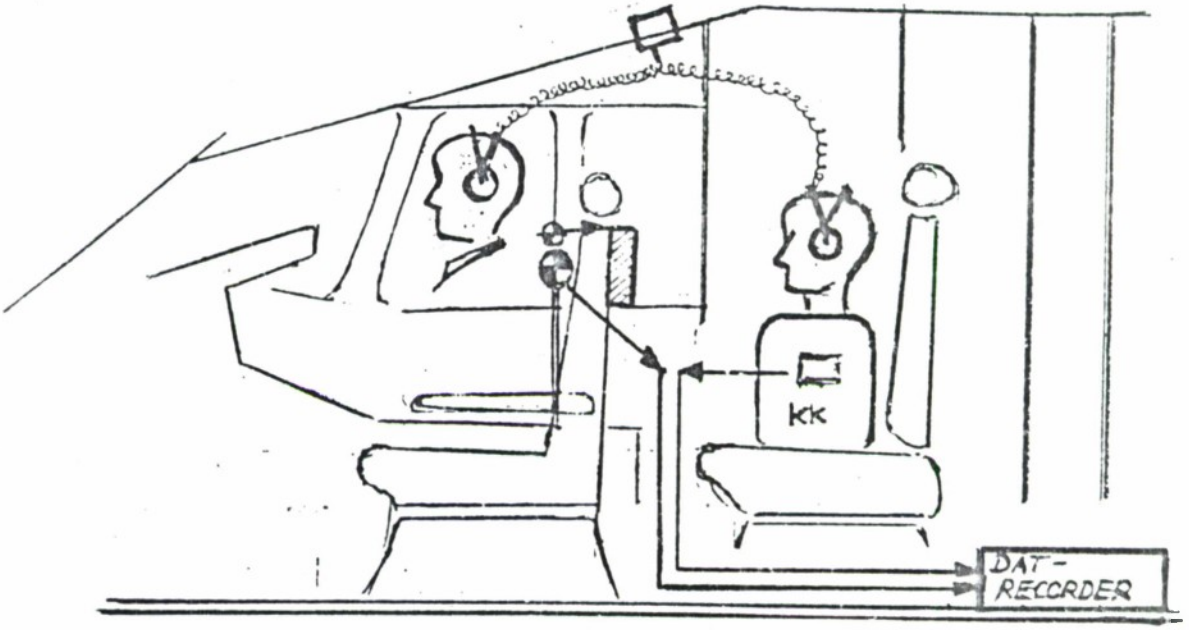

KK - MANIKIN KEMAR
DOSIMETER MICROPHON
BK 4166 MICROPHON
DOSIMETER METROSONICS

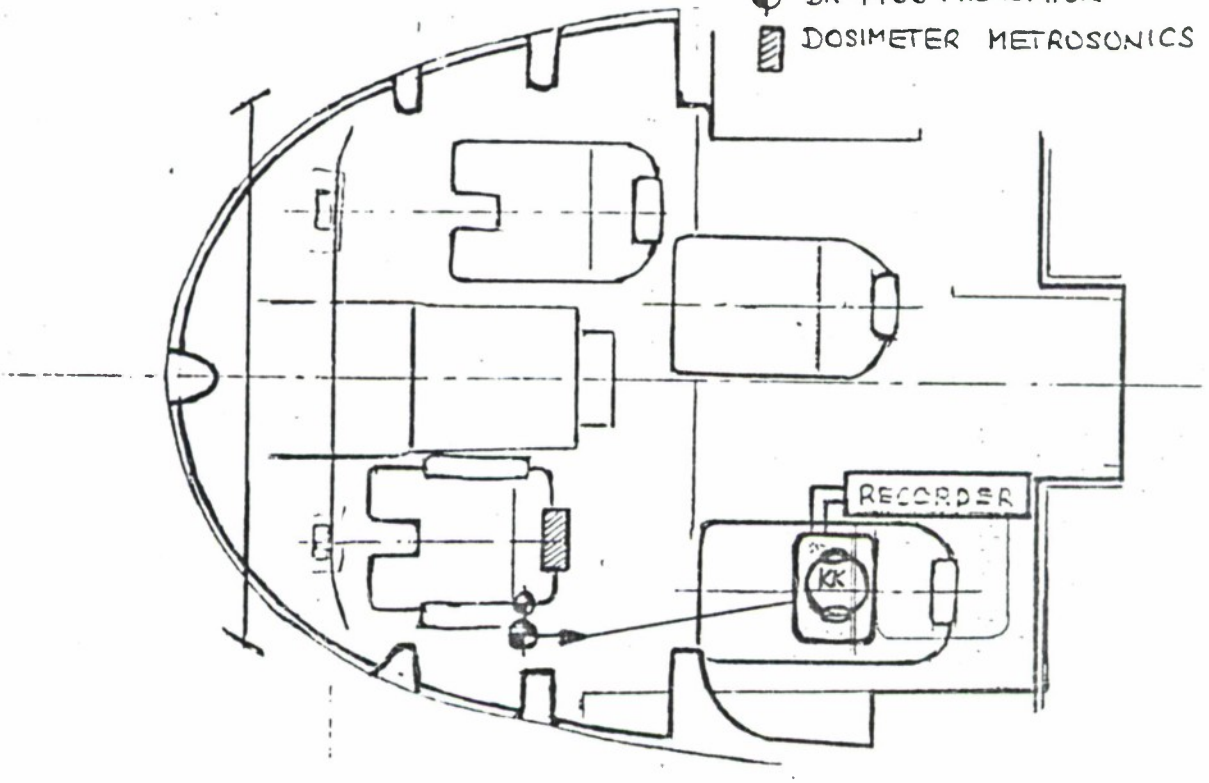

PX-21B
6.5.92

B747-400 D-ABTE FRA-SIN LH 778 6.6.91

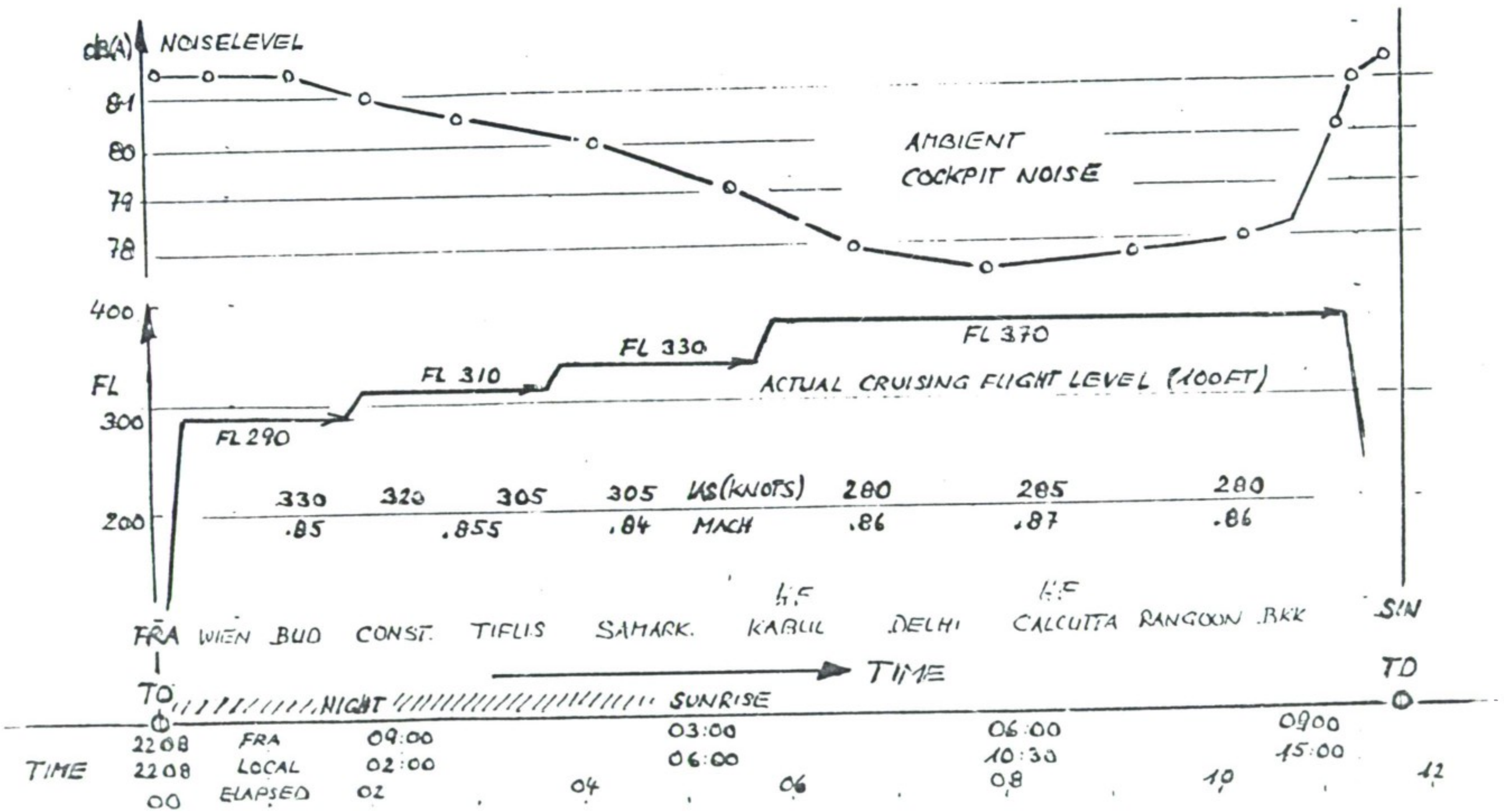

NOISE LEVEL DISTRIBUTION IN COCKPIT B747

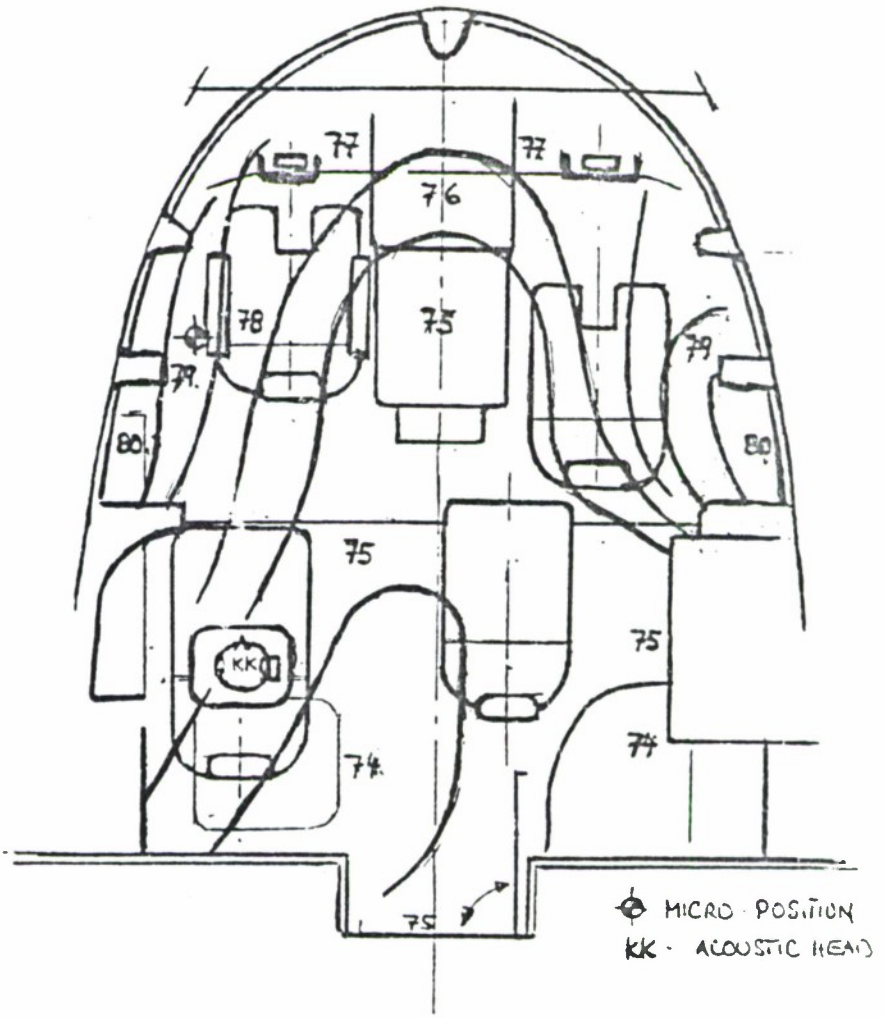

ALL VALUES IN dB(A) IN EAR LEVEL

B747-400 D-ABTE 3 PACKS

FL 370 .86 MACH 280 IAS CRUISE

LH 779 SIN-FRA 7.6.91

Px1 - HC
27.7.91

AMPLITUDE DISTRIBUTION

B747-400 AGTE FRA - SIN Leg

RECORDING TIME :
21:50 - 10:05 = 12 H 15 MIN

%	dB	SAMPLES	
	62	54	
	63	89	
	64	1217	.
	65	2609	+
	66	2399	+
	67	2948	+
	68	4887	+
	69	4353	+
	70	7271	*
	71	8388	*
	72	8116	*
	73	6650	+
	74	6812	+
	75	3262	+
1.6	76	23376	**
33.5	77	472720	**********
11.6	78	164302	**********
26.8	79	378675	**********
9.3	80	131107	********
10.1	81	142359	*********
1.1	82	16603	*
0.9	83	12763	*
0.5	84	7566	*
	85	894	.
	86	306	.
	87	187	.
	88	128	
	89	88	
	90	56	
	91	57	
	92	58	
	93	55	
	94	22	
	95	16	
	96	9	
	97	4	
	98	3	
	99	5	
	100	4	MAX

L_{AV} 79.2

Ln(0.0) = 100dB
Ln(10.0) = 81dB
Ln(50.0) = 78dB
Ln(99.9) = 65dB

Px 1 Ho
6.5.92

B747-400 COCKPIT NOISE

AMBIENT SOUND PRESSURE LEVEL dB(A)F - ISO/DIS 5129, LEVEL FLIGHT, CM1 LEFT EAR

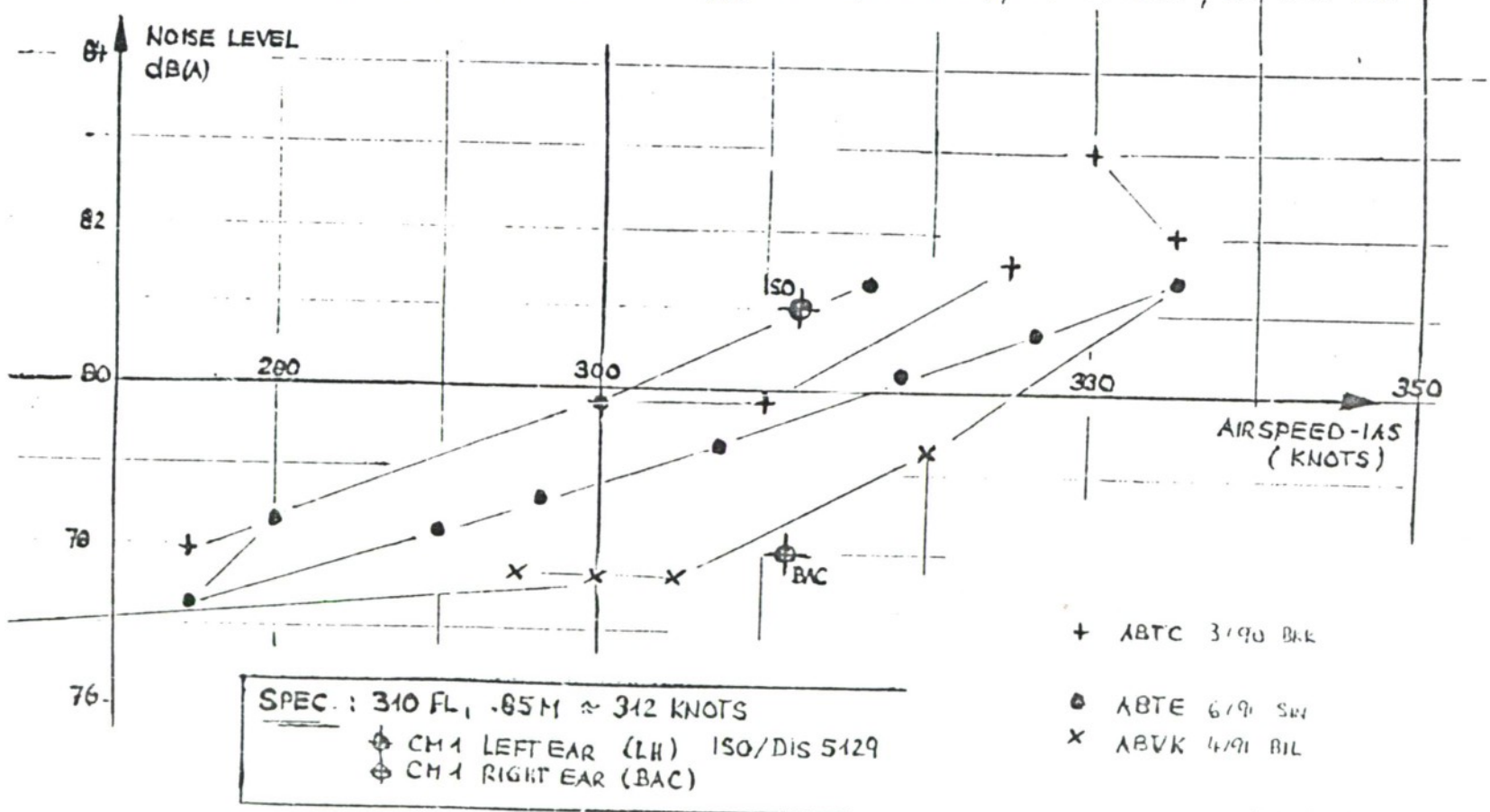

SPEC.: 310 FL, .85M ≈ 312 KNOTS

CM1 LEFT EAR (LH) ISO/DIS 5129

CM1 RIGHT EAR (BAC)

PX-1 Ho 6.5.92

ATC Signal VHF

KEMAR - Head recording (corrected)

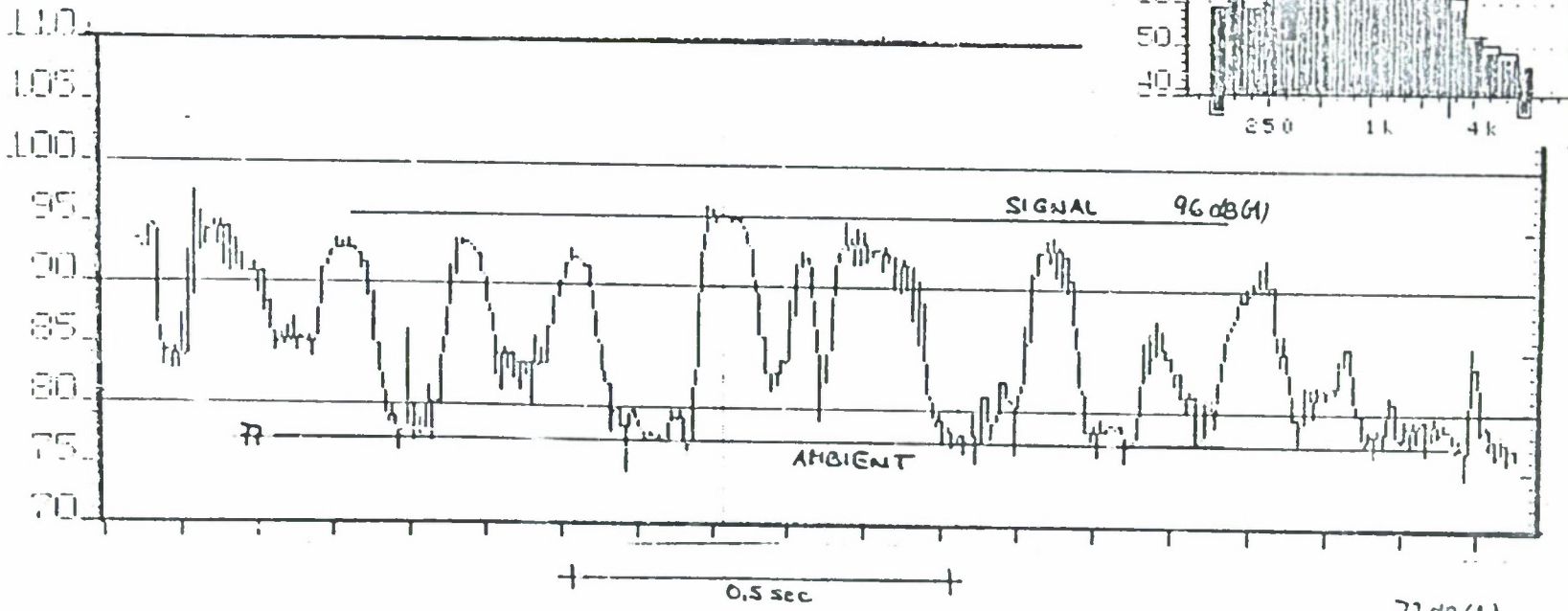

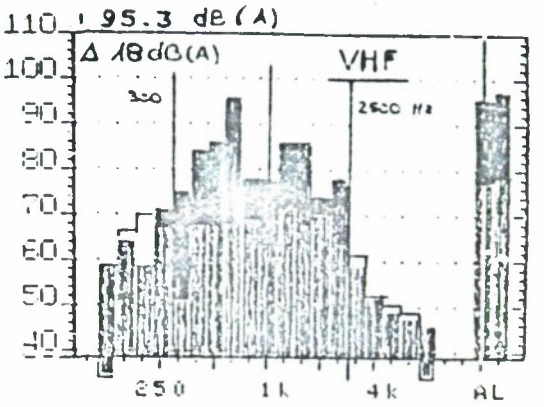

→ Luft hans sa seven two Po si ti one Ambient noise

HANDLA 40
12.5.91
DAT 67 : 41:05

ATC - Signal HF - Calcutta

KEMAR - Hedd recording (corrected)

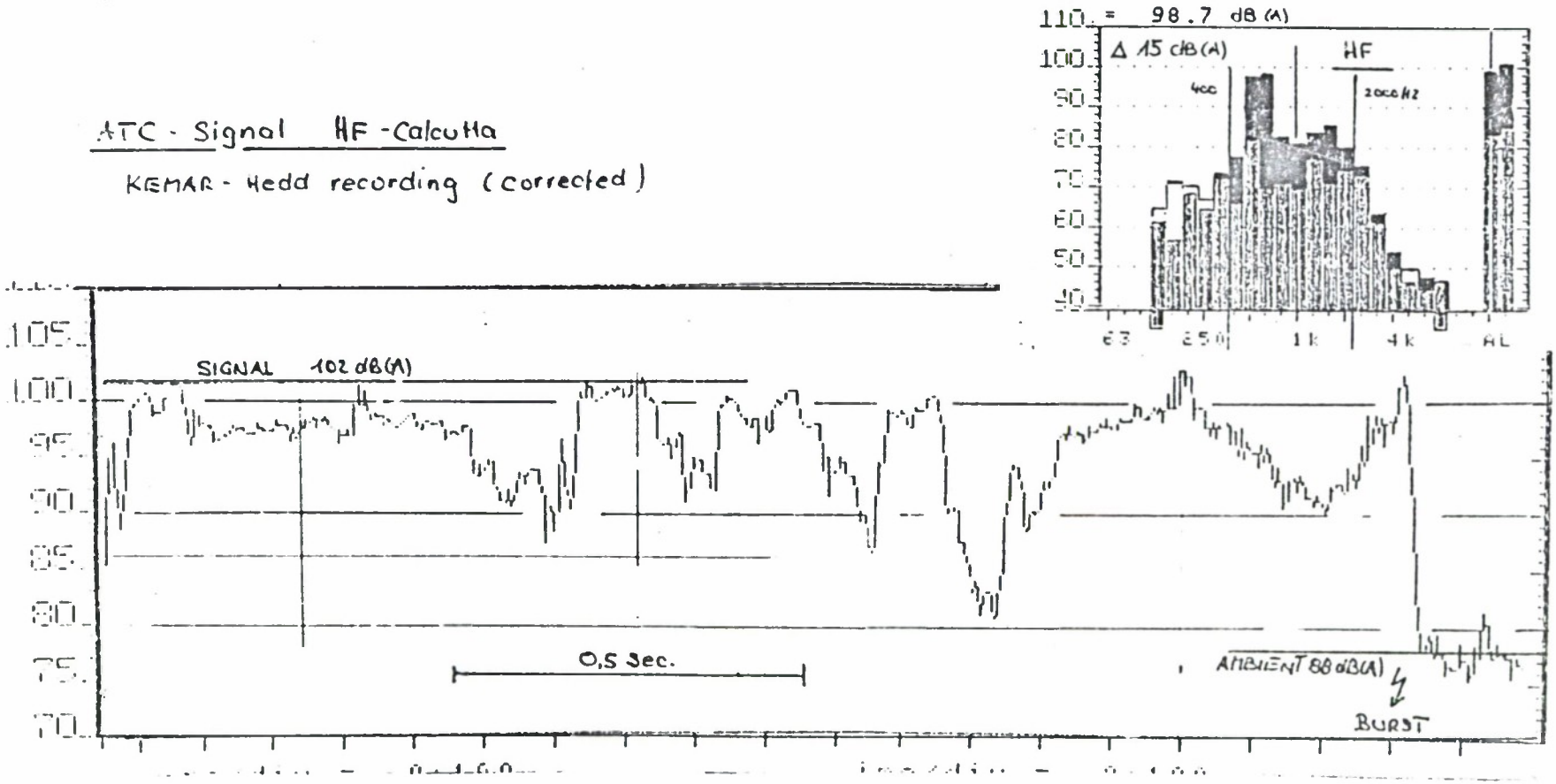

< RANGOON > > ONE TWO SEVEN SEVENTI ONE <

225

LH HAMPX1 HC
12.5.92

6:31

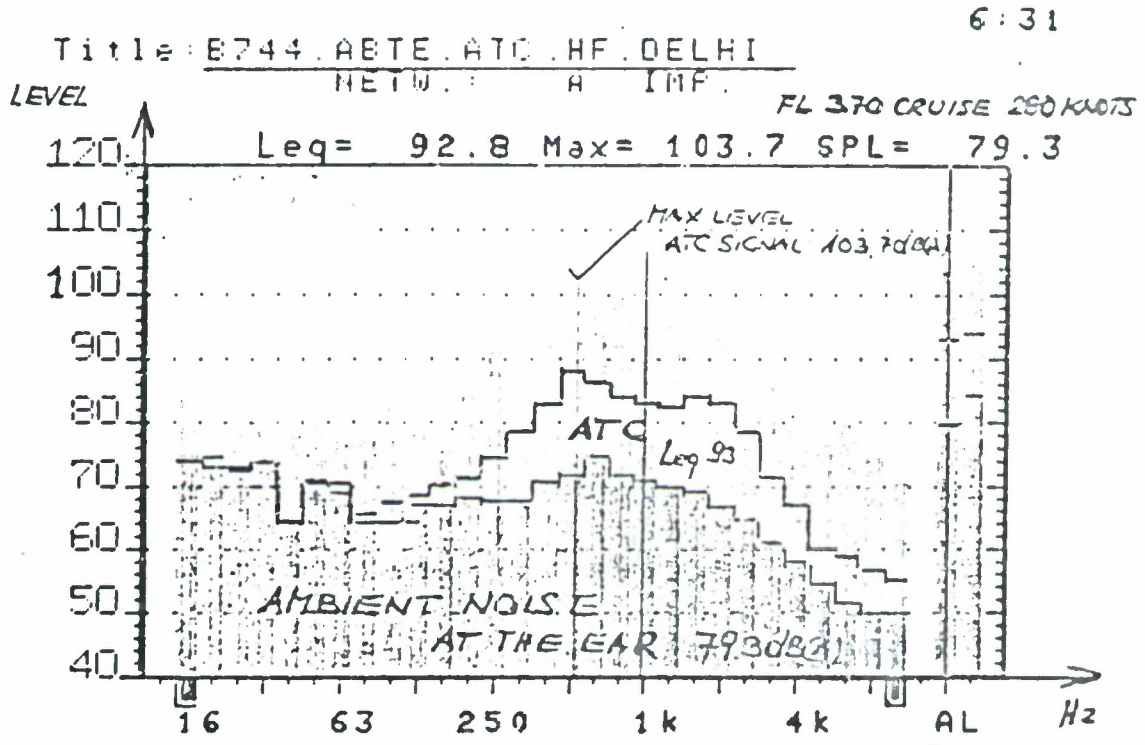

DX-1 Ho
6.5.92

Pilots Noise Exposure in Aircraft Cockpits

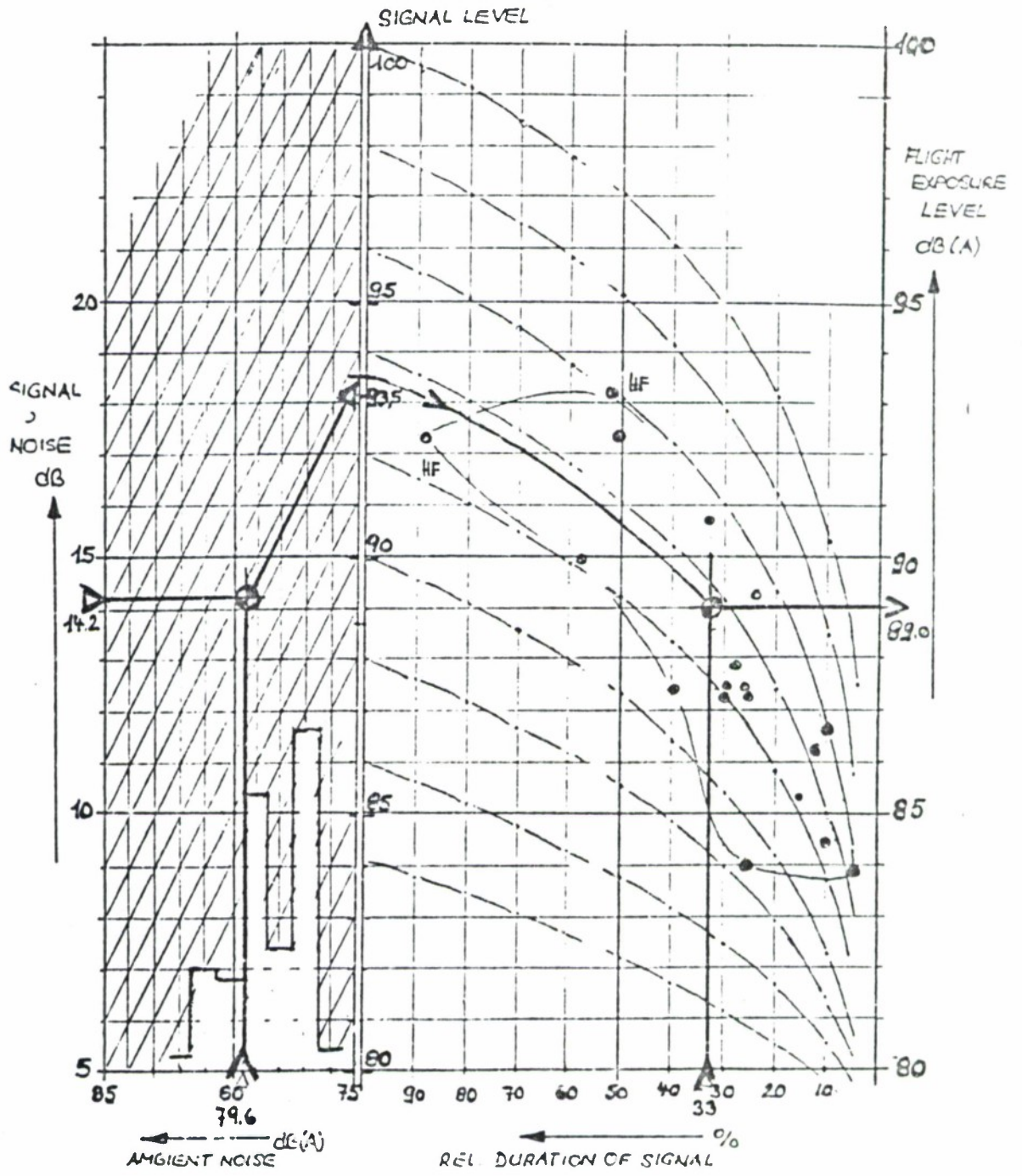

DLR HA 227K-1 Ho
12.5.92

Berufsgenossenschaft für Fahrzeughaltungen

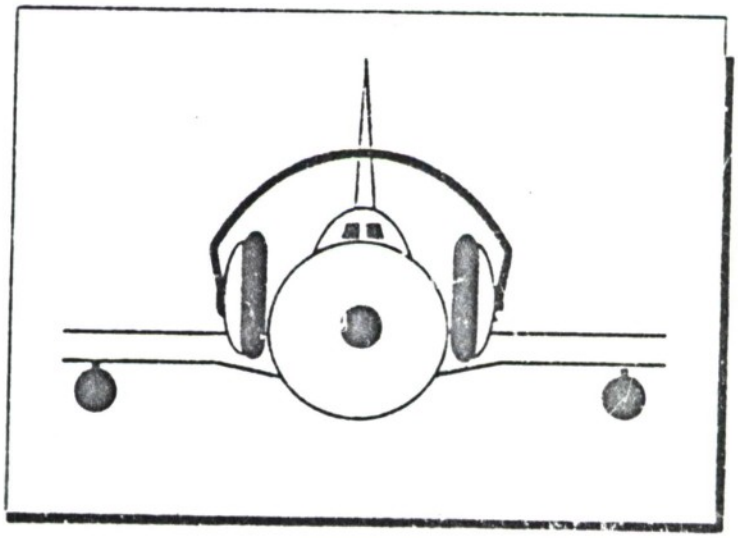

Judgment of noise analysis in respect to hearing impairment of pilots

May 19-20, 1992

Table of Contents

1. Introduction

In our capacity as Industrial Trade Association covering the vehicle sector (statuory accident insurance), in the Federal Republic of Germany we are required by law to prevent occupational accidents by all suitable means available. Our responsibility extends over

- the entire road-bound transport industry,
- commercial aviation, including all associated plant,
- All employees of non-commercial (private) vehicle, aircraft, riding and animal-drawn carriage operators (fig.1).

2. Noise level measurements in jet aircraft

For approximately 20 years we have been engaged in noise level measurements in and on surface vehicles and aircraft. In 1979 we started comprehensive noise level measurements in the cabins and cockpits of aircraft. So far we have made a total of 90 measurements in jet aircraft. Measuring results (fig. 23) have shown that most of the pilots work under conditions where noise constitutes a health hazard. The dominant noise level in these environments is constituted by the radiotelephone traffic, which has also been confirmed by measurements carried out by Mr. Hoffmann of the DLH.

3. Noise limit values and assessment of the measuring results

3.1 Assessment of noise levels below 85 dB(A)

We distinguish between noise limit values (noise levels) below approx. 85 dB(A) of extra-aural effects (non damaging to

hearing) and values equal to, or higher than, 85 dB(A) having aural effects (damaging to hearing).

In the case of noise ranges below the hearing damage level, extra-aural effects of many different manifestations have been proved by numerous investigations. Noise levels of 60 dB(A) and higher will already cause autonomic reactions. At a physiological level, an increased secretion of noradrenalin and also vanillin-almond acid has been established. Stomach secretions decrease, blood vessels contract and the pulse count and pulse and blood pressure increase. Patients with heart circulation disorders, as well as people suffering from high blood pressure are at special risk. In general, the tests show that reactions differ widely from person to person. Reactions were found to be not only dependent on the innate disposition, but also on the motivation towards the noise. The pathiological influence of extra-aural noise effects on human beings is frequently disputed. However, there can be no doubt that extra-aural noise effects must be considered as stress factors.

As a rule, noises inside aircraft show a high content of infrasound. Sound pressure level measurements at a linear frequency curve, i.e. without A-evaluation, then show values higher by up to 30 dB. In that case 100 dB (lin) instead of 70 dB(A).

In a series of tests, Messrs. Ising and Schwarze exposed 100 experimentees to noise and reported their findings in 1982. They have come to the conclusion that no distinct adverse effects of an objective nature occur, but that detrimental effects of a subjective nature are indeed felt. Other authors, especially in the United States, found visual defects, di-

gestive troubles and generally quicker signs of fatigue in the experimentees. Extreme amplitudes of these air vibrations in excess of 150 dB caused nausea, as well as headache, and ache in the testes.

As pilots are mainly subjected to psychic stress, it seems reasonable to base assessments of noise levels at work also on the "Ordinance on Work Places" as published on January 2, 1989. According to article 15 of this ordinance, a level of 55 dB(A) must not be exceeded, when predominantly intellectual work is involved. This ordinance is based on the fact that loid noises will impair the concentration and attention of such staff. Experimentees of widely varying background were found to produce a significantly higher rate of mistakes than those that were given the opportunity of solving the same test problems in peace and quiet. Noise has an activating effect, without a person being conscious of this fact, and also awakens a readiness to fight and to take to flight. Aggressive behaviour can, for instance, also be explained by a high inner noise level.

If it is to be ensured that a pilot can recognize an acoustic signal, a suitable low-noise aircraft has to be provided. This aspect is treated in DIN 33 404 "Safety requirements of acoustic danger signals", where it has been pointed out that the sound level of an acoustic signal can only be correctly heard when the interfering sound level in the reception range is lower by 10 dB(A). Otherwise the pilot of a loud aircraft will accordingly be warned later, i.e., for example, only when he moves closer to the signal transmitter. Note must be taken of the fact that radiotelephone noises will increase the noise level inside aircraft by approx. another 10 dB(A).

3.2 Assessment of values higher than 85 dB(A), i.e. above the hearing danger limit

In the presence of inside noises, as caused by radiotelephone traffic (LEP,d), the risk of hearing damage increases steeply (fig. 4). Apart from this, comprehension of the spoken word is very poor and almost impossible (fig. 5).

4. Evolution, costs and risks of the occupational desease "Noise Deafness" in the aviation sector

The development of the occupational noise deafness disease and the costs involved in all areas for which we are responsible, is shown in fig. 6. A not insignificant proportion of the total is represented by the occupational noise deafness disease in the aircraft industry (fig. 7).

From 1975 or thereabouts until the end of 1988, the Berufsgenossenschaft received notification of a total of 1,647 insured persons from these enterprises who were suspected of having defective hearing constituting the occupational disease known as noise deafness.

Of these notified cases, 410 were in the aviation sector, categorized as follows:

ground crew	387
air crew	23

The air crew are further categorized as follows:

cockpit pilots	12
cockpit flight engineer	1
cabin crew	10

Of the 1,647 insured persons reported up to the end of 1988 as having a suspected hearing defect, a total of 37 persons have been granted a pension, i. e. the hearing loss - in both ears - had reached or exceeded the prescribed 40 % level at which a pension becomes payable.

These 37 insured persons who were granted a pension included 3 pilots.

If these figures are placed in the context of the total number of insured persons, the situation in the aviation sector, with particular reference to air crew, is as follows:

a. Total insured number employed	approx. 560,000 persons
- in the aviation sector	approx. 80,000 persons
- as air crew	approx. 15,000 persons
- as cabin crew	approx. 11,000 persons
- as cockpit crew	approx. 4,000 persons

In other words, 14,3 % of all those insured are aviation workers (commercial and administrative staff, ground services and air crew). The persons who work on board aircraft constitute around 2,7 % of which 1,7 % are cabin crew and 0,7 % are cockpit crew (pilots, co-pilots and flight engineers).

b. Total number reported as having a suspected hearing defect	1,647 persons
aviation sector	410 persons
air crew	23 persons
pilots	12 persons
flight engineers	1 person
cabin crew	10 persons

In other words, approximately 25 % of all insured persons who were the subject of notification as having a suspected hearing defect work in the aviation sector, with air crew accounting for 1,4 % of the reported cases.

c. Total number granted a pension as a result of defective hearing	37 persons
pilots	3 persons

In other words, 8,1 % of all the insured persons who, by the end of 1988 had been granted a pension as a result of having suffered the prescribed level of hearing loss, were pilots.

This relatively small figure can be explained by the fact that pilots will lose their licence before their hearing deteriorates to the level of 40 % loss in both ears prescribed under the statutory accident insurance scheme as giving entitlement to a pension.

This in turn means that the quality of a pilot's life will be considerably impaired by factors such as reduced speech intelligibility and restricted directional hearing without the compensation of a pension which is granted to sufferers of the occupational desease known as noise deafness.

In summary, the statistics available at the end of 1988 show that the low figure of 0,7 % of all insured persons (pilots) represents 8,1 % of all cases in which a pension was granted. It is to be assumed that the figures at the end of 1989 will show an increase in this proportion, as some cases are being examined under the final statutory recognition procedure.

The final point to be noted is that the current average level of compensation payable in respect of occupational noise-induced deafness is a pension of 160.000 DM per person.

5. Required and possible measures

5.1 Legal basis in the EC

As early as 1974, the accident prevention regulations "Noise" (VBG 121) came into force in the Federal Republic of Germany. Preparation of the EC "Noise" regulations (Guidelines by the Council covering the protection of workers against health risks caused by noise at the work place, dated Dec. 5, 1986) was based on the accident prevention regulations already available at that time. The above EC Noise Protection Guidelines became national law in Germany on Oct. 1, 1990. The safety level existing then was not only maintained, but in some cases has been improved and has been defined in a more detailed fashion.

5.2 Noise level reduction

In article 5 of the EC-guidelines (article 9 of the accident prevention regulations "Noise") the following requirement is formulated:

1. The risks resulting from exposure to noise must be reduced to the lowest level reasonably practicable, taking account of technical progress and the availability of measures to control the noise, in particular at source.

2. Where the daily personal noise exposure of a worker exceeds 90 dB (A), or the maximum value of the unweighted instantaneous sound pressure is greater than 200 Pa:

   (a) the reasons for the excess level shall be identified and the employer shall draw up and apply a programme of measures of a technical nature and/for of organization of work with a view to reducing as far as reasonably practicable the exposure of workers to noise;

   (b) workers and their representatives in the undertaking or establishment shall receive adequate information on the excess level and on the measures taken pursuant to subparagraph (a).

In order to show means suitable to reduce the daily personal noise exposure (LEP.d) of cockpit crews, we have, in cooperation with Lufthansa, prepared a noise abatement program as detailed below which we would like to put forward for discussion:

5.3 Noise abatement program

1. Short-term measures, such as

1.1 Reduction of the ATC-level by means of the manual volume control to a level where communication is just adequate.

1.2 Improvement of the degree of modulation of the desired signal through personal discipline (loud and clear speach, holding the microphone immediately in front of the mouth) and by asking the ground staff to do likewise (e.g. via SINFO. Refer also to annex 14 of the radio VO and to CCIR-Recommendation no. 251).

1.3 Use of suitable ear protectors when performing outside checks, especially during AFU or GPU operations.

2. Medium-term measures, such as

2.1 Continued efforts to find an optimum headset for the cockpit crews as replacement for, or alternative to, the Telex and Sennheiser LH 400 set.

2.2 Practical testing of ear protectors worn under the headset to improve comprehension of the spoken word. In order to obtain a high degree of acceptance on the part of the test person, these investigations during flight operations will have to be carefully prepared.

2.3 Continual pressuring of the maker to provide technical upgrading of the onboard receiver. It would be desirable to obtain an even more effective separation of the intelligence signal from the spurious signal. Despite the fact that theorethical starting points can be seen, so far no promising avenue for realisation has been found.

2.4 Automatic maximum level limitation for the onboard receiver.

2.5 Compensating of the cockpit sound field by superimposing an inverted sound field (so-called destructive interference).

3. Long-term measures

Such measures are outside the sphere of influence of the aviation industry and are listed only to complete the range of potential measures and to show that modifications in this field will also result in changes in the noise-induced stress of cokpit crews.

3.1 Possible conversion of the radiotelephone traffic to satellite communication.

3.2 Increase in the degree of modulation of the ground stations.

3.3 Aerodynamic design of the outer cockpit contour.

3.4 Decreased sound emission of the jet power units towards the front.

Practical testing of ear protectors as mentioned under para. 2.2 has been successfully completed in the meantime. The relevant report can be supplied, if required.

5.4 Ear protectors and medical care

5.4.1 Ear protectors

The use of ear protectors is regulated in article 6 of the EC-guidelines.

"Article 6

1. Without prejudice to Article 5, where the daily personal noise exposure of a worker exceeds 90 dB (A) or the maximum value of the unweighted instanteous sound pressure is greater than 200 Pa, personal ear protectors must be used

2. Where the exposure referred to in paragraph 1 is likely to exceed 85 dB (A), personal ear protectors must be made available to workers.

3. Personal ear protectors must be supplied in sufficient numbers by the employer, the models being chosen in association, according to national law and practice, with the workers concerned.

The ear protectors must be adapted to the individual worker and to his working conditions, taking account of his safety and health. They are deemed, for the purposes of this Directive, suitable and adequate if, when properly worn, the risk to hearing can reasonably be expected to be kept below the risk arising from the exposure referred to in paragraph 1.

4. Where application of this Article involves a risk of accident, such risk must be reduced as far as is reasonably practicable by means of appropriate measures.

Article 7

1. Where it is not reasonably practicable to reduce the daily personal noise exposure of a worker to below 85 dB (A), the

worker exposed shall be able to have his hearing checked by a doctor or on the responsibility of the doctor and, if judged necessary by the doctor, by a specialist.

The wearing of ear protectors by flight crews must always comply with the applicable flight safety regulations, and in this case of pilots already suffering from partial loss of hearing, in compliance with the appropriate medical instructions.

6. Summary and concluding remarks

Even slight noise abatement measures involving a reduction of the noise level of, for example, only 5 dB would already considerably reduce the hearing damage risk of pilots (fig.4). If this is not possible, suitable ear protectors should be worn. A noise reduction of only 10 dB, as can alrady be achieved by using the slightly muffling ear plugs, can reduce the risk to below 5 per cent at noise levels of up to 95 dB(A).

The main source of noise in modern jet aircraft is constituted by the radiotelephone traffic noise. It could be said that pilots, by their very occupation, are carrying a walkman. This noise pollution is also present in other occupations and applies to

- air-traffic controllers,
- radio operators on sea-going vessels
- audio typists (secretaries)

For the above reasons a standard is already under discussion that is to define uniform regulations for "noise emissions by

sound sources located close to the ear" (DIN 45 683, part 1, draft).

In our opinion, incorporation of this measuring procedure in the ISO 5129 "Acoustics measurement of noise inside aircraft" would represent a major step forward. Only then would it be ensured that this problem is also brought to the attention of the aircraft makers (fig. 8).

In conclusion I would like to quote the pilot Prof. Dr. med. Niemeyer (Ear, Nose and Throat specialist) with regard to the subject of loss of hearing:

"Blindness is something that can be imagined, because everybody knows from his own experience the helplessness which results from the lack of information in the darkness of night or in dark rooms. Constant failure of the sence of hearing, however, is something most people cannot imagine and consequently fail to sympathize with. The helpless tapping of a blind person in strange surroundings motivates other people to offer assistance immediately. The helplessness of those who are hard of hearing scarcely moves anyone to compassion, but frequently to laughter, or the loss of hearing is simply found to be a cause of annoyance".

In the interest of flight safety, please help to eliminate these damaging conditions.

7. Bibliography

7.1 EG-Richtlinie "Über den Schutz der Arbeitnehmer gegen Gefährdung durch Lärm am Arbeitsplatz" (86/188 EWG)

7.2 Unfallverhütungsvorschrift "Lärm" (VBG 121, vom 1. Okt. 1990)

7.3 Verordnung über Arbeitsstätten in der Fasung vom 2. Jan. 1982)

7.4 ISO 5129 "Acoustics-Measurement of noise Inside Aircraft"

7.5 Entwurf der DIN 45683 Teil 1 "Bestimmung der Geräusche durch offene Kopfhörer und Einsteckhörer"

7.6 W. Niemeyer: Gehör und umweltbedingte Gehörschäden (Sonderdruck aus dem Berichtsband der MEDICENALE VV. Iserlohn 1985)

7.7 Wittenbecher, Hoormann: die Schallbelastung im Cockpit der LH-Flotte, Juli 1984

7.8 Bernhardt, H.: Konsequenzen aus der Durchführung der UVV "Lärm"; Die Berufsgenossenschaft, März 1980

7.9 Ising: Infraschallwirkung auf den Menschen - VDI-Verlag 1982

7.10 VDI-RL 2058 Blatt 3, "Beurteilung von Lärm am Arbeitsplatz unter Berücksichtigung unterschiedlicher Tätigkeiten; VDI-Verlag

7.11 DIN 33404 Teil 3 "Gefahrensignale für Arbeitsstätten-Akustische Gefahrensignale"

Berufsgenossenschaft für Fahrzeughaltungen

Wir betreuen

- das gesamte straßengebundene Verkehrsgewerbe
- den Flugverkehr mit seinen Einrichtungen
- die privaten Fahrzeug-, Luftfahrzeug-, Reittier- und Gespannhaltungen

We take care of

- the whole traffic trade engaged on public road
- the air traffic with its equipment for aircraft servicing
- the private owning of transport vehicles, aircraft, animal used for riding, horse and cart

Berufsgenossenschaft für Fahrzeughaltungen

Measurements from 1982 - 1990

results of 90 measurements

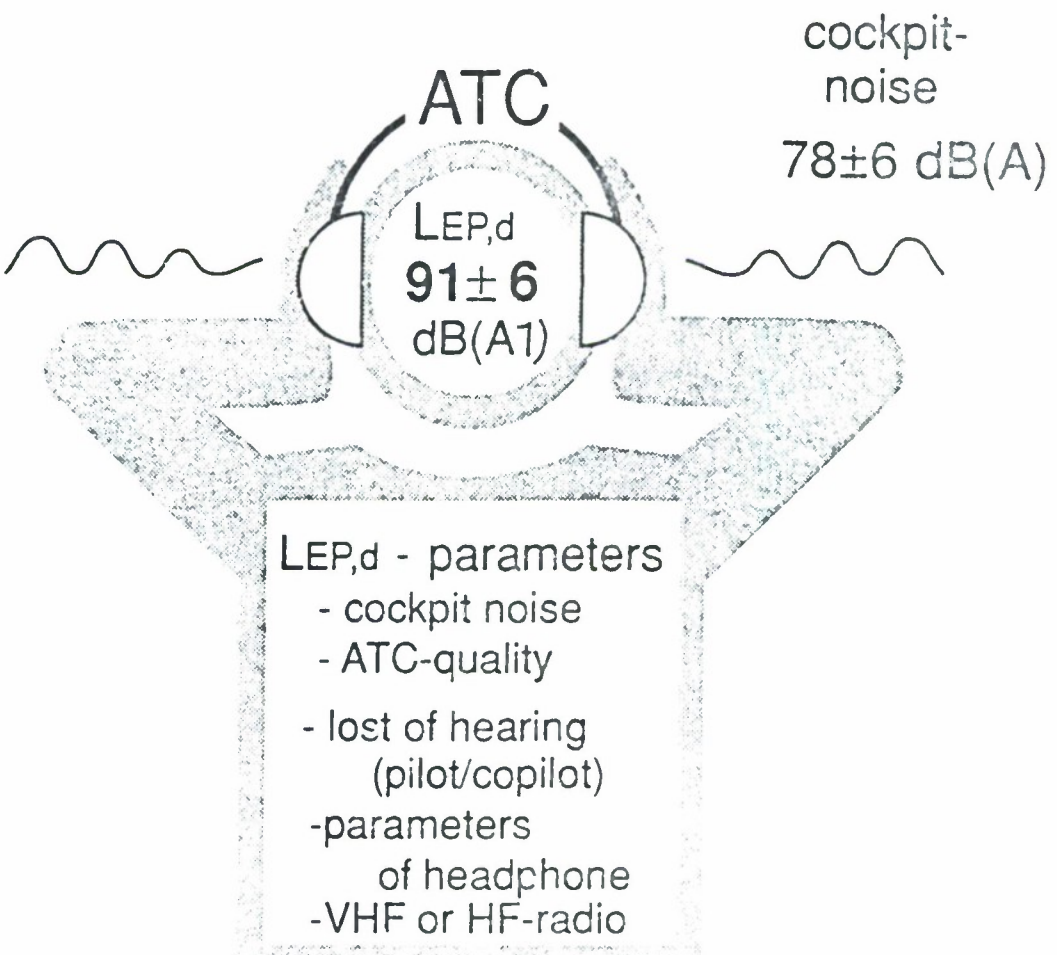

The daily personal noise exposure (LEP,d) of a worker is expressed in dB(A) using the formula:

$$L_{EP,d} = L_{AI,Te} + 10 \log_{10} \frac{T_e}{T_o}$$

$$L_{AI,Te} = 10 \log_{10} \{ \frac{1}{T_e} \int_0^{Te} [\frac{p_{A(t)}}{p_0}]^2 dt \}$$

245

Fig. 2

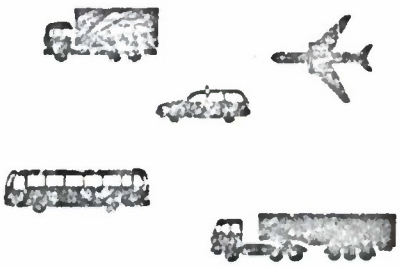

Noise limit values

Ordinance on workplaces

55 dB(A) = intellectual work
70 dB(A) = mechanized work

Accident prevention regulation "Noise"

85 dB(A) = hearing damage risk approx. 1% !
90 dB(A) = hearing damage risk approx. 10% !

As from 85 dB(A) "Assessment noise level"
Suitable ear protection to be used !

Ordinance on work places
Extra-aural effects = non-damaging to hearing

Accident prevention regulations "Noise"
Aural effect = damaging to hearing

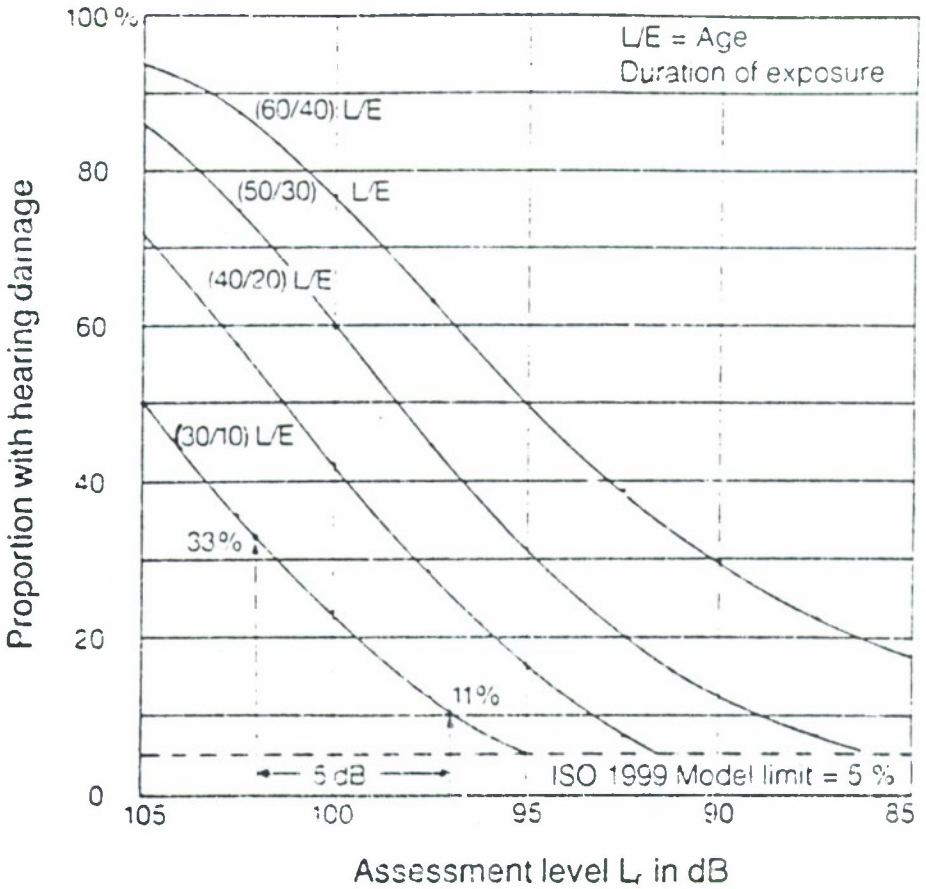

Probability of the development of hearing damage (loss of hearing in excess of 40 dB at 3 kHz) as a function of the hearing-effective assessment level to ISO 1999.

The parameter chosen is the combination age/years of exposure. The diagram makes possible an assessment of the effectiveness of ear protectors. Departing from the assessment level at the work place, the percentage of the group under review suffering from hearing damage is read off.
Read off then is the assessment level reduced by the effective sound attenuation. In this way the hearing damage risk for 30-year old men having been exposed to a noise of 102 dB(A) over a period of 10 years while wearing ear protectors offering an effective sound attenuation of only 5 dB is reduced from 33% to 11%.

Fig. 4

Interrelation between disturbing noise and speech communication over long distances

Enviromental disturbing noise at location of listener		Quality of speech communication
A-assessed sound level L_A dB	Speech disturbing sound level L_{SIL} dB	
up to 55	up to 47	satisfactory
over 55 up to 65	over 47 up to 57	slightly difficult
over 55 up to 80	over 57 up to 72	difficult
over 80	over 72	unsatisfactory

In the case of an A-assessed sound level of the environmental noise (spurious noise) between 70 and 80 dB(A), and a SIL of between 65 and 80 dB(A), speech communication over long distances is described as difficult to unsatisfactory in the DIN 33 410. In principle, this also applies to radio communication.

As a NOTE the DIN adds the following:

It is to be noted that it is the distant subscriber that becomes unintelligible first when the spurios noise increases at the location of the listener. Experience shows that the listener will raise his voice when the spurious enviromental noise increases. Apart from this, the signal-to-noise ratio at the microphone is still favourable, when the interfering noise penetrates via the microphone and the free ear and already shows a superimposing quality.

Berufsgenossenschaft für Fahrzeughaltungen

Exerpt from the list of occupational diseases
Statistics
Noise (BK 2301)

	Reported cases	Acknowledged cases	First compensated cases
1982	52	3	4
1983	46	3	3
1984	51	0	4
1985	54	0	8
1986	70	4	6
1987	96	6	4
1988	129	10	4
1989	137	--	1

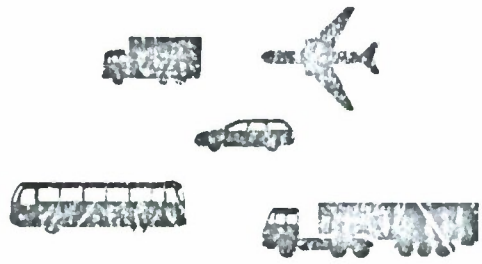

	Pensions still being paid in the current year	Pension payments in million DM
1982	8	1,28
1983	8	1,28
1984	8	1,28
1985	17	2,72
1986	25	4,00
1987	29	4,64
1988	33	5,28
1989	37	5,92

Fig. 6

Berufsgenossenschaft für Fahrzeughaltungen

Occupational diseases NOISE (BK 2301)

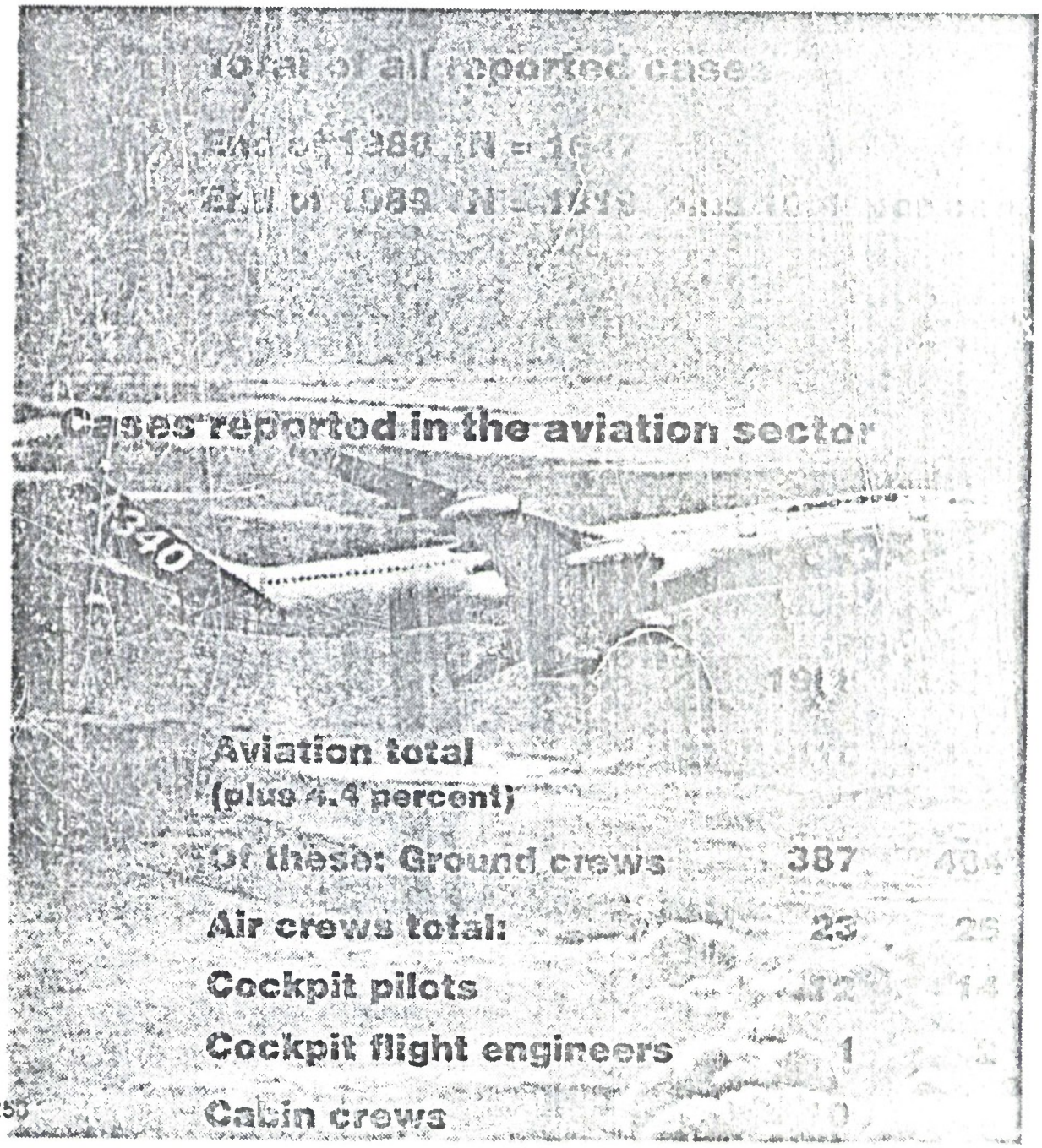

Fig. 7

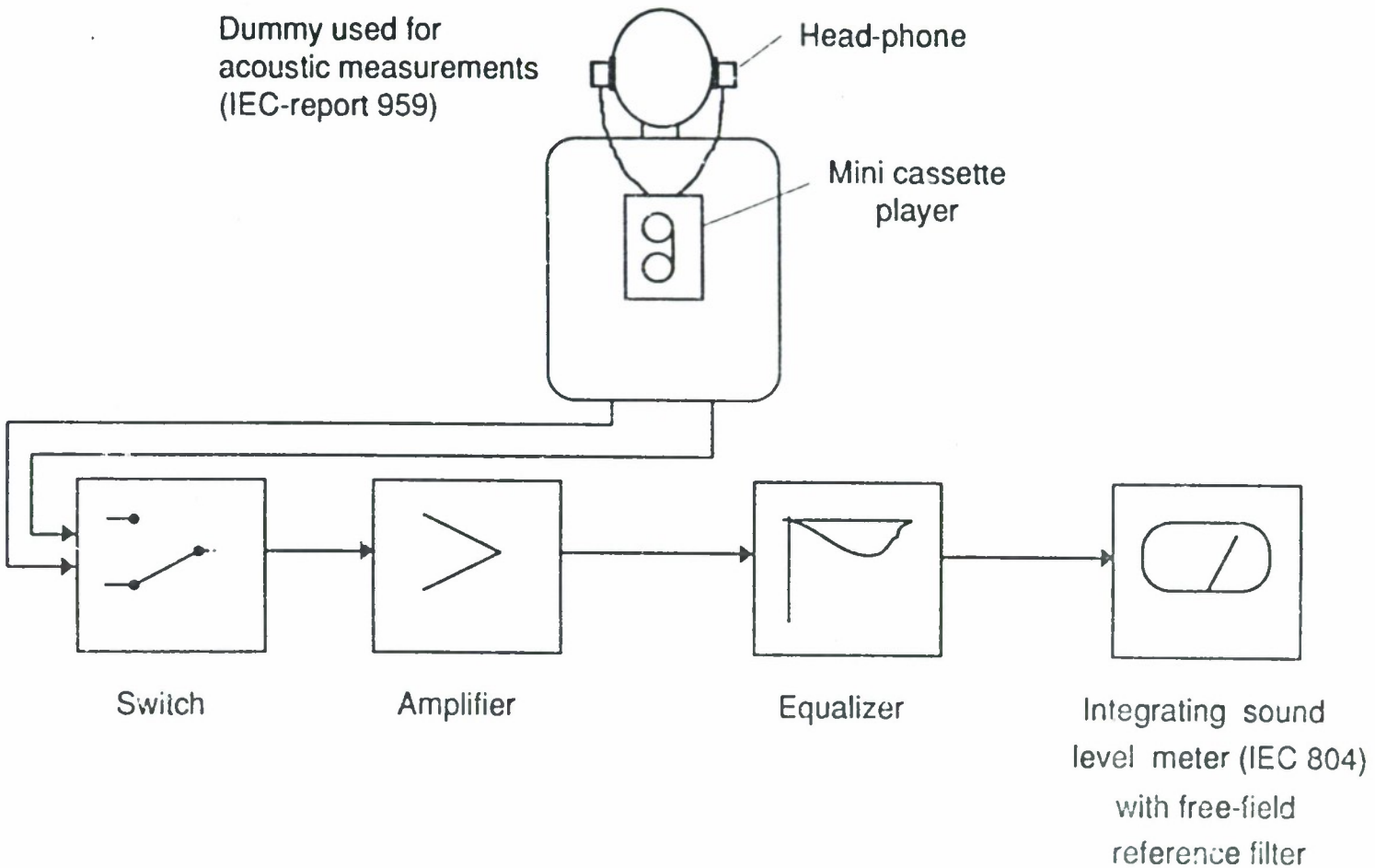

251

Fig. 9 Measuring arrangement for determining sound immission through open head-phones and plug-in head-phones

252

ALENIA

ALENIA AERONAUTICA

ACTIVE VIBRATIONS AND NOISE CONTROL FOR TURBOPROP APPLICATION RESEARCH PROGRAM ACTIVITIES

ALENIA/CIRA/IPV

A.PAONESSA ALENIA
A.CONCILIO CIRA
L.LECCE IPV

ALENIA

ALENIA AERONAUTICA

OBJECTIVES

- Development of Active noise control techniques to alleviate inefficiencies and drawbacks of Passive noise control approach especially at low frequencies.
- Reduction of structurally radiated noise applying external forces to the vibrating structure by means of force actuators made of piezoelectric material and actively controlled.
- Piezoelectric actuators are lightweight, are easily attached to the vibrating structure, take less space than other actuators and don't require any support structure.
- Reduction of fuselage vibration levels in propeller driven aircraft by means of distributed piezoelectric actuators actively controlled.

ALENIA

ALENIA AERONAUTICA

RESEARCH PROGRAM

- ALENIA has been involved in the investigation of piezoelectric material application since 1989 together with CIRA and IPV of University of Naples.
- Theoretically and experimentally activities about the use of piezoelectric material as sensing and actuating elements of active control systems have been undertaken.
- Theoretical studies of the system consisting of a simple structure with a piezoelectric actuator driven by different control laws have been performed by means of F.E.M..
- Tests of piezoelectric actuators on simple structures are currently under way. Application to more complex structures as a rectified aircraft frame and a fuselage double wall will follow soon.
- Design and development of software and hardware for vibration active control systems are also considered.

SUMMARY OF PERFORMED ACTIVITIES

THEOR.- NUMERICAL

- PIEZO-STRUCTURES INTERACTION MECHANICS (ACTUATORS AND SENSORS)
- FEM SIMULATION OF COMPLETE SYSTEM

  PIEZO + STRUCTURE + ACOUSTIC + CONTROL
- SIMPLE FEEDBACK AND LMS FEEDFORWARD CONTROL ALGORITHMS FOR BEAMS, PLATES AND DOUBLE WALL PARTITIONS
- NEURAL OBSERVER FOR STATE ESTIMATION IN ACTIVE CONTROL SYSTEM

EXPERIMENTAL

- PIEZO-ACTUATOR AND SENSOR MODEL VALIDATION ON SIMPLE STRUCTURES
- NEGATIVE POSITION FEEDBACK ACTIVE CONTROL SYSTEM (SISO) WITH APPLICATION ON BEAMS AND PLATES
- PIEZO-ACTUATION AND SENSING ON COMPLEX STRUCTURE (RECTILINEAR FRAME STRUCTURE)
- SPECIFICATION FOR A MIMO COMPLETE ACTIVE CONTROL SYSTEM

PIEZO - STRUCTURE INTERACTION

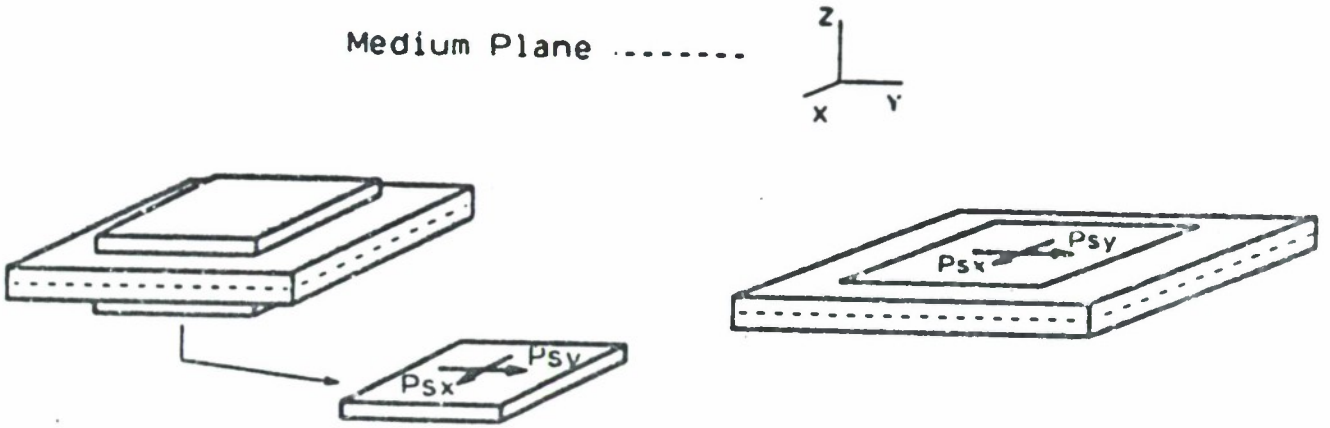

SLIDING FORCES ACTING ON THE PLATE
AND ON THE PIEZO ELEMENT

PIEZO - STRUCTURE INTERACTION

EXTENSION OF CRAWLEY'S AND DE LUIS' THEORY ON ID "STRAIN ACTUATION"

Resolving equations:

$$A_e\frac{\partial^2\epsilon_{x,e}}{\partial x^2}+\frac{\partial^2\epsilon_{x,e}}{\partial y^2}+B_e\frac{\partial^2\epsilon_{y,e}}{\partial x^2}-K_e(\epsilon_{xe}-\epsilon_{xp})=0 \qquad A_p\frac{\partial^2\epsilon_{x,p}}{\partial x^2}+\frac{\partial^2\epsilon_{x,p}}{\partial y^2}+B_p\frac{\partial^2\epsilon_{y,p}}{\partial x^2}+K_p(\epsilon_{xe}-\epsilon_{xp})=0$$

$$A_e\frac{\partial^2\epsilon_{y,e}}{\partial y^2}+\frac{\partial^2\epsilon_{y,e}}{\partial x^2}+B_e\frac{\partial^2\epsilon_{x,e}}{\partial y^2}-K_e(\epsilon_{ye}-\epsilon_{yp})=0 \qquad A_p\frac{\partial^2\epsilon_{y,p}}{\partial y^2}+\frac{\partial^2\epsilon_{y,p}}{\partial x^2}+B_p\frac{\partial^2\epsilon_{x,p}}{\partial y^2}+K_p(\epsilon_{ye}-\epsilon_{yp})=0$$

$$A_{e,p}=\frac{2}{1-\nu_{e,p}} \quad ; \quad B_{e,p}=\frac{1-3\nu_{e,p}}{1-\nu_{e,p}}$$

$$K_e=\frac{G_b/G_e}{t_b t_e} \quad ; \quad K_p=6\frac{G_b/G_p}{t_b t_p}$$

Hypotheses:

- Constant Strain along the thickness of piezoelectric elements
- Linear Strain along the thickness of the structural element
- Superposition Effect Principle (linearity) is valid

Compatibility equation:

$$\frac{\partial P_{ex}}{\partial x}+\frac{\partial P_{ey}}{\partial y}=0$$

It is not strictly dependent from the physical problem, but from the hypotheses we have assumed true

PIEZO - STRUCTURE INTERACTION

RESULTING STRAIN

If $\nu_p = \nu_s = 1/3$ the equations become (x direction):

$$3\frac{\partial^2 \epsilon_{xx}}{\partial x^2} + \frac{\partial^2 \epsilon_{xy}}{\partial y^2} - K_s(\epsilon_{xx} - \epsilon_{yy}) = 0$$

$$3\frac{\partial^2 \epsilon_{xy}}{\partial x^2} + \frac{\partial^2 \epsilon_{yy}}{\partial y^2} + K_p(\epsilon_{yx} - \epsilon_{yy}) = 0$$

integrating, we obtain:

$$\epsilon_{xx} = \frac{6}{6+\psi}\Lambda + \frac{\psi}{6+\psi}\frac{\cosh \Gamma_1 \bar{x}}{\cosh \Gamma_1}\Lambda$$

$$\epsilon_{xy} = \frac{6}{6+\psi}\Lambda - \frac{6}{6+\psi}\frac{\cosh \Gamma_1 \bar{x}}{\cosh \Gamma_1}\Lambda$$

where: $\psi = \frac{E_p t_p}{E_s t_s}$ $\qquad \Gamma_1^2 = \frac{8}{9}\frac{G_s/E_s}{t_s t_s}\left(\frac{\psi+6}{\psi}\right)a^2$

In the same way, along the y direction, there will be:

$$\Gamma_2^2 = \frac{8}{9}\frac{G_s/E_s}{t_s t_s}\left(\frac{\psi+6}{\psi}\right)b^2$$

- If $\Gamma \to \infty$, then the piezo may be assumed to be "perfectly bonded";
  in this case, the transmitted forces may be thought as applied at the end of the piezo

- But, generally speaking $\Gamma_1 \neq \Gamma_2$
  then, it may be incorrect to assume the "perfect bonding" hypothesis
  for a piezo with a very short side

PIEZO - STRUCTURE INTERACTION

RESULTS AND CONCLUSIONS

Compatibility Equation:

$$\frac{\partial P_{sx}}{\partial x} + \frac{\partial P_{sy}}{\partial y} = 0$$ is satisfied if: $\Gamma \to \infty$

Force (x direction), perfect bonding case:

$$F_x = \frac{3}{2}\frac{\psi}{6+\psi} 2bE_c d_{31} V = \frac{3}{2} F_{1D}$$

- So, the hypotheses we have assumed, are consistent if piezo is perfectly bonded.

- For usual cases, "perfect bonding" condition holds (thickness of bonding layer < .1 mm).

NUMERICAL SIMULATION VIA MSC/NASTRAN

$\nu_{STRUC.} = \nu_{PIEZO}$

PLATE AND PIEZO-ACTUATOR HEXA MODEL

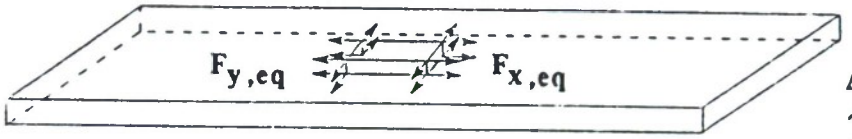

EQUIVALENT FORCES APPLIED AT EIGHT VERTICES OF PIEZO-ACTUATOR

PLATE HEXA MODEL

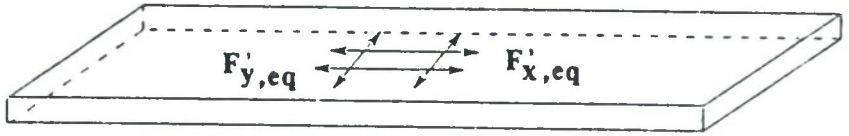

TRANSMITTED FORCES APPLIED ON THE CONTACT SURFACE

PLATE QUAD MODEL

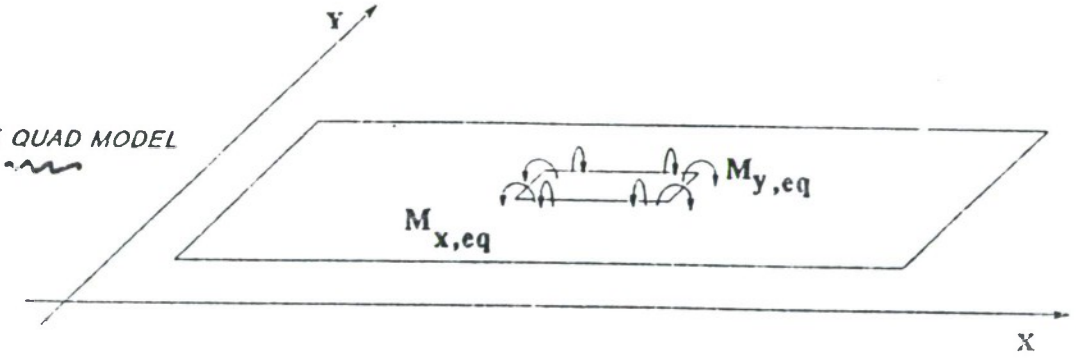

TRANSMITTED MOMENTS APPLIED ON THE CONTACT SURFACE

NUMERICAL MODELLING OF PIEZO SENSORS

STRAINS FROM FEM MODEL CAN BE DERIVED BY :

* DETAILED MODELLING OF PIEZO AND STRUCTURE ;
* APPROXIMATE EVALUATION FROM DISPALCEMENTS.

IN THIS 2nd CASE ,FOR BEAMS OR PLATES OF RECTANGULAR CROSS SECTION, WE CAN DERIVE :

$$\varepsilon_i = -\frac{t_b}{2}\frac{\partial^2 w}{\partial x_i} \simeq -\frac{t_b}{2}\frac{w_{i+1} - 2w_i + w_{i-1}}{\Delta x^2}$$

WHERE : w_i = VERTICAL DISPLACEMENT AT NODE i

ACTIVE CONTROL SCHEME AND ITS SIMULATION VIA MSC/NASTRAN

by DIRECT TIME INTEGRATION (BETA - NEWMARK)

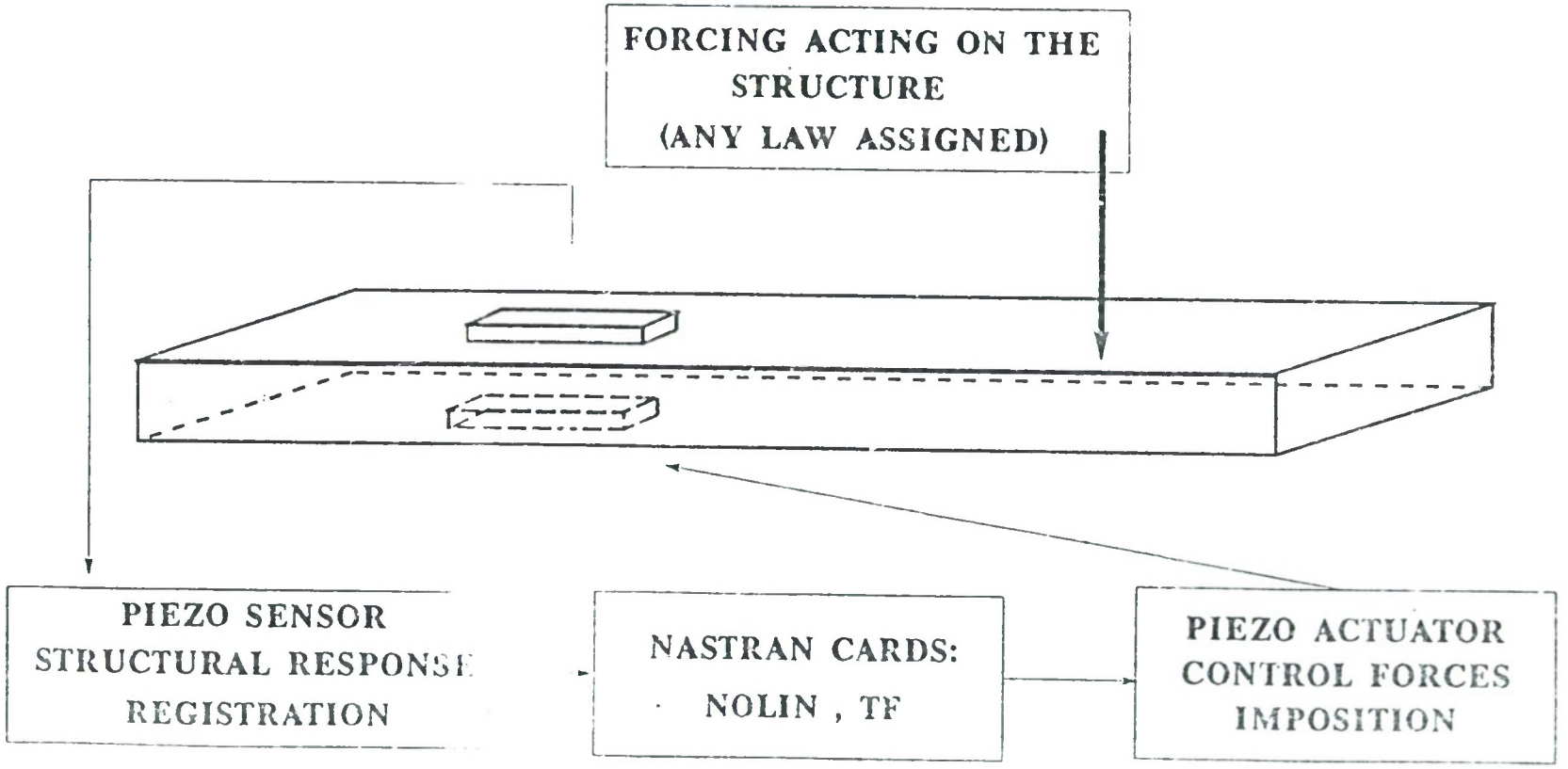

FREQUENCY RESPONSE OF AN ACOUSTIC ROOM

PRESSURE VALUES AT THE GRID ADJ. TO THE CENTRAL PLATE ONE

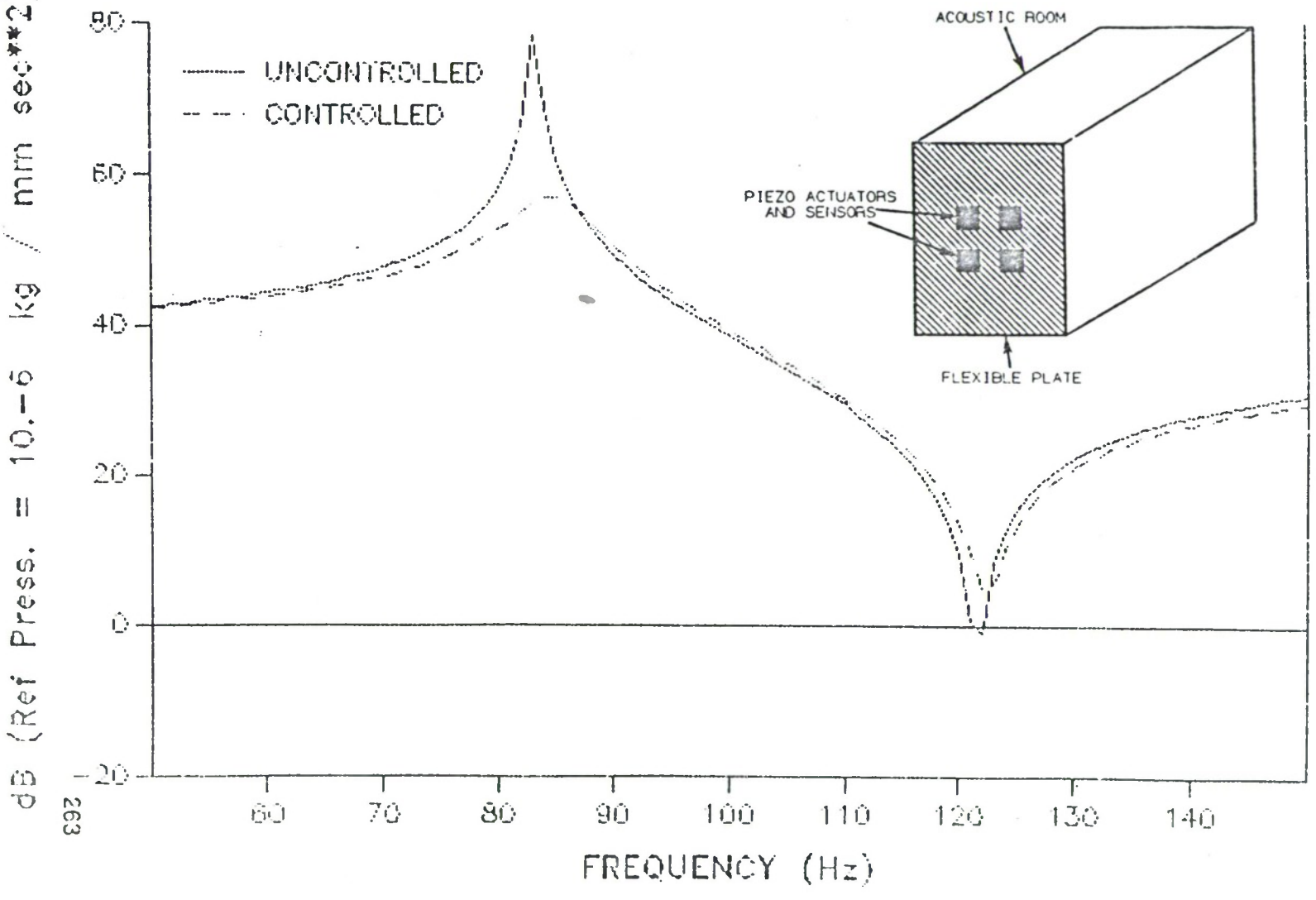

NEURAL OBSERVER (N.O.) FOR STATE ESTIMATION IN ACTIVE CONTROL SYSTEMS

- It is foreseen that this estimation structure is more advantageous than classic approaches
- The learning phase of N.O. can be implemented in real time
- Can be applied to non-linear structural systems (real ones)

NEURAL OBSERVER FOR STATE ESTIMATION IN ACTIVE CONTROL SYSTEMS

GENERAL ARCHITECTURE OF A NEURAL OBSERVER

NUMBER OF STATES = 4
NUMBER OF MEASUREMENTS = 2

WITH $e_i(k) = X_i(k) - \hat{X}_i(k) \longrightarrow 0$

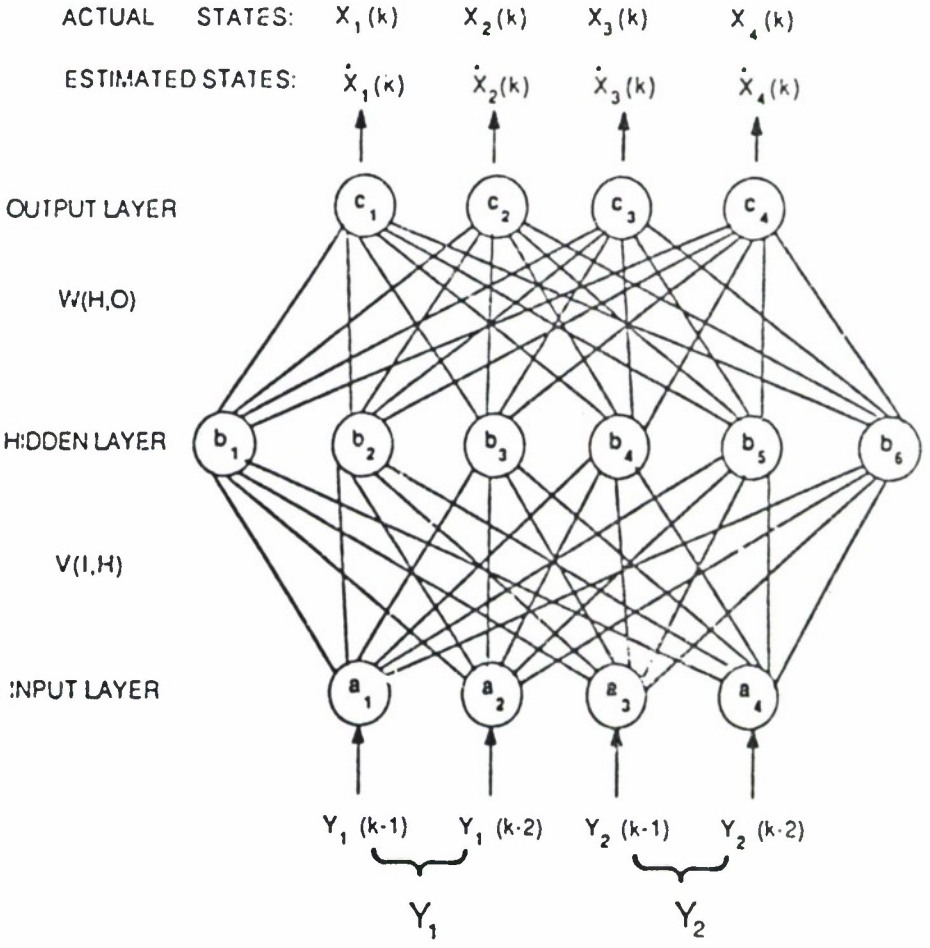

EACH CELL ◯ IS A PROCESSING ELEMENT (P.E.)

NEURAL OBSERVER FOR STATE ESTIMATION IN ACTIVE CONTROL SYSTEMS

BLOCK DIAGRAM OF A REAL NEURAL OBSERVER

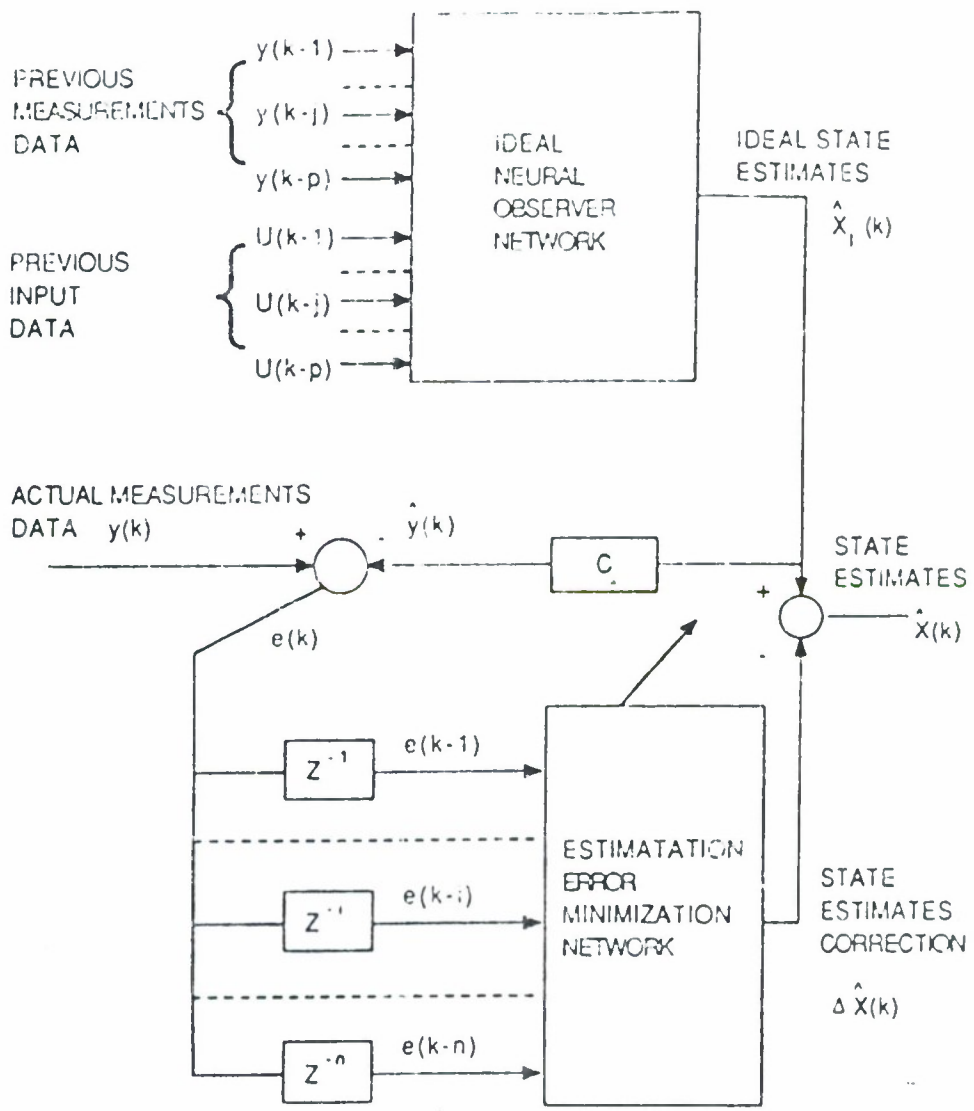

NEURAL OBSERVER FOR STATE ESTIMATION IN ACTIVE CONTROL SYSTEMS

(COMPUTER SIMULATION OF A VIBRATING BEAM)

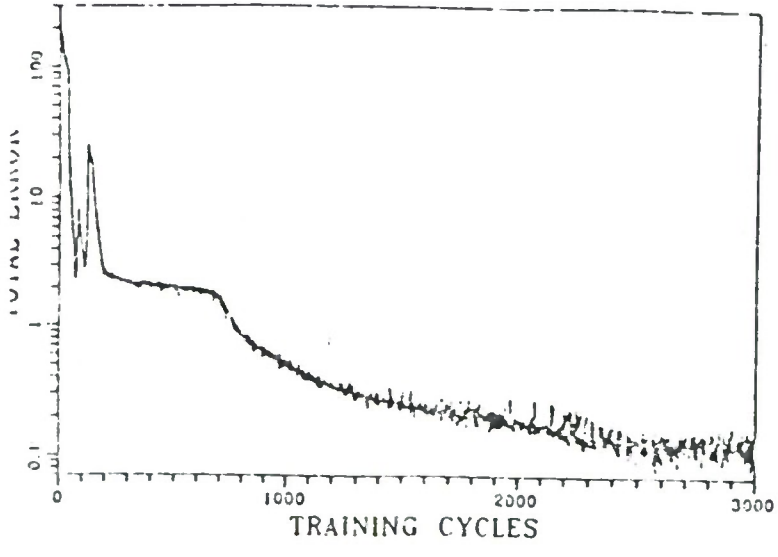

Estimation Error vs. Training Cycles

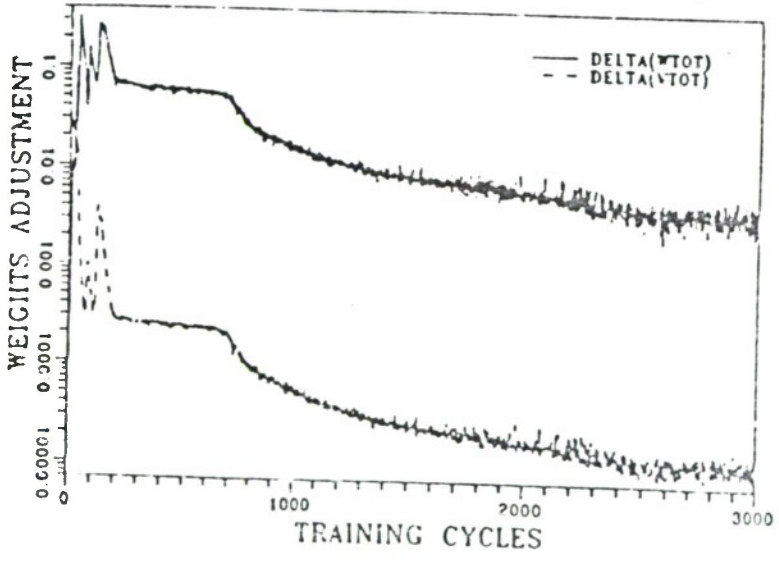

Weights Adjustment vs. Training Cycles

NEURAL OBSERVER FOR STATE ESTIMATION IN ACTIVE CONTROL SYSTEMS

(COMPUTER SIMULATION OF A VIBRATING BEAM)

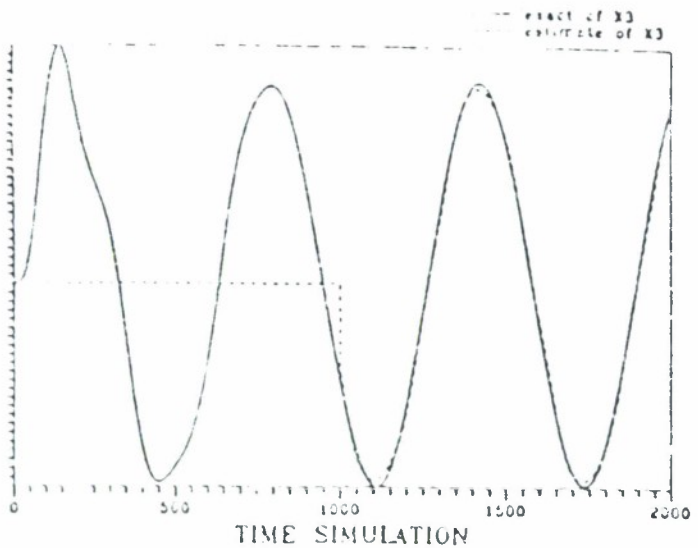

Dynamic Simulation Comparison of Exact and Estimate of X3 (Neural Observer turned on at instant k=1000)

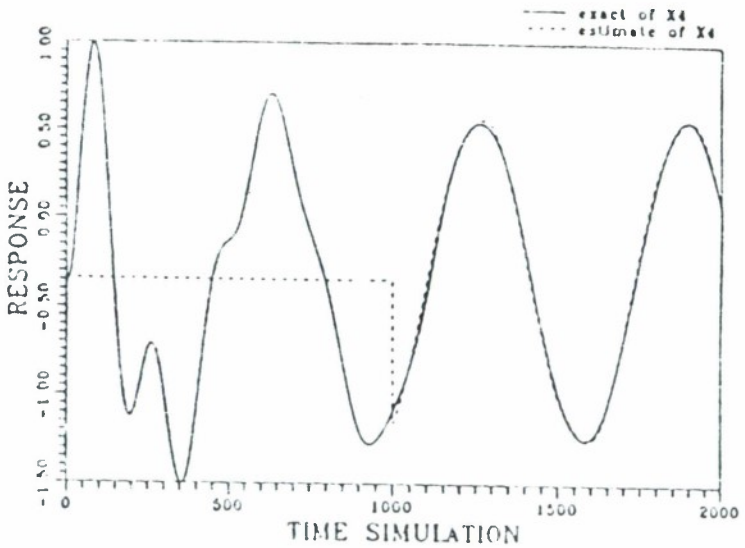

Dynamic Simulation Comparison of Exact and Estimate for X4 (Neural Observer turned on at instant k=1000)

OPTIMAL NOISE CONTROL ON DOUBLE WALL PARTITIONS

- Typical application of Active Control for Interior Noise in Aircraft Fuselage.

- Similar studies were previously conducted using Point Force (Shaker) Active Control.

- Piezoceramic Patches are candidate substitutes for Shakers.

OPTIMAL NOISE CONTROL ON DOUBLE WALL PARTITIONS
(cont.)

- Optimization criterion: research of the Minimal Vibrational Energy (Ev) or Sound Power Radiation (SWR).
- Characteristics of the algorythm:
  an application of the LMS routine
  feedforward-type (structure and external loads are known).
- External load: white-noise type (0-500 Hz).
- No algorythm has been implemented for the choice of the best location of piezo-actuators.
- <u>OBJECTIVE: to reduce SWR of the Trim Panel</u>
- Computation of the pressure field (free-field model):

$$p(y) = \frac{j\omega\rho S e^{-jkr}}{2\pi r} v(x)$$

FEM MODEL OF THE DOUBLE WALL PARTITION SYSTEM

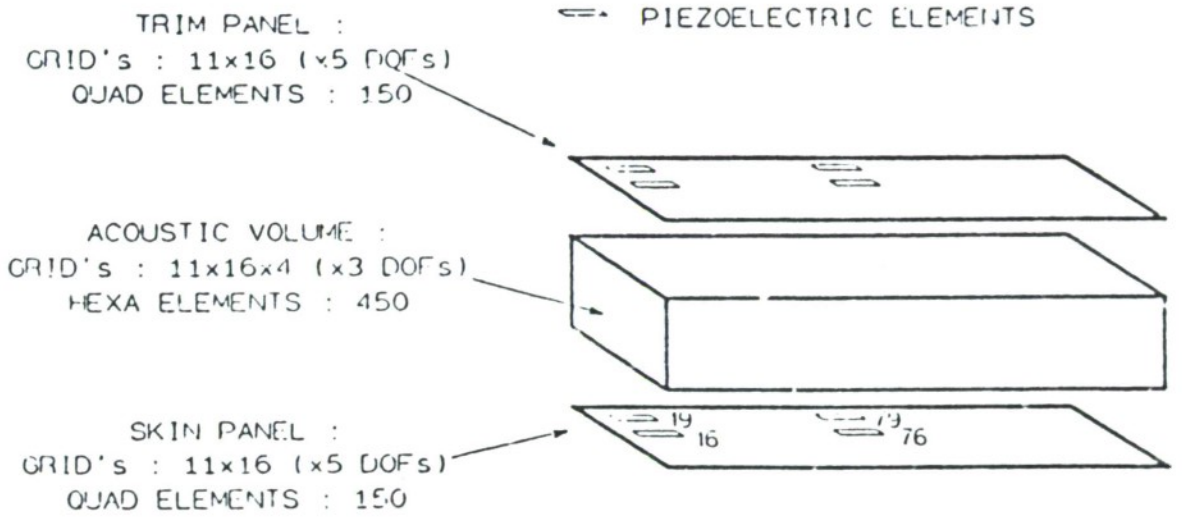

SWR EVALUED ON THE TRIM PANEL
CONTROL ON SOUND POWER, RADIATED BY THE TRIM PANEL

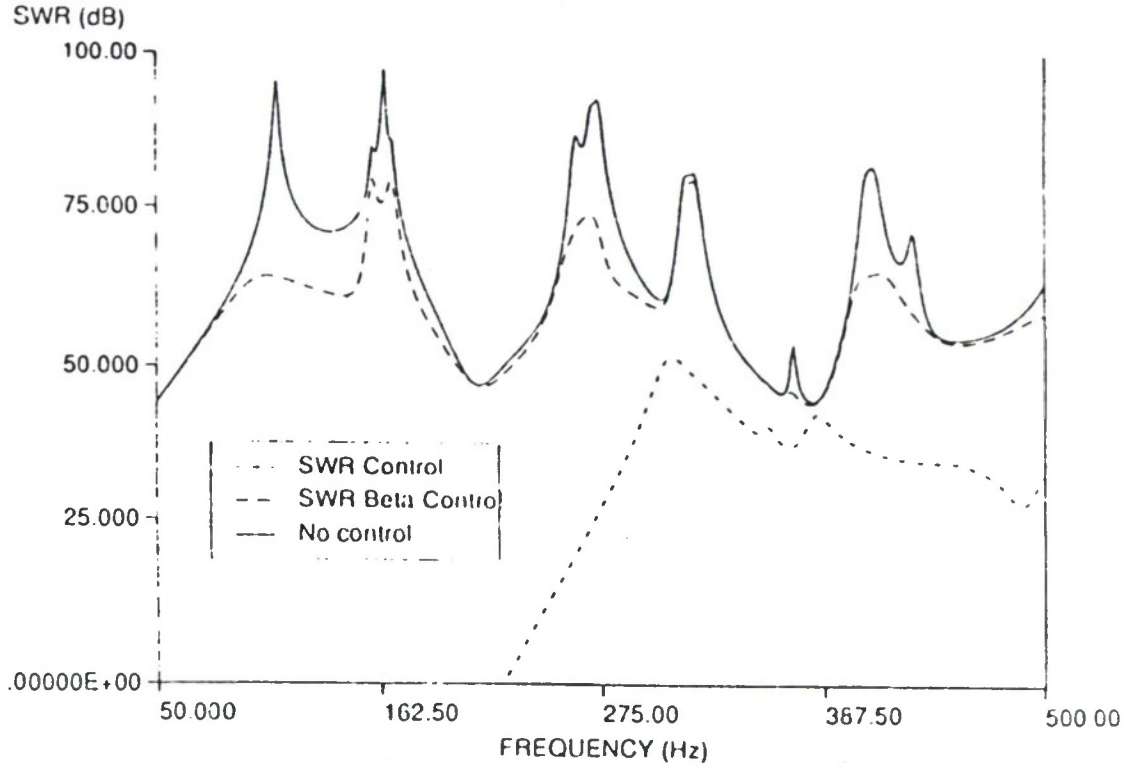

OPTIMAL NOISE CONTROL ON DOUBLE WALL PARTITIONS

(Preliminary Conclusions)

- SWR (direct) Control is a better way to minimize Sound Emission with respect to Ev Control.
- Actuators placed on the Trim Panel are less effective..
- All the four piezoes placed on the Skin Panel must be involved to obtain interesting noise reduction.
- Presented results are not comparable, because a different weight factor was used.
- Effect of Cost Factor introduction:
  - Control Forces (magnitude) reduction;
  - Control Effectiveness locaized at Resonance Frequencies.
- Further Objectives:
  - To improve Efficiency of Piezo Actuators (Best positioning)
  - To investigate about the effect of Physical and Geometrical characteristics on the Control System.

SIMPLE NEGATIVE POSITION FEEDBACK ACTIVE CONTROL SYSTEM (SISO) WITH APPLICATION TO BEAMS AND PLATES

DESIGN SPECIFICATION

- PRELIMINARY SIMPLE SYSTEM (SISO) TO ASSES CAPABILITIES
- MINIMUM HARDWARE AND COST
- ANALOGIC SIGNAL PROCESSING
- LIGHT AND SMALL
- PIEZO-ELEMENT AS ACTUATOR AND SENSOR
- MINIMUM SIGNAL CONDITIONING AND AMPLIFICATION

SUMMARY OF EXPERIMENTAL ACTIVITIES

MAIN CHARACTERISTICS OF THE FOUR SPECIMENS USED DURING TESTS

N	TYPE	CONTRAINT TYPE	SECTION [mm]	DIMENS. [mm]	MATERIAL
1	BEAM	CANTILEVER	Rectangular 50 x 5	Lenght 530	Alluminum Alloy
2	BEAM	FREE	Rectangular 40 x 4,4	Lenght 385	Steel
3	PANEL	DIFFERENT CONDITION	Thickness 2	400 x 500	2024 Al Alloy
4	RECT. FRAME	SIMPLY SUPPORTED	Fig.	Lenght 1500	2024 Al Alloy

PIEZOELECTRIC PCE-5 MATERIAL CHARACTERISTICS (furnished by SECI-SUD, Qualiano (NA))		
Density (gr/cm^3)	=	7.65
Curie Temperature (C)	=	355.
d31 (m/V)	=	18.6 e-12
g31 (mV/N)	=	12.3 e-3
Young's module (N/m^2)	=	6.3 e+10
Poisson's module	=	.33

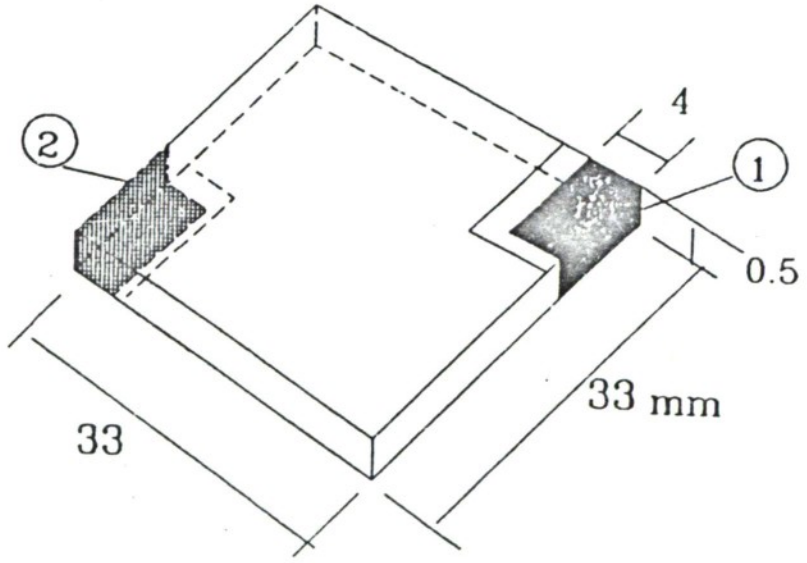

PIEZO–ACTUATOR AND SENSOR MODEL VALIDATION

Numerical (A)
Experimental (B)
Comparison
FRF's of a Plate in Open-Loop Configuration.

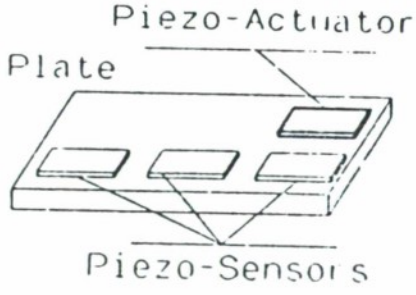

(A)

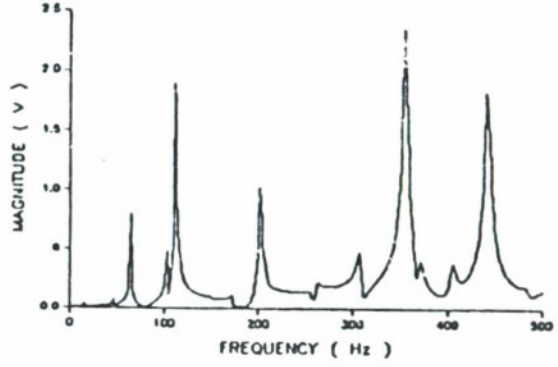

(B)

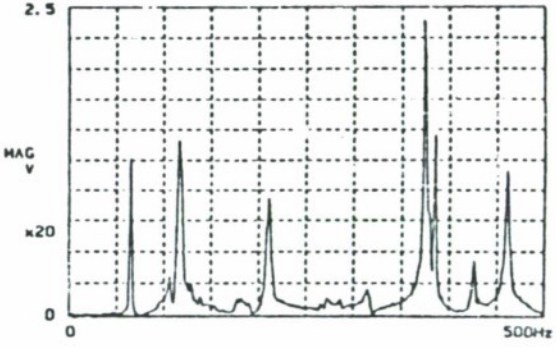

PIEZO-ACTUATOR AND SENSOR MODEL VALIDATION

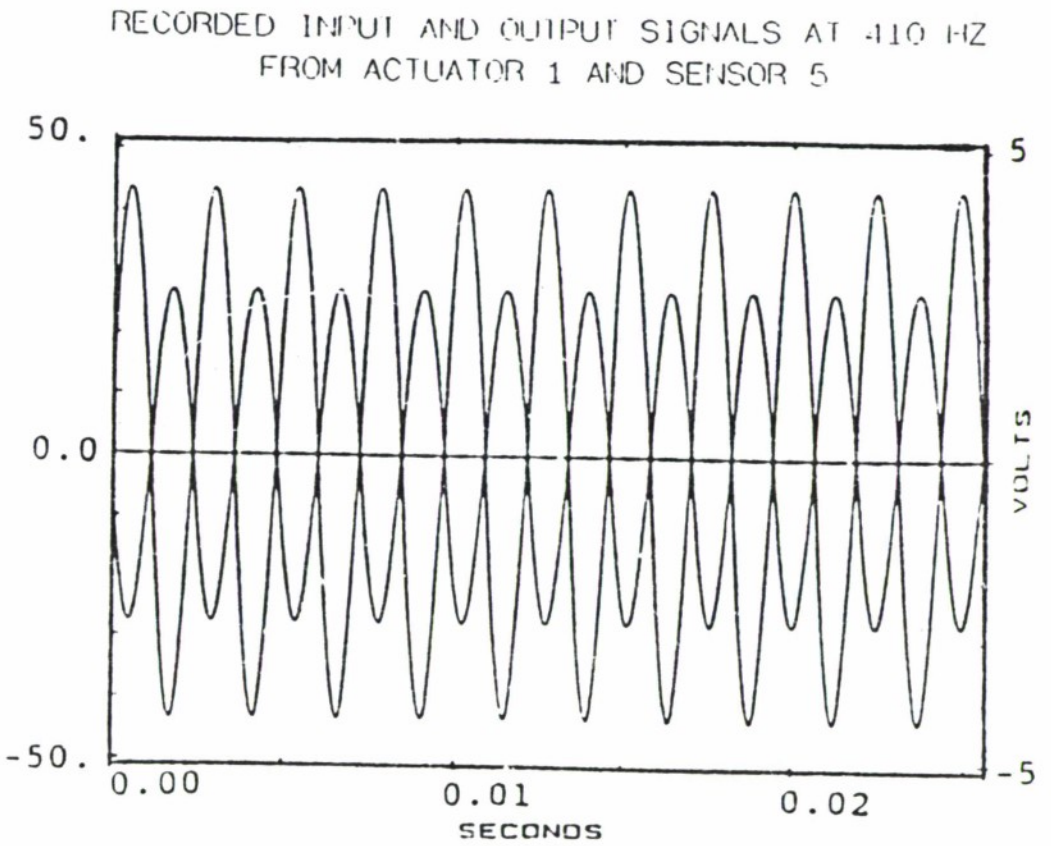

PIEZO–ACTUATOR AND SENSOR MODEL VALIDATION

PIEZO–ACTUATOR AND SENSOR COUPLE

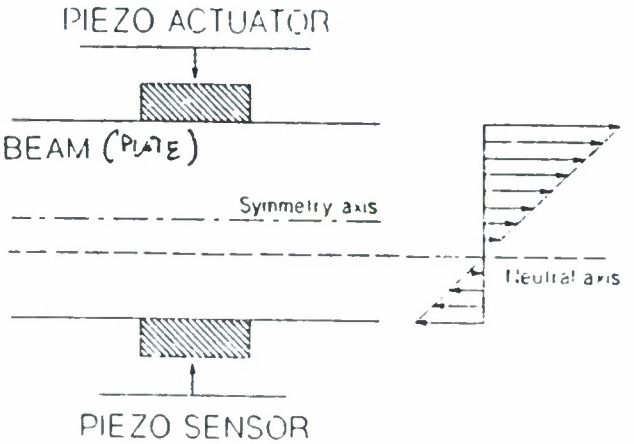

$$\epsilon_1 = \frac{12 + 4\psi}{(2 + \psi)(6 + \psi)}\Delta$$

$$\epsilon_2 = -\frac{2\psi}{(2 + \psi)(6 + \psi)}\Delta$$

INPUT(Vi)–OUTPUT(Vu) STATIC RELATIONSHIP

$$\frac{V_u}{V_i} = 2g_{31}d_{31}\frac{E_c}{1 - \nu c}\frac{2\psi}{(2 + \psi)(6 + \psi)}$$

	NUM	EXP	Δ%
Vi/Vu	17.20	16.99	1.23

PIEZO-ACTUATOR AND SENSOR MODEL VALIDATION

SCHEMATIC VIEW OF THE TEST PANEL (ITEM 3) WITH THE DISTRIBUTION OF THE PIEZO ELEMENTS

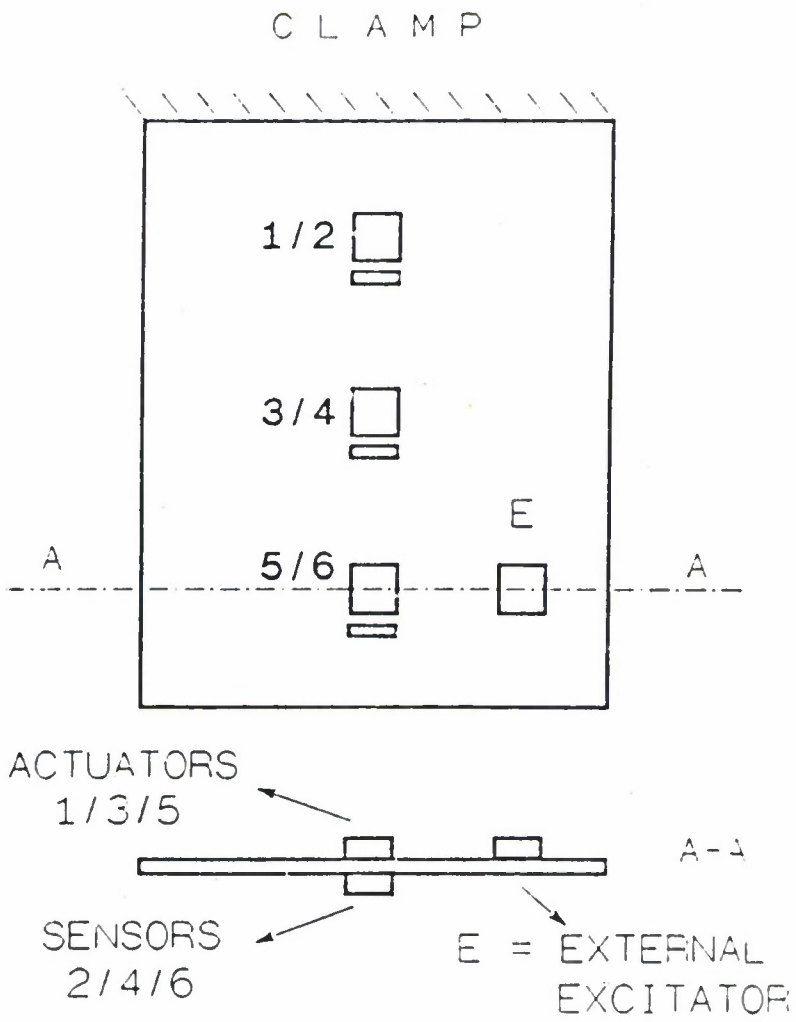

CONTROL LAW

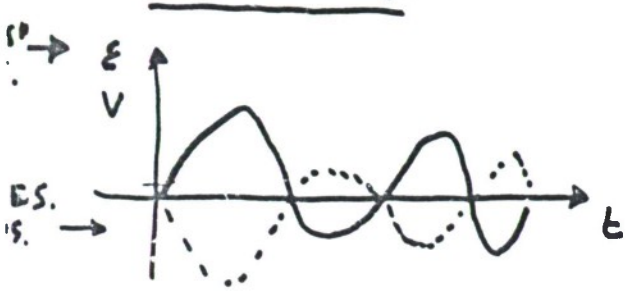
ε
V
t

PLOTTER
DATA ANALYZER (ONO SOKKI)
OSCILLOSCOPE (DATA 6000)
SIGNAL AMPLIFIER
SIGNAL TRANSFORMER
PIEZO ACTUATOR
CONTROL BLOCK
CONTROL SYSTEM PIEZO-ACTUATOR
STRUCTURE
PIEZO SENSOR
AUTOMATIC GAIN REGULATOR
CONTROL SYSTEM PIEZO-SENSOR
POWER
CONTROL SYSTEM

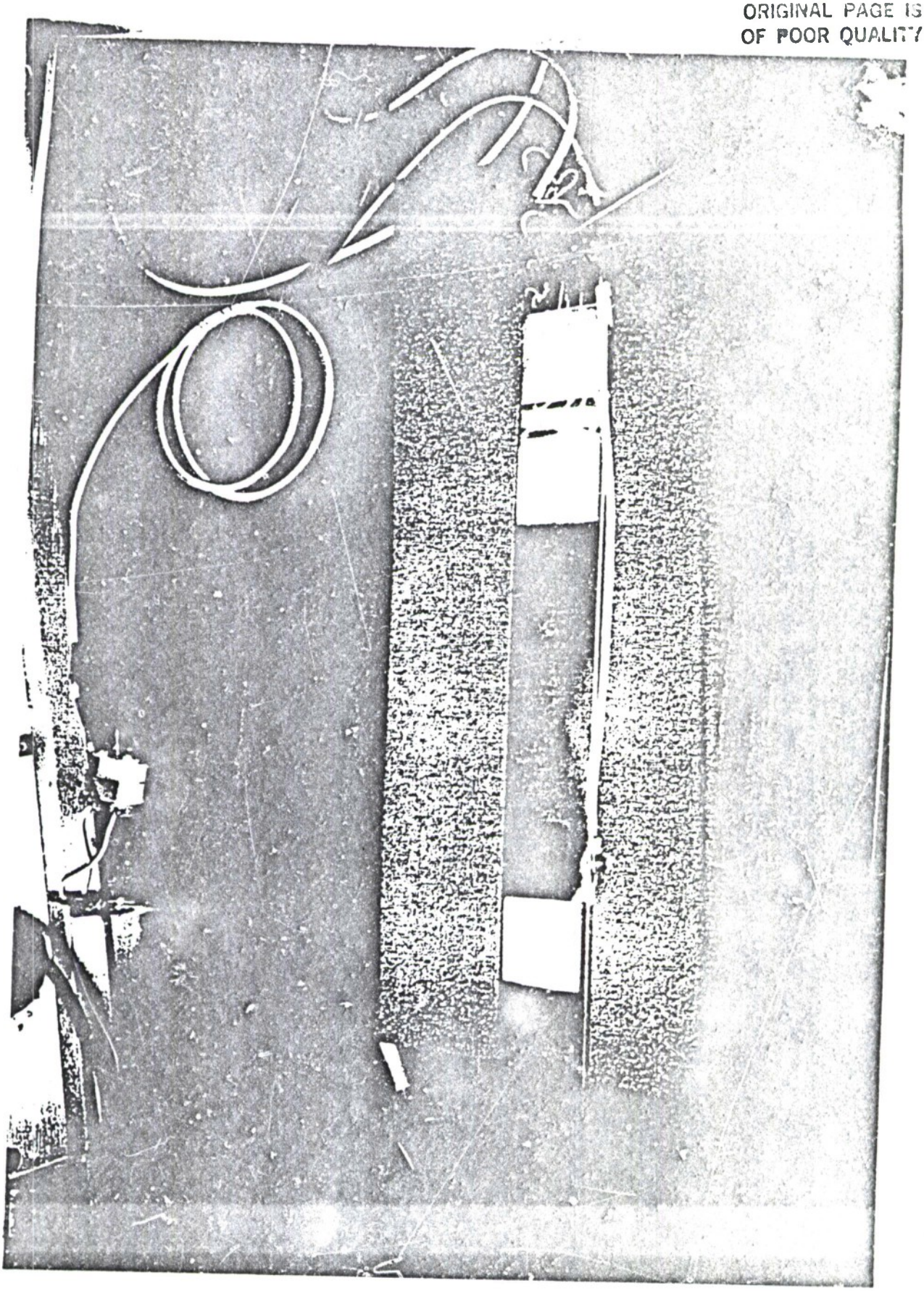

Alenia
ALENIA AERONAUTICA
DIREZIONE TECNICA
TRASPORTO

SLIDE X EVIDENZIARE LA "CONTROL BOX" !!

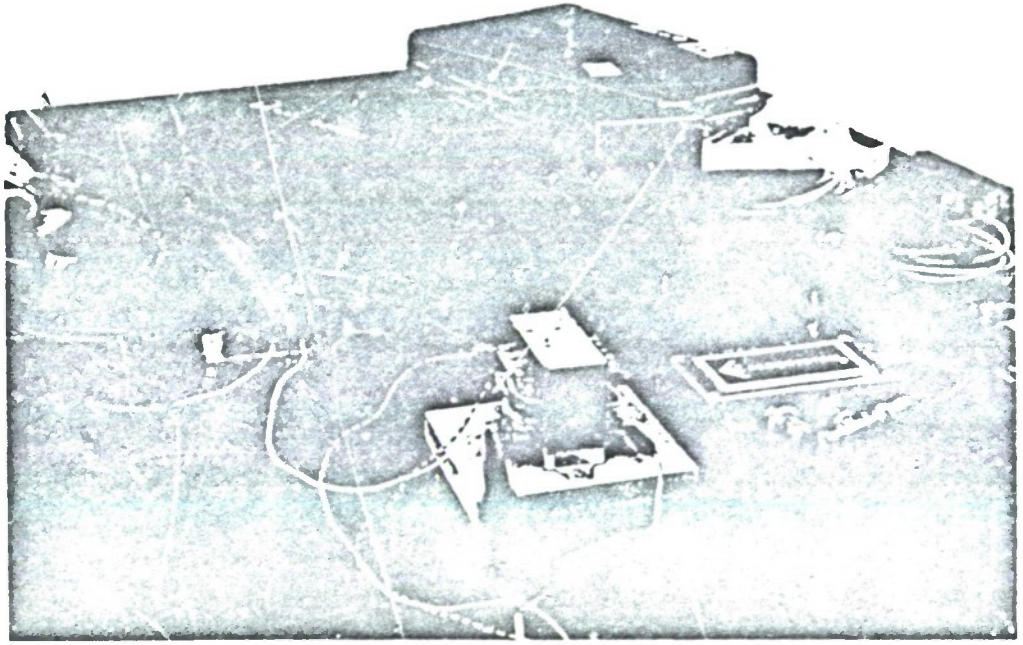

TYPICAL RESULTS OF ACTIVE CONTROL ON SPECIMEN N.2

RESPONSE FROM PIEZO-SENSOR OF CONTROL SYSTEM

(a) IMPULSIVE EXCITATION (HAMMER)
(b) SINE EXCITATION AT 400 Hz (2nd FLEX. MODE)

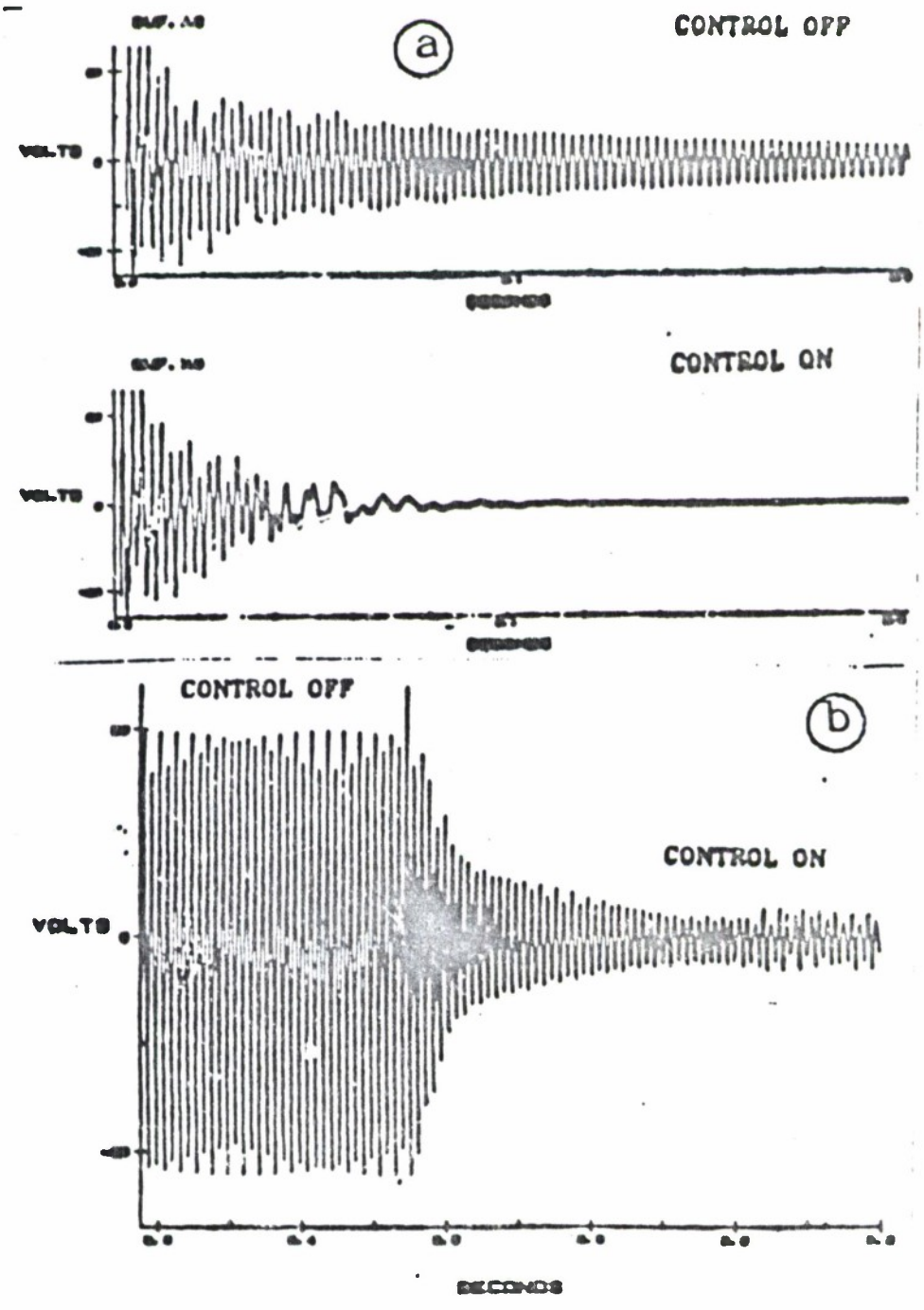

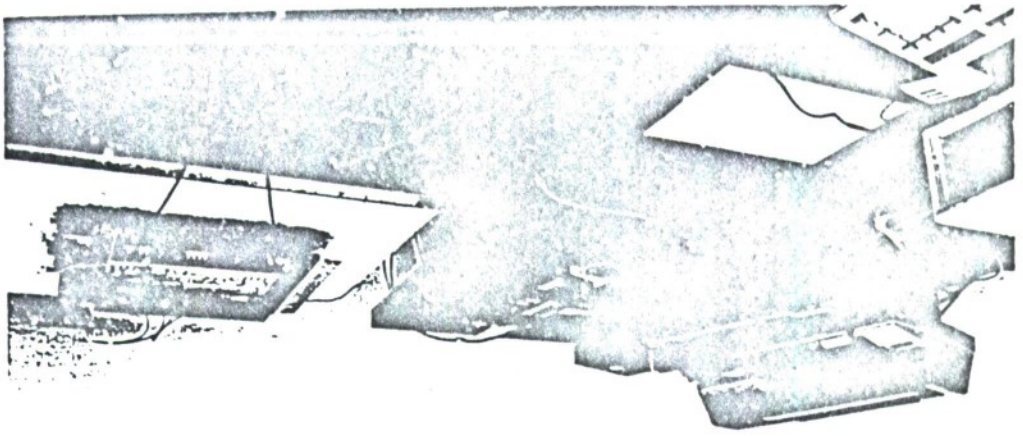

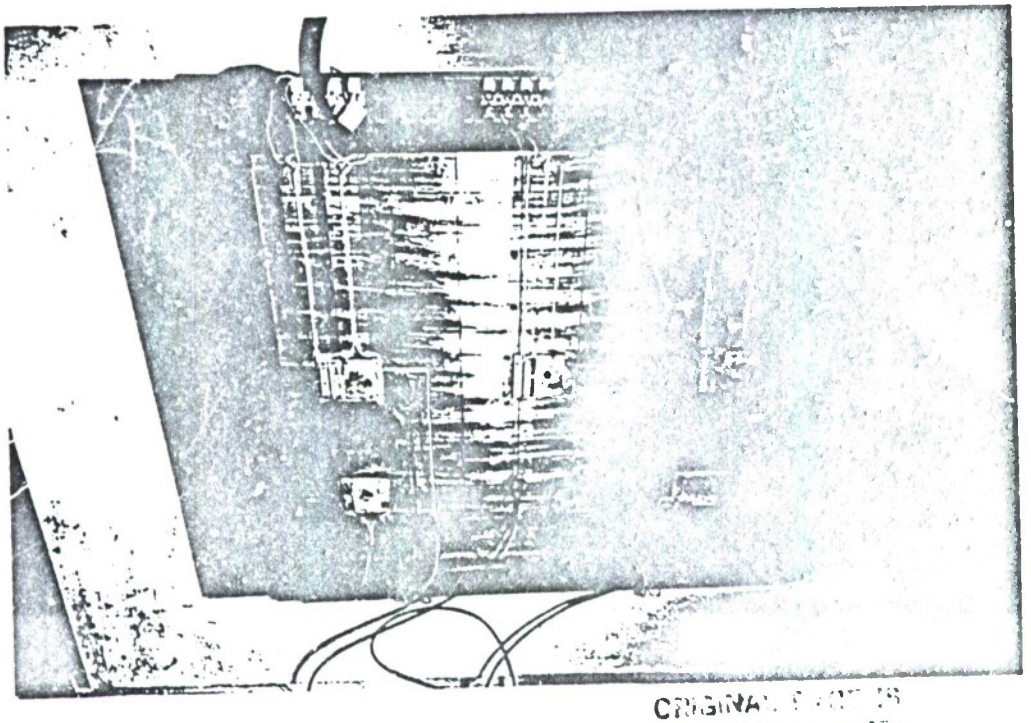

SIMPLE NEGATIVE POSITION FEEDBACK ACTIVE CONTROL SYSTEM (SISO) WITH APPLICATION TO BEAMS AND PLATES

TYPICAL RESULTS ON PLATE STRUCTURE

FRF (OPEN AND CLOSED LOOP) BETWEEN PIEZO EXCITATION IN ① AND ACCELERATION RESPONSE IN ① WITH CONTROL ON IN ③

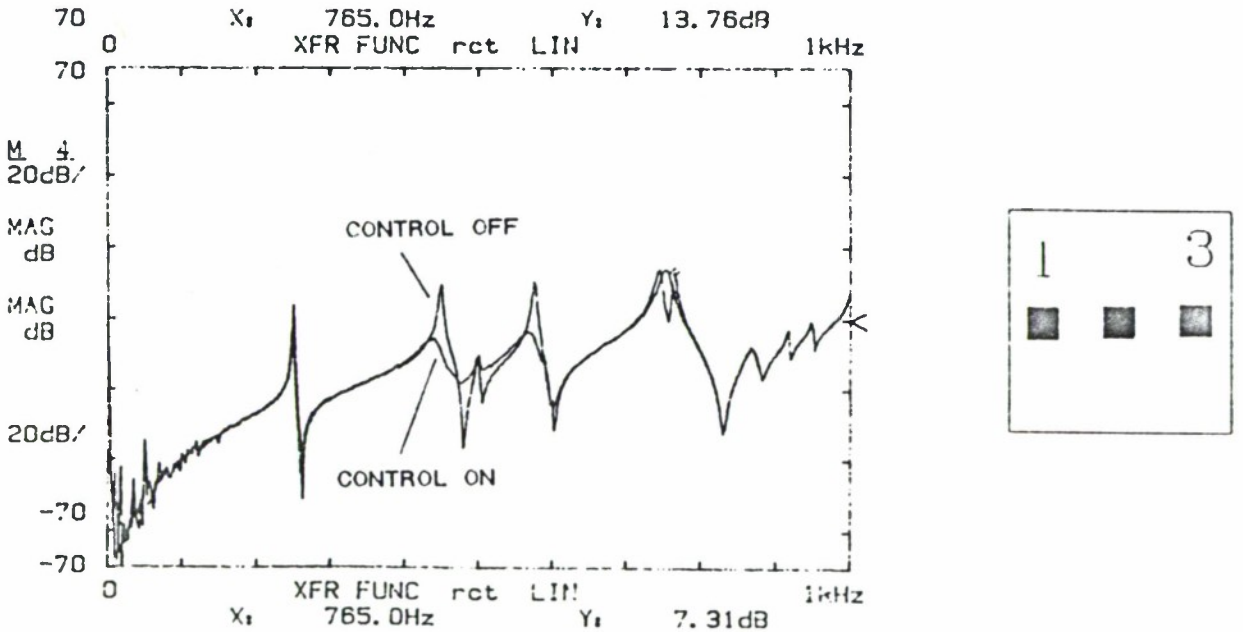

SIMPLE NEGATIVE POSITION FEEDBACK ACTIVE CONTROL SYSTEM (SISO) WITH APPLICATION TO BEAMS AND PLATES

TYPICAL RESULTS ON PLATE STRUCTURE

FRF (OPEN AND CLOSED LOOP) BEETWEN PIEZO EXCITATION IN (1) AND ACCELERATION RESPONSE IN (1) WITH CONTROL ON IN (3)

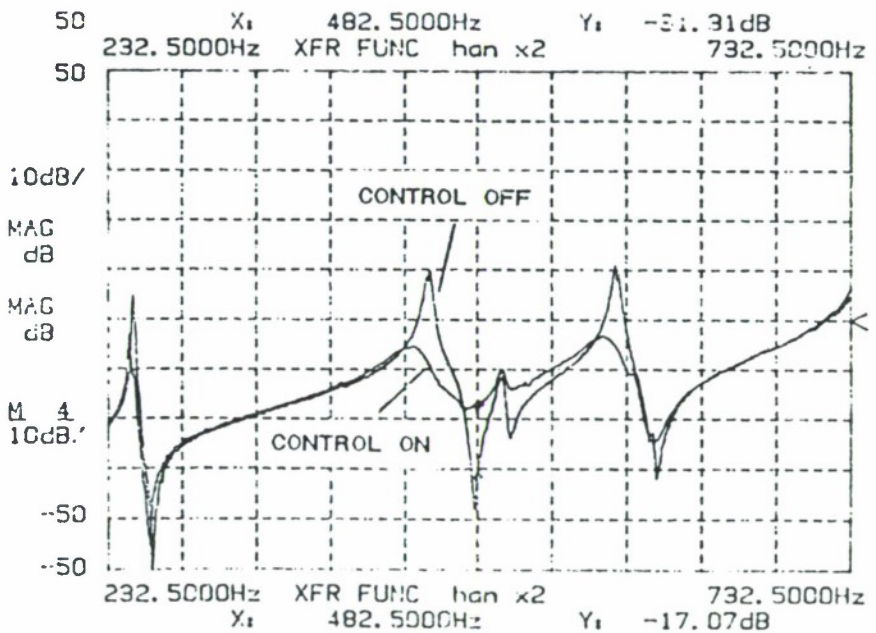

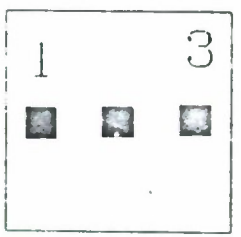

ZOOM FROM PREVIOUS FIGURE

ORIGINAL PAGE IS
OF POOR QUALITY

SPECIMEN N. 4 (FRAME)

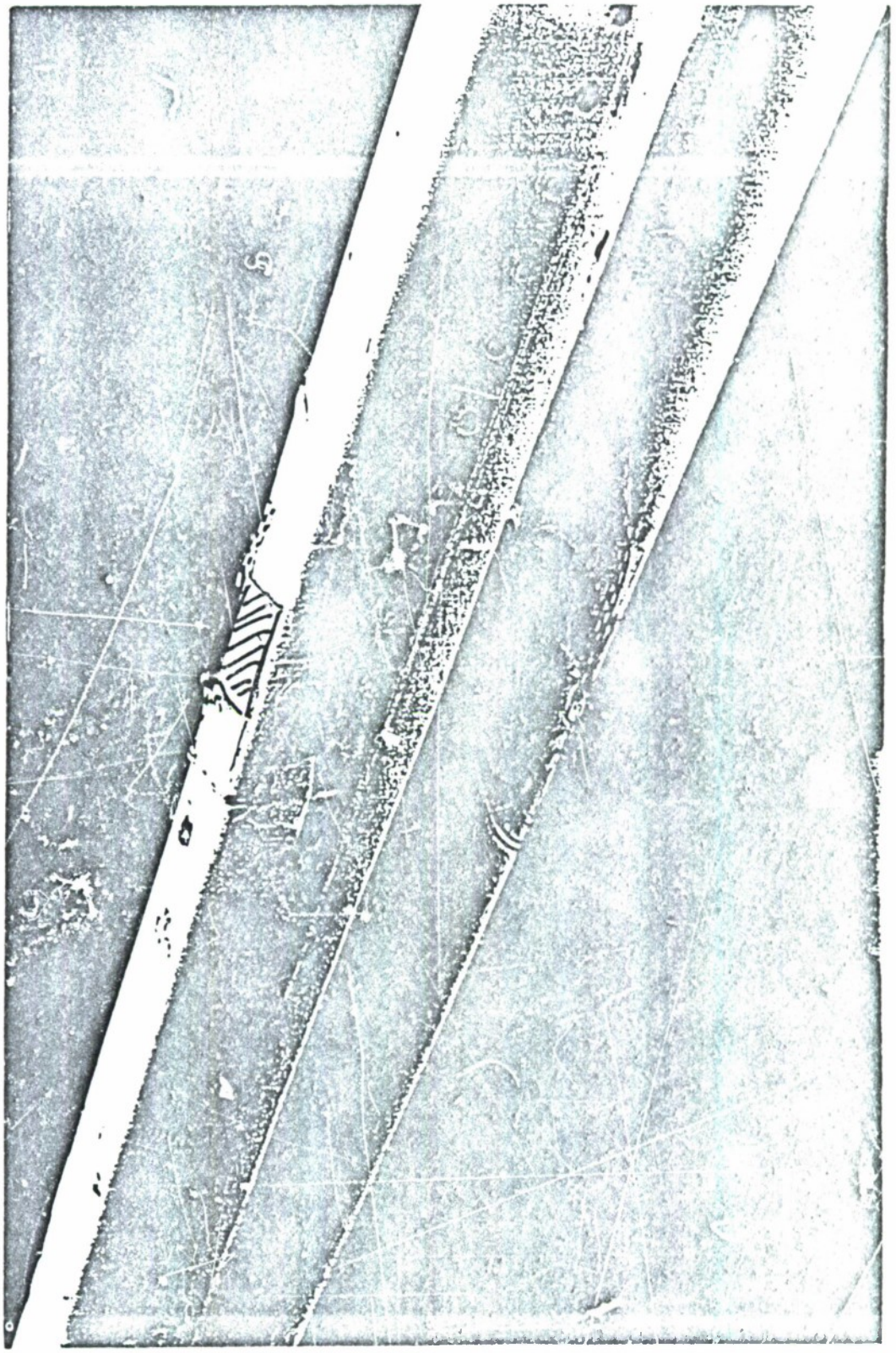

PIEZO-ACTUATION CAPABILITIES ON COMPLEX STRUCTURES
RECTIFIED PARTIAL FRAME OF TURBOPROP AIRCRAFT

VERTICAL ACCELERATION RESPONSE AT MIDSPAN DUE TO A SINGLE
OR A COMBINATION (in parallel) OF PIEZO-ACTUATORS

SWEPT-SINE EXCITATION : 0 - 200 HZ ; 90 V AMPLITUDE
RESPONSE EVALUATED AT 98 HZ (1st Vertical Bending Freq.)

SINGLE PIEZO ACTUATOR						
PIEZO ID.	PIEZO N. SECT. A	ACC.RESP. [g*10-3]	PIEZO N. SECT. B	ACC.RESP. [g*10-3]	PIEZO N. SECT. C	ACC.RESP. [g*10-3]
a	1		3	27	5	20
b	2	8	4	16	6	18
c	7	23	9	30	11	15
d	8		10	24	12	

MULTI. PIEZO ACTUATORS (in parallel)	
PIEZO N. COMBIN.	ACC.RESP. [g*10-3]
2+7	25
4+9	38
3+9	38
9+10	33
6+11	28
5+11	28
3+5	36
2+6	20
7+9	34
2+4+6	34
7+9+11	42
4+9+6+11+ 2+7	45

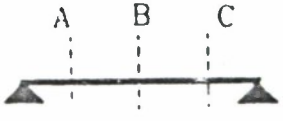

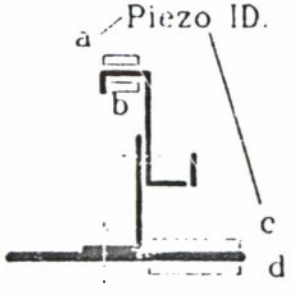

PIEZO-ACTUATION CAPABILITIES ON COMPLEX STRUCTURES
RECTIFIED PARTIAL FRAME OF TURBOPROP AIRCRAFT

VERTICAL ACCELERATION RESPONSE AT MIDSPAN DUE TO A SINGLE
OR A COMBINATION (in parallel) OF PIEZO-ACTUATORS

SINE EXCITATION : 98 Hz ; 90 V AMPLITUDE
(1st Vertical Bending Freq.)

		SINGLE PIEZO ACTUATOR				
PIEZO ID.	PIEZO N. SECT. A	ACC.RESP. [g*10-3]	PIEZO N. SECT. B	ACC.RESP. [g*10-3]	PIEZO N. SECT. C	ACC.RESP. [g*10-3]
c	7	150	9	246	11	173
d	8		10	212	12	

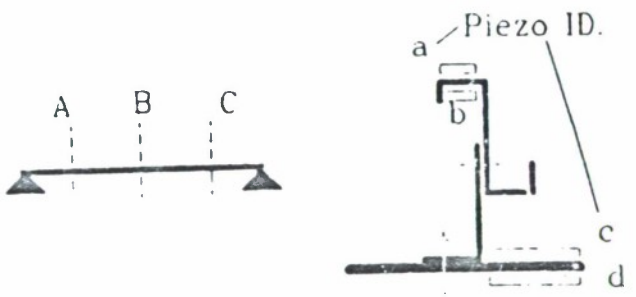

MULTI. PIEZO ACTUATORS (in parallel)	
PIEZO N. COMBIN.	ACC.RESP. [g*10-3]
9+10	325
9+11	302
7+9+11	375
9+10+11	360
4+9+6+11+ 2+7	500

Alenia
ALENIA AERONAUTICA
DIREZIONE TECNICA
TRASPORTO

292

PIEZO-ACTUATION AND SENSING ON COMPLEX STRUCTURES

Z SHAPED STRINGER-FEM SIMULATION

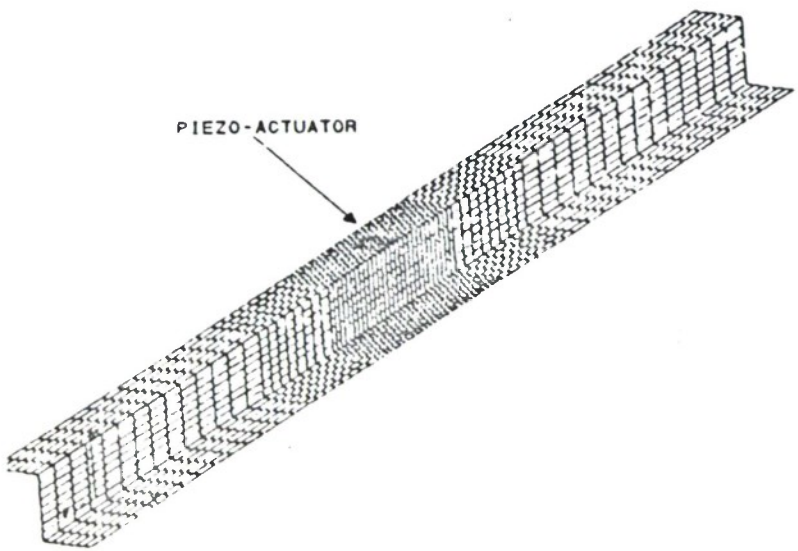

UNDEFORMED MODEL

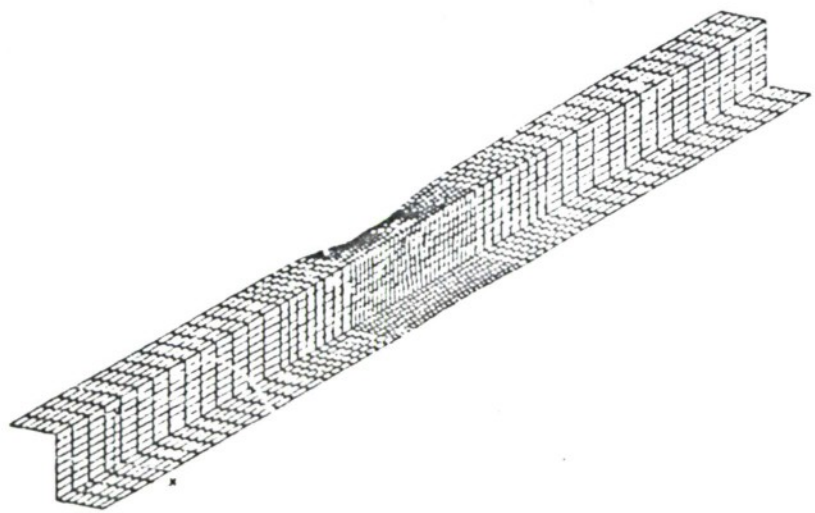

STATIC DEFORMATION

ALENIA

ALENIA AERONAUTICA

FUTURE PROGRAM

- Development of theoretical and numerical models for complex systems :

  - Circular Fuselage Frame
  - Fuselage Sidewall Panel
  - Real Aircraft Fuselage.

- Test of active vibration control systems applied to the following structures :

  - Stiffned flat panel inside an anechoic chamber
  - Aircraft fuselage on the ground
  - Aircraft fuselage in flight.

REFERENCE

[1] VITIELLO P., NELSON P.A., PETYT M.; "Numerical Studies of the Active Control of Sound Transmission through Double Wall Partitions", ISVR University of Southampton; Technical Report N. 181, Southampton (U.K.), Sept. 1989.

[2] LECCE L., CONCILIO A., DE ROSA S., CAVALIERE M.; "Riduzione della Trasmissione del Rumore attraverso Pannelli mediante l'uso di Attuatori Piezoelettrici", Proceedings del X Congresso Nazionale AIDAA, Pisa, 16-20 Ottobre 1989, ETS Editrice, Pisa, 1990, pp. 769-780.

[3] LECCE L., CONCILIO A., DEL GATTO F.S.; "Active Vibration Control using Distributed Actuators and Sensors", Proceedings Inter-noise '90, Goteborg (Sweden), 13-15 Aug 1990, Acoustic Society of Sweden, Goteborg, 1990, pp. 1375-1378.

[4] LECCE L., MARULO F., DE ROSA S., CONCILIO A., PEZZULLO G.; "Finite Element Simulation of the Active Noise Control in Small Enclosures using Piezoelectric Materials", FEM in the Design Process, Proceedings of the 6th World Congress, edited by J. Robinson and Ass., N. 16, 1990, pp. 94-102.

[5] LECCE L., VITIELLO P., MARULO F.; "Il Controllo Attivo del Rumore in Velivoli Turboelica", IPV Universita' di Napoli, Report SPEI 9025, Marzo 1990.

[6] LECCE L., CONCILIO A., DEL GATTO F.S.; "Numerical and Experimental Results on Vibroacoustical Active Control of Structural Elements with Piezoelectric Materials", "Workshop on Smart Materials System and Structures", DLR, AIAA, RAE, International Forum on Aeroelasticity and Structural Dynamics, Aachen (Germany), 3-6 June 1991.

[7] LECCE L., VITIELLO P., CONCILIO A., DEL GATTO F.S.; "Esperienze di controllo Attivo delle Vibrazioni e del Rumore mediante Materiali Piezoelettrici su Pannelli"; to be published "L'Aerotecnica, Missili e Spazio", edited by AIDAA (Italian Association of Aerospace Eng.).

[8] CONCILIO A., DEL GATTO F. S., LECCE L., VITIELLO P.; "Active Noise Control on Plates and Double Wall Partitions Using Discrete Piezoelectric Devices"; Invited Paper to the 14th DGLR/AIAA Aeroacoustics Conference, 11-14 May 1992, Aachen, Germany.

ACTIVE SYNCHROPHASING OF PROPELLER UNBALANCE

Dick Kaptein

Fokker Aircraft B.V.

4th NASA/SAE/DLR Interior Noise Workshop

Friedrichshafen, Germany, May 19-20 1992

ACTIVE SYNCHROPHASING OF PROPELLER UNBALANCE

Dick Kaptein, Fokker Aircraft B.V.

SUMMARY

This presentation describes the results of a survey to reduce the inflight propeller unbalance vibrations in the cabin of Fokker50 airplanes. Several approaches have been investigated. Active synchrophasing of the unbalance vibrations of both propellers has appeared to be most successful. Such system is now introduced in series airplanes. It is protected by patents all over the world.

THE FOKKER50 AIRPLANE

The Fokker50 turbopropeller airplane is well known for its low cabin noise levels which provide this airplane with a jet comfort. The careful selection of 6-bladed propellers with a very accurate and stable control system is one of the main reasons of this result. The system controls the shaft speed within ± 2 rpm and the phase angle between both propellers within ± 2 degree.

1P-VIBRATIONS

After delivery of the 30th airplane it happened that several customers complained about vibrating seat tables in the middle of the cabin. A short survey showed that propeller unbalance was the source of the vibrations and that the lateral direction of the seat tables was very sensitive for these 1P-vibrations. It was tried to attack the vibrations along 3 routes:
1- Reduction of the sensitivity of the seat table construction.
2- Reduction of the transmission by improvement of the Engine Vibration Isolators.
3- Reduction of the source by improvement of the balancing procedures.

1. Attempts to reduce the sensitivity of existing seats appeared to require unacceptable weight penalties and needed space which was not available. This approach was stopped and vibration sensitivity requirements were incorporated in specifications for new seats.
2. The metal-mesh rear engine vibration isolators were replaced by elastomeric isolators with lower dynamic stiffnesses. This reduced the 1P-vibration transmission with about 30 %. However, this improvement was not sufficient to avoid vibration complaints.
3. Dynamic balancing of the propellers was more successful in several cases. However, during test flights to verify the result of the balancing actions it appeared that the vibration level was dependent on the flight speed and that the vibration level changed due to a shut-down and relight of one of the engines. After some experiments it was found that the 6P-synchrophasing system was the cause of latter behaviour. This system has an important influence on the interference between the unbalance forces of both propellers.

ACTIVE SYNCHROPHASING

The 6p-phase angle requirement can be met with 6 combinations of blades of the LH and RH propeller. However, with each of these 6 combinations the phase relationship between the unbalances is shifted 60 degrees. In the cabin this results in 6 different 1P-vibration levels. On basis of this phenomenon Fokker has developed an active control system which is able to generate the 6 blade combinations, to measure the 1P-vibration levels for each combination and to select the combination with the lowest level. After realisation of the best combination the system monitors the vibration level. If it increases above some limit the system starts the search and selection procedure again. This means that it is able to respond on changes in flight conditions such as the flight speed or changes in propeller unbalance. The system also has to be active because, due to differences between propeller unbalances, each airplane needs a different optimum blade combination.
The newly delivered Fokker50 airplanes are provided with this Propeller Blade Matching System (PBMS). It is also available for existing Fokker50 aircraft. The PBMS box is installed below the cabin floor close to the wing mounting frames. The PBMS reduces the chance of 1P-vibration complaints to zero.

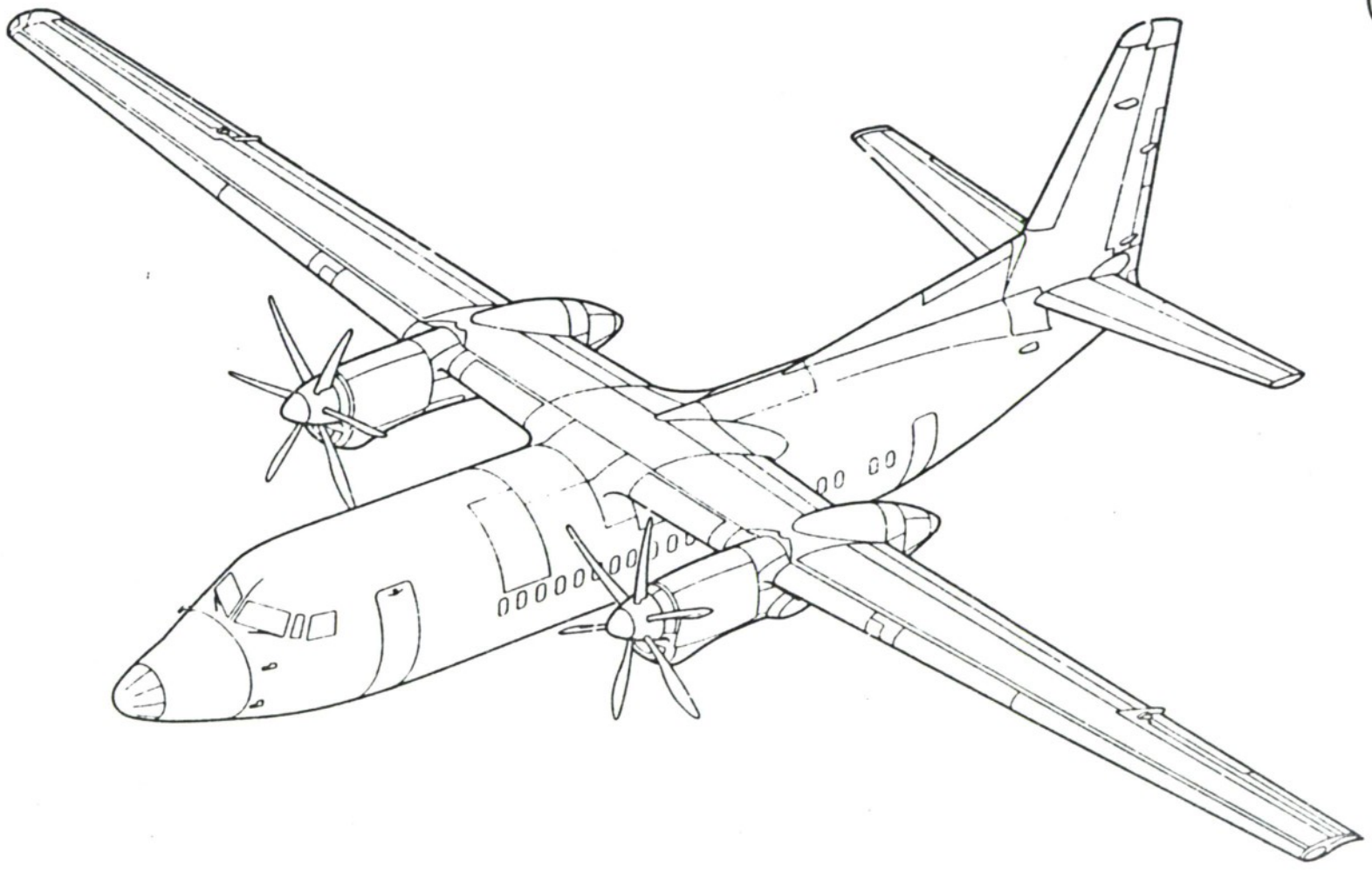

FOKKER50 AIRPLANE WITH 6-BLADED PROPELLERS

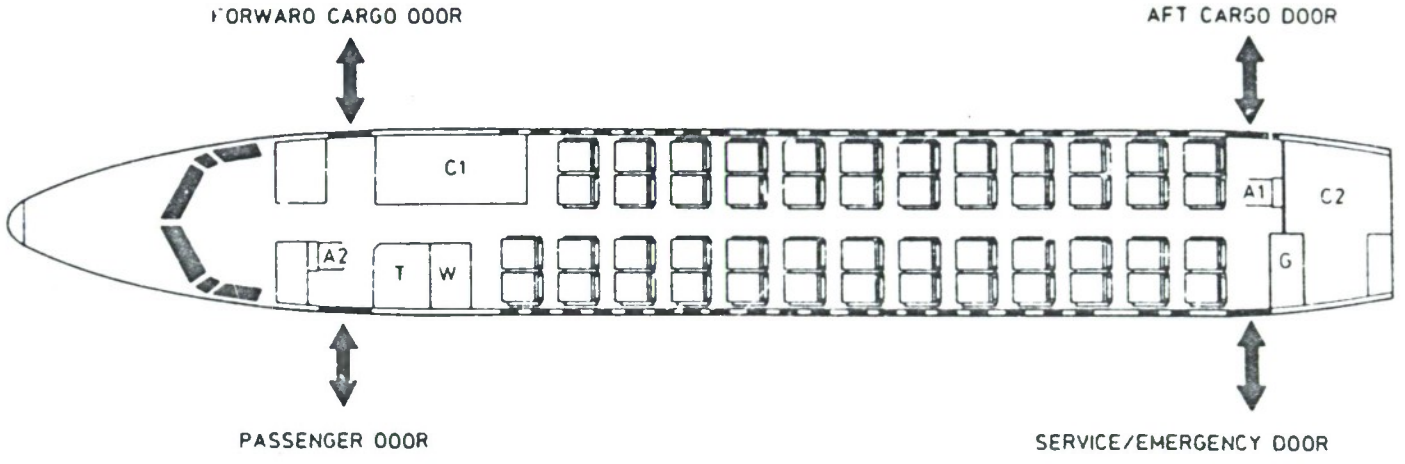

FOKKER50 CABIN LAY-OUT FOR 50 PASSENGERS

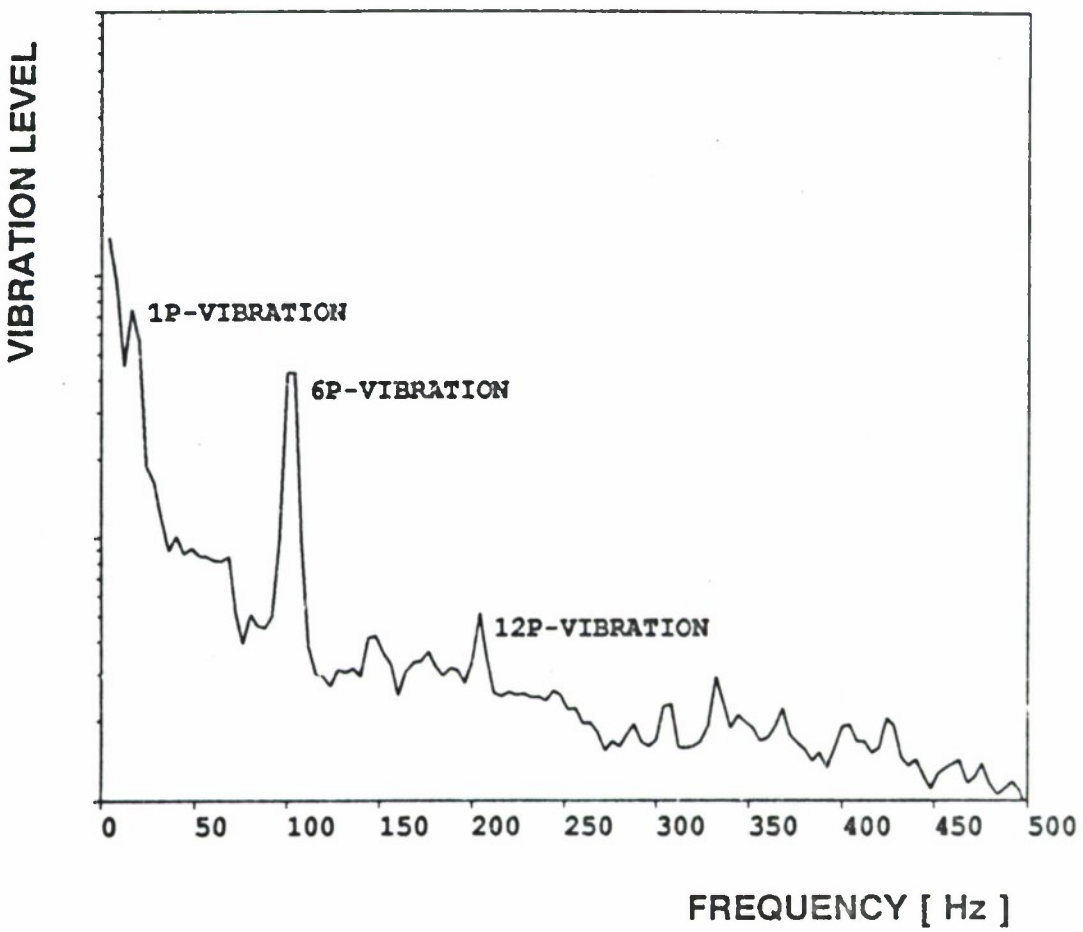

TYPICAL VIBRATION SPECTRUM IN THE MID CABIN

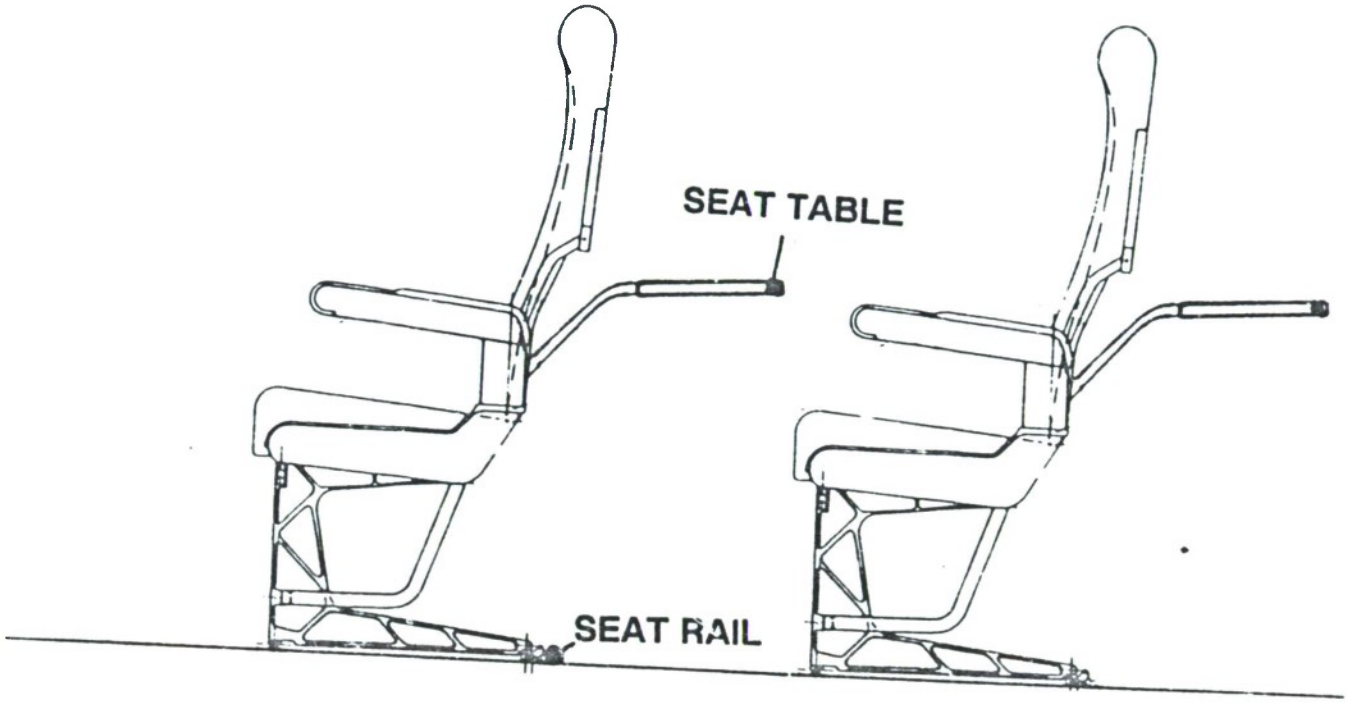

FOKKER50 SEAT WITH MEASUREMENT LOCATIONS

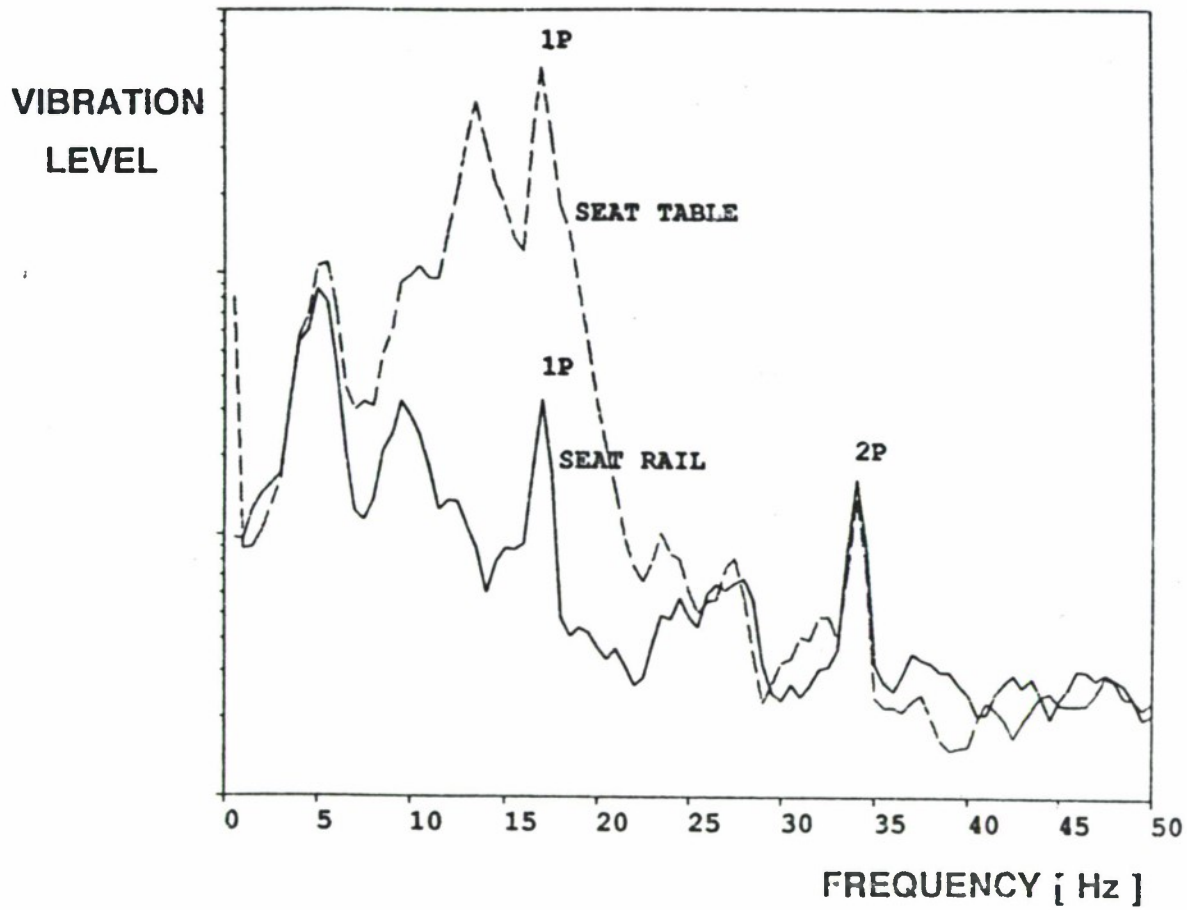

1P-VIBRATIONS OF SEAT TABLE AND SEAT RAIL

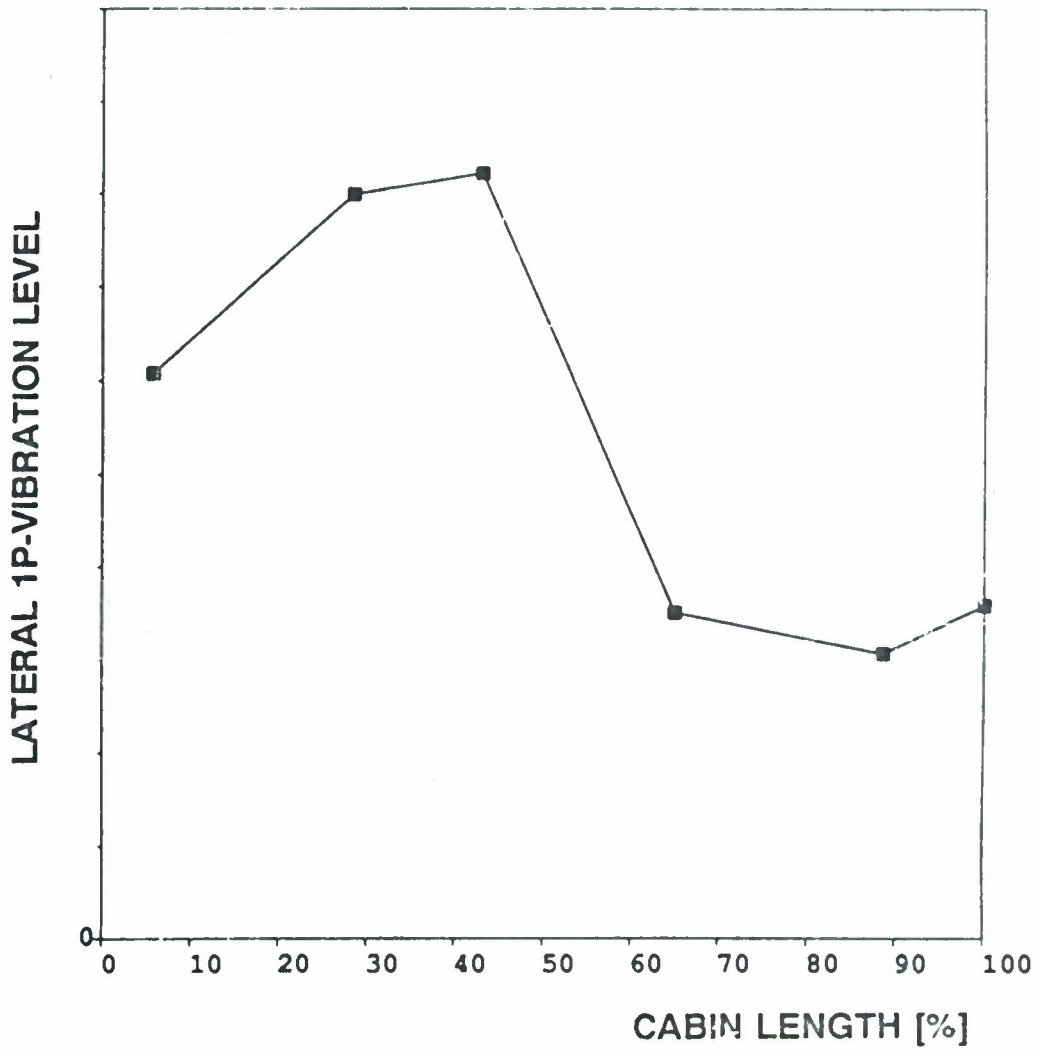

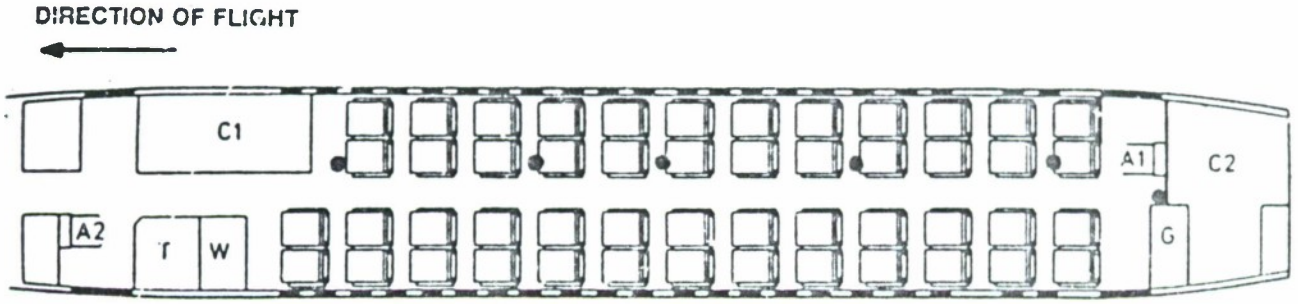

LATERAL 1P-VIBRATION vs CABIN LENGTH

1- REDUCTION OF SEAT TABLE SENSITIVITY.
(RESPONSE)

2- IMPROVEMENT OF ENGINE VIBRATION ISOLATORS.
(TRANSMISSION)

3- IMPROVEMENT OF PROPELLER BALANCING PROCEDURES.
(SOURCE)

3 APPROACHES TO ATTACK 1P-VIBRATIONS

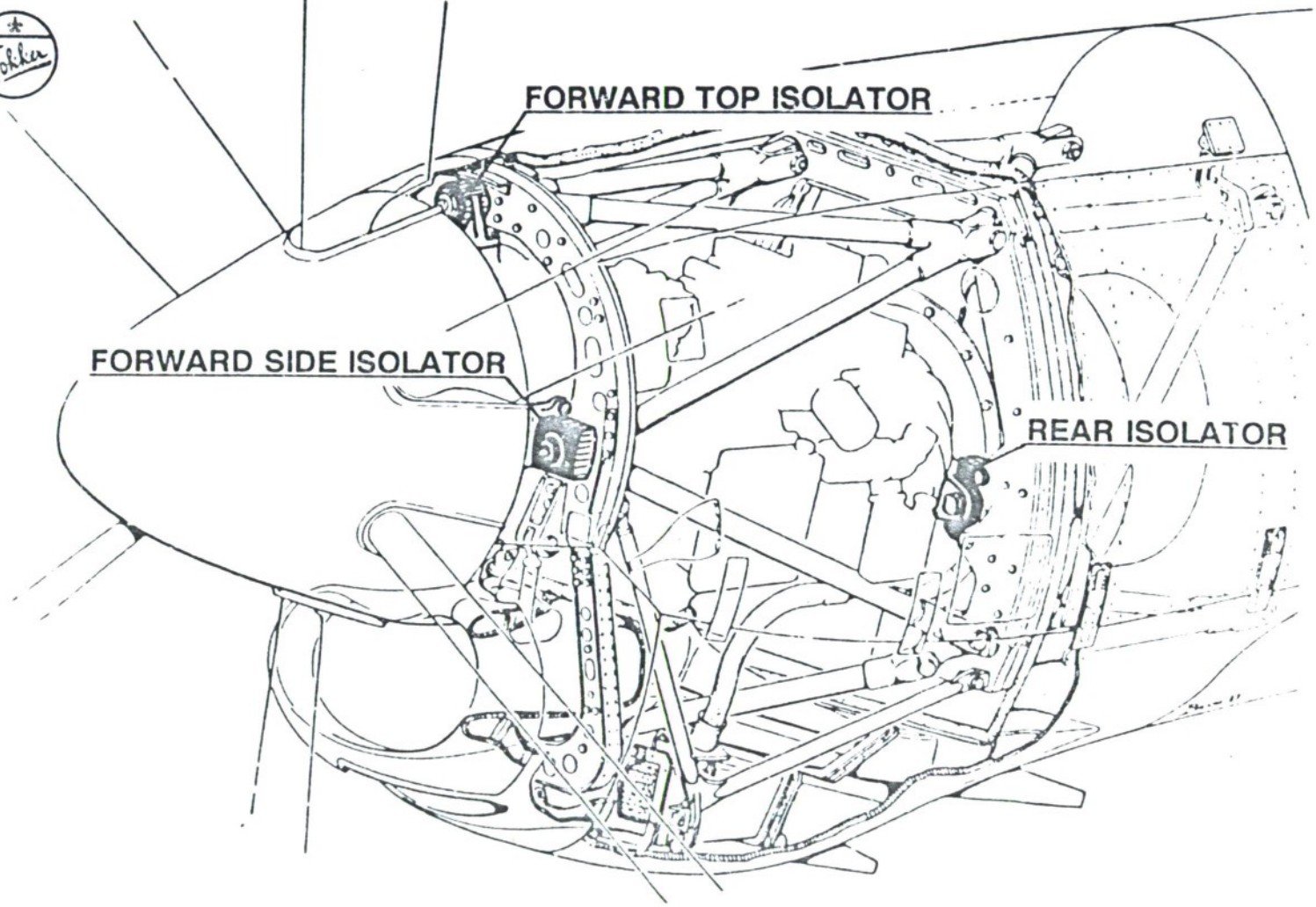

FOKKER50 ENGINE MOUNTING SYSTEM

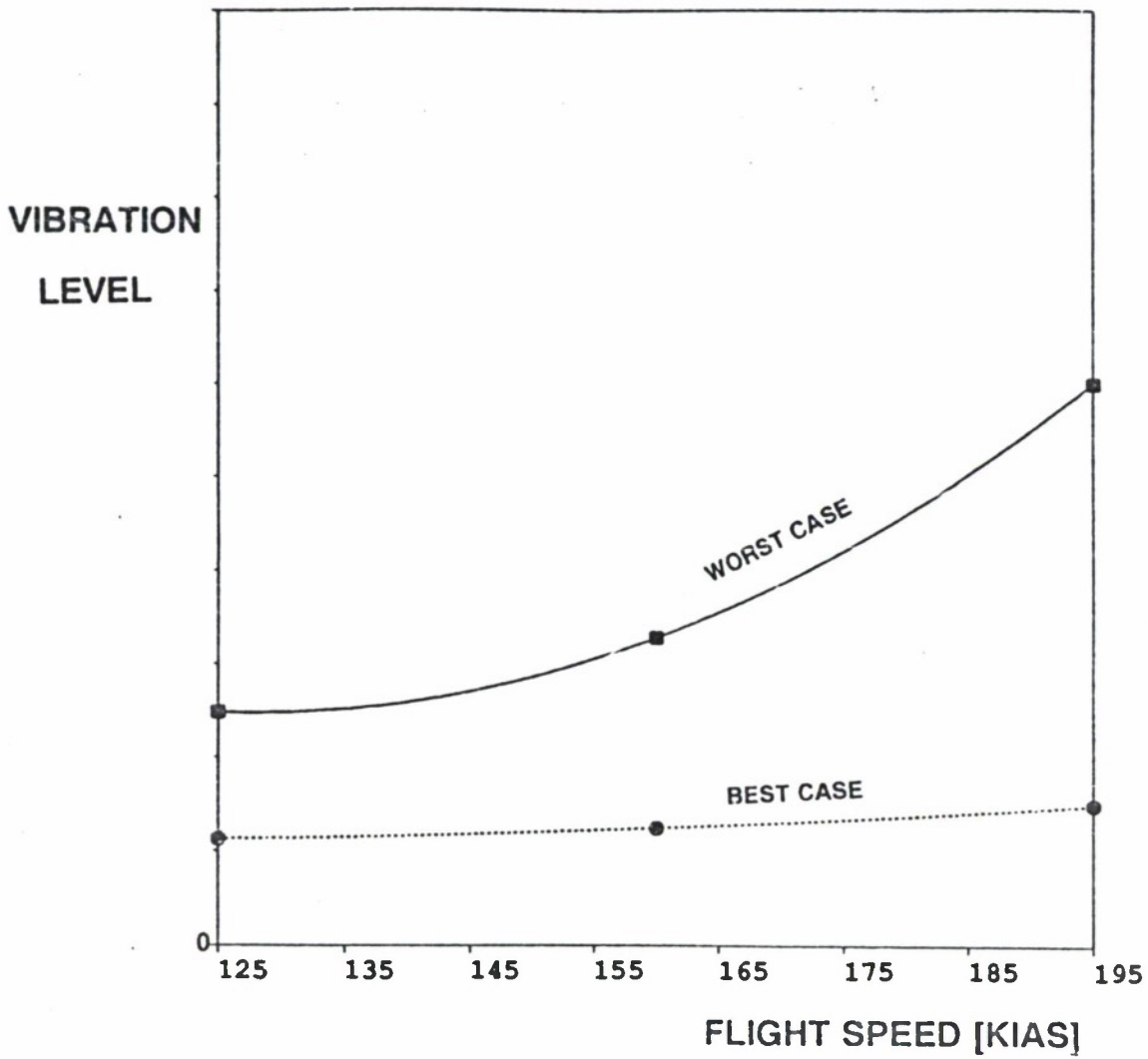

INFLUENCE OF FLIGHT SPEED ON 1P-VIBRATION LEVEL

VIBRATION LEVELS

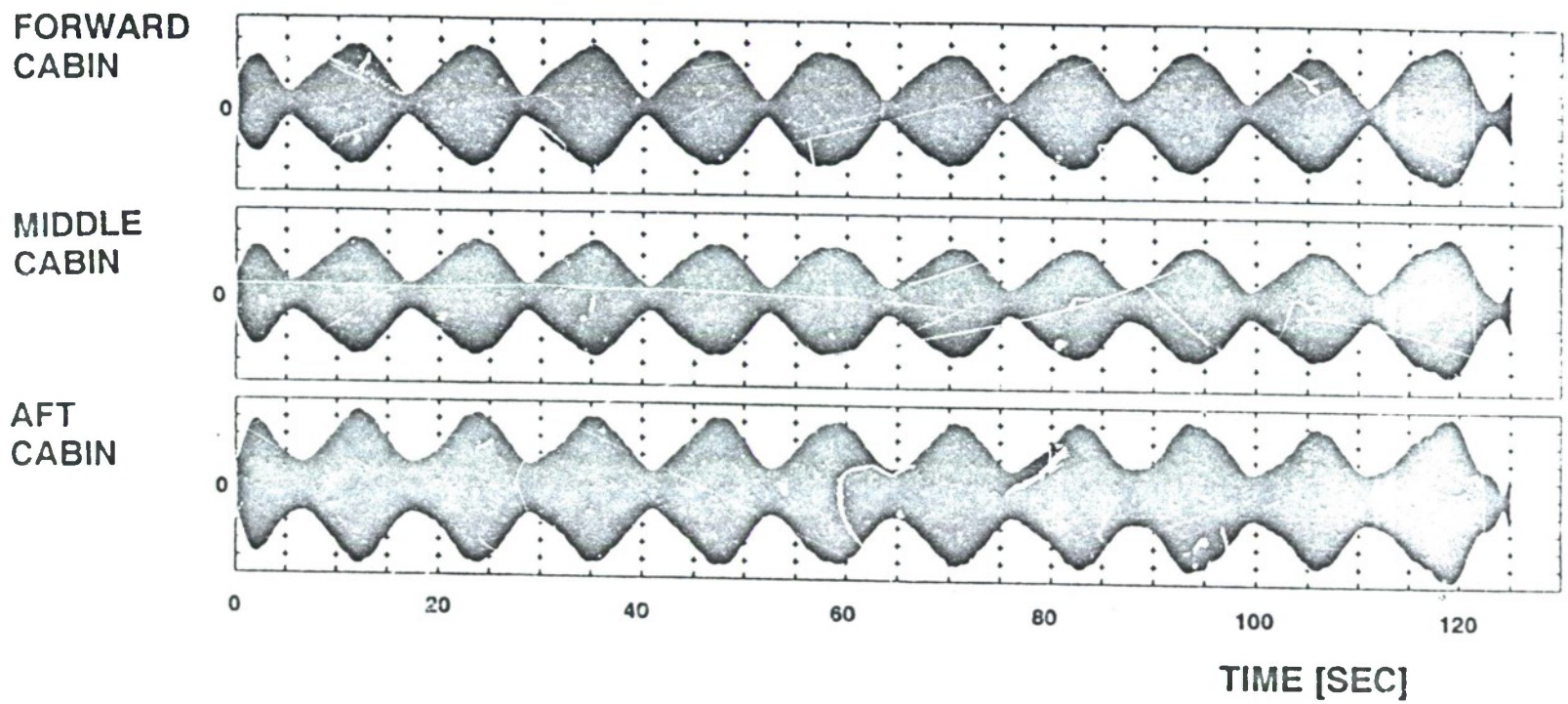

1P-BEAT DUE TO ASYNCHRONOUS PROPELLERS

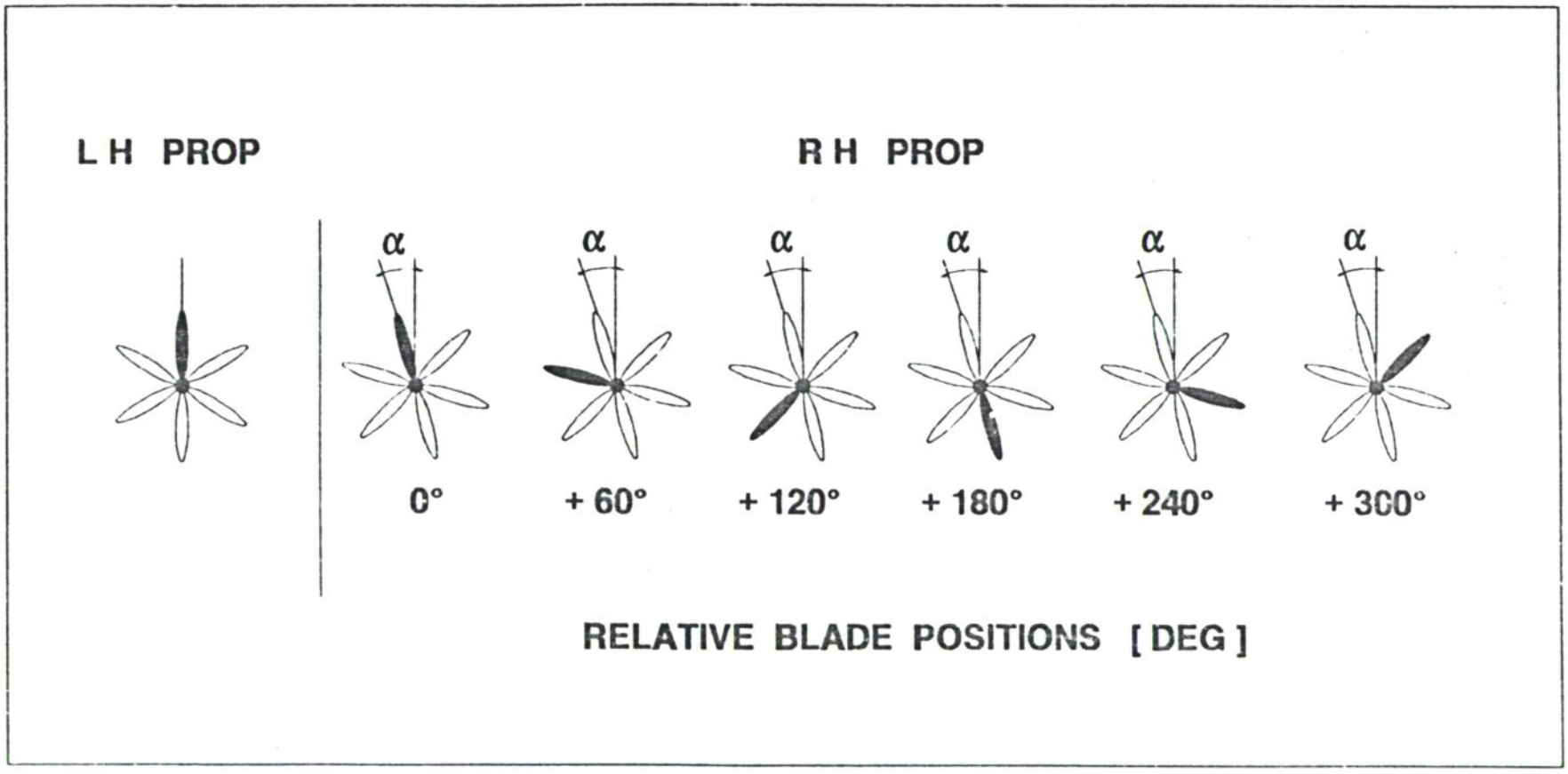

6 BLADE COMBINATIONS

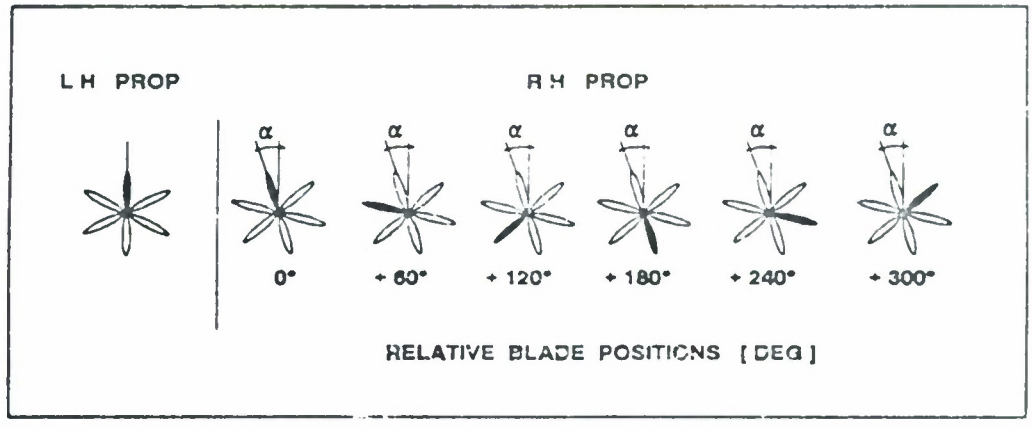

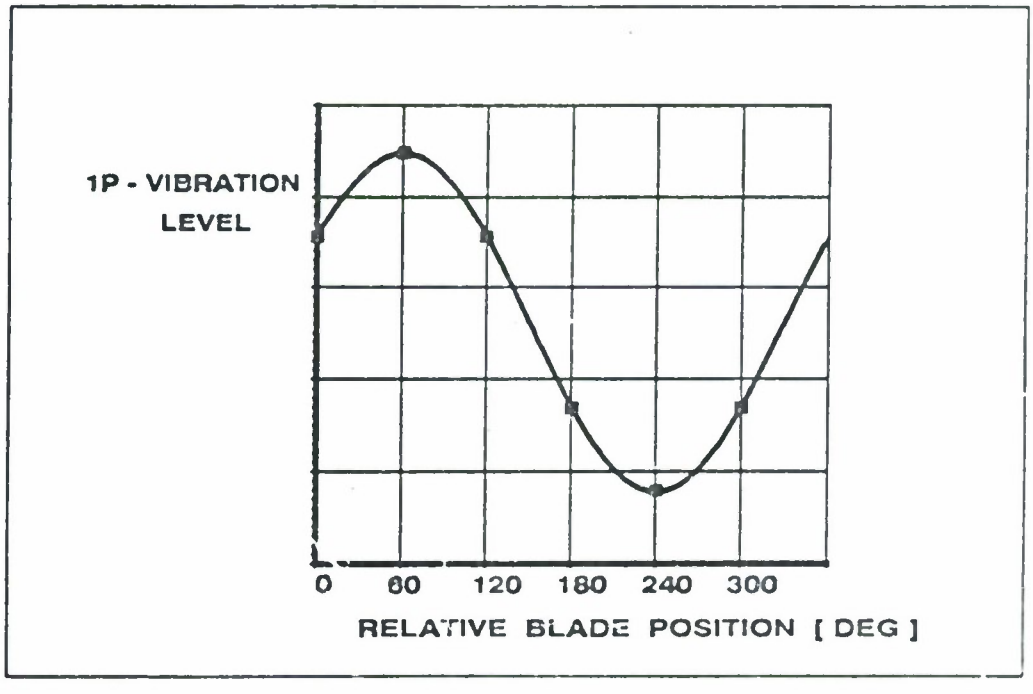

VIBRATION LEVEL vs RELATIVE BLADE POSITION

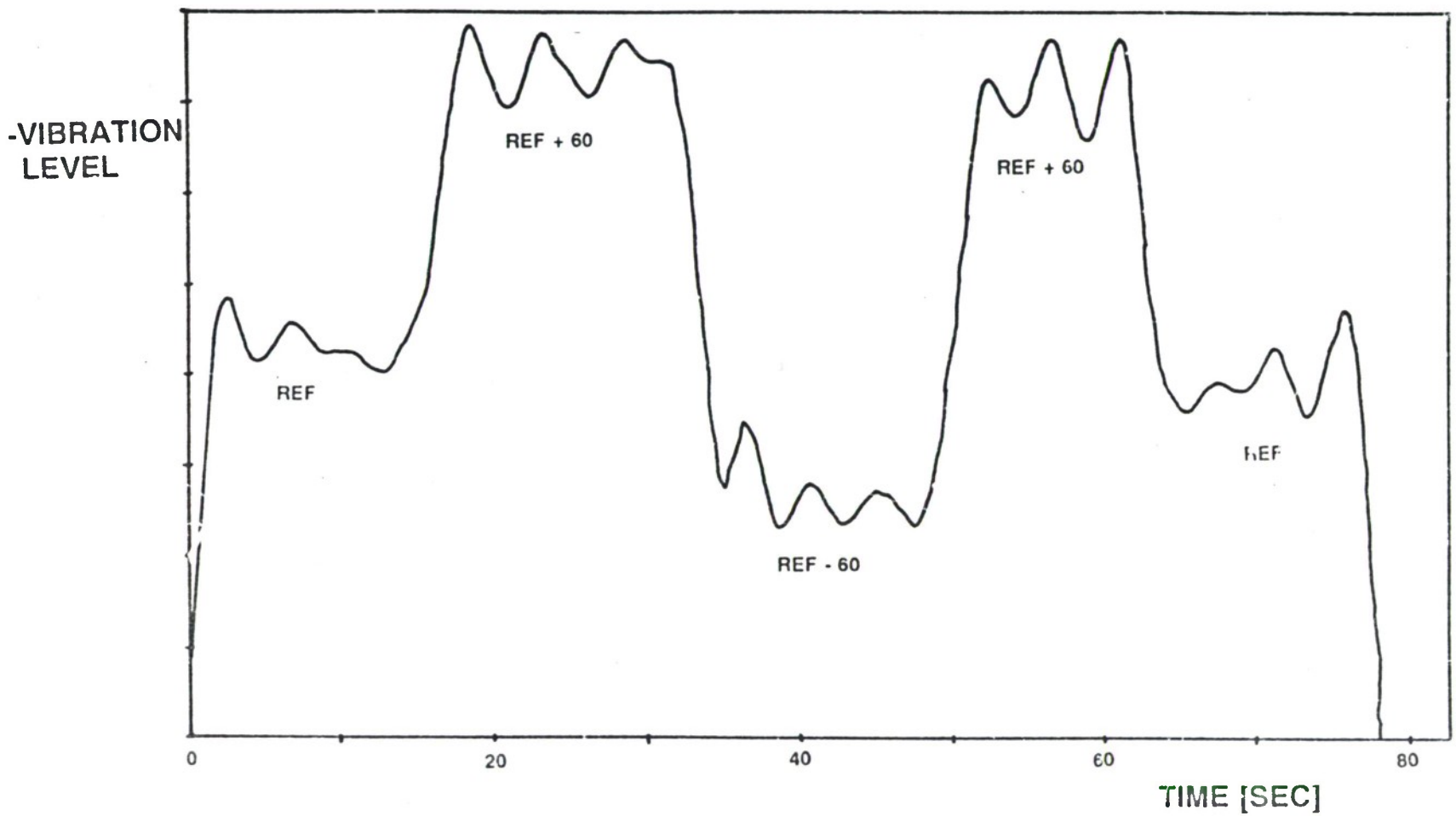

309

VIBRATION LEVEL vs BLADE POSITION STEPS

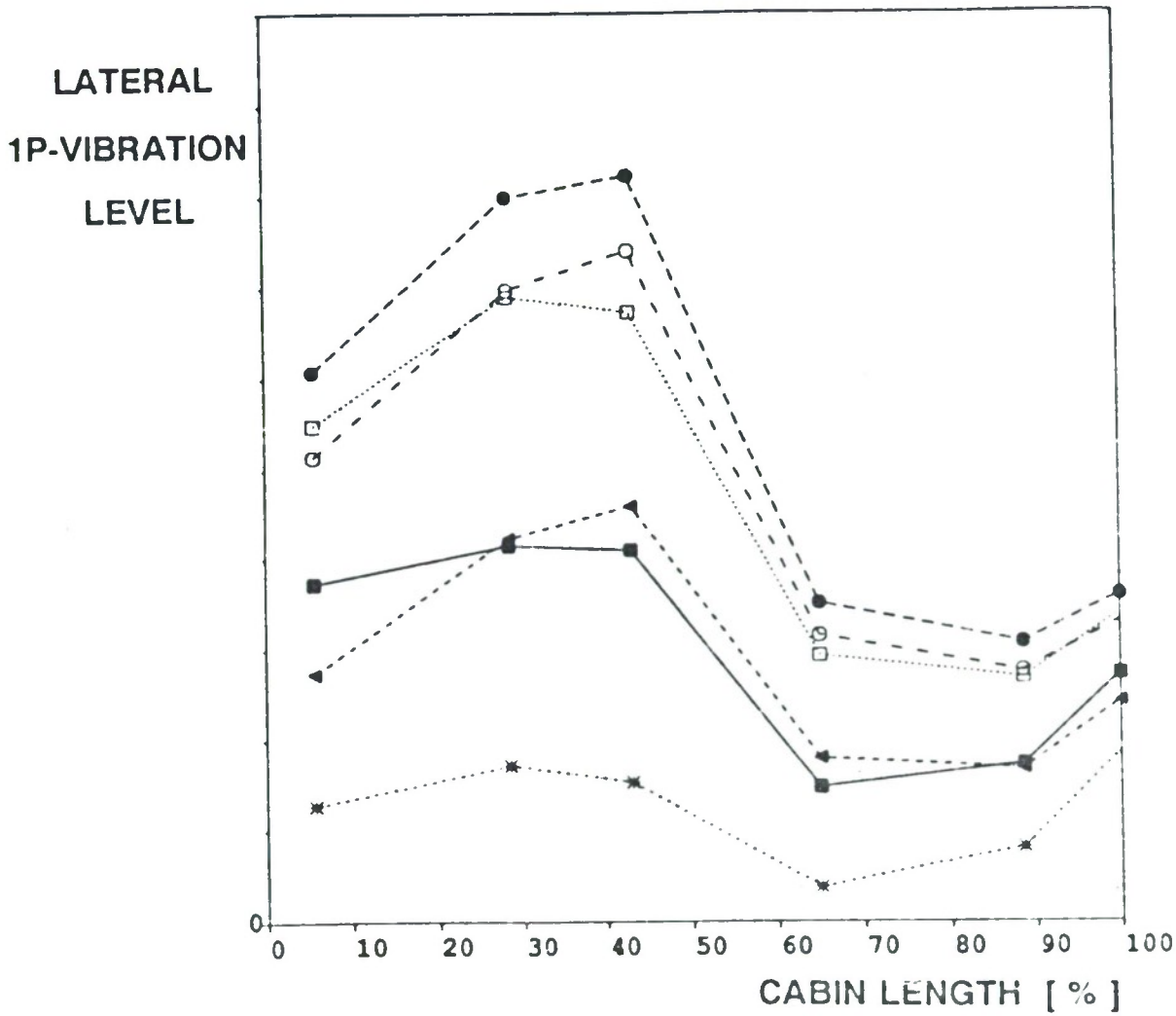

6 BLADE COMBINATIONS vs CABIN VIBRATION SHAPE

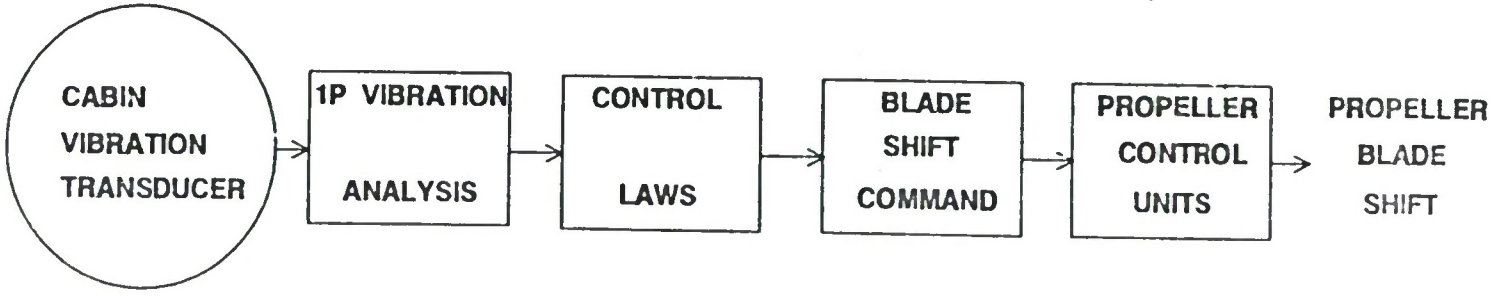

SYSTEM FUNCTIONAL BLOCK DIAGRAM

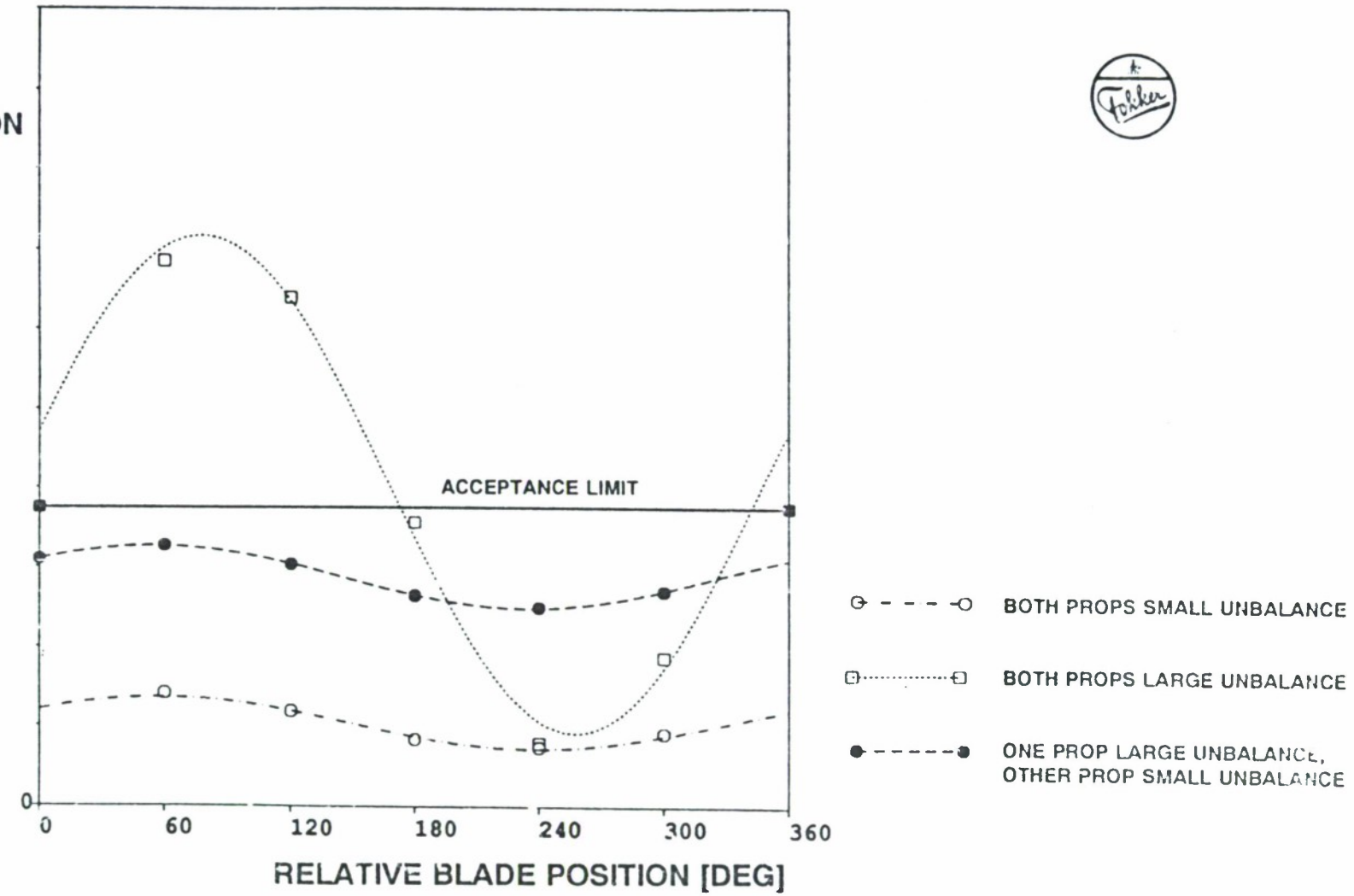

PROPELLER UNBALANCE vs PBMS PERFORMANCE

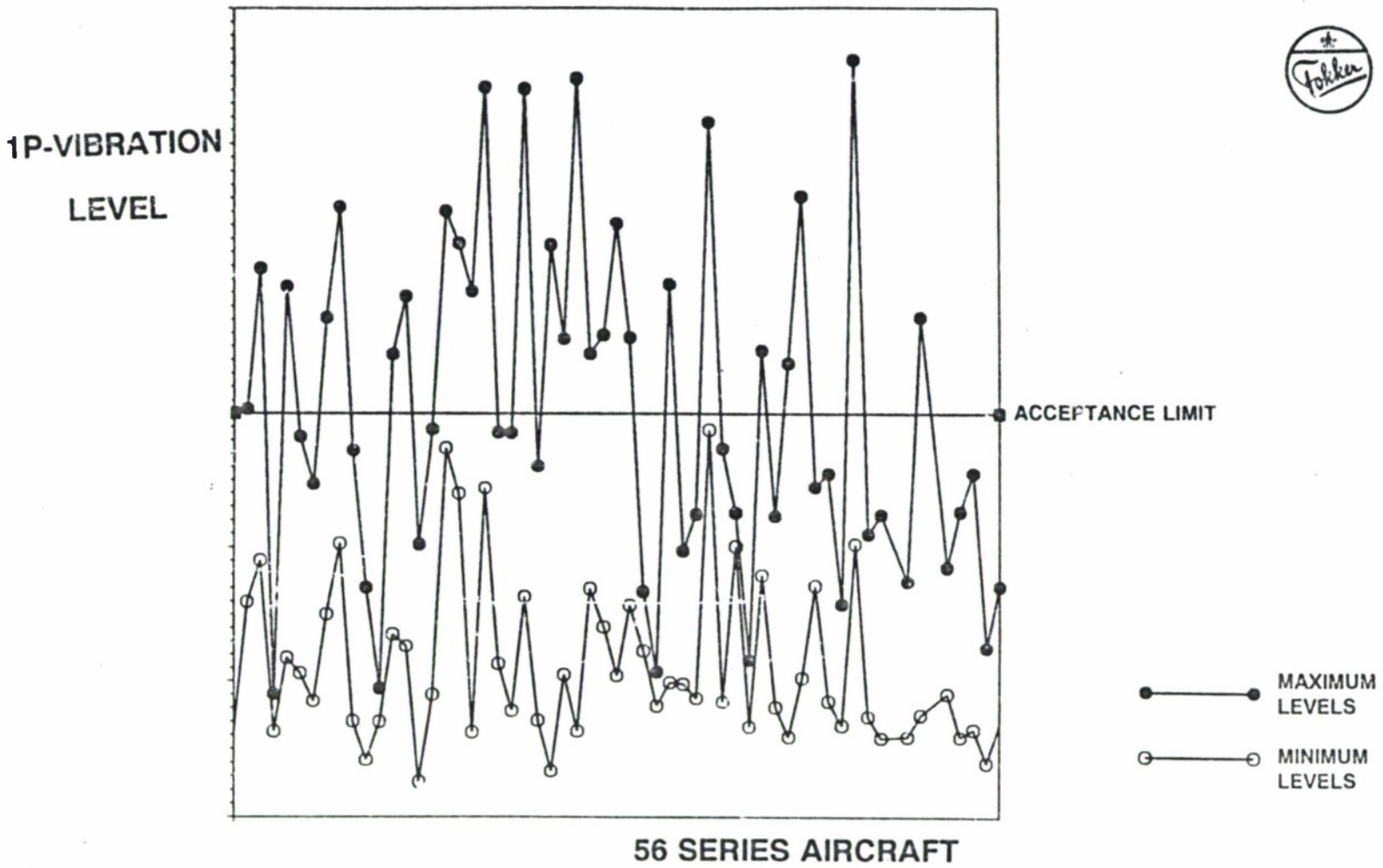

MAXIMUM AND MINIMUM VIBR LEVELS IN 56 AIRCRAFT

PBMS REDUCES ACCEPTANCE LIMIT EXCEEDANCES FROM 45 % TO 0

1- PBMS IMPROVES THE VIBRATION COMFORT IN PROPELLER AIRPLANES

2- PBMS SAVES MAINTENANCE COSTS, IT REDUCES THE NEED FOR PROPELLER BALANCING

ADVANTAGES PROPELLER BLADE MATCHING (PBMS)

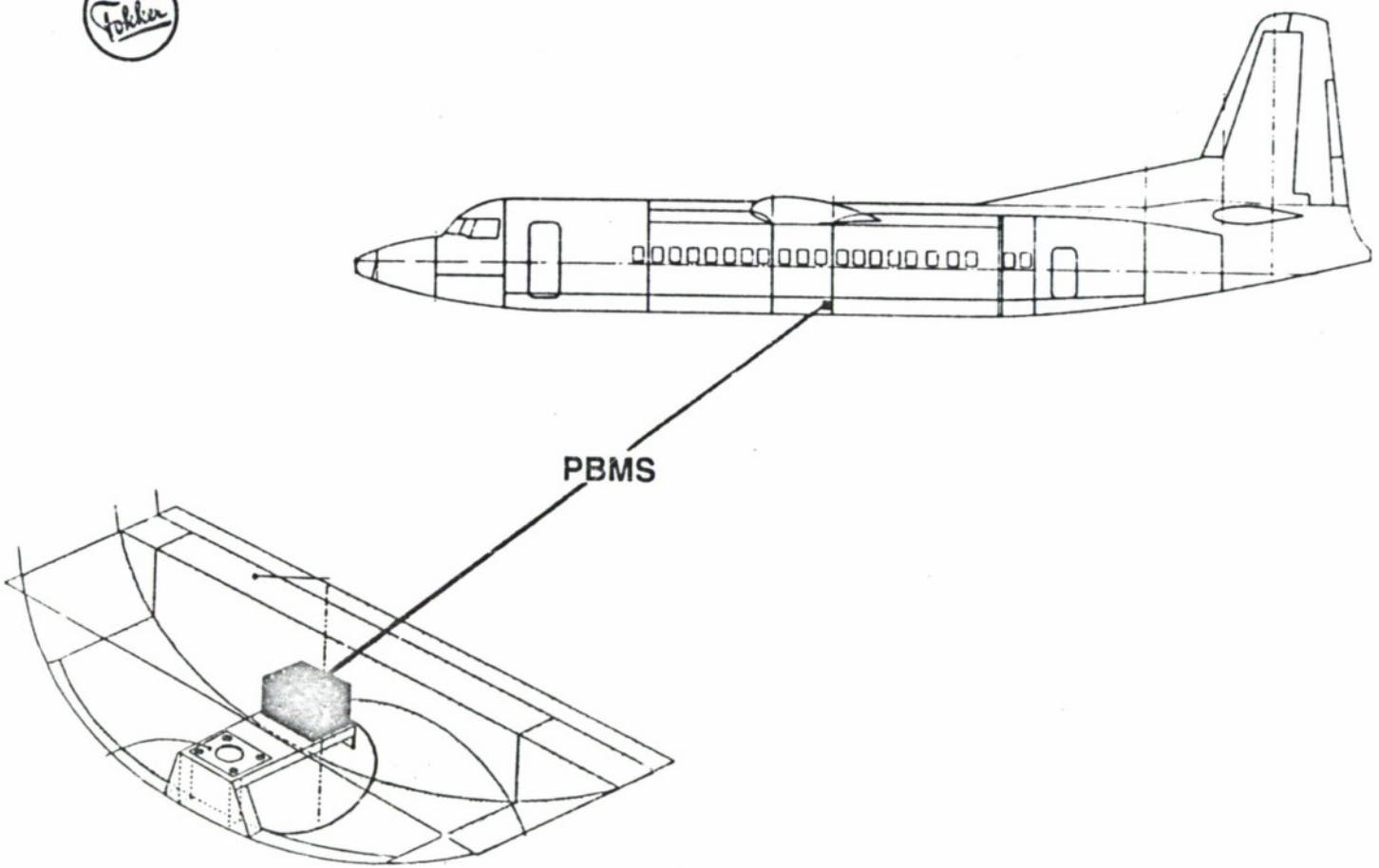

LOCATION OF PBMS IN THE FOKKER50 CABIN

N92

A LIGHTWEIGHT LOUDSPEAKER FOR AIRCRAFT COMMUNICATIONS AND ACTIVE NOISE CONTROL

Glenn E. Warnaka
APPLIED ACOUSTIC RESEARCH
PO Box 10369 Calder Square
State College, PA 16805
USA

Mark Kleinle
Parry Tsangaris
Michael J. Oslac
Harry J. Moskow
OXFORD SPEAKER COMPANY
A Division of OXFORD INTERNATIONAL LIMITED
4237 West 42nd Place
Chicago, IL 60632
USA

Presented to The 4th NASA/SAE/DLR
Aircraft Interior Noise Workshop
19 and 20 May 1992
Graf Zeppelin Haus
Friedrichshafen, Germany

Summary

A series of new, lightweight loudspeakers for use on commercial aircraft has been developed. The loudspeakers use NdFeB magnets and aluminum alloy frames to reduce the weight. In the cases where high voltage transmission lines are employed, the transformers used on conventional loudspeakers are replaced by high impedance voice coils of 1000Ω to 2000Ω DC resistance to lower the weight still further. The lightweight cabin loudspeakers are 15cm in diameter and weigh only 39% as much as conventional designs without transformers and only 27% as much as conventional designs with transformers. A 10cm diameter loudspeaker for use in avionics equipment weighs only 70g. The lightweight loudspeakers can replace current designs and meet all U.S. aircraft requirements. These loudspeakers are now being produced and installed in commercial aircraft.

The NdFeB magnet is virtually encapsulated by steel in the new speaker designs. As a result, the stray magnetic fields are extremely low and cannot be detected by standard means beyond about 25cm. This means that they will not cause magnetic interference with equipment on board. Since the loudspeakers also have reduced height and smaller volume, they may be used with tightly packed avionics packages.

The field intensity of the magnet may be increased 15% by adding a small "bucking" magnet of inexpensive ferrite to the design. This increases the weight by only 6% or 7%. If an NdFeB bucking magnet is used, the weight penalty is only about 0.6% to 0.8% for a 15% gain in magnetic field strength. In addition, the loudspeakers were tested for back emf. The back emf was found to be low and will produce no electrical problems.

Active noise reduction using internal loudspeakers was demonstrated to be effective in aircraft in 1983. A weight, space, and cost efficient method for creating the active sound attenuating fields is to use the existing cabin loudspeakers for both communications and noise attenuation. To accomplish this the loudspeakers must produce a speech to noise ratio of +4dB or +5dB in a noise field of approximately 75dB SIL. At the same time, the loudspeakers must be capable of several decibels of "headroom" to accommodate the active noise reduction signal without speech distortion. The lightweight loudspeakers are capable of achieving this or can easily be made capable of doing so. However, the dual usage of the cabin loudspeakers would raise their duty cycle from 4% or 5% to 100%. This would require some additional loudspeaker design considerations. An overall system design of the combined communication and active noise control sub-systems to provide proper equalization and amplification of both functions would also be required.

TABLE I

	CONVENTIONAL	LIGHT WEIGHT	WEIGHT RATIO: LIGHT WEIGHT / CONVENTIONAL
15 cm Diameter Cabin Loudspeaker With Transformer	686 g	185 g with high impedance voice coil and resistor network	0.27
15 cm Diameter Cabin Loudspeaker Without Transformer	387 g	151 g	0.39
10 cm Diameter Cockpit/ Avionic Loudspeaker	-------	70 g	------

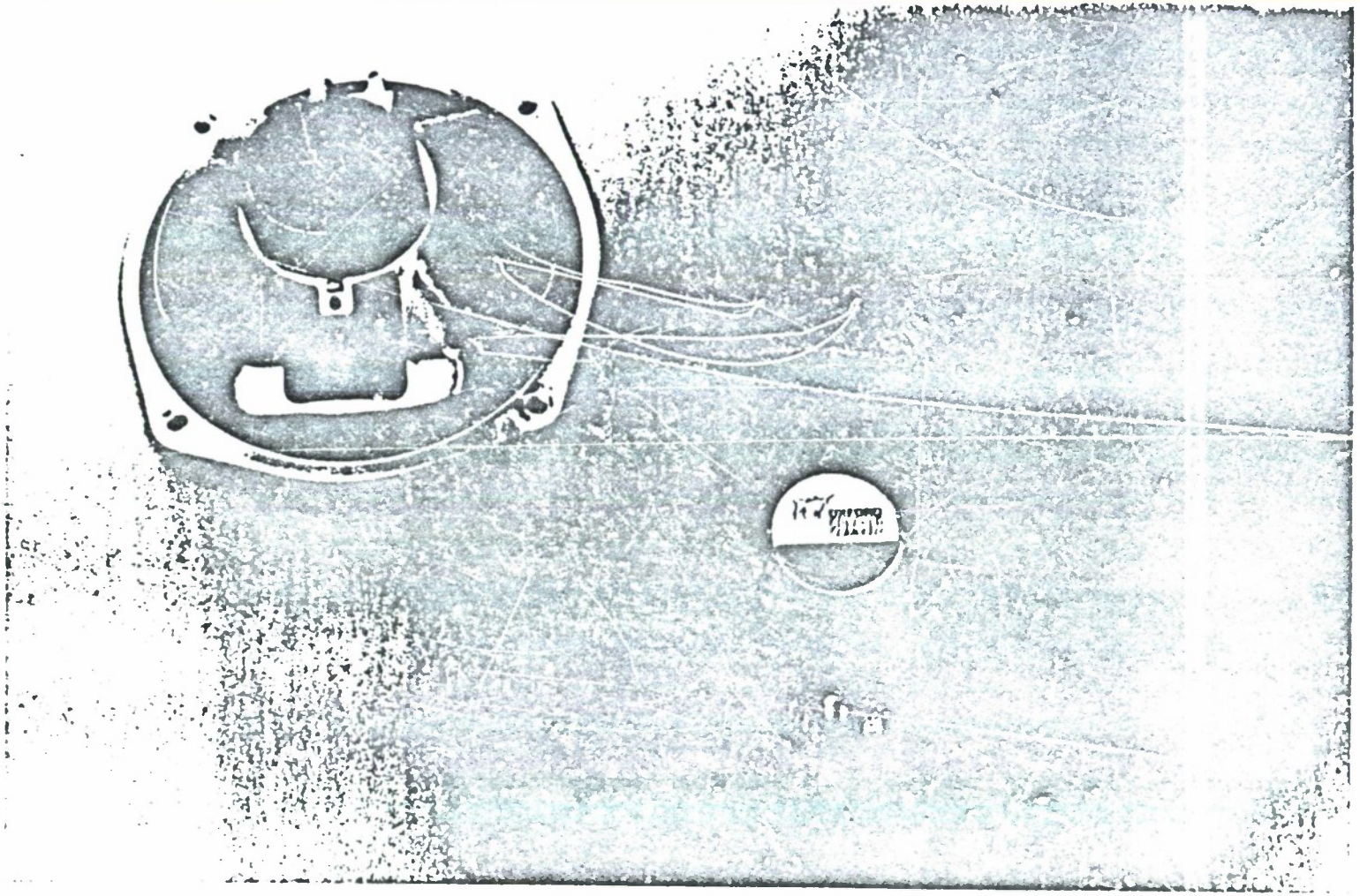

Figure 1. Conventional 15cm Diameter Loudspeaker (left) and Lightweight Loudspeaker (right).

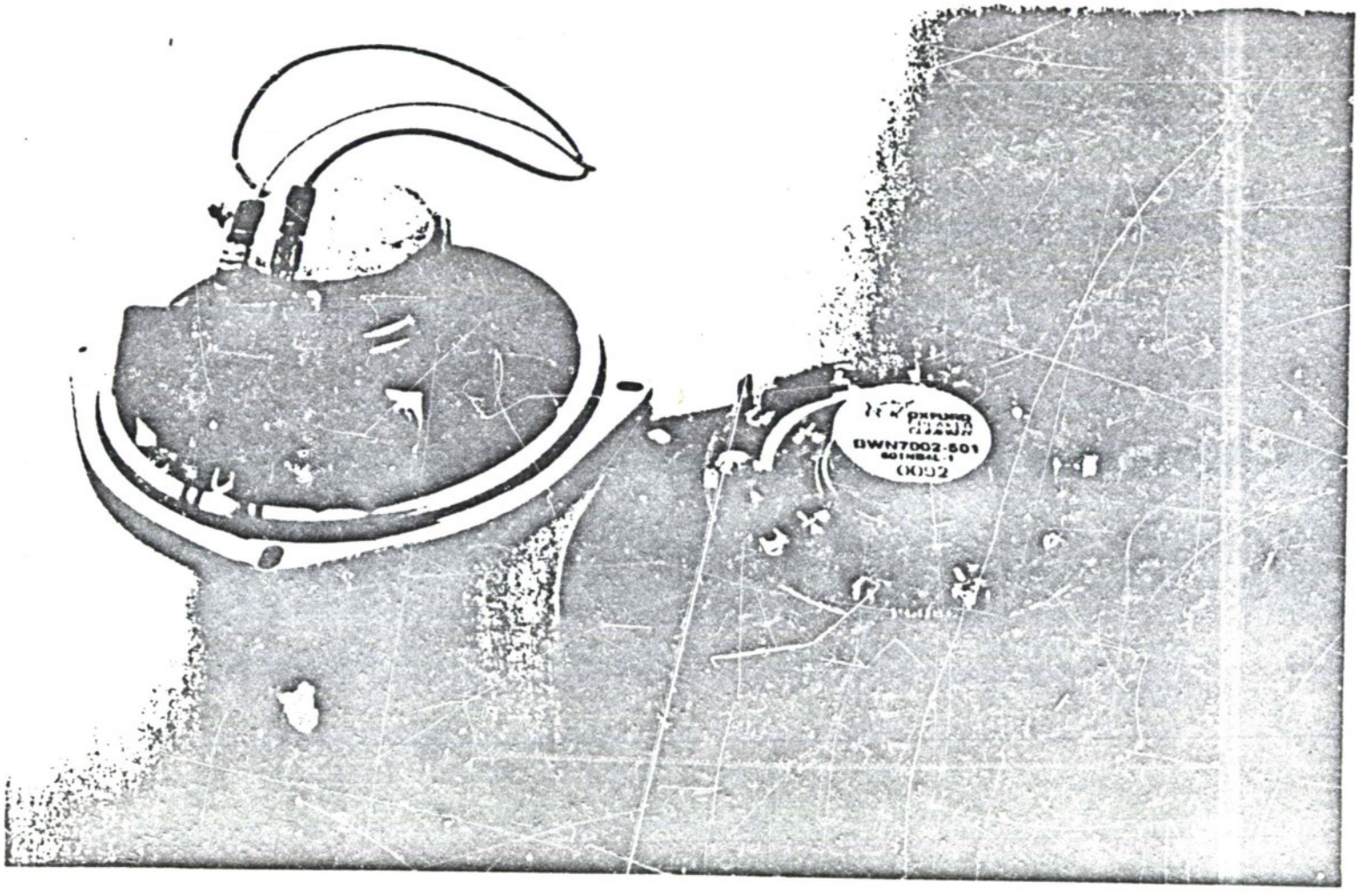

Figure 2. Conventional 15cm Loudspeaker with Transformer (left) and Lightweight Loudspeaker with High Impedance Voice Coil and Resistor Network (right).

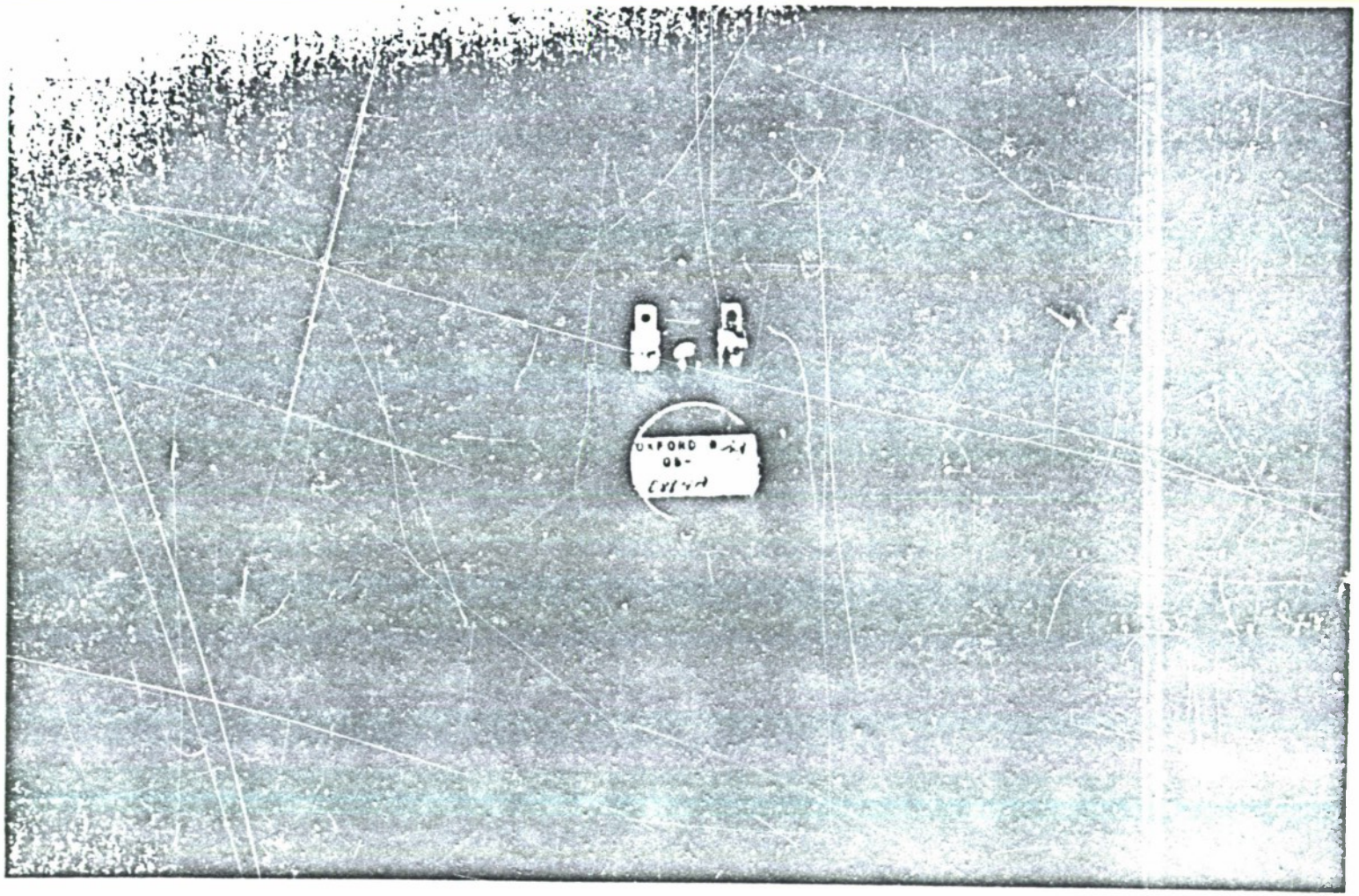

Figure 3. Lightweight 10cm Diameter Loudspeaker.

Figure 4. BACK emf TEST CONFIGURATION

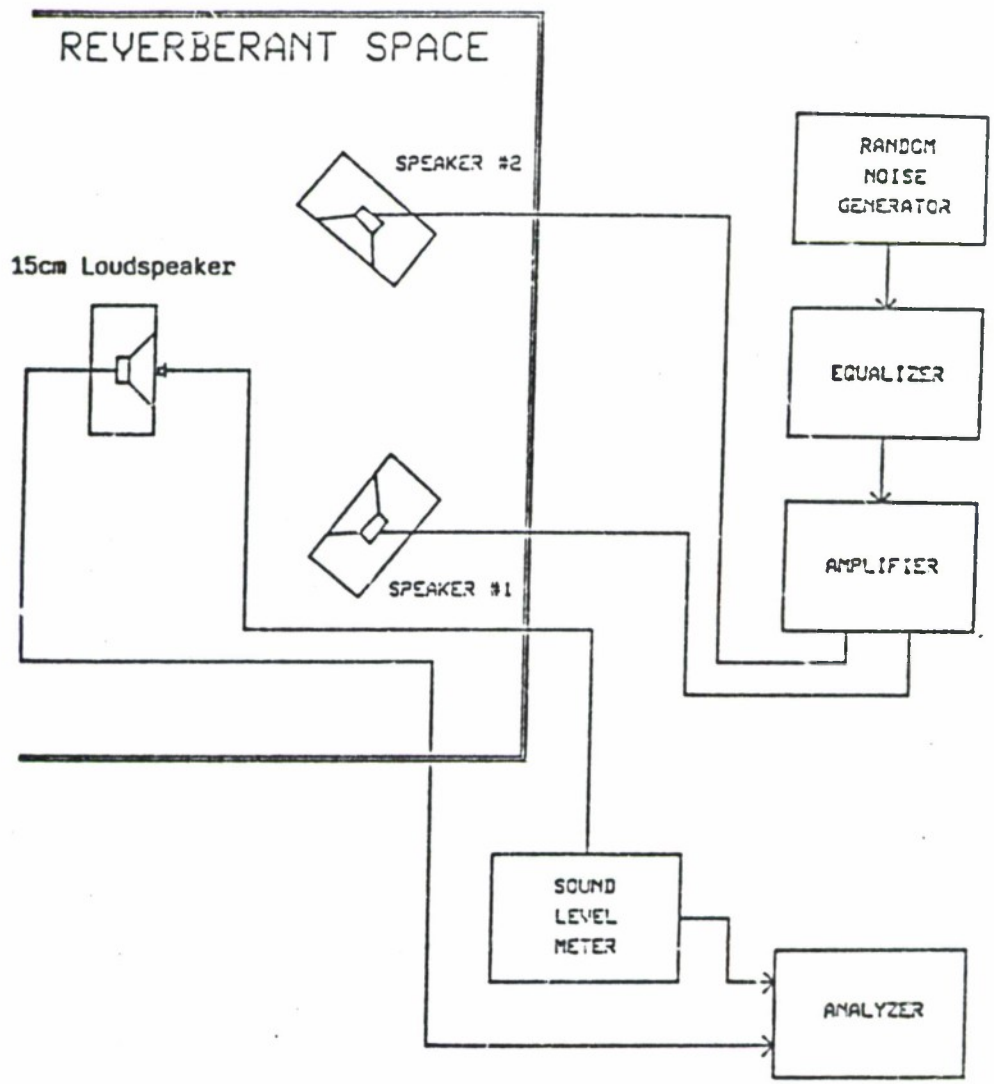

Figure 5. Back emf of 15cm Lightweight Loudspeaker
to Steady State Excitation and Electrical Noise Floor
4 Watt Connection. Data to 12.8 kHz

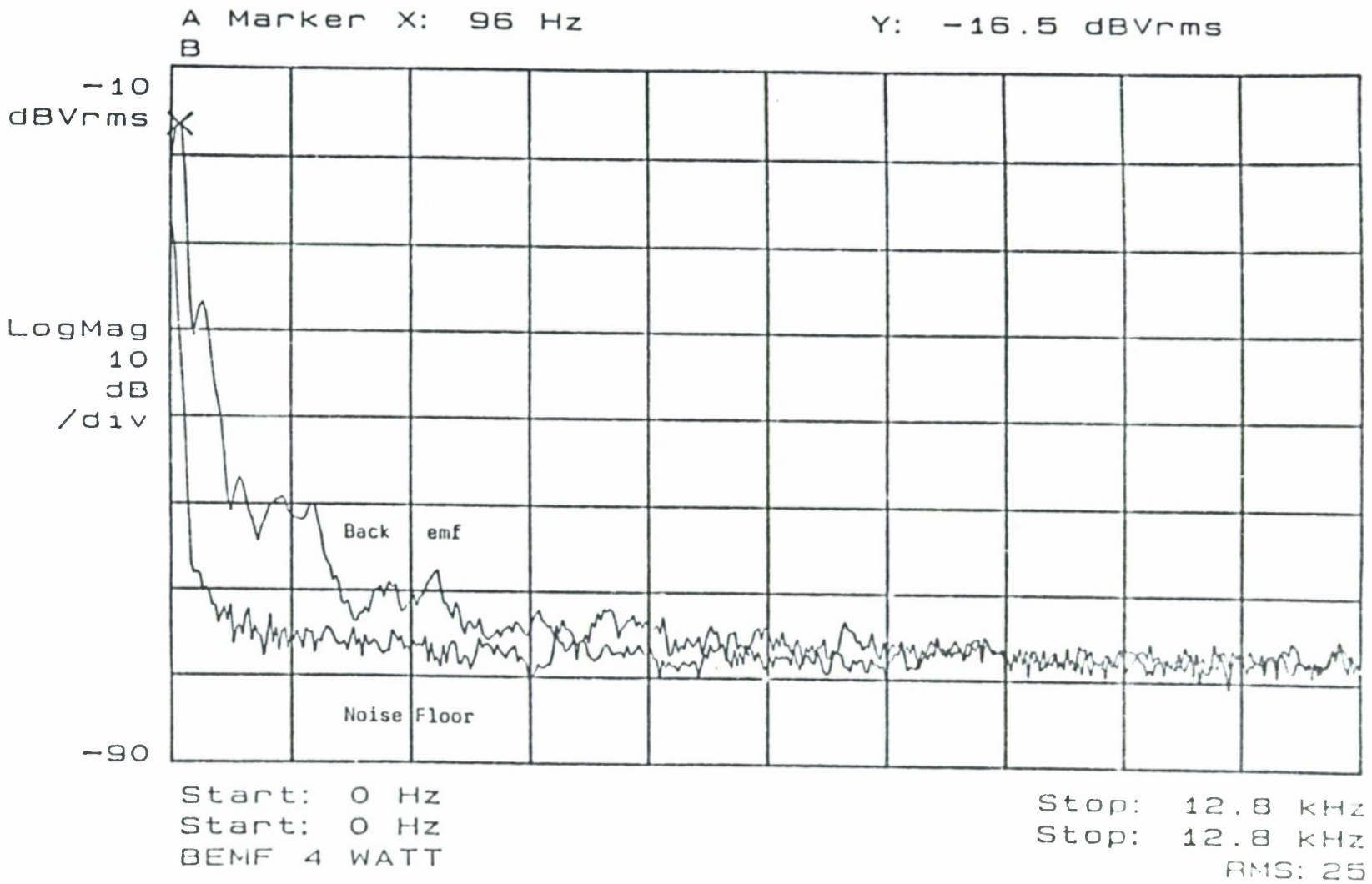

Figure 6. Transient Electrical Response of 15cm Lightweight Loudspeaker
4W Connection. 70 Volt Excitation.

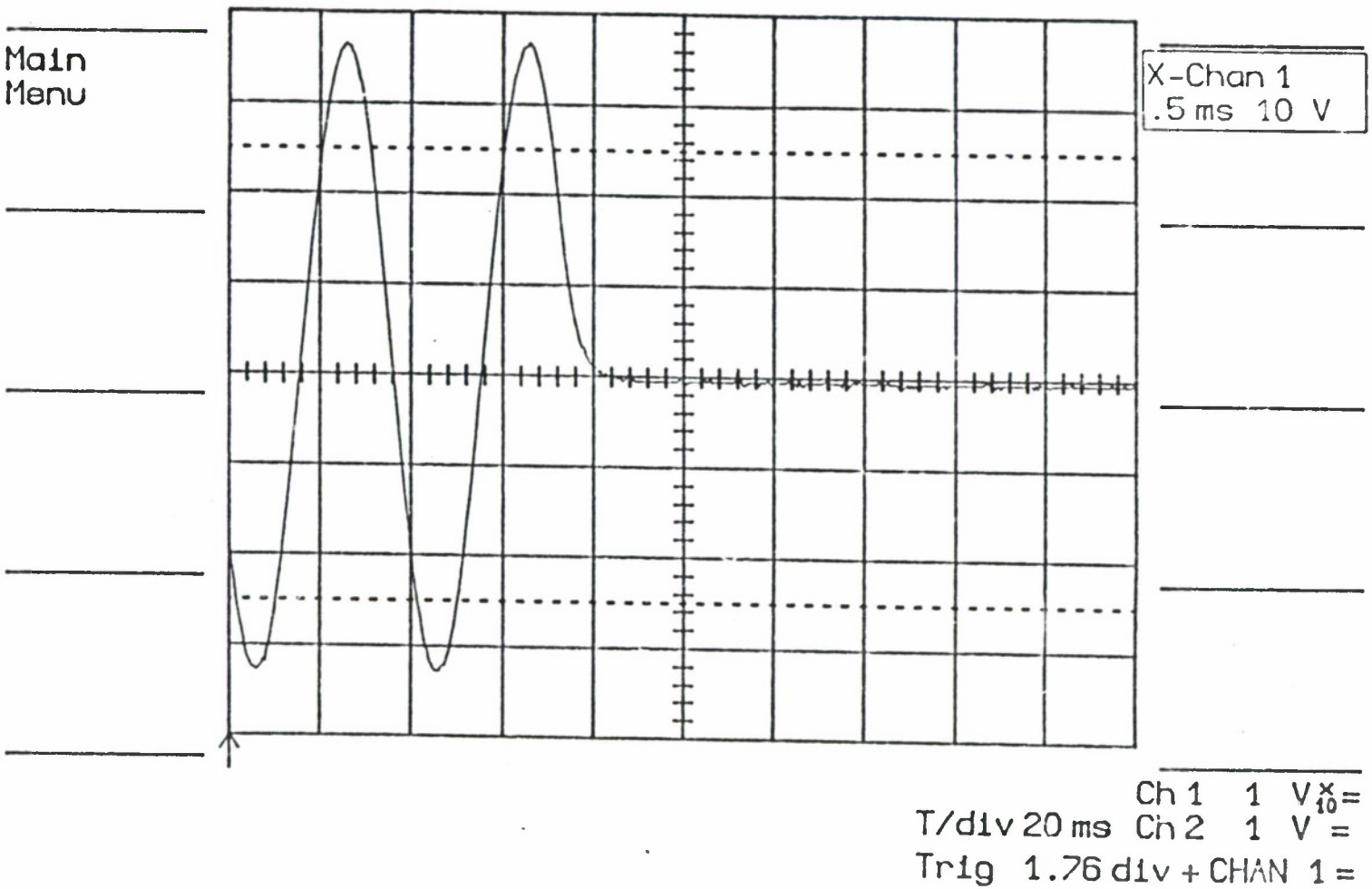

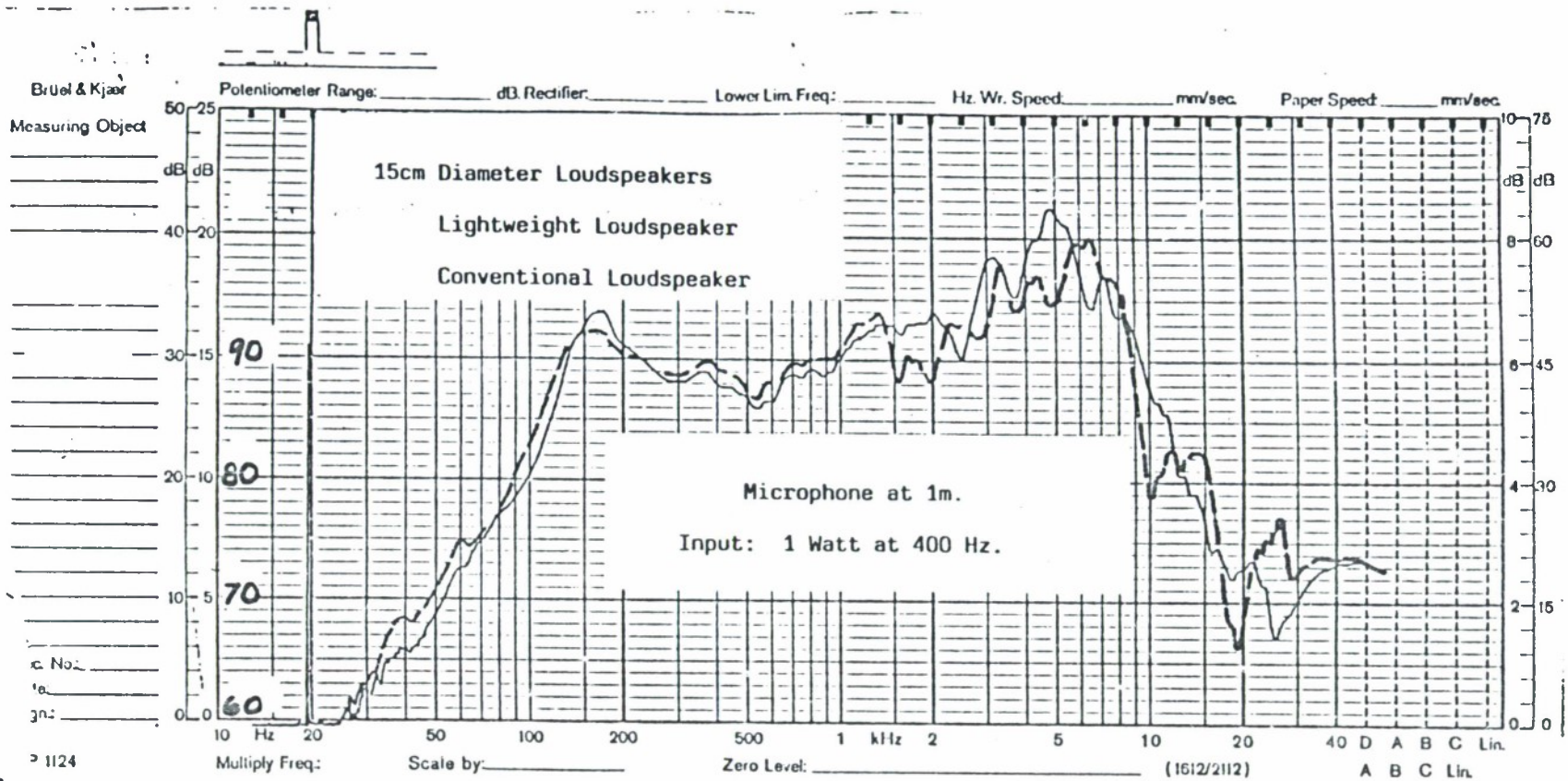

Figure 7. Comparison of the Frequency Response of a 15cm Diameter Lightweight Loudspeaker and a Conventional Loudspeaker.

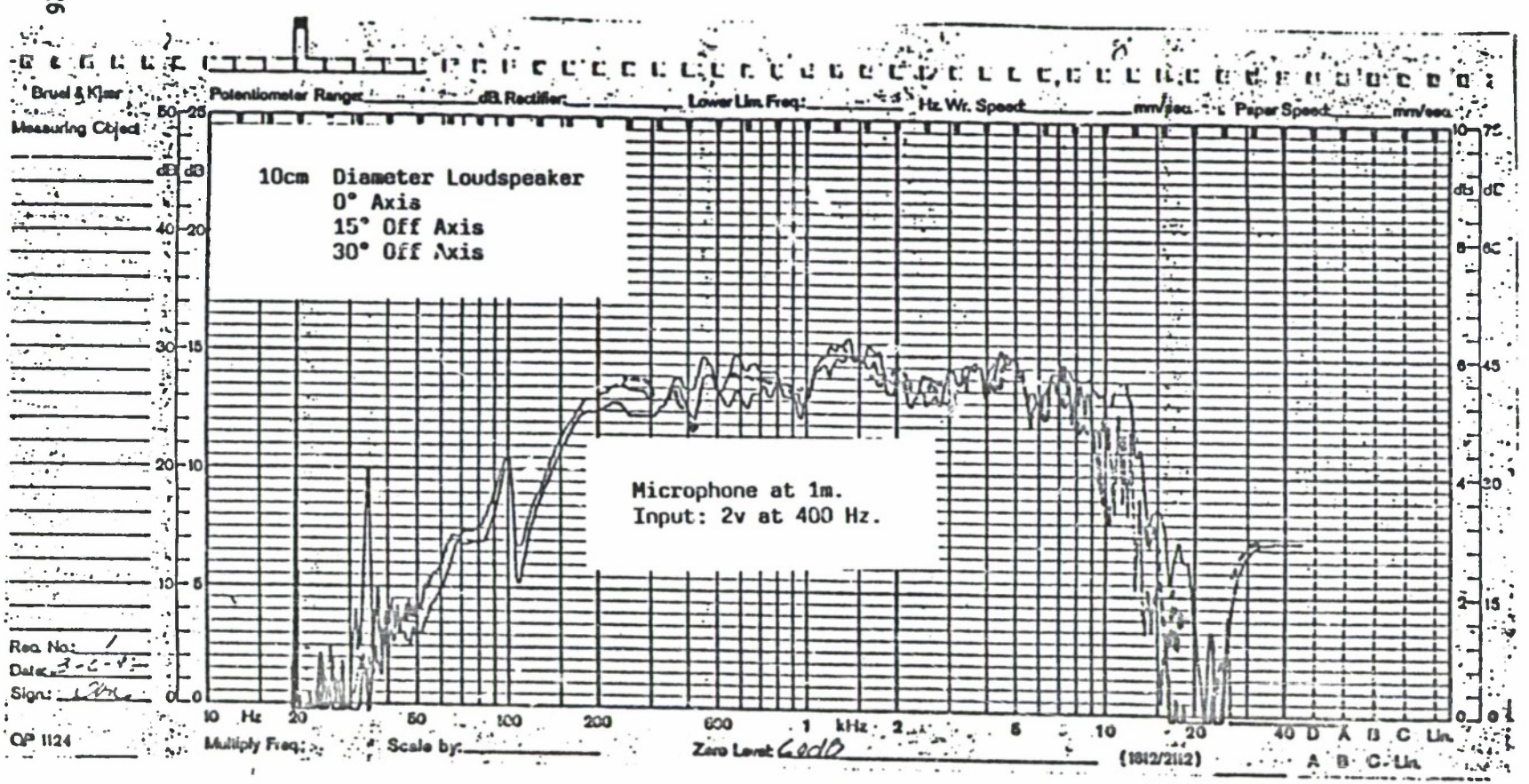

Figure 8. Off Axis Measurements of 10cm Diameter Lightweight Loudspeaker.

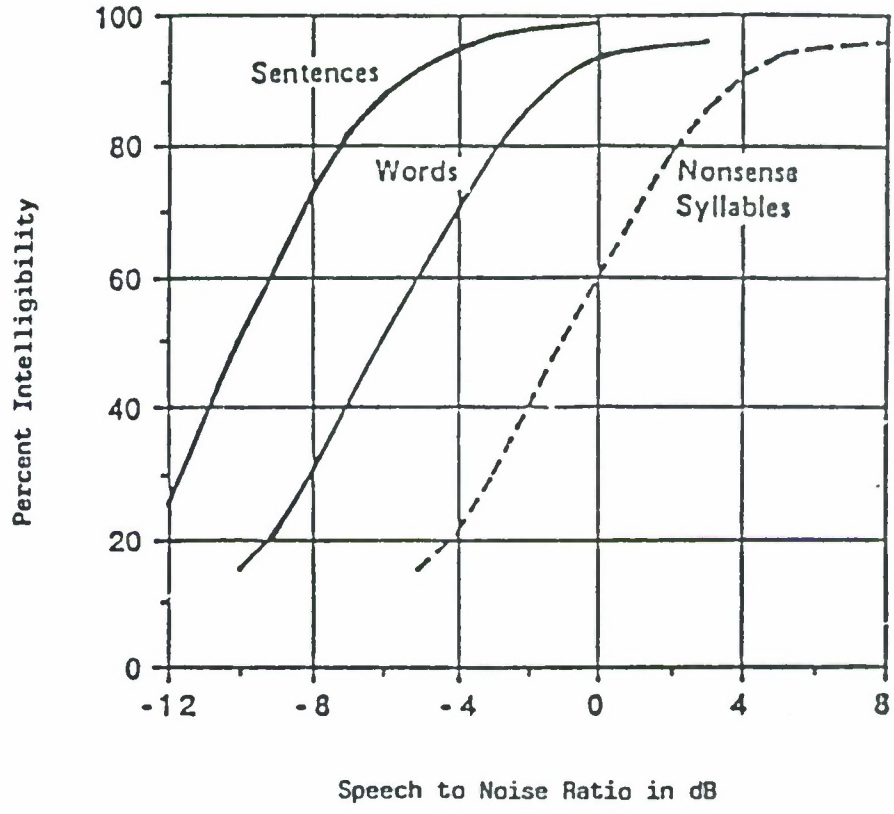

Figure 9. Intelligibility of Different Spoken Material in a Noisy Environment.

REPORT DOCUMENTATION PAGE

Form Approved

1. AGENCY USE ONLY (Leave blank)	2. REPORT DATE	3. REPORT TYPE AND DATES COVERED
	July 1992	Conference Publication

4. TITLE AND SUBTITLE
Fourth Aircraft Interior Noise Workshop

5. FUNDING NUMBERS
535-03-11-03

6. AUTHOR(S)
David G. Stephens, Compiler

7. PERFORMING ORGANIZATION NAME(S) AND ADDRESS(ES)
NASA Langley Research Center
Hampton, VA 23665-5225

8. PERFORMING ORGANIZATION REPORT NUMBER

9. SPONSORING MONITORING AGENCY NAME(S) AND ADDRESS(ES)
National Aeronautics and Space Administration
Washington, DC 20546-0001
Society of Automotive Engineers and
German Aerospace Research Establishment

10. SPONSORING/MONITORING AGENCY REPORT NUMBER
NASA CP-10103

11. SUPPLEMENTARY NOTES

12a. DISTRIBUTION AVAILABILITY STATEMENT
Unclassified - Unlimited

Subject Category - 71

12b. DISTRIBUTION CODE

13. ABSTRACT (Maximum 200 words)

The fourth in a series of NASA/SAE Interior Noise Workshops was held on May 19 and 20, 1992, at the Graf Zeppelin Haus in Friedrichshafen, Germany. The theme of the workshop was new technology and applications for aircraft interior noise with emphasis on source noise prediction; cabin noise prediction; cabin noise control, including active and passive methods; and cabin interior noise test procedures. This report is a compilation of the presentations made at the meeting which addressed the above issues.

14. SUBJECT TERMS	15. NUMBER OF PAGES
Interior noise Source noise prediction	335
	16. PRICE CODE A15

17. SECURITY CLASSIFICATION OF REPORT	18. SECURITY CLASSIFICATION OF THIS PAGE	19. SECURITY CLASSIFICATION OF ABSTRACT	20. LIMITATION OF ABSTRACT
Unclassified	Unclassified		

END

DATE

FILMED

OCT 14 1992

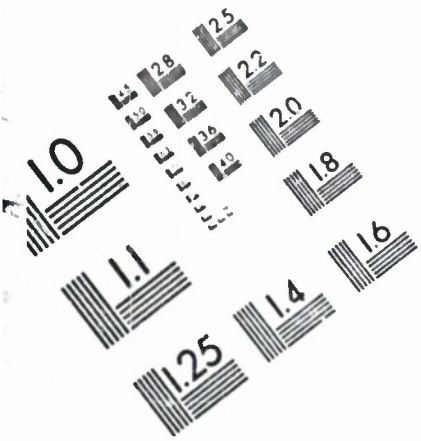

Association for Information and Image Management
1100 Wayne Avenue, Suite 1100
Silver Spring, Maryland 20910
301/587-8202

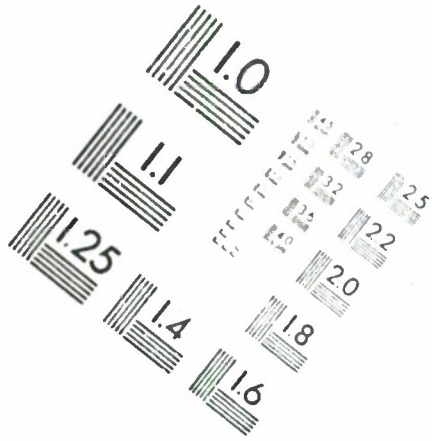

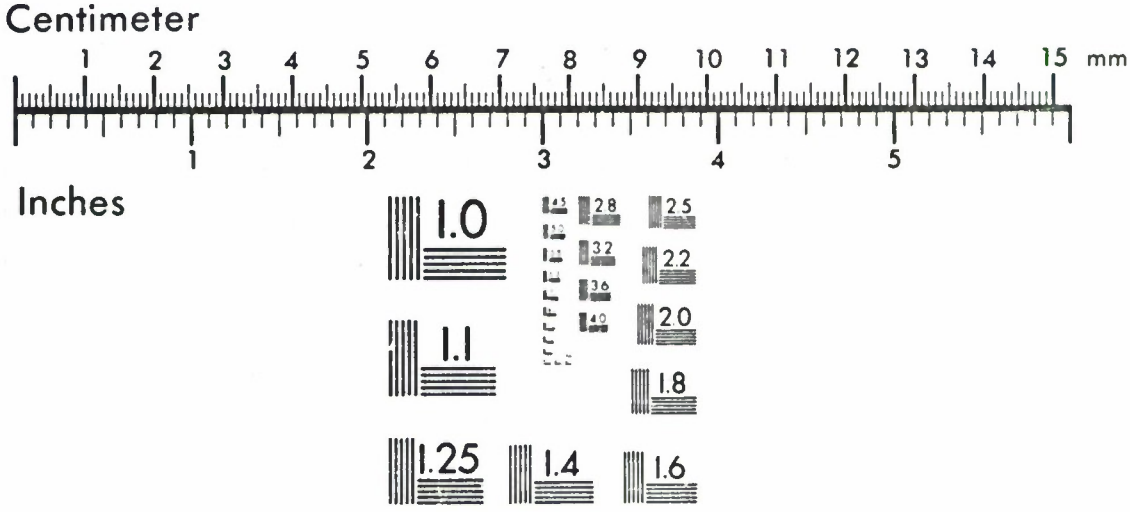

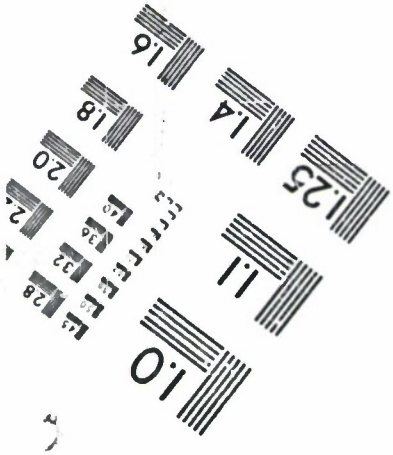

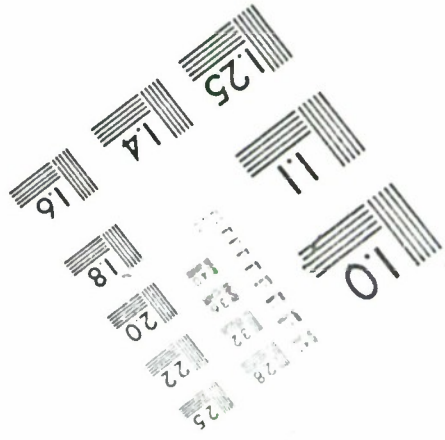

MANUFACTURED TO AIIM STANDARDS
BY APPLIED IMAGE, INC.